

NASA-CR-189055
19920010443

NASA CR189055
RI/RD90-214

Orbital Transfer Rocket Engine Technology Program

**Contract NAS3-23773
Task B.5**

Soft Wear Ring Seal Technology

FINAL REPORT

February 1992

**Prepared for:
National Aeronautics and Space Administration
Lewis Research Center
Cleveland, Ohio 44135**



Rockwell International
Rocketdyne Division

LIBRARY COPY

FEB 25 1992

LANGLEY RESEARCH CENTER
LIBRARY NASA
HAMPTON, VIRGINIA

Rocketdyne Division
Rockwell International Corporation
6633 Canoga Avenue
Canoga Park, California 91303

Telex: 698478
ROCKETDYN CNPK



Rockwell
International

14 February 1992

In reply refer to 92RC01849

NASA/Lewis Research Center
21000 Brookpark Road
Cleveland, OH 44135

Attention: Albert A. Spence, MS 500-305

Subject: NAS3-23773; "Orbit Transfer Rocket Engine Technology
Program", CDR NO. 7, Task B.5, Approved-Final Report, dated
February 1992, RI/RD90-214, NASA CR 189055

Reference: NASA letter 5320, dated October 30, 1991

Gentlemen:

We are transmitting an enclosure in accordance with the subject contract
for your information and retention.

Very truly yours,

ROCKWELL INTERNATIONAL CORPORATION
Rocketdyne Division

P. R. Wesley
Manager
Configuration and Data Management

G.O. 95285

Encl: One copy of the Approved Final Report, Soft Wear Ring Seal
Technology, dated February 1992, RI/RD90-214, NASA CR 189055

cc: NASA/Lewis Research Center
21000 Brookpark Road
Cleveland, OH 44135
Attention: Margaret P. Proctor, MS SPTD-2
(one copy)

See attached list for distribution

9887o

A. A. Spence
M.S. 500-305
NASA Lewis Research Center
21000 Brookpark Rd.
Cleveland, OH 44135

S. B. Foust
M.S. SPTD-3
NASA Lewis Research Center
21000 Brookpark Rd.
Cleveland, OH 44135

Technical Util. Office
M.S. 7-3
NASA Lewis Research Center
21000 Brookpark Rd.
Cleveland, OH 44135

Report Control Office
M.S. 60-1
NASA Lewis Research Center
21000 Brookpark Rd.
Cleveland, OH 44135

AFSC Liaison Office
M.S. 501-3
NASA Lewis Research Center
21000 Brookpark Rd.
Cleveland, OH 44135

Library
M.S. 60-3
NASA Lewis Research Center
21000 Brookpark Rd.
Cleveland, OH 44135

M. P. Proctor
M.S. SPTD-2
NASA Lewis Research Center
21000 Brookpark Rd.
Cleveland, OH 44135

G. P. Richter
SPTD-2
NASA Lewis Research Center
21000 Brookpark Rd.
Cleveland, OH 44135

Frank D. Berkopec
SPTD-2
NASA Lewis Research Center
21000 Brookpark Rd.
Cleveland, OH 44135

J. A. Hemminger
M.S. SPTD-2
NASA Lewis Research Center
21000 Brookpark Rd.
Cleveland, OH 44135

NASA Headquarters
Attn: Director/MD
Washington, D. C. 20546

NASA Headquarters
Attn: Director/RP
Washington, DC 20546

NASA Headquarters
Attn: W. Escher/RP
Washington, D.C. 20546

NASA Ames Res. Center
Attn: Library
Moffett Field, CA 94035

NASA Flight Res. Center
Attn: Library
P. O. Box 273
Edwards CA, 93523

NASA MSFC
Attn: J.F.Thompson/PD13
Huntsville, AL 35812

NASA MSFC
Attn: Library
Huntsville, AL 35812

NASA MSFC
Attn: R. J. Richmond
Code ER21
Huntsville, AL 35812

NASA MSFC
Attn: O. K. Goetz
Code EE21
Huntsville, AL 35812

NASA MSFC
Attn: L. A. Gross
Code EE21
Huntsville, AL 35812

NASA MSFC
Attn: H. P. Stinson
Code EP62
Huntsville, AL 35812

NASA MSFC
Attn: S. P. McIntyre
Code EP53
Huntsville, AL 35812

NASA MSFC
Attn: C. F. Huffaker
Code PT31
Huntsville, AL 35812

NASA MSFC
Attn: C. S. Cornelius
Code EP61
Huntsville, AL 35812

NASA MSFC
Attn: J. P. McCarty
Code EP01
Huntsville, AL 35812

NASA MSFC
Attn: J. R. Redus
Code EP51
Huntsville, AL 35812

NASA MSFC
Attn: L. W. Jones
Code EP53
Huntsville, AL 35812

NASA MSFC
Attn: J. M. Cramer
Code EP53
Huntsville, AL 35812

NASA MSFC
Attn: J. E. Clark
Code ER21
Huntsville, AL 35812

NASA Goddard Space Flight
Center
Greenbelt, MD 20771
Attn: Library

NASA KSC
KSC, FL 32899
Attn: Library

NASA Johnson Space Center
Houston, TX 77001
Attn: Library

NASA Johnson Space Center
Attn: C. A. Vaughan/EP
Houston, TX 77001

NASA Johnson Space Center
Attn: R.J. Taueber/EP11
Houston, TX 77001

NASA Johnson Space Center
Attn: W.C. Boyd/EP43
Houston, TX 77001

NASA Langley Research
Center
Langley Station
Hampton, VA 23665
Attn: Library

NASA Center for Aero Space
Information/P. O. Box 8757
B-W Int. Airport
Baltimore, MD 21240
Attn: Access.Dept.

Jet Prop. Laboratory
4800 Oak Grove Drive
Pasadena, CA 91103
Attn: Library

NASA WSTF
P. O. Drawer MM
Las Cruces, NM 88004
Attn: Kevin Farrah

NASA WSTF
P. O. Drawer MM
Attn: Joel Stoltzfus
Las Cruces, NM 88004

NASA WSTF
P. O. Drawer MM
Attn: Frank Benz
Las Cruces, NM 88004

Defense Doc. Center
Cameron Station/Building 5
5010 Duke Street
Alexandria, VA 22314
Attn: TISIA

Def. Advanced Research
Projects Agency
1400 Wilson Blvd.
Washington, D.C. 22209
Attn: Library

Aeronautical Sys.Div
WL/DOOP
Wright-Patterson AFB
Dayton, OH 45433-6503
Attn: Library

Air Force Phillips Lab
6510-TW/TSTL
Edwards AFB, CA 93523-6343

Air Force Phillips
Laboratory
Attn: AL/RKL/R. L. Wiswell
Edwards AFB, CA 93523-6343

Air Force Phillips
Laboratory
Edwards AFB, CA 93523-6343
Attn: AL/RKLB/M. Connally

Air Force Phillips
Laboratory
Edwards AFB, CA 93523-6343
Attn: AL/CR L. Meyer

Space Division
Los Angeles Air Force
Station, CA 90009
Attn: Library

U. S. Naval Weapons Center
China Lake, CA 93555
Attn: Library

Picatinny Arsenal
Dover, NJ 07801
Attn: Library

U. S. Naval Research
Laboratory
Washington, DC 20375-5000
Attn: Library

Marquardt Corporation
16555 Saticoy Street
Box 2013 South Annex
Van Nuys, CA 91409
Attn: Library

Martin-Marietta Corp.
P. O. Box 179
Denver, CO 80201
Attn: Library

McDonnell Douglas Space
Systems/Attn:Library
5301 Bolsa Avenue
Huntington Beach, CA 92647

P & W Aircraft Group
UTC/Attn: Library
P. O. Box 109600
West Palm Beach, FL 33410-9600

P & W Aircraft Group
UTC/Attn: J. R. Brown
M.S. 731-25
P. O. Box 109600
West Palm Beach, FL 33410-9600

Rocketdyne Division
Rockwell International
Attn: Library
6633 Canoga Avenue
Canoga Park, CA 91303

Rocketdyne Division
Rockwell International
Attn: R. P. Pauckert
6633 Canoga Avenue
Canoga Park, CA 91303

Rocketdyne Division
Rockwell International
Attn: T. J. Harmon
6633 Canoga Avenue
Canoga Park, CA 91303

Space Division
A Div. of Rockwell Int.
Attn: Library
12214 Lakewood Blvd.
Downey, CA 90241

Rocket Research Corp.
Willow Rd.at 116th St.
Redmond, WA 98052
Attn: Library

Boeing Aerospace Co.
P. O. Box 3999
Seattle, WA 98124
Attn: Library

Johns Hopkins Univ.
Applied Physics Lab
John Hopkins Road
Laurel, MD 20810
Attn: Library

Curtiss-Wright Corp.
One Passaic St.
Woodridge, NJ 07075
Attn: Library

GD/Convair
P. O. Box 80847
San Diego, CA 92138
Attn: Library

General Electric Co.
Valley Forge SC
P. O. Box 8555
Philadelphia, PA 19101
Attn: Library

Grumman Aerospace
Corporation
Bethpage, NY 11714
Attn: Library

Hughes Aircraft Company
Space & Comm. Group
Attn: Library
P. O. Box 92919
Los Angeles, CA 90009

Lockheed Missiles & Space
Company
P. O. Box 504
Sunnyvale, CA 94087
Attn: Library

U. S. Army Missile
Command/RSIC
Attn: Document Section
Redstone Arsenal, AL 35808

U. S. Naval Air Station
Point Mugu, CA 93041
Attn: Tech Library

Aerospace Corporation
2350 E. El Segundo Blvd.
Los Angeles, CA 90045
Attn: Library

Garrett Turbine Engine Co.
402 South 36th Street
Phoenix, AZ 85034
Attn: Library

Aerojet Propulsion Div.
P. O. Box 13222
Sacramento, CA 95813-6000
Attn: Library

Aerojet Propulsion Div.
P. O. Box 13222
Attn: R. Diepenbrock
Sacramento, CA 95813-6000

Aerojet Propulsion Div.
P. O. Box 13222
Attn: B. Reimer
Sacramento, CA 95813-6000

Aerojet Propulsion Div.
P. O. Box 13222
Attn: L. Schoenman
Sacramento, CA 95813-6000

Aerojet Propulsion Div.
P. O. Box 13222
Attn: R. LaBotz
Sacramento, CA 95813-6000

Aerojet Propulsion Div.
P. O. Box 13222
Attn: F. Viteri
Sacramento, CA 95813-6000

Aerojet Propulsion Div.
P. O. Box 13222
Attn: A. Martinson
Sacramento, CA 95813-6000

Aerojet Propulsion Div.
P. O. Box 13222
Attn: P. Buckmann
Sacramento, CA 95813-6000

Aerojet Propulsion Div.
P. O. Box 13222
Attn: L. Bedrosyan
Sacramento, CA 95813-6000

Avco Systems Division
201 Lowell St.
Wilmington, MA 01887
Attn: Library

Bell Aerospace Textron
Box 1
Buffalo, NY 14240
Attn: Library

Sundstrand Avia. Mech.
2421 Eleventh Street
Rockford, IL 61101
Attn: Library

TRW Systems Group
1 Space Park
Redondo Beach, CA 90278
Attn: Library

Vought Corporation
3811 Van Dyke Avenue
Sterling Heights, MI
48077
Attn: Library

AiResearch L A Division
Attn: Alston Gu
Allied Signal Aero Co.
2525 West 190th Street
Torrance, CA 90509

MTI
Research & Development Div.
Attn: Wilbur Shapiro
968 Albany-Shaker Rd.
Latham, NY 12110

CPIA
JHU/Attn: Librarian
10630 Little Patuxent Pkwy.
Suite 202
Columbia, MD 21044-3200

Rocketdyne Division
Rockwell International Corporation
6633 Canoga Avenue
Canoga Park, California 91303

Telex: 698478
ROCKETDYN CNPK



Rockwell
International

NASA CR189055
RI/RD90-214

Orbital Transfer Rocket Engine Technology Program

Contract No. NAS3-23773

Soft Wear Ring Seal Technology - Task B.5

Final Report

14 February 1992

Prepared By

Brian Lariviere
Member of Technical Staff

Approved By

R. F. Sutton
Manager
Advanced Rotating
Machinery Projects

R. P. Pauckert
Project Manager
Cryogenic Upper Stage
Engines

TABLE OF CONTENTS

FORWARD	iii
LIST OF FIGURES	iv
LIST OF TABLES	vi
INTRODUCTION	1
SUMMARY	5
TECHNICAL DISCUSSION	8
Technology Assessment and Requirements	8
Candidate Material Selection	9
Soft Seal Tests and Results	16
Oxygen Compatibility Tests	16
Autogenous Ignition and Promoted Ignition Tests	17
Tester Description	17
Autogenous Ignition Test Results	17
Promoted Ignition Test Results	20
LOX Impact Tests	23
Tester Description	23
LOX Impact Test Results	25
Low Speed Friction and Wear Tests	29
Tester Description	29
Test Plan	39
Test Facility Configuration	43
Instrumentation and Redline Limits	49
Low Speed Test Results	49
Soft Seal Data Correlation	73
Frictional Heating Theory	73
Heat Inputs	73
Heat Dissipation Mechanisms	76
Conduction	76
Convection	76
Radiation	78
Mechanical	78
Chemical	79

TABLE OF CONTENTS (cont'd)

Frictional Heating Model Description	79
Frictional Heating Model Results	81
Kel-F - WS03C	81
Vespel SP211 - WS30F	84
Vespel SP211 - WS31	84
Vespel SP211 - WS04C	89
Seal Specimen Wear Description	95
Seal Specimen Wear Results	96
Kel-F Wear Analysis	96
Vespel SP211 Wear Analysis	101
Polybon M Wear Analysis	107
CONCLUSIONS	108
REFERENCES	111
APPENDIX A:Test WS31 Failure Investigation Report by White Sands Test Facility .	112

FORWARD

The efforts presented herein were conducted from May 1985 to November 1990 by personnel from Engineering functional units at Rocketdyne, a division of Rockwell International, under the Orbit Transfer Rocket Engine Technology contract, NAS3-23773-B.5. The program was monitored by Messrs. D. Scheer, G. P. Richter, and J. A. Hemminger of the NASA-Lewis Research Center. At Rocketdyne, Messrs. R. P. Pauckert, T.J. Harmon, and B. W. Lariviere were responsible for the overall program direction and implementation. Autogenous ignition, promoted ignition, and low speed friction and wear tests were conducted under the supervision of F. Benz and J. Stoltzfus of NASA-JSC White Sands Test Facility, and J. Homa of LEMSCO.

Important contributions to this program and the preparation of this report were made by the following Rocketdyne personnel:

Advanced Rotating Machinery Projects

R.F. Sutton
A. N. Little
T. B. Irvin

Materials Engineering and Technology

A. R. Brown
C. L. Swingler

Aerothermodynamics/Heat Transfer

B. R. Hemmings
P. Rutherford

LIST OF FIGURES

FIGURE	DESCRIPTION	PAGE
1.	Mark49-F Turbopump Cross-Section with Potential Soft Seals	3
2.	Mark49-O Turbopump Cross-Section with Potential Soft Seals	4
3.	Promoted Ignition Tester	18
4.	Post Auto Ignition Test - Vespel SP211 Sample	19
5.	Post Auto Ignition Test - Polybon M Sample	21
6.	Post Auto Ignition Test - Torlon 4301 Sample	22
7.	LOX Impact Test Chamber	24
8.	Photograph of the LOX Impact Test Tower	26
9.	LOX Impact Test Facility Schematic	27
10.	High Pressure O ₂ Impact Tester Housing	28
11.	WSTF Rubbing Cylinder Frictional Heating Tester	31
12.	Low Speed Friction and Wear Tester	32
13.	Soft Seal (Vespel SP211) Mounted in Seal Retainer	34
14.	Illustration of Soft Seal Specimen Configuration	36
15.	Photograph of Low Speed Soft Seal Specimens	37
16.	Photograph of Soft Seal in High Velocity Ratio Diffusing Crossover Inlet	38
17.	Low Speed Friction and Wear Tester Internal Flow Paths	40
18.	Low Speed Tester Rotor Contact Tooth Configurations	41
19.	Photograph of Original Low Speed Test Rotors	42
20.	Typical PV Profile of a Static Friction Test	44
21.	Typical PV Profile of a Running Friction Test	45
22.	Illustration of the Low Speed Friction and Wear Tester	46
23.	Photograph of Low Speed Friction and Wear Tester installed in Facility	47
24.	Low Speed Friction and Wear Tester LOX Facility Schematic	48
25.	Low Speed Friction and Wear Instrumentation Schematic	51
26.	Test WS30F: Temperature Profiles within the Seal	54
27.	Test WS31: Load, Speed, Torque, and Incursion Profiles	55
28.	Test WS31: Temperature Profiles within the Seal	56
29.	Test WS31: Post Test Rotor Photograph	58
30.	Photograph of Re-Designed Rotors	59
31.	Test WS01C: Axial Load vs. Time	62
32.	Test WS03C: Photograph of Wear Debris in Test Chamber	63

LIST OF FIGURES (continued)

FIGURE	DESCRIPTION	PAGE
33.	Test WS03C: Photograph of Wear Debris around Test Shaft	64
34.	Test WS03C: Incursion Profile	65
35.	Test WS04C: Incursion Profile	67
36.	Test WS04C Seal Temperature Distribution	68
37.	Test WS04C: Photograph of Rotor Face with Heat Effected Areas	69
38.	Test WS04C: Measured Shaft Axial Load	70
39.	Test WS04C: Photograph of Test Rotor Failure	71
40a.	Thermal Conductivity of Ni Based Alloys vs. Temperature	75
40b.	Thermal Conductivity Comparison of a Thermoset Resin and Ni Based Alloy	75
41.	Frictional Heating Model Finite Element Model	80
42.	Test WS30F: TC-702 Data vs Model Comparison	85
43.	Test WS30F: TC-703 Data vs Model Comparison	86
44.	Test WS30F: TC-708 Data vs Model Comparison	87
45.	Test WS30F: Data vs Model Composite Comparison	88
46.	Test WS31: Data vs Model Composite Comparison	90
47.	Test WS04C: Data vs Model Composite Comparison	91
48.	Test WS03C: Temperature Contour Plot	92
49.	Test WS30F: Temperature Contour Plot	93
50.	Test WS04C: Temperature Contour Plot	94
51.	Typical Wear Track Measured using Profilometry	97
52.	Test WS03C: Kel-F Worn Seal Specimen	100
53.	Specific Wear Rate vs. Contact PV for Vespel SP211	102
54.	Test WS04C: Test Rotor showing Surface Oxidiation	103
55.	Test WS04C: Test Rotor showing Material Transfer	104
56.	Test WS04C: Photograph of Vespel SP211 Wear Track (Close Up)	105
57.	Test WS04C: Vespel SP211 worn Seal Specimen	106

LIST OF TABLES

TABLE	DESCRIPTION	PAGE
1.	Desired Soft Seal Material Properties	10
2.	Material Properties Test Results	11
3.	Selected Candidate Soft Seal Materials	15
4.	Identified Soft Seal and Rotor Combinations	15
5.	Promoted Ignition Test Results	24
6.	LOX Impact Test Results	30
7.	Low Speed Friction and Wear Tester Parts List	34
8.	Low Speed Friction and Wear Test Instrumentation and Redline List	51
9.	Low Speed Friction and Wear Test History in LOX	53
10.	Selected Running Friction Tests Reduced Data	73
11.	Frictional Heating Model Inputs	83
12.	Frictional Heating Model Tabular Results	84
13.	Low Speed Tests Seal Wear Summary	98
14.	Low Speed Tests - Kel-F Seal Wear Summary	99

INTRODUCTION

High specific impulse liquid rocket engines require high speed, high efficiency cryogenic turbopumps to deliver the propellants at the required pressures and flows. As is the case with the Orbital Transfer Vehicle Engine (OTVE) concepts, performance parameters, such as, engine thrust to weight ratio and specific impulse, are at a premium, which requires the turbopumps to push the state-of-the art. Some mission profiles indicate the need for manned operations, which imposes stringent reliability standards as well. Similar to the Space Shuttle Main Engine (SSME) turbopumps, the OTVE turbopumps must provide high performance with high reliability.

Turbopump performance, defined by its efficiency, is greatly effected by the amount of propellant that flows around the pumping elements. Although detrimental to the overall efficiency of the pump, this flow can be used for other functions, such as bearing coolant, turbine housing coolant, and rotor axial thrust control. However, it is generally best to minimize these flows to improve the turbopump performance. For example, reduced inducer tip clearances improves suction performance capability and thereby reduces the Net Positive Suction Pressure (NPSP) or pump inlet pressure requirements. Potentially, reduced inlet pressure requirements can be translated into thinner tank walls, lower tank weights, and consequently, lower vehicle weights.

High efficiencies for small high speed turbopumps are complicated by the fact that annular seal clearances do not scale with turbopump size due to current manufacturing capabilities and assembly tolerances. Seals made from soft, non-metallic materials were identified as a means of improving the efficiency of these turbopumps by allowing the rotor to wear into the seal material during operation, essentially creating its own unique and minimum clearance. The magnitude of the seal clearance would be determined by the radial shaft motion driven by hydrodynamic radial loads and inherent shaft unbalance. In super-synchronous machines, the clearance could be effected by transitions through the rotor natural frequencies, where rotor displacements may be at their greatest.

Historically, Rocketdyne has benefitted from the use of Kel-F, a fluoropolymer, for shrouded inducer seals and impeller wear rings in the Mark 3, Mark 4, Mark 10, and Mark 15 LOX turbopumps. More recently, Kel-F was used in the SSME High Pressure Fuel Turbopump (HPFTP) and High Pressure Oxidizer Turbopump (HPOTP) to improve performance and reliability. Further demonstration of this technique came from the Mark49-F turbopump which utilized Kel-F in both the impeller front wear ring labyrinth seal and the pump interstage seal locations. The

assembled clearances in the Mark49-F, however, were greater than the expected radial deflections of the rotor, so contact was not anticipated, and the full performance benefits of the soft seal design were not achieved.

Using Kel-F as a baseline material for comparison, the goal of this program was to broaden the use of rubbing soft seals by demonstrating new soft seal materials for both liquid oxygen (LOX) and liquid hydrogen turbopump applications. Particular attention was placed on the potential applications identified for the high performance turbopumps in advanced expander cycle rocket engines like the OTVE. Figures 1 and 2 show the potential locations for minimum clearance soft seals within the Mark 49-F liquid hydrogen and the Mark 49-O LOX turbopumps, respectively.

MK49-F Liquid Hydrogen Turbopump with Potential Soft Seal Applications

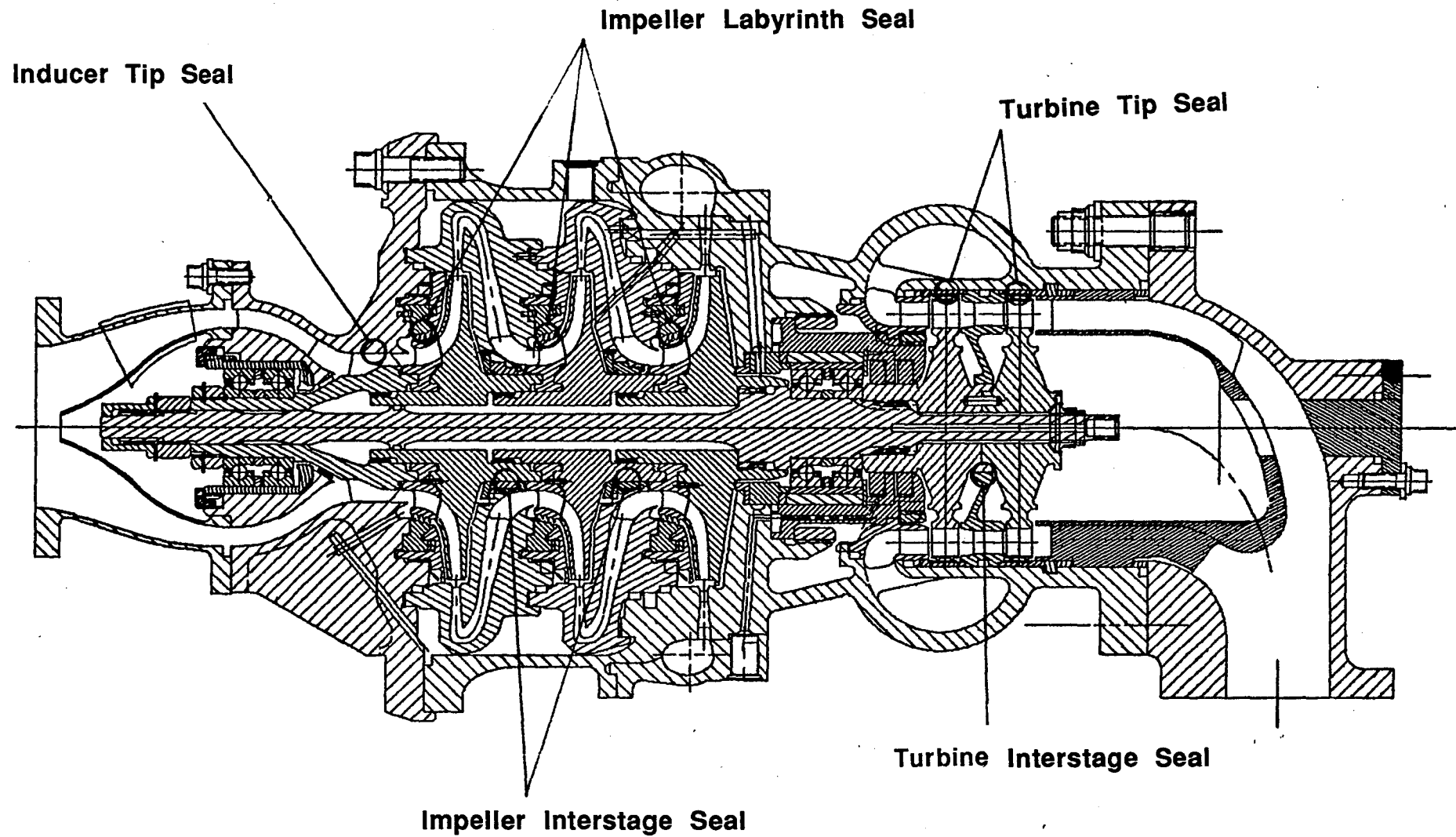


Figure 1

MK49-O Liquid Oxygen Turbopump with Potential Soft Seal Applications

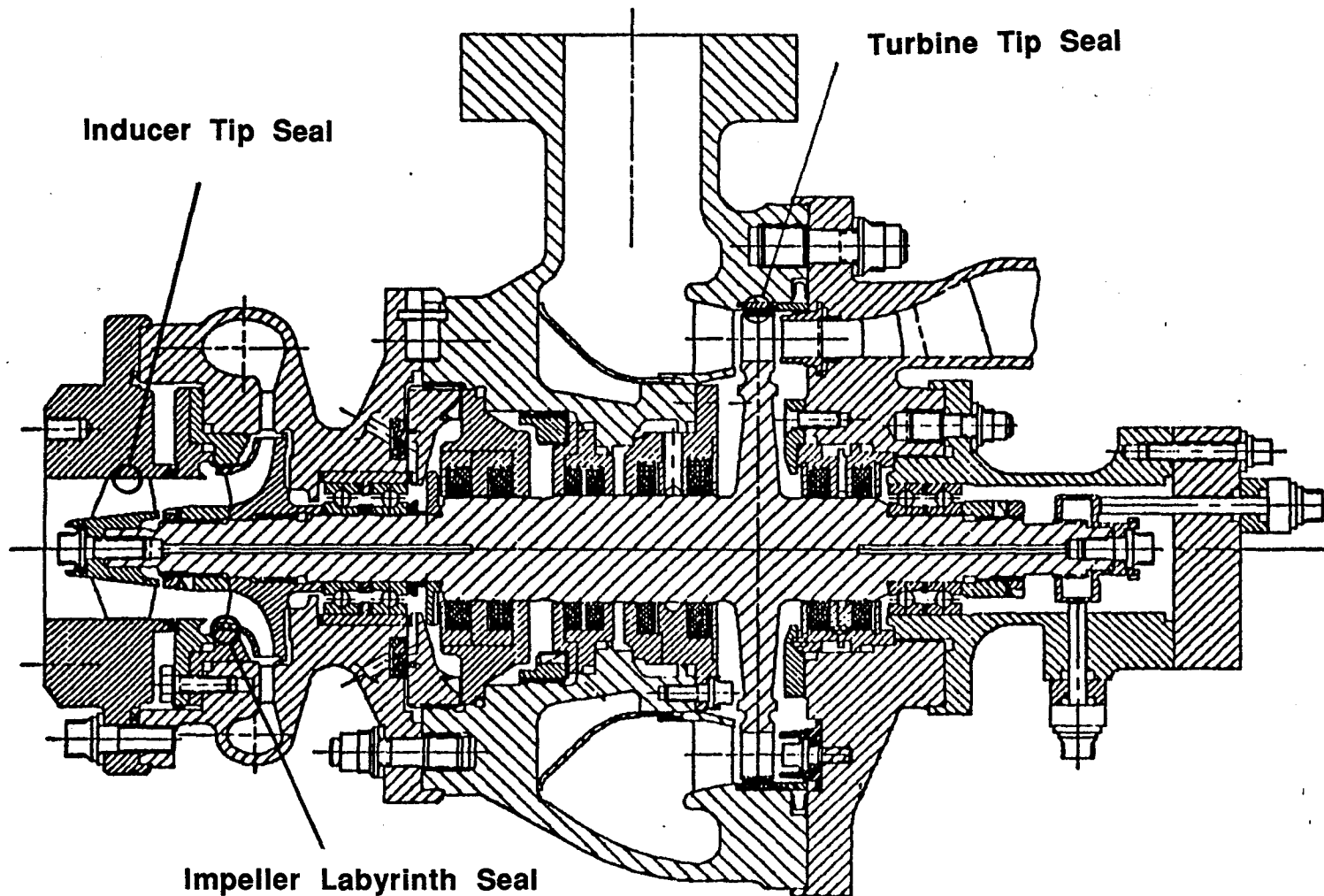


Figure 2

SUMMARY

The Soft Wear Ring Seal Development Program provided a systematic and comprehensive technical approach that explored new polymeric materials for cryogenic turbopump seals. The Soft Wear Ring Seal Technology program was funded under the Orbital Transfer Rocket Engine (OTRE) contract, NAS3-23773, by the NASA-Lewis Research Center. Divided into two task orders, NAS3-23773-B.3 and NAS3-23773-B.5, the project plan included a total of five technical subtasks and one reporting subtask. The Task B.3 efforts were performed from 11 May 1984 to 11 February 1985, and included:

Subtask 1: Technology Assessment and Requirements Definition

Subtask 2: Material Selection, Design, and Test Plans.

Based on the operational requirements passed down from the OTVE systems, the turbopump dynamic seal environment required that the soft seal materials maintain certain mechanical, thermal, and chemical characteristics to survive. Initial candidate soft seal materials and their material properties were summarized from tests conducted during Task B.3. Based on the results of these tests, a down-selection was conducted, isolating those materials with superior properties in the various turbopump seal applications that had been identified. These selected candidate seal materials included Vespel SP211, Polybon MT747, and Torlon 4301, while Kel-F was used as the baseline material for comparison.

A soft seal Energy Dissipation Factor (EDF) model was formulated which rated these new seal materials based on their mechanical and thermal properties, the particular seal location, and the particular fluid medium. Task B.3 was completed when the soft seal test plan and the low speed and high speed friction and wear test rigs were designed. A final report was submitted on 15 May 1985 (1).

Upon completion of the technical effort of Task B.3, the plans for Task B.5 were formalized. The subtasks performed during Task B.5 included:

Subtask 3: Hardware Fabrication

Subtask 4: Testing

Subtask 5: Data Correlation.

Due to the sensitivity of LOX environments to heat generation, the test program focused on materials that were identified for a liquid oxygen environment. The test program was to establish the basic chemical compatibility and mechanical survivability attributes of the seal materials. To fully evaluate these candidate materials, autogenous ignition tests, promoted ignition tests, LOX impact tests and low speed friction and wear tests were conducted. Additional tests were planned to evaluate liquid hydrogen turbopump and gaseous hydrogen expander cycle turbine configurations, however they were only partially completed due to test hardware malfunctions.

The LOX compatibility tests series, including the auto-ignition, promoted ignition, and LOX impact tests, identified Kel-F, Vespel SP211, and Polybon MT-747 as demonstrating sufficient resistance to reaction. Torlon 4301 showed more reactivity during the LOX impact tests at 2000 psig, reaching only the 4 kg-m level, while all the other materials achieved at least the 8 kg-m level. Torlon 4301's poorer performance in these tests were grounds for eliminating testing with this material in the low speed friction and wear tester.

An existing frictional heating tester was modified and used to conduct the low speed friction and wear tests at the White Sands Test Facility (WSTF). Two types of friction and wear tests, static friction and running friction, were conducted to simulate the characteristics of the different seal operation approaches. A total of 28 tests were conducted at PV products (normal contact pressure times the sliding velocity) ranging from 4,000 to 21,000 psi-ft/sec. These low speed tests were used as a demonstration for the new seal materials as well as a concept verification. Material wear rate, debris size, and frictional heat management of the seal were of particular interest. High speed tests were planned as a final verification of the soft seal concept, but these efforts were not pursued.

To better correlate the interactions at the rubbing surface from the low speed test data, a 2-D axisymmetric frictional heating model was constructed. Temperature distributions measured within the seal specimen were compared with the output of the model. By adjusting the frictional heat rate input in the model, the seal temperature profiles were matched. This model was used to help isolate the energy dissipation mechanisms consistent with a rubbing contact.

Wear track depths were measured in the seal specimens, and the wear rate correlated with the surface temperatures predicted by the frictional heating model. Specific wear rates were also calculated from the wear track data and were compared with the literature. The specific wear coefficients calculated from the low speed friction and wear tests were an order of magnitude

greater than the literature, possibly due to the higher sliding velocities (four orders of magnitude greater) and highly oxidizing environment.

In general, the data generated by this program helped strengthen the understanding of the rubbing environment within a stationary polymeric seal ring. Due to the unique differences between the polymeric materials used in this program, interesting and varied heat generation and dissipation mechanisms were witnessed. Kel-F produced higher wear and essentially no internal temperature rise, while Vespel SP211 produced low wear and higher internal temperatures. The chemical complexity and differences between the polymers selected, increased the difficulty in predicting the specific operational (PV) limitations of these materials. Most importantly, the friction and wear test program demonstrated that an interplay existed between the thermal, mechanical, and chemical characteristics of the soft wear ring seal materials. However, a quantitative method could not be implemented to isolate the contributing mechanisms with the available data. This report documents the technical efforts of Task B.5, which were performed from March 1985 to November 1990.

TECHNICAL DISCUSSION

The Soft Wear Ring Seal Technology program was organized into a comprehensive analytic prediction and test verification program which focused on broadening the use of soft polymeric materials in turbopump dynamic seal applications. Task B.5 was the proving grounds for the candidate materials in liquid oxygen pump, liquid hydrogen pump, and gaseous hydrogen expander cycle turbine seal locations. Much of the analytical work and test plan preparation for this program was completed during Task B.3. To maintain program and report continuity, the important contributions from the Task B.3 activities will be summarized briefly before discussing in more depth the test program and data correlation completed during Task B.5.

TECHNOLOGY ASSESSMENT AND REQUIREMENTS DEFINITION

Operationally, the OTVE system will be designed for 20 hours service-free life, 10:1 throttling, multiple start, man-rated, and space-based maintenance and operations capabilities. This places great demands on the turbopumps, which require light weight, high performance, high reliability, and no maintenance. These requirements place strict constraints on the turbopump design and operation.

Pump performance improvements, including head, efficiency, and NPSH margin were predicted for soft seals within the Mk49-F and Mk49-O turbopumps using various Rocketdyne analytic codes. The results of these studies showed a significant improvement in head and efficiency in the impeller and interstage seal locations and increased suction performance for the inducer for both fuel and oxidizer turbopumps. Inducer efficiency and head, although improved, had a very small effect on the overall pump performance. The benefits of reduced required NPSH far outweighed the minor improvement in the overall pump head and efficiency (1).

In order to meet the stringent component and system reliability requirements, the turbopump seals must possess sufficient environment survivability characteristics. The dynamic seal environment in a high performance cryogenic turbopump is one of the most severe, combining high velocity fluid flow, mechanical impacts, and high velocity rubbing contact. Mechanical survivability was the key issue when defining requirements for the turbopump seal materials. If the seal withstood the environment, the performance benefits of the turbopump would be achieved. Therefore, understanding the seal environment was paramount in establishing the physical requirements of the seal material.

The design goal of the soft seal was to incorporate a small radial clearance, approximately line-to-line to 0.0005" in the chilled condition, just prior to start. As the rotor speed increased, the rotor would grow due to centrifugal effects, and the shaft would orbit due to shaft unbalance and radial loads created by the impeller. Prior to reaching the operating speed, the rotor would contact the seal face. Increased rotor deflections are also possible as the machine transitions through its critical speeds. The load carrying capability, contact load, and sliding velocity are the key components in determining the wear of the seal material.

The seal must also possess significant structural capabilities to be retained rigidly in its metallic housing. Large radial interference fits were required at assembly to maintain concentricity, thermal cycles, and load reaction at operation. Since most polymeric materials have significantly higher coefficients of thermal expansion than their metallic housings, high stresses are encountered within the part at assembly and at operation, requiring ductility at both room and cryogenic temperatures.

Most importantly, the seal materials must be compatible with the specific propellant application. Heat generated by the impact loading and rubbing contact of the seal and rotor interface intensifies the need for a compatible material selection, especially in an oxygen environment.

Table 1 describes, qualitatively, some of the desired properties that a soft seal material should possess to withstand the environment.

An Energy Dissipation Factor (EDF) model was developed which ranked the individual materials based on their mechanical and thermal properties, as well as the particular seal location, using a figure of merit approach. This computer code was developed as a method of comparing new materials against the experience of test materials. As an overall objective, this project was to establish a data base of soft seal materials properties based on the information gained from testing, with the plan of using these data to predict the performance of new materials as they became available. A logic diagram and supporting analysis for the EDF model can be found in Reference 1.

CANDIDATE MATERIAL SELECTION

Candidate soft seal materials were selected based on a survey of several areas of information. In Task B.3, a literature search was conducted to identify any current or past applications of nonmetallic materials used as dynamic seals. Non-metallics were chosen over metallic materials based on Rocketdyne's experience with copper, silver, and aluminum used as turbopump rotor

seal materials. Beyond this, manufacturer's recommendations and Rocketdyne experience led to the final selection of specific products. Original seal materials for this project were selected for their mechanical strength and toughness at cryogenic temperatures. Thermoset resins, such as the polyimides, were selected for their elevated temperature capabilities in addition to their cryogenic properties.

Table 1
Desired Soft Wear Ring Seal Properties

Desired Properties	Rationale
Propellant Compatibility	Minimizes Property Degradation
Thermal Coefficient of Expansion Compatibility with Housings	Minimizes Radial Fits
Tensile Strength at Ass'y & Operating Temperature	Maintain Radial Fits
Ductility/Toughness at Operating Temp	Withstand Impact Loading
Thermal Shock Insensitivity	Survive Thermal Stresses @ Chill
High Thermal Conductivity	Improves Heat Removal From Contact
High Frequency Viscoelastic Heating	Prevents Property Degradation
Low Coefficient of Dynamic Friction	Low Coefficient of Dynamic Friction
Wear Process Generates Fine Debris	Reduce opportunity for Down-stream Blockage
High Maximum Useable Temperature	More Potential Applications and Increased Rubbing Capability

These products, once selected, were tested at Rocketdyne for evaluation of material properties needed for data analysis of the seal environment. Many of the materials initially selected for this program were not commonly used for these applications or at cryogenic temperatures; consequently, very little published material properties data were available. During the Requirements Definition phase of Task B.3, material properties that influenced the seal performance in a rubbing or frictional heating environment were identified. Based on these studies, material properties tests at ambient and cryogenic temperatures were completed to develop the material properties database, as well as support future frictional heating analyses. Material strength, hardness, specific heat, thermal expansion, thermal conductivity, and specific gravity were determined using standardized testing processes. Table 2 presents the results of

Table 2

Material Properties Test Results

Material	Tensile Strength (psi)	Elongation (in/in.) (Values are at -320°F)	Modulus (psi)	Specific Gravity (75°F)	Specific Heat (BTU/lb - °F)	Shore D Hardness (75°F)	Thermal Conduct. (BTU in./hr ft ² °F)	Thermal Expansion (in/in.) from 70°F	Maximum Service Temperature (°F)
System 10 (Polathane)	18,000	0.040	410,000	1.07	0.447	40	1.28	-0.0250 (-410F)	400
Alasco 6928	20,000	0.042	525,000	1.26	0.393	40	1.20	-0.0190 (-410F)	400
Vespel SP211	10,000	0.022	565,000	1.55	0.255	70	3.38	-0.0070 (-320F)	750
Hexcel 3125	24,000	0.048	608,000	1.08	0.426	80	1.47	-0.0140 (-320F)	300
Hexcel 3124	24,000	0.046	651,000	1.19	0.444	75	1.40	-0.0130 (-320F)	300
Kel-F	17,000	0.030	850,000	2.15	0.215	70	1.00	-0.0090 (-320F)	350
Glass Reinforced Teflon (Armalon)	80,000	0.020	1,900,000	2.14	0.213	50	1.40	-0.0040 (-320F)	600
Torlon 4301	21,000	0.035	400,000	1.47	0.256	80	3.46	-0.0033 (-320F)	500
Torlon 4347	16,000	0.018	361,000	1.49	0.256	75	3.47	-0.0029 (-320F)	500
Torlon 4275	19,000	0.031	750,000	1.52	0.241	75	2.86	-0.0026 (-320F)	500
Crest 810	13,000	0.025	288,000	1.06	0.411	35	1.34	-0.0200 (-410F)	275
CPR 2116	10,000	0.034	333,000	1.26	0.415	20	1.48	-0.0160 (-410F)	400
Polybon MT747	6,000	0.017	125,000	1.51	0.243	80	6.52	-0.0049 (-320F)	600

Urapol 35

(Dropped from further testing: Could not be cured, processing and handling extremely difficult)

Urabond 835

(Dropped from further testing: Very low tear strength, cannot be cured in thick enough sections)

the material properties tests that were conducted. A more detailed description of the test methods and individual test results can be obtained from Reference 1.

A brief description of these materials, highlighting the properties thought to be uniquely beneficial for a soft seal material applications, is presented below.

Polathane XPE System 10

Polathane XPE System 10 was manufactured by Polaroid Corporation, Commercial Chemicals Department and was an ether based polyurethane material. The material was translucent amber in color and had very high tear strength and flex resistance. This material was a rubber-like polyurethane at room temperature, but was only slightly ductile in the cryogenic range.

Alasco 6928

This material was molded by Alasco Rubber and Plastic Company. This company was recommended by a representative of Mobay Chemical Corp., formulators of basic polyurethane systems. Alasco 6928 was a polyether based polyurethane that was opaque and was smokey white in appearance. This material also had high strength and elongation at ambient conditions, but was only slightly ductile at cryogenic temperatures.

Hexcel 3125

This polyurethane material was formulated by Hexcel Corporation and was a terminated methylene diphenyl diisocyanate monomer (MDI) system with a polyol catalyst. This material was translucent, black-purple in appearance and was quite hard at room temperature. Results showed that this material retained good elongation at cryogenic temperatures. Hexcel 3125 was an elastomeric casting system with higher strength and less elongation at ambient conditions than the polyether based polyurethanes.

Hexcel 3124

This polyurethane material was also formulated by Hexcel Corp. and was a terminated toluene diisocyanate (TDI) system with a polyol catalyst. This material was not as hard as the 3125, but is a higher density material. This material was an opaque amber color in appearance and was ductile at room temperature. Hexcel 3124 retained good elongation at cryogenic temperatures and had high strength.

Crest 810

Crest 810 was a toluene diisocyanate monomer (TDI) polyurethane catalyzed by an amine paste catalyst. It was specially formulated for cryogenic applications by Crest Products Corp., primarily for adhesive applications. However, its high strength and elongation at low temperatures made it a potential dynamic seal material. At room temperature this material was also very ductile and rubber-like. It was opaque and bright yellow in appearance.

CPR 2116

Castethane CPR 2116 was a MDI/polyester based polyurethane system formulated by the CPR Division of Upjohn. This material was translucent, yellow in color and was soft with high elongation at room temperature. It retained sufficient elongation at cryogenic temperature to have potential benefits as a soft seal material.

Vespel SP211

Vespel SP211 was a polyimide filled with Teflon and graphite formulated by DuPont. It was LOX compatible as tested to date on a batch-to-batch acceptance plan. (This material will have to out-perform the current test results, however, as it will be used in a more severe application as a soft seal.) This material had a low coefficient of friction and performed well in wear and abrasion tests. This material was capable of higher temperatures than other non-metallics and was selected for potential high as well as low temperature applications. The graphite filler helped increase the thermal conductivity and decrease the thermal expansion from the base polyimide which was desirable. It was hard and black in appearance.

Polybon MT-747

Polybon M was a polyimide filled with graphite and chopped carbon fiber fabricated by Tribon Bearing Company. It was usable in a similar temperature range as the Vespel material and may perform at least as well. Like Vespel SP211, the graphite filler increased the thermal conductivity significantly from the base polyimide. The LOX compatibility of this material was not known. Polybon M polyimide was hard and black in appearance.

Kel-F

Kel-F was the 3-M trade name for polychlorotrifluoroethylene. It was translucent white in color and retained some elongation at cryogenic temperature. It was inert to a liquid oxygen environment in previous testing. This material was used as the baseline for comparison, since it had already demonstrated satisfactory performance as a soft seal in the SSME turbopumps. Kel-F has also

been shown to melt under certain high frequency vibrations. This phenomena is called viscoelastic heating.

Glass Reinforced Teflon (Armalon)

Armalon was a glass fabric reinforced Teflon produced by American Durafilm. Teflon on its own was not a good soft seal material due to its creep behavior even at cryogenic temperature. Glass-reinforced Teflon may have corrected for this problem. It was light brown in appearance and was commonly available in tubes. LOX compatibility was required on a batch to batch basis.

Torlon

Torlon is the Amoco trade name for a series of filled and unfilled polyamide-imides. This material contained a hybrid nylon and polyimide chemical structure. The bearing grades were chosen due to their low coefficients of friction and good wear and abrasion characteristics. Torlon 4301 contained 12% graphite powder and 3% Teflon. Torlon 4275 contained 20% graphite powder and 3% Teflon. Torlon 4347 contained 12% graphite powder and 8% Teflon. These materials retained some elongation at cryogenic temperatures and may prove to be LOX compatible. These materials could have been used for applications up to 700°F for short durations. These materials were all dark green to black in appearance and were opaque.

Based on the results of the material properties tests, a final material selection was made to identify the materials which showed superior mechanical and thermal properties. The results of the final material selections are shown in Table 3. From the fluoroplastic category, Kel-F was selected because wear information and oxygen compatibility records existed from actual liquid oxygen and hydrogen turbopump applications. This experience made Kel-F the "baseline" material and was used for direct comparison with turbopump disassembly records and for relative comparisons with the other seal materials. In addition, the low shear strength of the teflon and the potential glass wear particles of the glass reinforced teflon were considerations which promoted the selection of Kel-F.

Torlon 4301 was selected over the other Torlon products (polyamide-imides) due to its higher cryogenic tensile strength and elongation. Both the polyimide materials, Vespel SP211 and Polybon MT-747 were selected because of their relatively high thermal conductivity and maximum temperature capabilities. Of the polyurethane materials, the Hexcel 3124 and 3125 were selected because of their superior castability, cryogenic strength and elongation.

The materials selected were then assigned potential turbopump seal application, and the potential rotor counterface material was identified. Table 4 illustrates the rotor and seal combinations that were selected. This table was used to help construct the Task B.5 test program.

Table 3
Selected Candidate Soft Seal Materials

Category	Materials Initially Selected	Materials Selected for Testing
Fluoroplastics	Kel-F Glass Filled Teflon	Kel-F
Polyamide-imides	Torlon 4301 Torlon 4327 Torlon 4275	Torlon 4301
Polyimides	Vespel SP211 Polybon MT-747	Vespel SP211 Polybon MT-747
Polyurethanes	Hexcel 3124 Hexcel 3125 Crest 810 Alasco 6928 Polathane System 10 Castethane CPR 2116	Hexcel 3124 Hexcel 3125

Table 4
Soft Seal Material and Rotor Combinations

Fluid	Typical Rotor Mat'ls	Soft Seal Materials	Turbopump Seal Application
LOX	K-Monel	Kel-F, Vespel SP211, Polybon M, & Torlon 4301	Inducer Tip
LOX	INCO 718	Kel-F, Vespel SP211, Polybon M & Torlon 4301	Imp Wear Ring & Interstage
LH ₂	INCO 718	Hexcel 3124 & Hexcel 3125	Inducer Tip
LH ₂	Titanium	Hexcel 3124 & Hexcel 3125	Imp Wear Ring & Interstage
GH ₂ 500°F	A-286	Vespel SP211 & Polybon M	Expander Turbine Tip/ Interstage

SOFT SEAL MATERIAL TESTS AND RESULTS

Soft wear ring seal applications in cryogenic turbopumps can provide increased performance and reliability benefits in both liquid hydrogen and liquid oxygen turbopumps. However, prior to using the soft seals in a more aggressive manner than previously demonstrated, the materials must be tested to verify their capability to survive the operating environment, as well as maintain chemical inertness. Since the LOX turbopump environment is far more sensitive to rubbing contact situations, the soft wear ring seal test program focused on these materials.

The materials selected for LOX turbopump service were initially put through a series of LOX compatibility tests to assess their thermal and mechanical sensitivity to the oxygen environment. Upon successful completion of the compatibility tests, the materials were placed in a low speed friction and wear tester that simulated low speed turbopump operations. Low speed friction and wear tests, only, were planned for candidate materials selected for liquid hydrogen pump and gaseous hydrogen-driven expander cycle engine turbine applications. The low speed friction and wear tests were designed as a verification of the soft seal materials in a rubbing environment only. Final demonstration was planned in high speed friction and wear tester, originally designed during Task B.3, that could simulate actual turbopump rotor tip speeds. The low speed tests originally planned in high pressure LOX, liquid hydrogen, and warm gaseous hydrogen were not completed, however, due to test hardware malfunctions. Hardware for these tests, including rotor specimens and seal specimens were fabricated. The description of the tests conducted, test hardware used, and test results are presented in the remainder of this section.

Oxygen Compatibility Tests

The oxygen compatibility tests were organized into a series of demonstration tests that determined oxygen environment sensitivity. Autogenous ignition and ignition promotion tests were used as a means of screening the candidate materials for oxygen compatibility as well as establish their characteristic behavior in an oxygen environment under severe heating. To ensure that the soft seal materials met established safety requirements for materials intended for oxygen service, LOX impact tests were conducted at atmospheric pressure and at an elevated pressure per NASA Handbook NHB 8060.1B. Recently, promoted ignition tests were proposed in the "C" revision of NASA Handbook NHB 8060.1 indicating its credibility as a compatibility assessment tool. Only materials that had been identified for potential applications within a LOX turbopump were subjected to these tests. As mentioned earlier these candidate materials were Kel-F, Vespel SP211, Polybon MT-747, and Torlon 4301. Upon completion of the oxygen compatibility

test series the results were reviewed and the materials showing adequate chemical compatibility were used in the low speed friction and wear tests.

Autogenous and Promoted Ignition Tests.

Tester Description. The autogenous ignition (auto-ignition) and promoted ignition tests were used to determine the reactivity, burn rate, and combustion characteristics of the candidate materials in an atmospheric pressure pure oxygen environment. Both the auto-ignition and promoted ignition tests were conducted using the promoted ignition tester located at the White Sands Test Facility (WSTF). The tester, as shown in Figure 3, consisted of a $7.4 \times 10^{-4} \text{ m}^3$ (45 in³) stainless steel test chamber rated for a working pressure of 10,000 psig and utilized a copper sleeve and copper baseplate for protection against burning. The test sample, in the form of a rod or cylinder, was held at the top of the sample support column and connected to the bottom of the sample heater feed through. The chamber utilized inlet and outlet ports which provided the capability to run both static and dynamic (flowing oxygen) tests, although only static tests were conducted. Chamber pressure and temperature, as well as sample temperature were measured during the tests. Three thermopiles mounted to the sight glass ports in the chamber all monitor the burning sample. The thermopiles, which measured the radiant heat, were used to determine the sample propagation rates. The test data was recorded on strip charts and stored digitally. The promoted ignition tests were also recorded on VHS formatted videotape.

Autogenous Ignition Test Results. The tests were conducted in compliance with the ASTM G-72 test procedures. The auto-ignition tests were conducted by slowly heating the test sample to a maximum temperature of 427°C (800°F) in an oxygen environment to determine if the specimen would combust or physically degrade. Five tests on each candidate soft seal materials Vespel SP211, Polybon M, Torlon 4301, and Kel-F, were conducted in a pure oxygen environment starting initially with atmospheric pressure in the test chamber. The sample was heated by passing current through the sample, which was grounded to the chamber.

Five each Vespel SP211 samples showed no reactions up to the 427°C (800°F) test point. The samples showed no signs of deformation or distortion. The sample holder showed no evidence of residue or reaction, as seen in the photograph in Figure 4. No pre-test samples were available for the photograph because all the specimens were tested. The physical condition of the pre-test and post-test samples appeared to be the same. For Vespel SP211, the calculated maximum temperature was 400°C (750°F). This maximum temperature was defined as the temperature at which the material degraded or deteriorated, as calculated by a thermal analyses and supported by discussions with the material supplier.

Promoted Ignition Tester

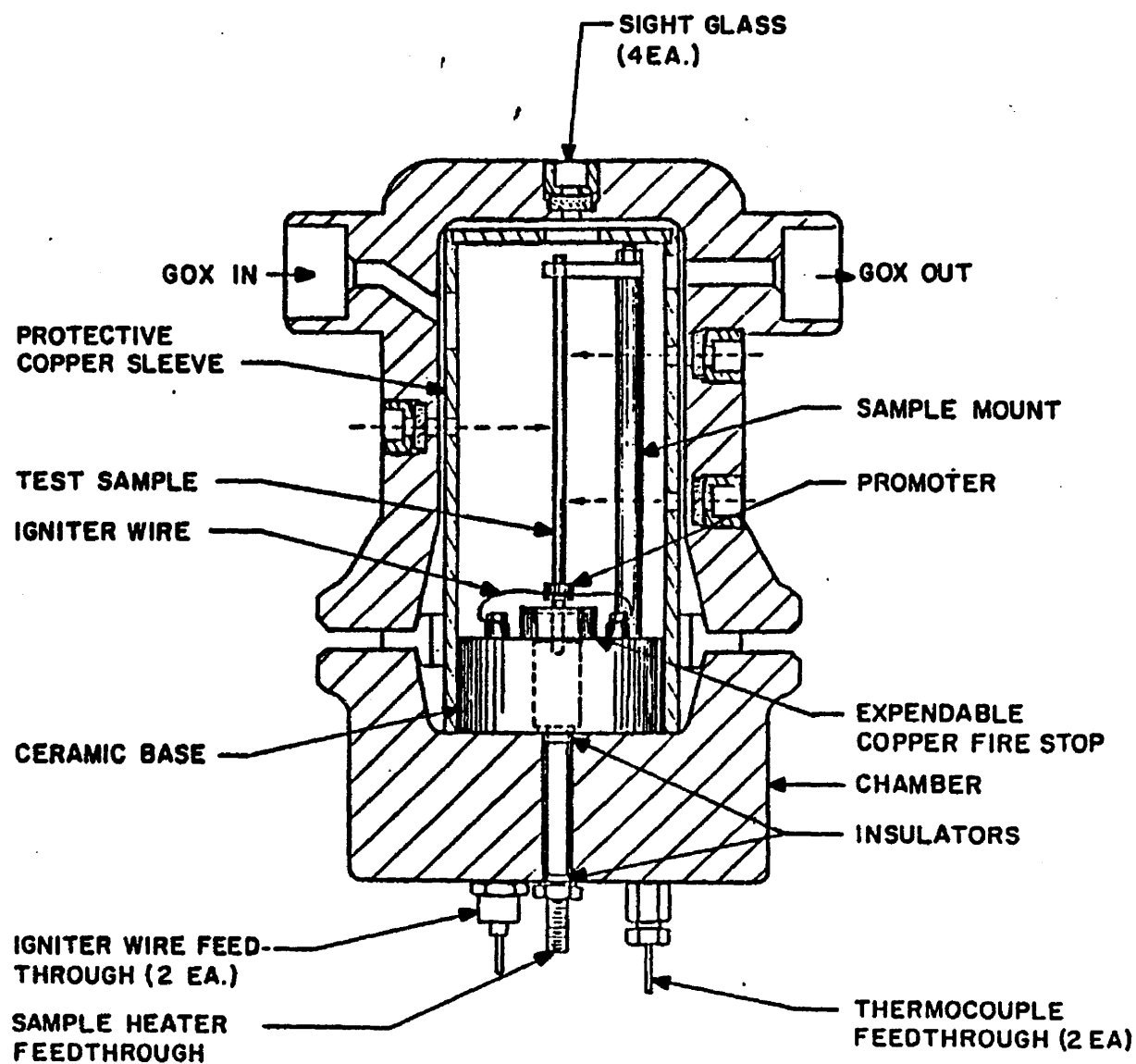


Figure 3

Auto-Ignition Test Vespel SP211 Sample

SAMPLE

*

SAMPLE
HOLDER

PRETEST

POSTTEST

VEPEL SP - 211
(Typical)

* Pretest sample not available



Figure 4

No reactions were evident on the five each Polybon M samples up to the 427°C (800°F) test limit. Post-test inspections found the specimens were elongated and slightly disfigured. The specimen holders were coated with a small amount of a brown residue indicating some decomposition or "charring", as seen in the photograph in Figure 5. The calculated maximum service temperature was 316°C (600°F).

Torlon 4301 was tested, and likewise, no reactions were detected up to the 800°F temperature limit. The test samples were deformed and swollen which was evidence of severe out gassing at the elevated temperatures. The sample holders were discolored by a small amount of black to brown colored residue, as seen in the photograph in Figure 6. The calculated maximum service temperature was 260°C (500°F).

Lastly, the Kel-F specimens (Lot #847) were tested, and like the other materials, no reactions were detected up to 427°C (800°F). However, the Kel-F specimens were totally sublimated during the test. No specimens were available for post-test inspections, but the sample holders were discolored a cloudy white. A white flaky residue was recovered from the sample holder. The calculated maximum service temperature of Kel-F was 177°C (350°F).

Promoted Ignition Test Results. The promoted ignition tests were initiated by heating a nichrome wire, which ignited the promoter and subsequently the test sample. The combustion characteristics of each sample were monitored and recorded by a video camera from the viewing sightglass of the tester. Test sample burn rates were calculated from the data and verified by the video playback.

This test was considered exceptionally severe for non-metallic materials such as the soft seal candidates due to their poor thermal conductivity and relatively low ignition temperatures. If the promoted ignition test were to be accepted and implemented as part of the NHB 8060.1 procedures, then many materials, such as Kel-F and Teflon, which have supported many aerospace applications, would not pass this stringent test.

As the results in Table 5 indicate, the candidate materials burned rapidly and completely in the test chamber. These results were expected, and should not lead to the conclusion that these materials were not acceptable for use in this application. With proper design and conservative system considerations, these materials can perform satisfactorily.

Auto-Ignition Test Polybon MT747 Sample

NASA-WSTF
0186-0049

SAMPLE

SAMPLE
HOLDER

PRETEST

POSTTEST

POLYBON M
(Typical)



Figure 5

**Auto-Ignition Test
Torlon 4301 Sample**

NASA-HSTF
0186-0048

SAMPLE



SAMPLE
HOLDER



PRETEST



POSTTEST



TORLON 4301
(Typical)

Figure 6

TABLE 5
Promoted Ignition Test Results

Material Specimen	Calculated Burn Rate	Burn Characteristics
Polybon MT747	0.078 In/sec	Burned outside then inward. Sparking witnessed.
Torlon 4301	0.102 In/sec	Burned outside then inward. Some sparking seen.
Vespel SP211	0.113 In/sec	Burned upward then outward.
Kel-F (Lot #847)	0.290 In/sec	Burned upward. Kel-F dripping witnessed.

Although Torlon 4301 and Polybon M displayed the slowest burn rates, undesirable sparking, possibly due to the breakdown of the polymer chains or by the graphite fillers, were observed. This type of reaction during combustion makes these materials less desirable than the Kel-F or Vespel specimens. The Kel-F specimen was consumed the fastest, nearly three times faster than the other specimens.

LOX Impact Tests.

Tester Description. The industry standard for demonstrating oxygen environment sensitivity is the LOX impact test as described in NASA Handbook NHB8060.1B. The NASA Handbook NHB8060.1B prescribed a simple mechanical impact or drop tower test to screen materials for oxygen compatibility. In this test, the material specimen, a flat test button, was placed in a pressurized oxygen chamber and a plummet was dropped, driving a striker pin into the specimen, as illustrated in Figure 7. Oxygen pressure, plummet weight, and tower height were all known variables. The reaction of the material from the imparted blow must be fully benign. Any observed difference in material surface texture, noises, obvious flashes, or color was reported as a reaction. Maximum allowable reactions were zero in twenty (20) consecutive trials, or one (1) in sixty (60) consecutive trials. For this program, the zero in twenty reactions was sufficient to demonstrate compatibility.

For non-metallic materials that are used in the Space Shuttle Main Engine LOX Turbopumps, such as glass reinforced Teflon, batch-to-batch testing is still required for each process lot to verify oxygen compatibility.

LOX IMPACT TEST CHAMBER

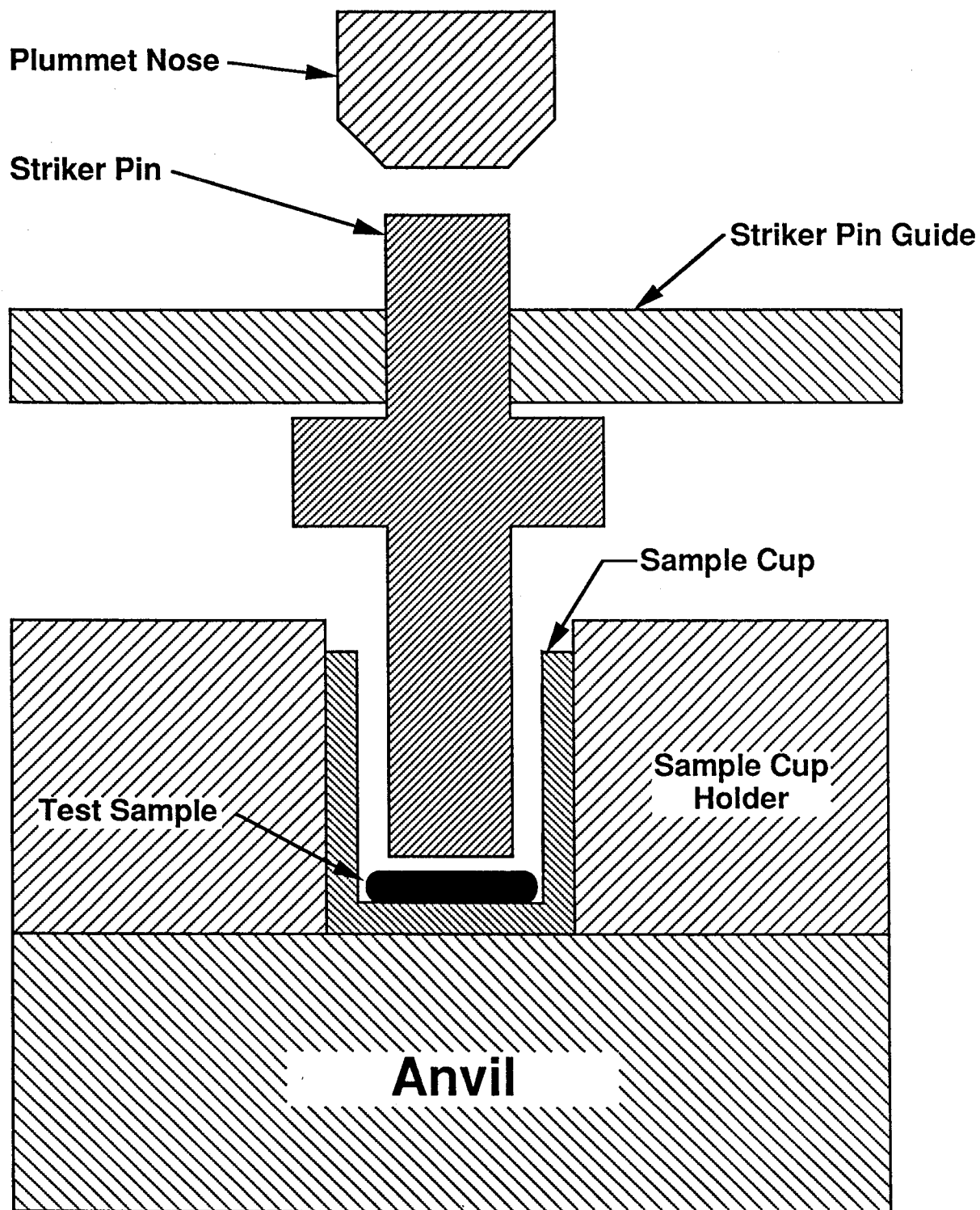


Figure 7

The LOX impact tester, located at the Rocketdyne facility, consisted of three major components: impact tower, pneumatic enclosure, and control console. The impact tower and pneumatic enclosure were housed in a remote test cell, as shown in Figure 8, while the console was located in the control center. The oxygen test system schematic showing the propellant feed and pressurization system is shown in Figure 9.

Low and high pressure test cavities, or impact cells, were designed to minimize the amount of oxygen in the sample cavity at the moment of impact. This feature minimized the possibility of damage to the impact test cell in the event of a positive reaction. Both the striker tip and the sample cup were removable to permit resurfacing of any affected areas between tests. The striker was balanced at the desired operating pressure by a diaphragm located on the striker shaft (Figure 10) which was supplied by an automatically regulated GN₂ system.

Additional control circuit logic was built into a graphic control panel to enhance convenience, reliability, repeatability, and safety. All high pressure operations were remotely conducted. A camera attached to a two channel, dual beam oscilloscope allows recording two parameters at the moment of impact: plummet velocity and system pressure. Sample temperature and impact cell pressure were monitored continuously during the tests.

LOX Impact Test Results. Two oxygen pressure levels, atmospheric and 2000 psia, were used to characterize the soft seal materials. Sufficient data were available which showed that Kel-F and Vespel SP211 had demonstrated 10kg-m compatibility at ambient pressure. These tests were felt to be repetitive, and were not conducted. No oxygen compatibility data were available for the Torlon 4301 and Polybon M, so these materials were tested at the atmospheric pressure condition. All four materials were tested at the 2000 psia pressure level. The tests were initially run at the 10 kg-m level (the product of the mass of the plummet times the height at which it was dropped). Should a reaction be witnessed, the 8 kg-m level was attempted. Subsequent reactions were cause for further reductions in the test level until the test material passed with zero reactions in twenty (20) trials. As the results indicate in Table 6, the Polybon M and Torlon 4301 seal materials passed the minimum requirements for oxygen compatibility at ambient pressure. This was expected for the Polybon M, which was chemically similar to the Vespel, while the Torlon 4301 results were encouraging.

LOX Impact Test Tower

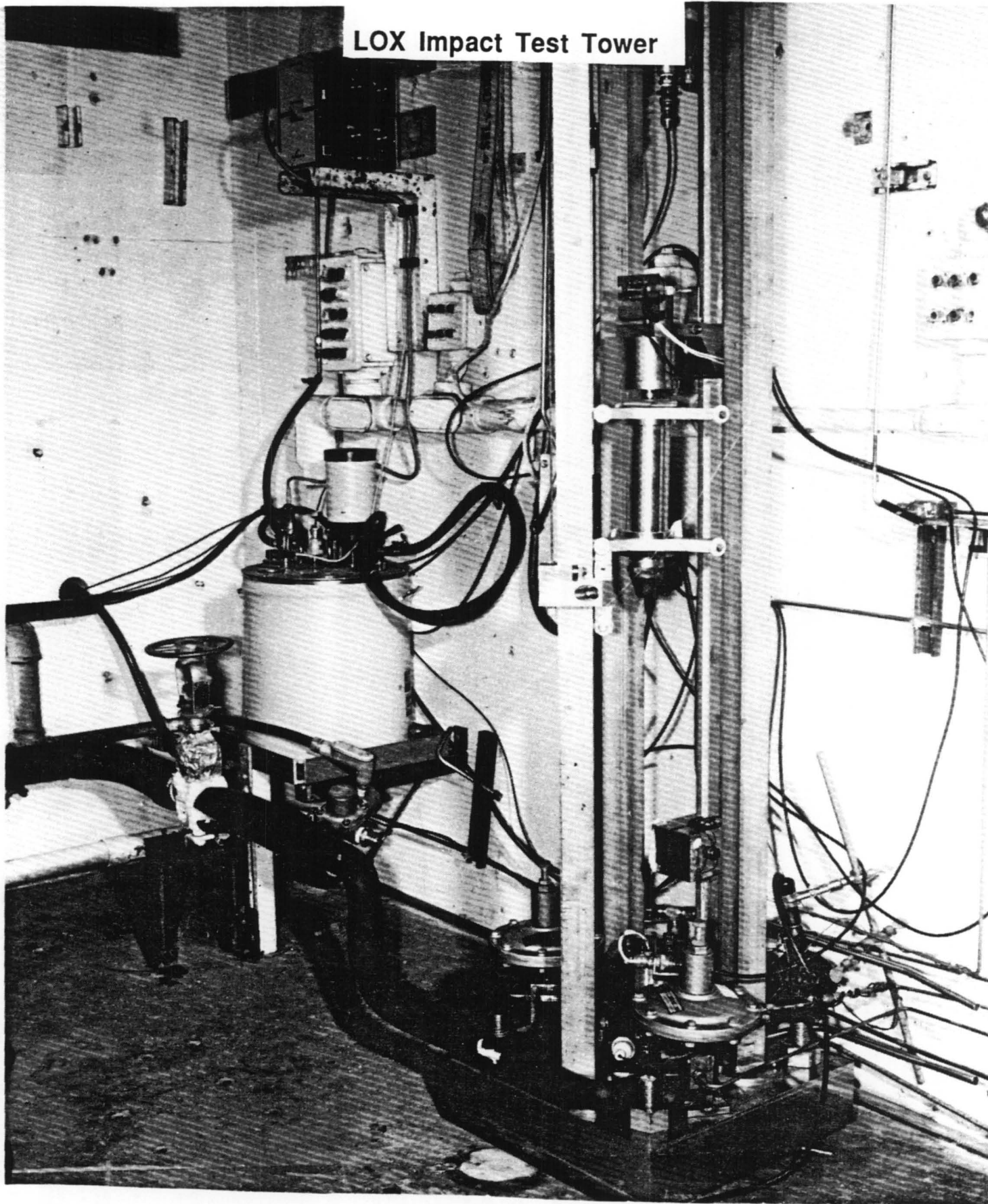


Figure 8

LOX Impact Test Facility Schematic

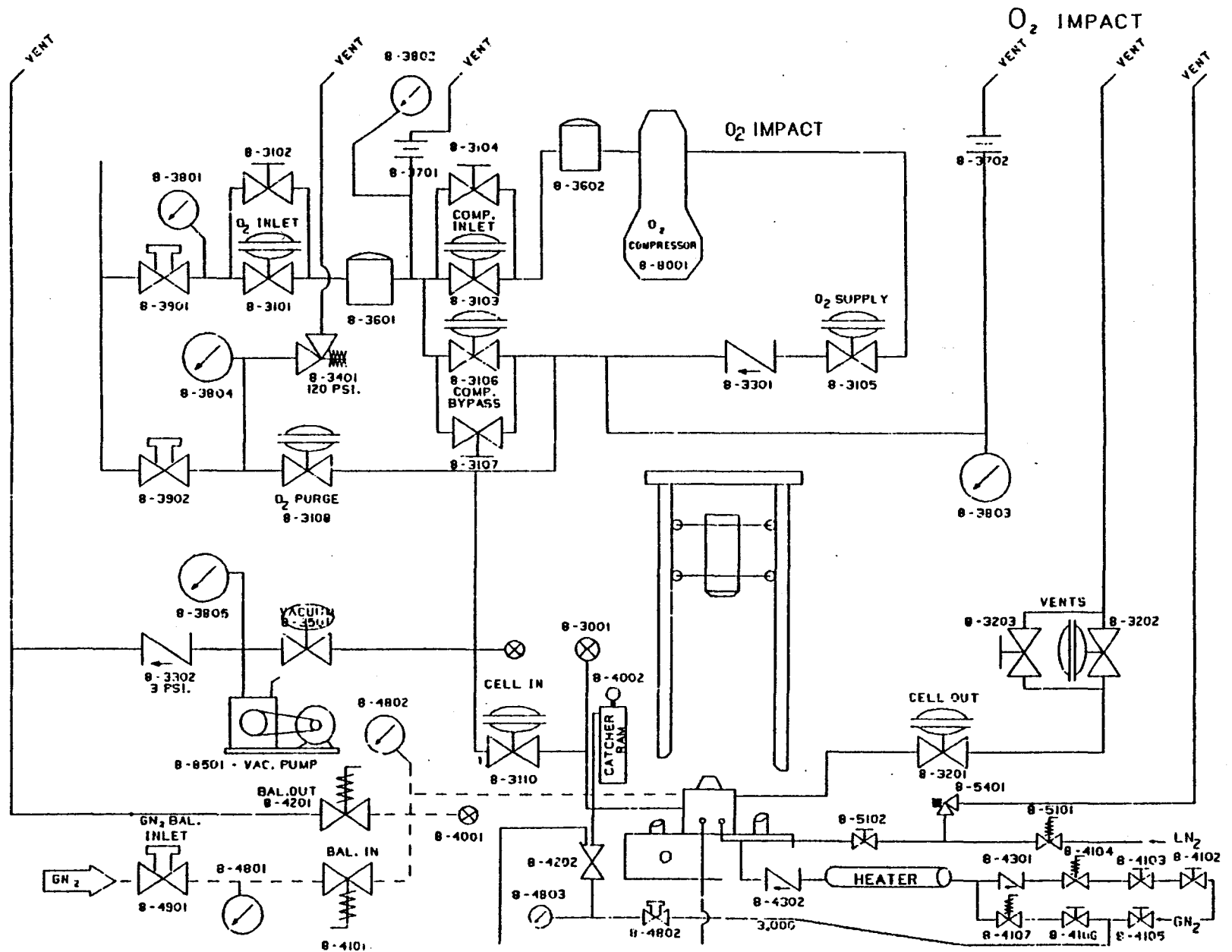


Figure 9

RI/RD90-214

High Pressure O₂ Impact Tester Housing

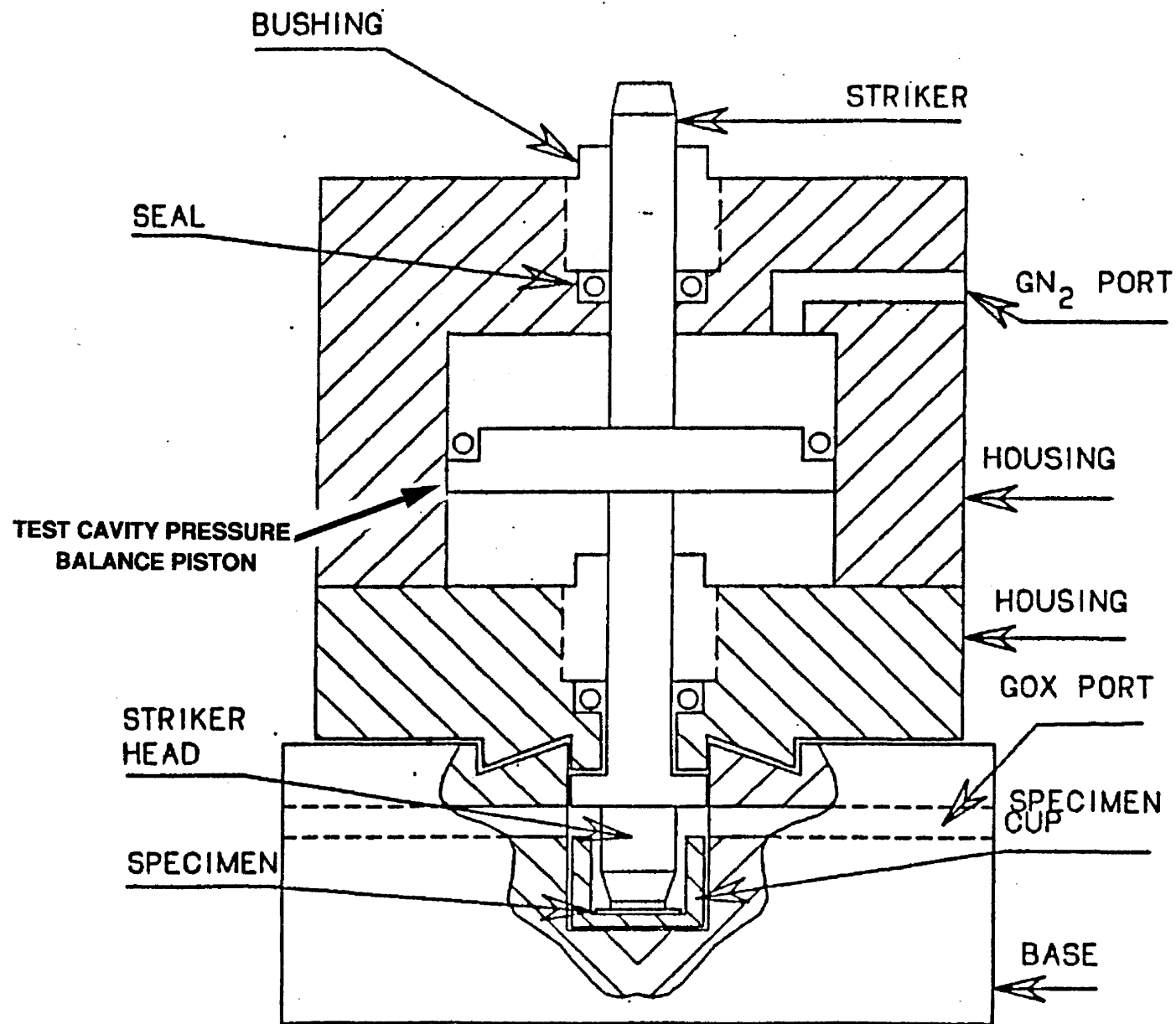


Figure 10

The results of the high pressure tests showed that Vespel SP211 was the most chemically compatible of the polymeric materials selected for this program demonstrating 10 kg-m level. Kel-F and Polybon M were just below this mark at 8 kg-m. Torlon 4301 compatibility was demonstrated at a disappointing 4 kg-m level. Based on the poor results in the three compatibility tests, Torlon 4301 was not considered for testing in the low speed friction and wear tests.

Table 6
LOX Impact Test Results

Material Identification	SUCCESSFUL IMPACT TEST LEVELS	
	Atmospheric Pressure 14.7 psia (kg-m)	Elevated Pressure 2000 psig (kg-m)
Torlon 4301	10	4
Polybon M	10	8
Kel-F	10 *	8
Vespel SP211	10 *	10

* Tests not conducted in this program, sufficient data exists at this level.

Low Speed Friction and Wear Tests

Tester Description. The low speed friction and wear tests were designed to evaluate the rubbing interactions between a typical metallic turbopump shaft material and one of the candidate soft seal materials in a simulated turbopump seal environment. The "low speed" preface in the friction and wear test title simply indicates that the tests planned were at speeds lower than those predicted in an actual turbopump operation. These demonstration tests were conducted to examine whether the new materials were capable of surviving the rubbing contact in a cryogenic environment. Reduced leakage, performance improvements, and minimum operating clearances were not the objective of this test program, but rather to evaluate mechanical survivability of the candidate materials. The test program obtained data that would help quantify the effects and interactions of rubbing friction within a soft seal. Wear, heat generation, heat dissipation, and wear process debris characteristics were the data of interest.

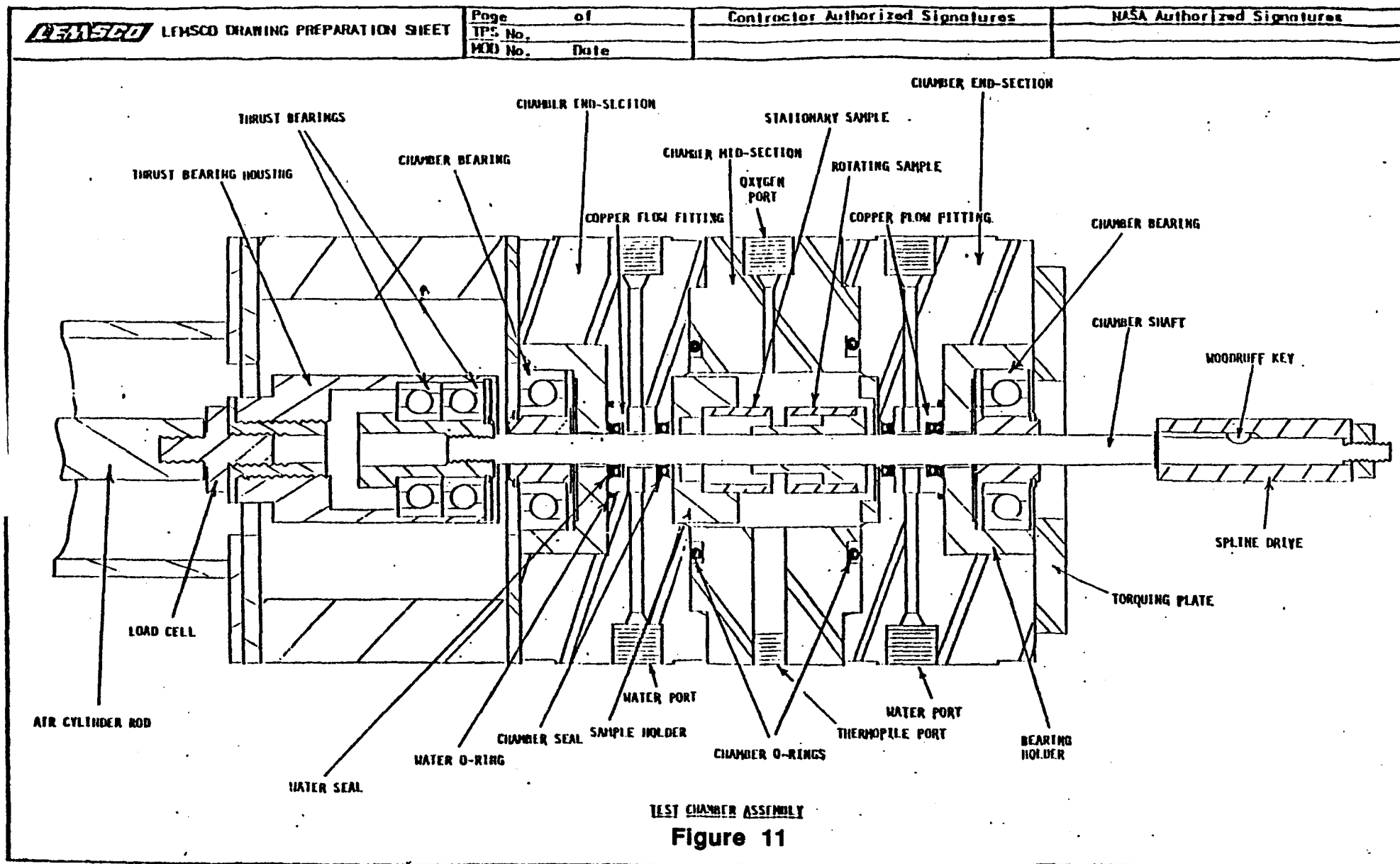
The Rubbing Cylinders tester located at the WSTF was uniquely suited for the type of testing being proposed by this project. However, the tester in its original configuration did not meet all the needs of this task, so minor modifications were incorporated. The low speed tester design was an adaptation of the tester, shown in **Figure 11**, which was primarily used to test rubbing metallic cylinders in a pressurized gaseous oxygen atmosphere. The majority of the design modifications were made in the mid-chamber section of the tester to incorporate larger stationary and rotor specimens for increased sliding velocity capability. Other minor changes were made to incorporate cryogenic temperature capabilities.

The low speed tester, **Figure 12**, consisted of a cylindrical pressure chamber fabricated from Monel 400, which contained an inner cavity over 2.1 inches in diameter and 2 inches long. The chamber was provided with a rotating shaft that extended through the chamber via a series of bushing bearings for radial support and purged seals for propellant separation. The soft seal test specimens P/N's, 7R030264 or 7R030265, were secured to the tester housing via the retainer, P/N 7R030263 which provided both radial and axial positioning of the samples. The parts list for the soft seal low speed tester components are shown in **Table 7**. The remaining tester components outside the test chamber, including the shaft bearings, gas purged seals, and shaft axial load application and measurement systems, were unchanged and were furnished by the WSTF.

The tester shaft was radially supported by a ball bearing on either side of the test chamber, each with a bushing pressed on the inner diameter of the bearing inner race. A nominal diametral clearance of 0.001 inch was provided between the bushing and the shaft to allow axial motion. This bushing was initially made from bronze which rubbed against the CRES 321 shaft, P/N 7R030267.

The stationary soft seal specimens, P/N's 7R030265 and 7R030264, were 2.115 inches in diameter which was much larger than the 1" diameter rubbing cylinder specimens. The seals made per P/N 7R030265 were machined from the raw polymeric material billet provided by the manufacturer. The Kel-F, Vespel SP211, Polybon M, and Torlon 4301 were all machined specimens. These soft seals were mounted in the tester by four screws. **Figure 13** shows the Vespel SP211 sample installed in the Low Speed tester.

WSTF Rubbing Cylinders Frictional Heating Tester



R/RD90-214
31

Low Speed Friction and Wear Tester Cross-Section

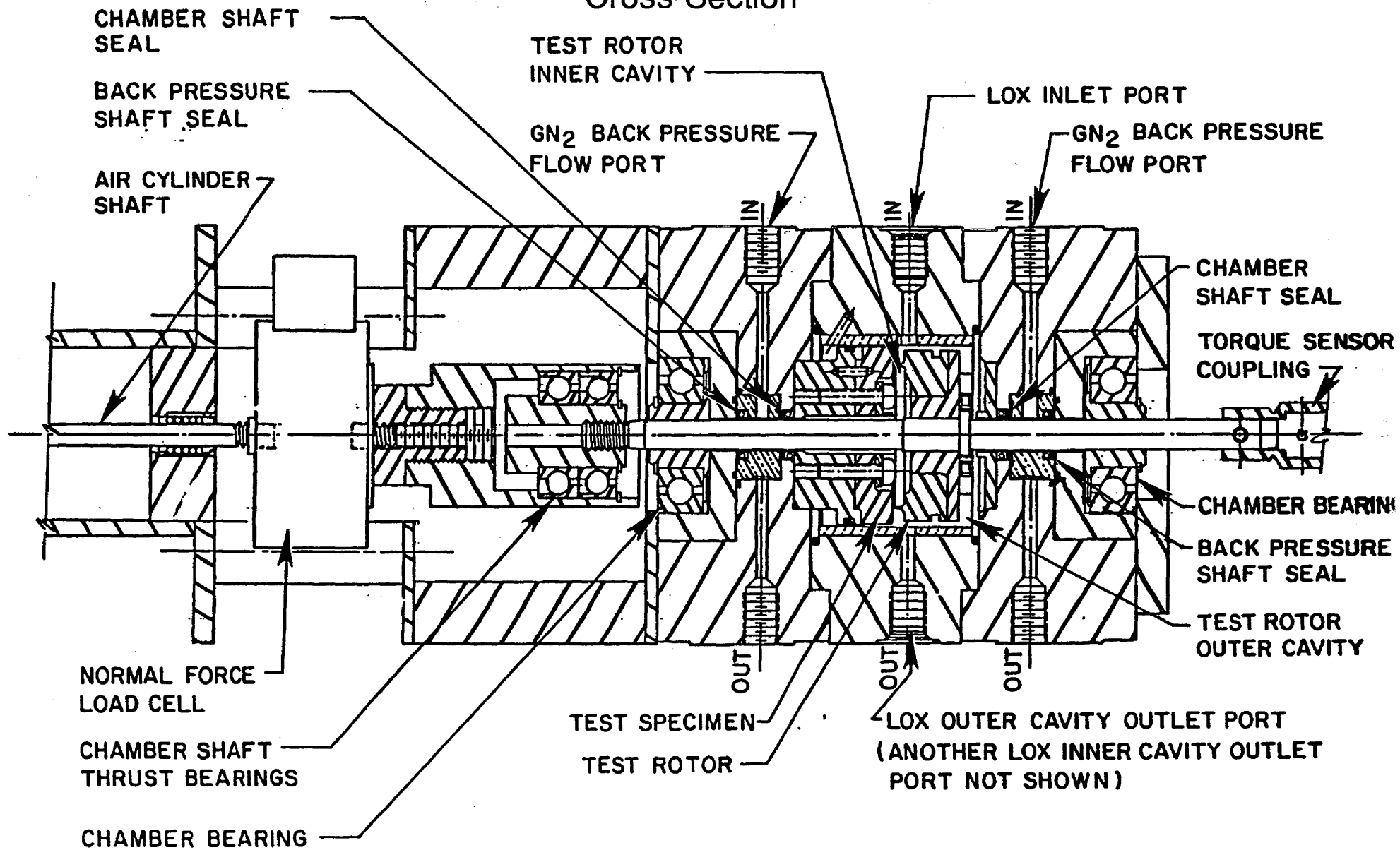


Figure 12

Table 7
Low Speed Tester Parts List

Part Number	Description
7R030261	Mid-Chamber Ass'y
7R030262-1	Body, Mid-Chamber
7R030263	Retainer, Ass'y
7R030264	Retainer, Castable Seal Ass'y
7R030264-3	Retainer
7R030264-7	Castable Sample: Hexcel 3124
7R030264-9	Castable Sample: Hexcel 3125
7R030265-19	Sample, Mach. Soft Seal: Torlon 4301
7R030265-23	Sample, Mach. Soft Seal: Polybon M
7R030265-25	Sample, Mach. Soft Seal: Kel-F
7R030265-27	Sample, Mach. Soft Seal: Vespel SP211
7R030266	Ring, Soft Seal Retaining
7R030267-1	Shaft, Low Speed Tester, Ass'y of
7R030268-3&-5	Rotor Config. 1: Alloy718 & Titanium
7R030268-7&-9	Rotor Config. 2: Alloy718 & A-286
7R030268-13&-15	Rotor Config. 3: Titanium & K-Monel
7R030268-15	Rotor Config. 4:
7R030269	Key, Rotor Drive
7R030270-3	Screw
7R030270-5	Screw
7R030271-3	Washer
7R032078-3	Rotor, Integral: K-Monel
7R032078-5	Rotor, Integral: Alloy 718
7R032078-7	Rotor, Integral: A-286
7R032079	Rotor, Ass'y: Titanium 5-2.5 ELI
MS171523	Spring Pin
MS9390-170	Pin
MS9390-220	Pin
MS9880-09	Cup Washer
Parker #2-135	O-Ring
Parker #2-143	O-Ring
RD112-5007-2607	Screw
RD112-5007-2612	Screw

Vespel SP211 Mounted into Seal Retainer

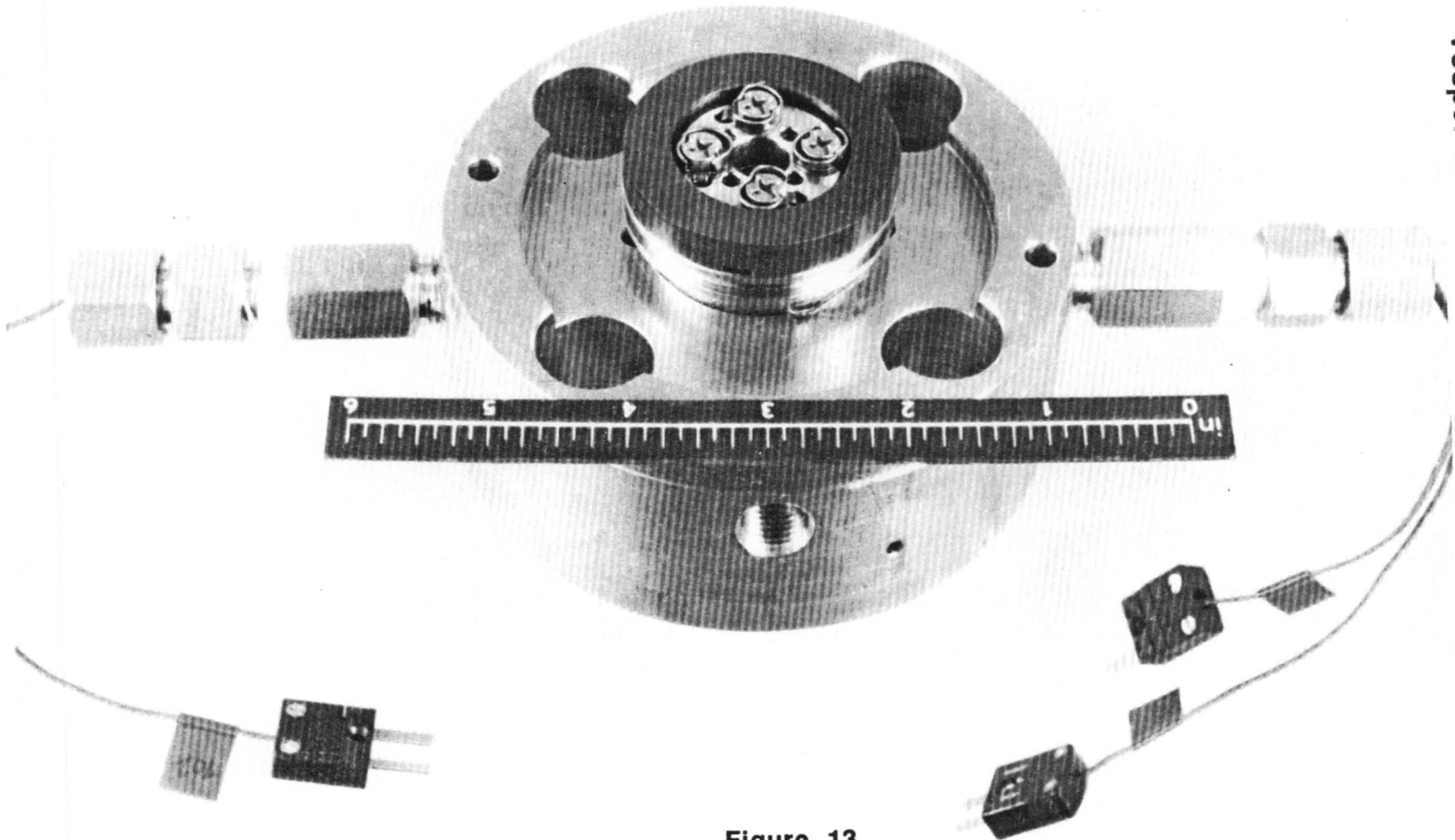


Figure 13

On the back of the P/N 7R030265 seal specimens, three thermocouples were inserted different depths from the rubbing surface; 0.125 inch, 0.172 inch, and 0.219 inch. **Figure 14** illustrates the basic configuration of the seal specimens. The temperature sensors were placed at a diameter of 1.700 inches, which was aligned with the rotor tooth, at three circumferential locations. The thermocouples were potted in the holes using two different adhesives. The first adhesive, called Ecobond, was used to set the thermocouple into the drilled hole. This adhesive utilizes silver particles within the resin matrix to maintain a high thermal conductivity to ensure rapid heat transfer and maximize the sensor response time. The second adhesive, Refset, was used to cover the thermocouple installation because of its proven chemical compatibility in liquid oxygen. This method worked well, however, great care was required to remove any excess adhesive from the back of the seal sample. Upon installation into the tester, extruded adhesive would cock the seal in the retainer, losing axial alignment with the rotor and, consequently, creating an uneven contact.

The second type of seal that was fabricated was the castable seals made from the polyurethanes, Hexcel 3124 and 3125, per P/N 7R030264. Instead of machining these specimens, the seal was formed by casting raw material into a metallic receptacle. After the curing cycle was completed, the seal was machined to final dimensions. Although the castable materials were more desirable from a manufacturing point of view, due to their chemical composition, they were not compatible for LOX service and were identified for LH2 service only. **Figure 15** shows a photograph of the machined and the cast seal samples.

This manufacturing technique was very desirable, in that the seal could be poured right into a turbopump housing. No mechanical fasteners or restraint systems are required to support or locate the seal. An example of this technique was demonstrated in Orbital Transfer Rocket Engine Technology Program - Task B.2. Using a dove-tailed groove, Hexcel 3125 was centrifugally cast into the inlet flange of the High Velocity Ratio Diffusing Crossover tester to produce the inducer tip seal, as shown in **Figure 16**. A similar approach was used to pour the interstage seal on the inner diameter of the crossover housing. Both seals performed well but were damaged when a tester ball bearing failed. The seals were sacrificed as protection for the more expensive crossover and inducer components. With only minor repair these very expensive components could be reused. The seals could also be repaired by removing the remaining material and casting new material back into the dove-tailed groove.

Low Speed Test

Soft Seal Specimen Configuration

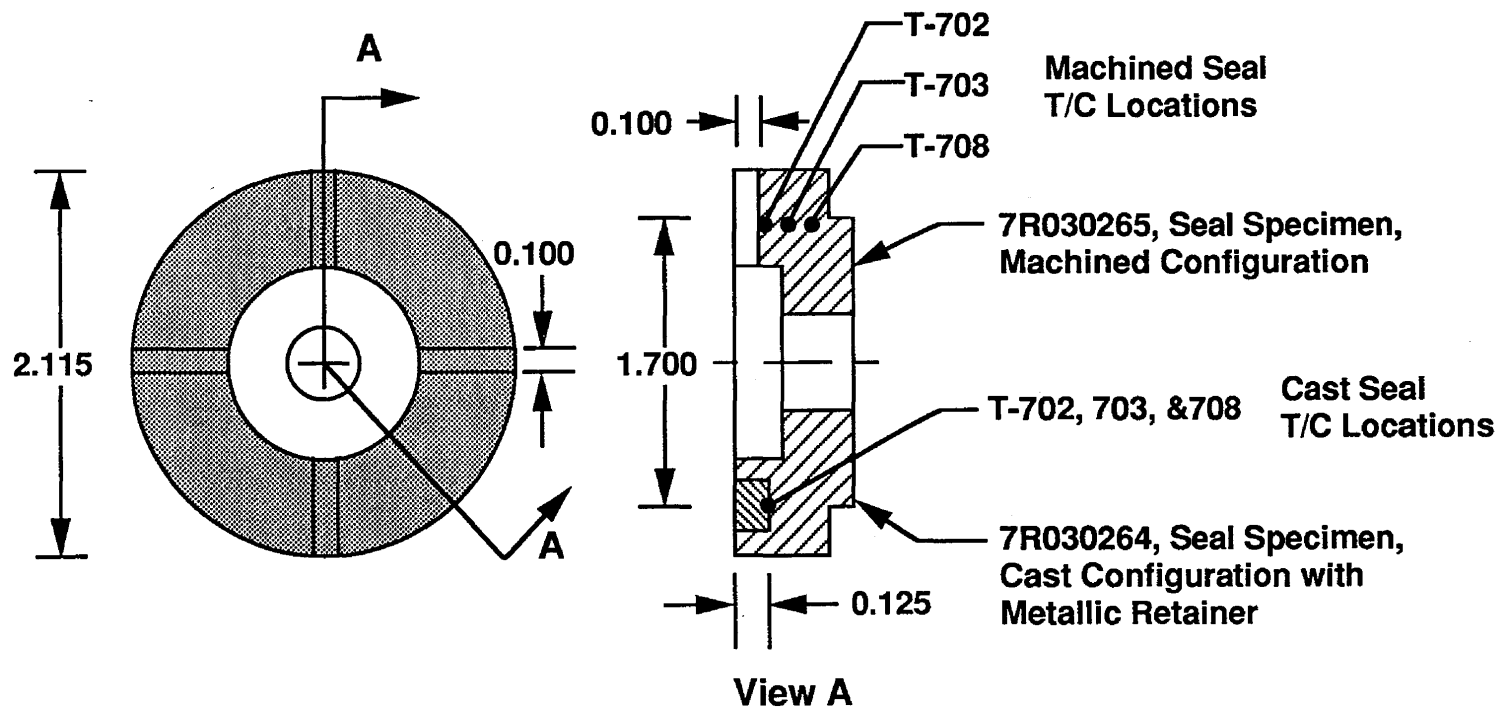


Figure 14

Low Speed Friction and Wear Tester Soft Seal Specimens

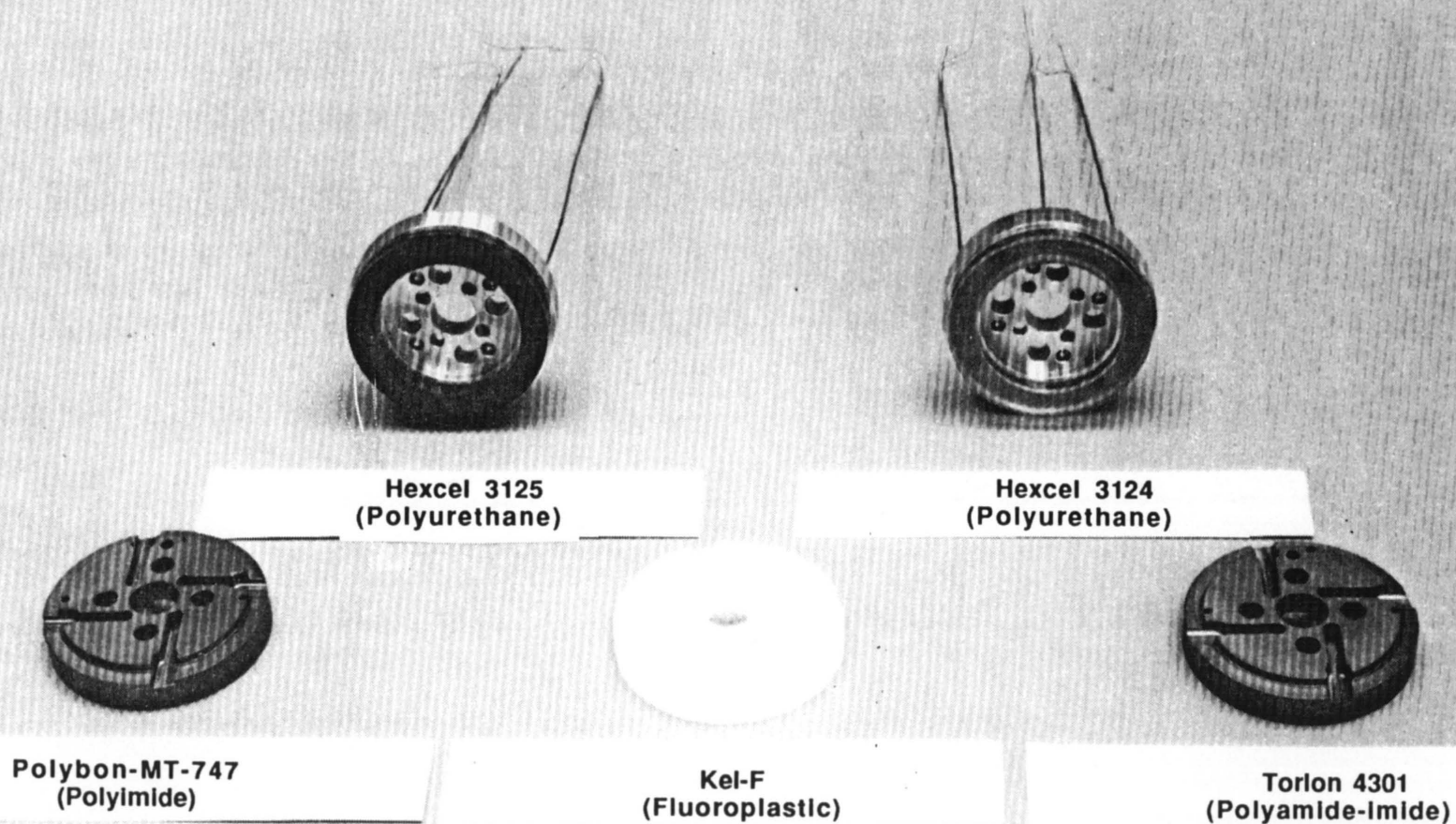


Figure 15

High Velocity Ratio Diffusing Crossover Tester
Inlet Flange

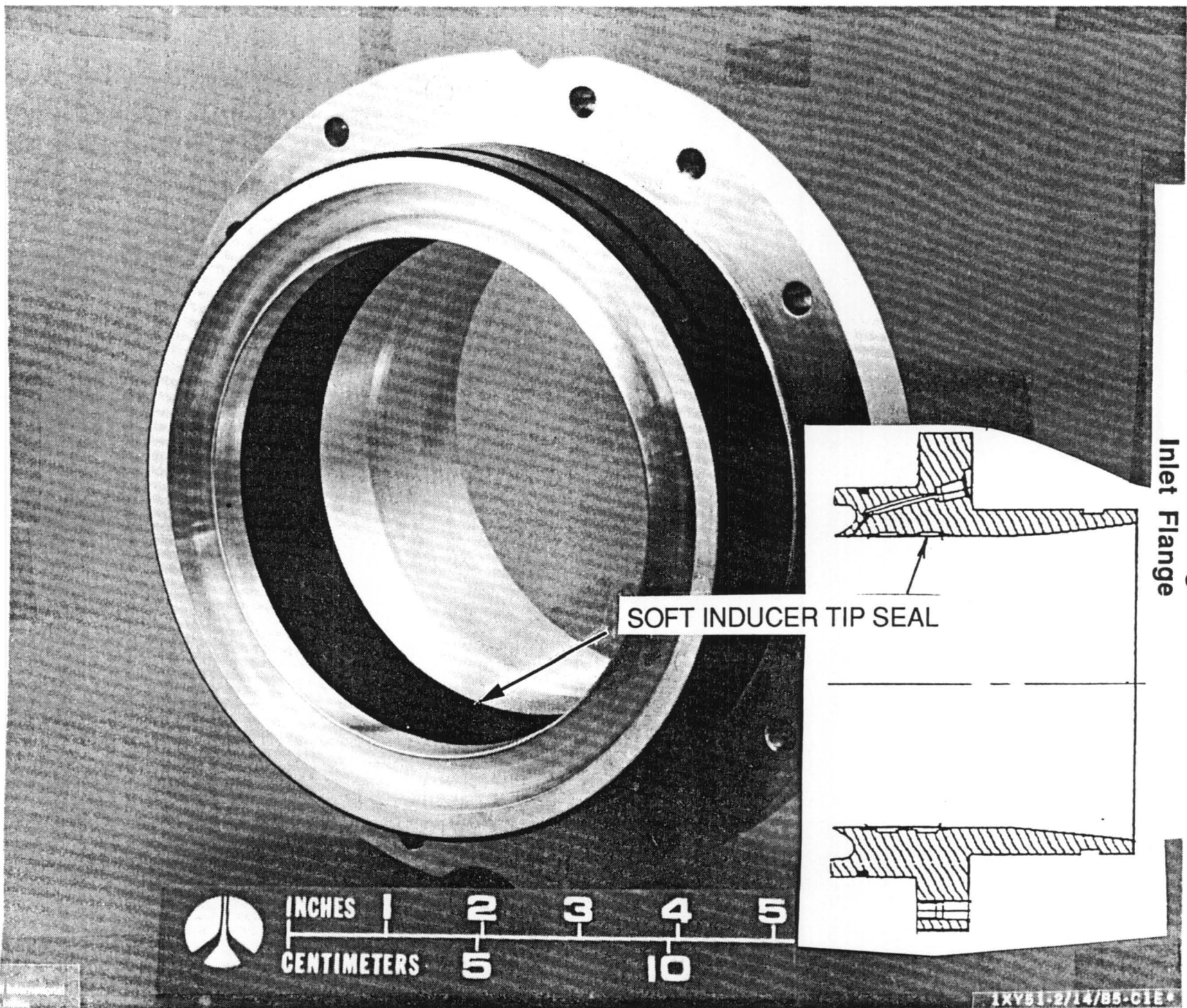


Figure 16

RI/RD90-214
38

The test fluid entered the test chamber of the low speed friction and wear tester through an inlet port on the top of the tester and drained through two ports on the bottom of the tester. The fluid flow path was complicated by the axial contact of the rotor and the seal specimen. Flow passed around the contacting specimens to the test chamber outlet, as well as between the seal and the seal retainer, as seen in **Figure 17**. Several holes and channel patterns, as seen previously in **Figure 15**, were machined into the seal specimens to allow the test fluid flow all around the specimen to obtain the maximum cooling. In a turbopump seal, the flow is basically axial with a strong tangential component. This tester could not provide the identical flow distribution and rubbing condition that a typical seal would see, so the additional passages were included to maintain sufficient coolant.

The initial shaft design employed in the Low Speed tester utilized a replaceable rotor specimen, P/N 7R030268. The rotor specimen was configured to simulate a labyrinth type seal, except the seal tooth was on the axial face of the rotor, instead of the circumference. As seen in **Figure 18**, various seal contact tooth widths were designed to allow flexibility of applied contact stress which would simulate various seal rotor types, such as a labyrinth tooth, a smooth rotor, and a turbine tip seal configuration. Rotor contact areas ranged from 440 mm² (0.682 in²) with the 3.2 mm (0.126 inch) wide contact area, simulating the smooth seal, to 34.8 mm² (0.054 in²) for the 0.254 mm (0.010 inch) wide knife-edged rotor which simulates the labyrinth tooth. These test rotor specimens were fabricated of Monel K-500 and INCO718 for LOX testing, Titanium-5Al-2.5Sn ELI and INCO 718 for LH₂ testing, and A-286 for GH₂ testing. The rotor materials selected for testing were based on their common use in cryogenic rocket engine turbopumps, for example the Mark49-F and Mark49-O turbopumps. In this configuration, four bolts were used to secure the metallic test rotor to the 321 CRES shaft, P/N 7R030267, as shown in **Figure 19**.

Test Plan. Two operating scenarios can be employed using soft wear ring seals. The first technique would require the soft seal in contact with the rotor in the pre-start or chilled condition. This can be achieved by taking advantage of the natural shrinkage of the housing and seal components at cryogenic temperatures. The second technique would incorporate a small clearance, near line-to-line, between the rotor and the stationary seal at pre-start. Contact between the rotor and the stator would be accomplished at speed. Consistent with these different assembly techniques, two types of tests were planned to demonstrate the soft seal and rotor interactions.

The first test was the static friction (SF). In this test, once the fluid and seal temperatures within the test cavity were at the pre-start conditions, the rotor was pulled against the seal with the air

Low Speed Tester Internal Flow Paths

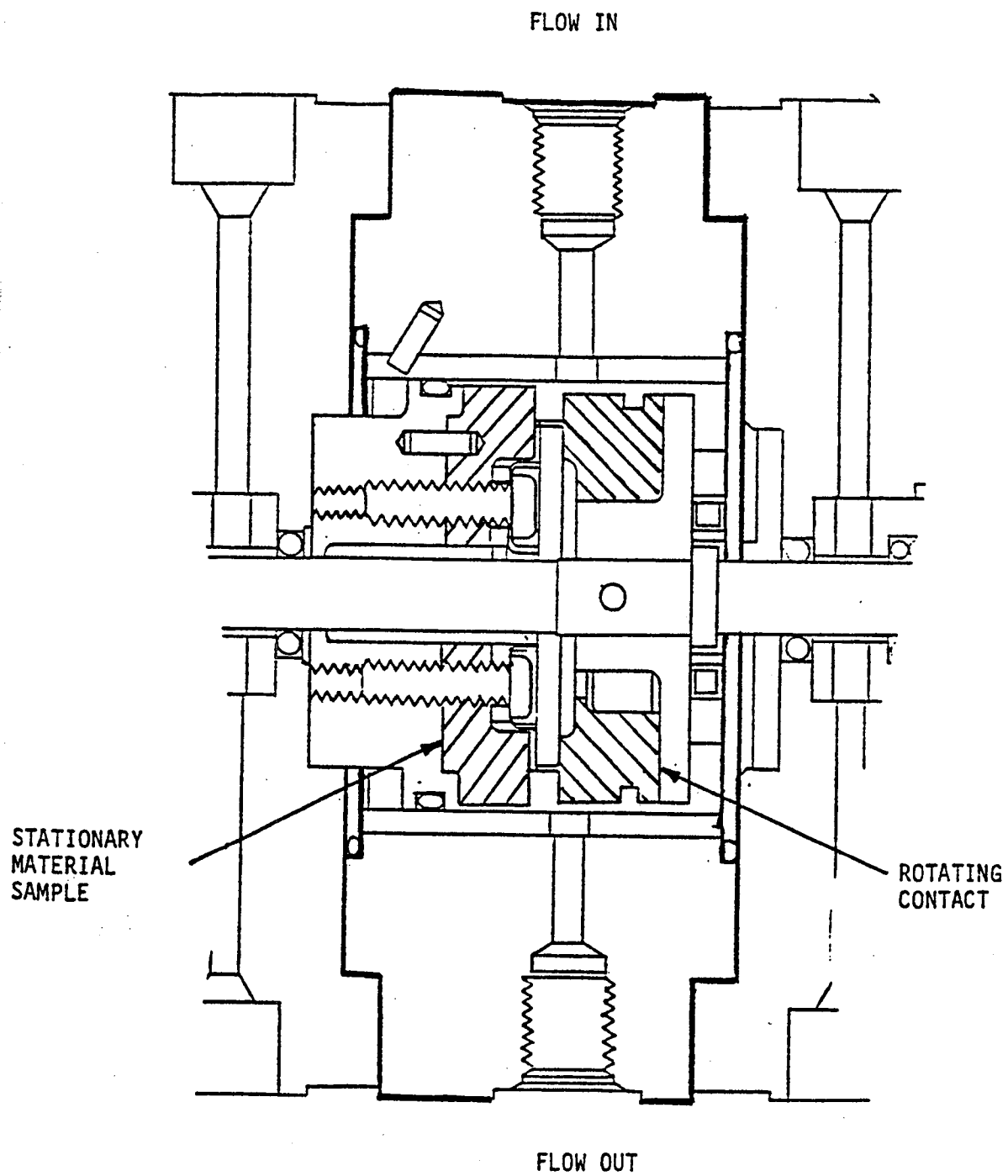
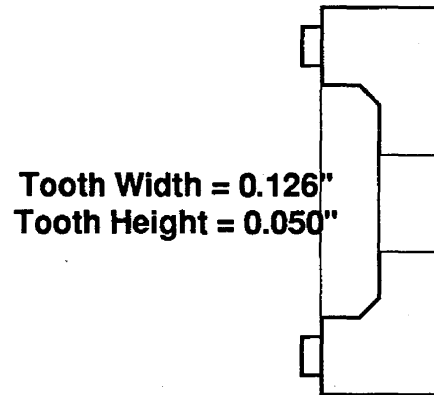


Figure 17

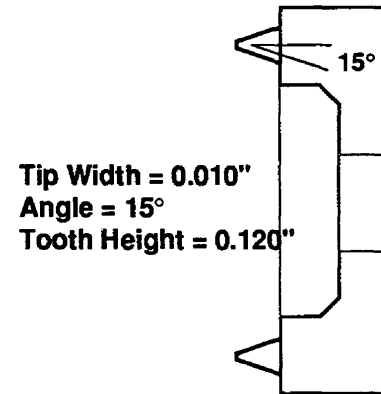
Low Speed Tester

Rotor Contact Tooth Configurations



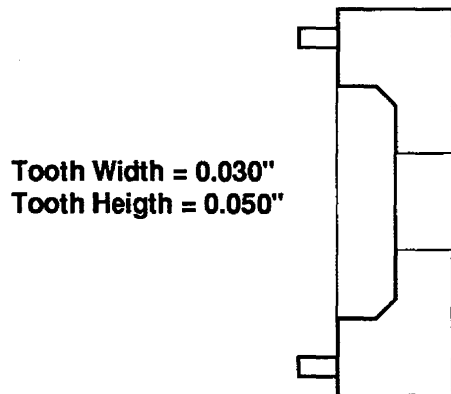
Tooth Width = 0.126"
Tooth Height = 0.050"

Smooth Seal Rotor



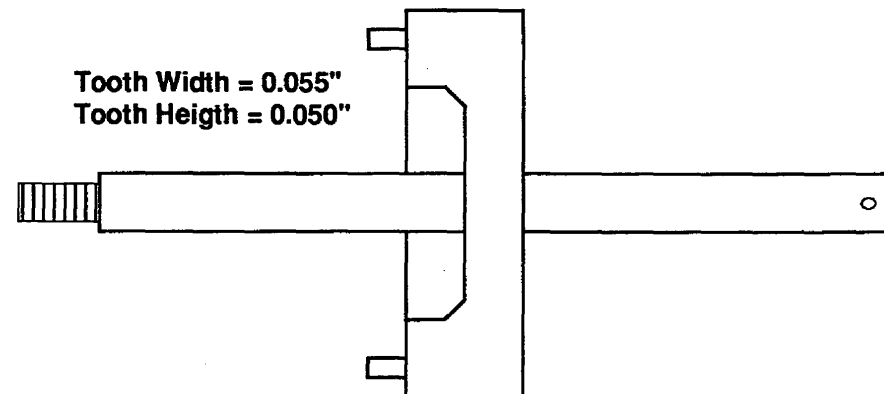
Tip Width = 0.010"
Angle = 15°
Tooth Height = 0.120"

Labyrinth Seal Rotor



Tooth Width = 0.030"
Tooth Height = 0.050"

Turbine Tip Seal



Tooth Width = 0.055"
Tooth Height = 0.050"

Redesigned Configuration

Figure 18

Low Speed Friction and Wear Tester
Rotor Specimens

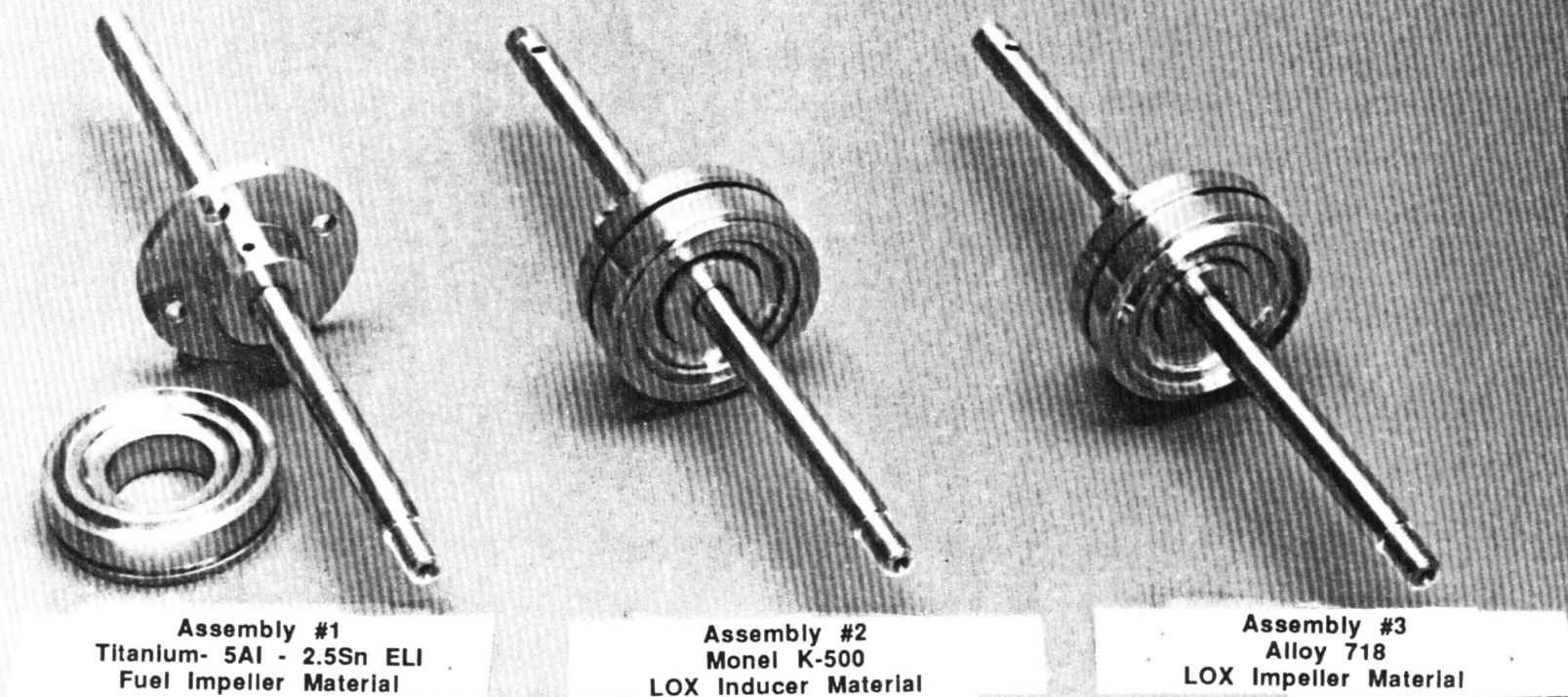


Figure 19

actuated cylinder to apply the desired force. This would be similar to the stationary seal shrinking around the rotor as the temperature dropped during pre-start cooldown. At this point, the rotor would be accelerated to the test speed allowing the rotor to wear into the seal. A mechanical stop was utilized during this test to limit the progress of the wear which allowed the applied load to decay. This test is comparable to the situation where the rotor reaches the operating speed, the growth stops, and hence the load decays. A typical PV profile for this type of test is shown in **Figure 20**. Data such as breakaway torque, running torque, applied load, and seal incursion were measured.

The second test was called the running friction (RF) test. This test simulated the second assembly condition, where the rotor contacted the seal at speed. During this test, the fluid and tester conditions were established as before, then the rotor was brought to the operating speed of 17,000 rpm (except test WS30F, where 6200 rpm was employed). This speed was held constant for several seconds so that the shaft torque could reach steady state. The rotating tester shaft was then pulled into the stationary seal material specimen at the prescribed load. A typical PV profile is shown in **Figure 21**. Running torque was compared against the previously measured steady state or tare torque to determine the torque transmitted to the seal specimen. From this the seal/rotor dynamic coefficient of friction, μ , was determined as shown:

(Eq. 1)

$$\mu = (T_r - T_t)/F_n r$$

where T_r is the running torque, T_t is the tare torque, F_n is the applied normal load, and r is the mean radius of the rotor contact tooth.

Test Facility Configuration. The Low Speed Friction and Wear Tester was connected at one end to the drive motor and transmission assembly, which was capable of speeds ranging from 1,000 to 17,000 rpm. The other end of the tester was connected to a load cell in series with an air actuator cylinder which provided axial motion and load capability (**Figure 22**). A photograph of the tester installed in the facility is shown in **Figure 23**.

The test facility, located in 800 Area Cell 111 of the White Sands Test Facility, was designed to provide continuous LOX flow through the test chamber during the performance of the static and running friction tests. The Low Speed friction and wear test facility schematic for the LOX test series is shown in **Figure 24**. Prior to the start of the test, LOX was fed into the system from a 568 liter (150 gallon) dewar to chill the hardware. A gaseous nitrogen purge system was used to

Typical Static Friction Test Profile

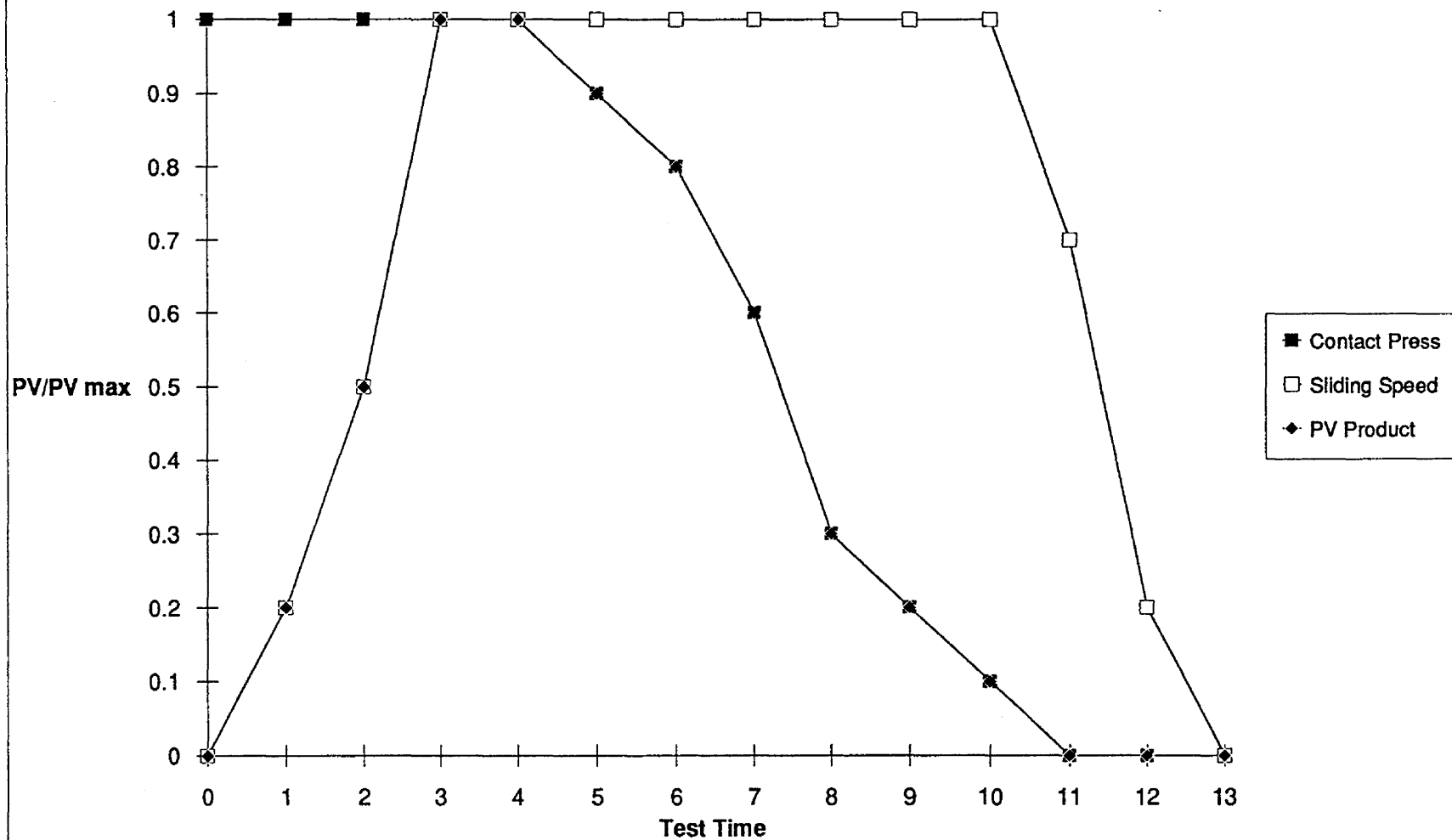


Figure 20

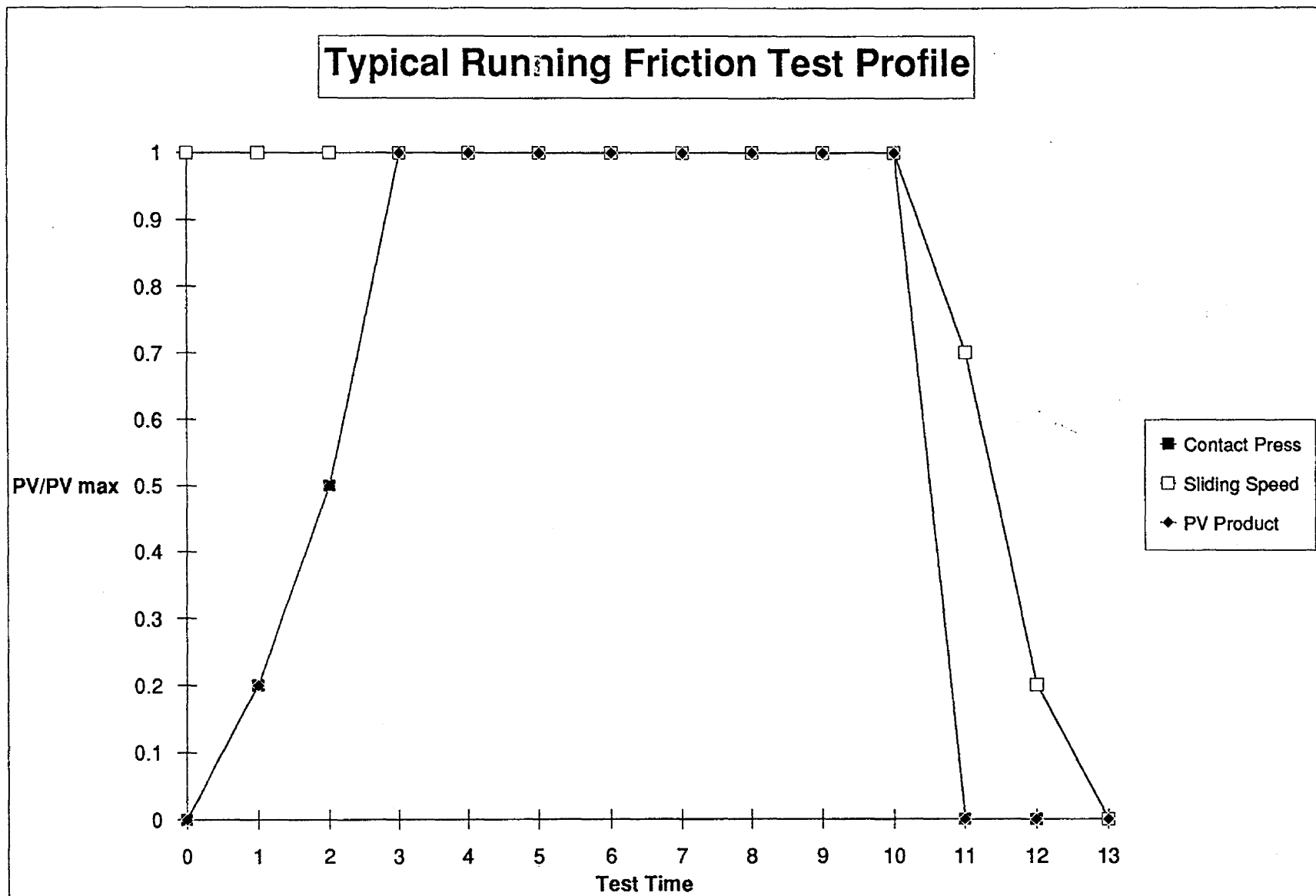


Figure 21

Low Speed Friction and Wear Tester

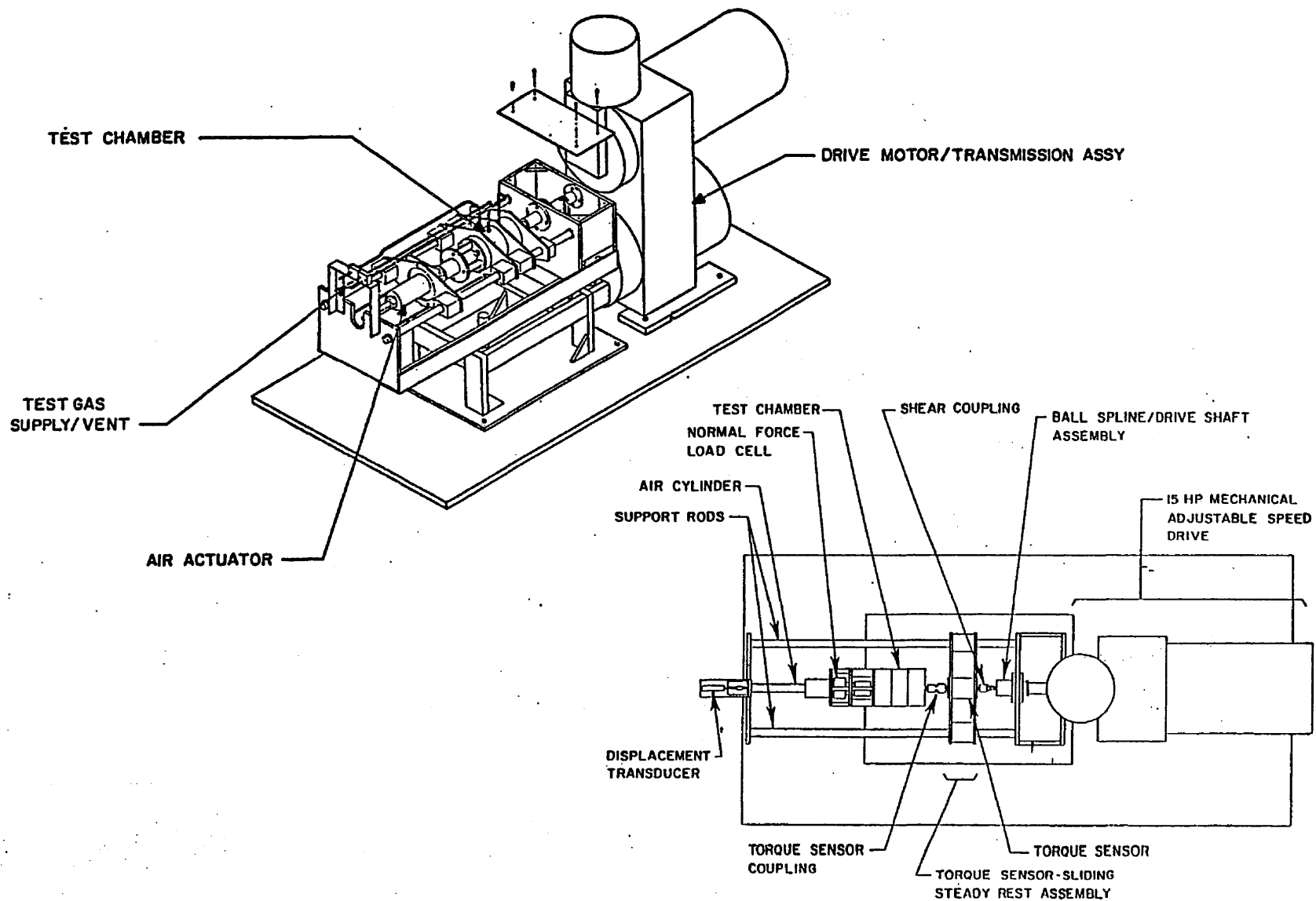
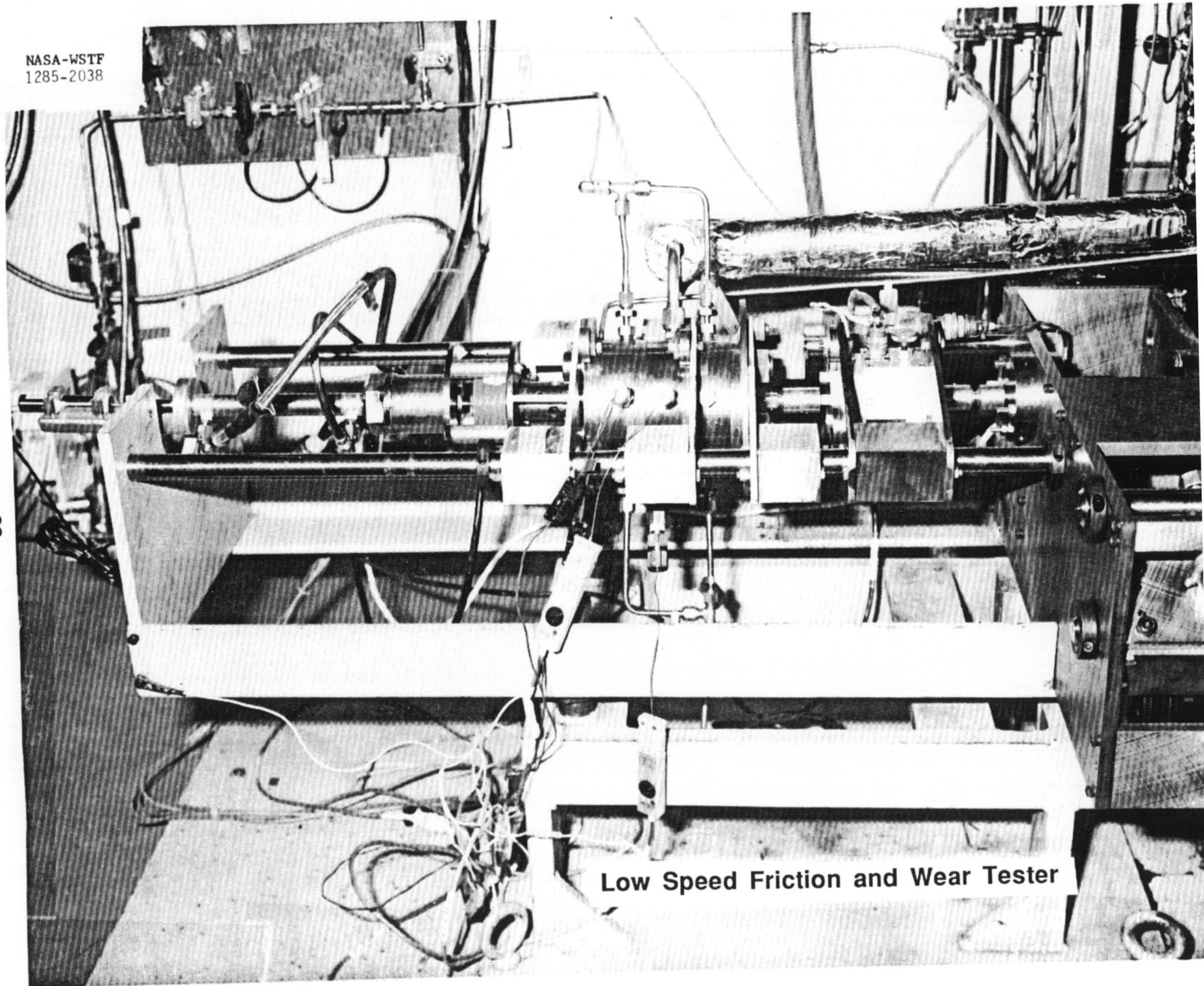


Figure 22

NASA-WSTF
1285-2038



Low Speed Friction and Wear Tester

Figure 23

R/RD90-214
47

LOX Low Speed Test Facility Schematic

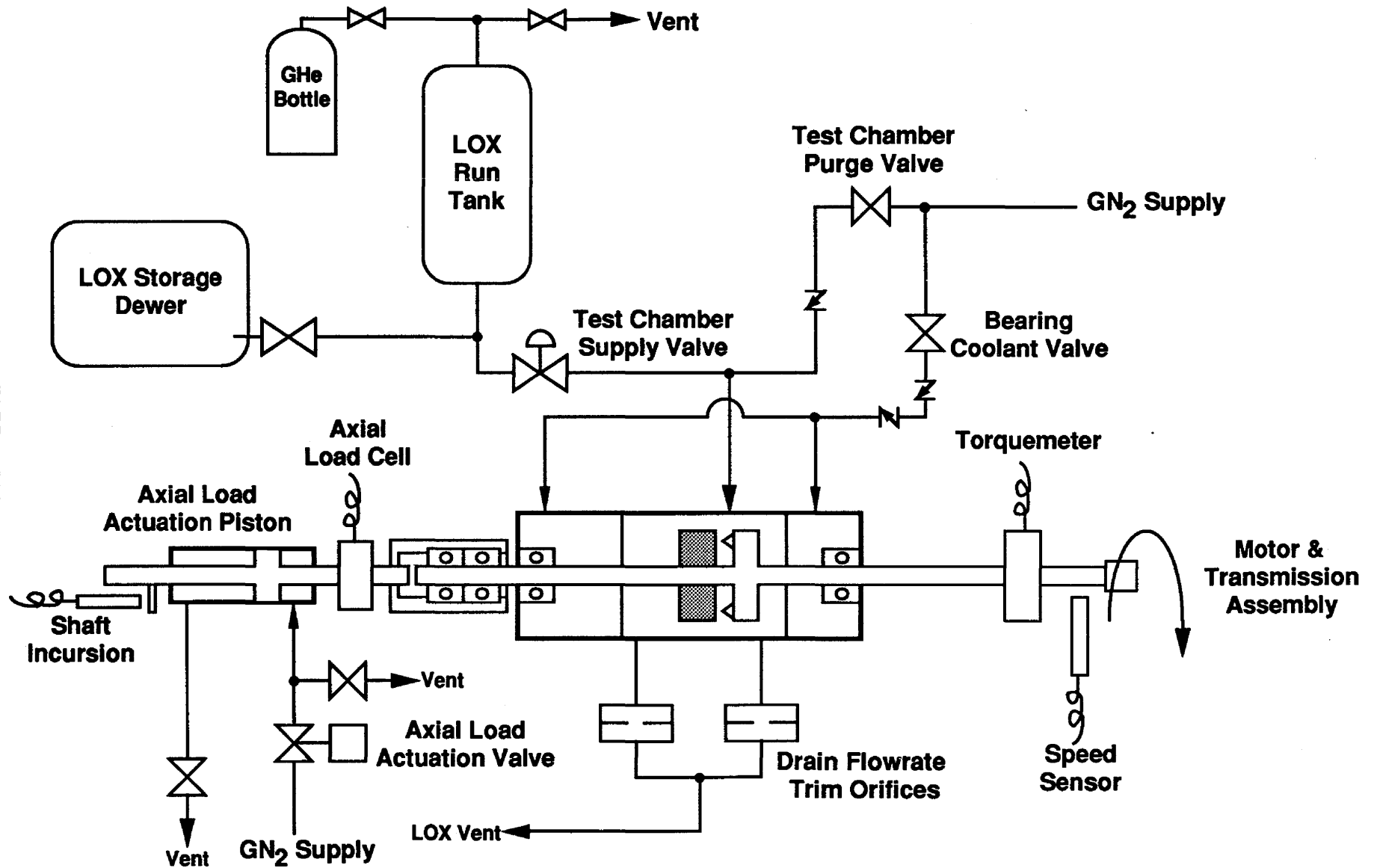


Figure 24

prevent excessive chilling of the chamber shaft seals, and was later used to inert the test chamber at the conclusion of the test. Upon completion of the pre-test chill, the LOX accumulator with an approximate 11.4 liter (3 gallon) capacity was filled, and the dewar was isolated from the test system. A gaseous helium system provided ullage pressurization to the accumulator. This system, although duration limited by the supply of LOX, could provide propellant at 12.5 MPA (1800 psig). Later in the test program, the accumulator system was replaced with a positive displacement pump which delivered flow right from the dewar for extended test durations. Downstream of the test chamber, the metering valve was adjusted to set the desired flowrate through the tester. A second metering valve in parallel with the first was added later in the test program to help balance the tester drain pressures in an attempt to minimize the hydrodynamic forces acting on the rotor.

The tests were controlled by a pre-programmed microprocessor which automatically commanded many of the test events, such as the pre-chill, motor start, pneumatic cylinder operation, and automatic emergency shutdown steps, for maximum safety and repeatability. This control system was remotely located away from Cell 111 in a common control center.

Instrumentation and Redline Limits. The test data was collected at 100 millisecond intervals throughout each test by the microprocessor system. The low speed tester was instrumented with sufficient measurements to safely run the tests as well as conduct post test diagnostics. Table 8 shows the instrumentation and redline list used on the LOX Low Speed test program. Figure 25 illustrates schematically the locations of the instrumentation used during these tests. In addition to the typical instrumentation shown in the list, the low speed friction and wear tester was monitored using VHS formatted video recording equipment rolling at 30 frames/second.

Low Speed Test Results. Summarized in Table 9 are the test chamber pressure, planned test duration, actual rubbing duration, seal material, rotor material, test type, planned PV, and other key test parameters for the tests conducted during the Low Speed LOX test program. The major objectives of these tests were to determine the frictional heating characteristics, LOX compatibility, wear rate, and wear particulate size of the selected polymeric materials.

Tests WS27 through WS30E were SF tests which utilized a Vespel SP211 seal sample running against a Monel K-500 rotor with the largest contact area of 4.40 mm^2 (.682 inch²). From test WS27, the first Low

Table 8

**Low Speed Friction and Wear Test
Instrumentation and Redline List
Liquid Oxygen Test Series**

Parameter ID Number	Parameter Description	Units	Lower Range	Upper Range	Nominal Value	Redline Limit
PT-814	OUTER CHAMBER HUB PRESS	PSIG	0	4000	300	2300 max
PT-819	OUTER/INNER CHAMBER ΔP	PSID	0	100	0	
TS-710	ROTOR TORQUE	IN-LB	0	88	20	100 max
PT-210	PNEUMATIC CYLINDER PRESS	PSIA	0	300	60	
PT-517	BEARING COOLANT PRESS	PSIG	0	4000	60	
LC-706	ROTOR AXIAL LOAD	LBS	0	100	60	
PT-806	TANK ULLAGE PRESS	PSIA	0	3000	300	
DP-701	ROTOR AXIAL DISPLACEMENT	INCH	0	0.100	0.010	0.020 max
TC-REFK	"K" TYPE T/C REFERENCE TEMP	°F	-	-	60	
TC-702	SAMPLE TEMP @ 0.125"	°F	-217	2250	-285	450 max
TC-703	SAMPLE TEMP @ 0.172"	°F	-217	2250	-285	450 max
TC-704	OUTER CHAMBER TEMP	°F	-300	2500	-285	
TC-708	SAMPLE TEMP @ 0.219"	°F	-217	2250	-285	450 max
TC-803	TANK OUTLET TEMP	°F	-300	2500	-285	
TC-807	TANK ULLAGE TEMP	°F	-300	2500	-285	
TC-812	METER VALVE INLET TEMP	°F	-300	2500	-285	
PM-717	MOTOR INPUT POWER	WATTS	0	20000	5000	
TC-820	CHAMBER OUT TEMP 1	°F	-300	2500	-285	
TC-823	CHAMBER OUT TEMP 2	°F	-300	2500	-285	
TC-JREF	"J" TYPE T/C REFERENCE TEMP	°F	-	-	70	
FM-844	LOX INLET FLOWRATE	LB/MIN	0	100	50	
RPM	TESTER SHAFT SPEED	RPM	0	30000	17000	21000 max
PT-815	OUTER CAVITY PRESSURE	PSIA	0	10000	300	2300 max

Low Speed Friction and Wear Tester Instrumentation Schematic

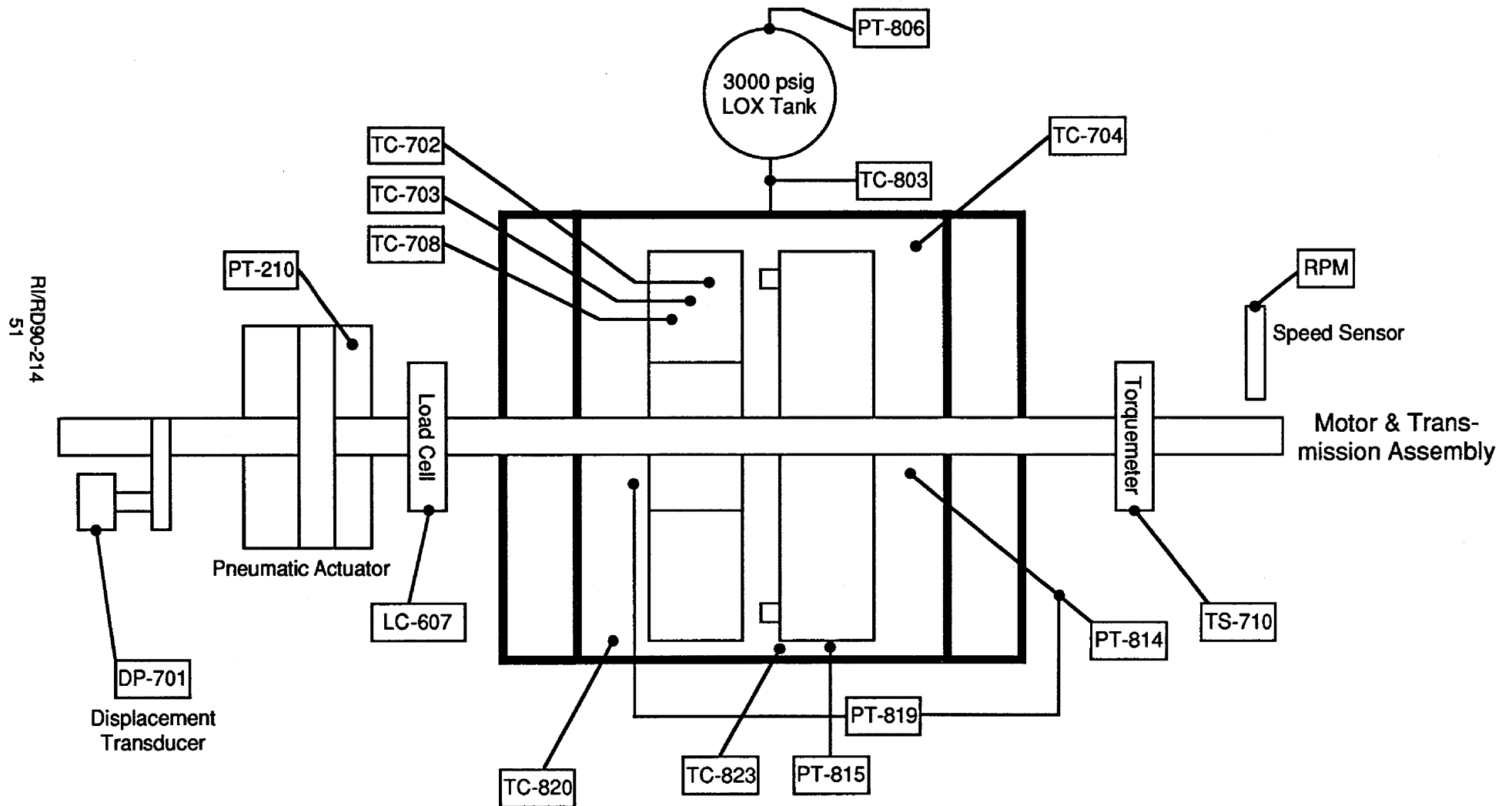


Figure 25

Table 9

Soft Wear Ring Seal Low Speed Test History

Test Number	Test Date	Test Type	Soft Seal Sample	Test Rotor Sample	Test Fluid Media	Chamber Press (psia)	Applied Shaft Load (lbf)	Rotor Pumping Load (lbf)	Shaft Speed (rpm)	Rotor Rub Vel. (ft/sec)	Break Torque (in-lbf)	Tare Torque (in-lbf)	Run Torque (in-lbf)	Planned PV (psi-ft/sec)	Comments
WS27	12/3/85	C/O	Vespel #1	K-500 #1	LOX	300	-	-	17,000	-	-	-	4	-	Successful Chillover and Check Out
WS28	12/3/85	C/O	Vespel #1	K-500 #1	LOX	300	-	-	17,000	-	-	-	3	-	Successful Chillover and Check Out
WS29	N/A	-	-	-	-	-	-	-	-	-	-	-	-	-	Optional Check Out Test Not Used
WS30A	12/4/85	SF	Vespel #1	K-500 #1	LOX	300	15.0	110.0	17,000	127.81	10.0	-	7	-	Oblique contact due to mating flange burrs. Pumping Observed.
WS30B	1/7/86	SF	Vespel #1	K-500 #1	LOX	300	-	-	17,000	127.81	-	-	-	-	No Data Recorded. Test Repeated.
WS30C	1/8/86	SF	Vespel #2	K-500 #1	LOX	300	75	125	17,000	127.81	15.0	-	6	-	No Contact on Seal Specimen.
WS30D	1/9/86	SF	Vespel #2	K-500 #1	LOX	300	125	135	17,000	127.81	22.5	-	6	-	No Contact on Seal Specimen.
WS30E	1/14/86	SF	Vespel #2	K-500 #1	LOX	300	150	175	17,000	127.81	26.0	-	6	-	
WS30F	1/17/86	RF	Vespel #2	K-500 #1	LOX	300	220	15	6,200	46.61	-	2	22	13991	Light, Uneven Wear.
WS31	1/31/86	RF	Vespel #3	INCO718	LOX	300	383	135	17,000	127.81	-	6	25	586969	Test Terminated By Redline Cut. Tester Fire caused by Seal Overload. Used Knife-Edged Rotor for WS31.
WS01	1/21/87	C/O	Kel-F #1	K-500 #2	LN2	300	-	-	17,000	124.77	-	-	-	-	Bronze Bushing Seizure. Testing Delayed for SSME C7B Tests
WS03A	10/26/88	SF	Kel-F #1	K-500 #2	LOX	300	31	-	17,000	124.77	18.2	-	7	-	Light, Uneven Wear. Epoxy on Back of Seal caused Misalignment.
WS04A	11/1/88	RF	Kel-F #1	K-500 #2	LOX	300	32	23	17,000	124.77	-	4	5	3859	
WS05A	11/1/88	RF	Kel-F #1	K-500 #2	LOX	300	31	22	17,000	124.77	-	4	5	3859	Light, Uneven Wear.
WS03B	11/17/88	SF	Kel-F #1	K-500 #2	LOX	300	31	-	17,000	124.77	20.2	-	6	-	Light Wear Slightly Uneven. Tester Shaft/Housing Not Concentric.
WS04B	11/18/88	RF	Kel-F #2	K-500 #2	LOX	300	31	20	17,000	124.77	-	6	7	4716	
WS05B	11/18/88	RF	Kel-F #2	K-500 #2	LOX	300	31	18	17,000	124.77	-	6	6	5574	
WS06	11/18/88	RF	Kel-F #2	K-500 #2	LOX	300	30	16	17,000	124.77	-	6	6	6003	Light Even Wear to .003". 60 seconds Total Duration. Stringers Visible.
WS07	11/23/88	SF	Vespel #4	K-500 #2	LOX	300	31	-	17,000	124.77	14.4	-	6	-	Light Even Wear. 60 seconds Duration. Reused Seal WS04C.
WS08	11/28/88	RF	Vespel #5	K-500 #2	LOX	300	32	17	17,000	124.77	-	6	6	6431	
WS09	11/28/88	RF	Vespel #5	K-500 #2	LOX	300	32	23	17,000	124.77	-	6	6	3859	
WS10	11/28/88	RF	Vespel #5	K-500 #2	LOX	300	31	22	17,000	124.77	-	6	6	3859	Light Uneven Wear. 60 seconds Total Duration.
WS11	12/1/88	SF	Polybon #1	K-500 #2	LOX	300	31	-	17,000	124.77	15.6	-	6	-	Light Uneven Wear. 60 seconds Total Duration.
WS12	12/9/88	RF	Polybon #2	K-500 #2	LOX	300	32	15	17,000	124.77	-	7	7	7289	
WS13	12/9/88	RF	Polybon #2	K-500 #2	LOX	300	33	21	17,000	124.77	-	5	7	5145	
WS14	12/9/88	RF	Polybon #2	K-500 #2	LOX	300	31	21	17,000	124.77	-	6	6	4288	Light Uneven Wear. 60 seconds Total Duration.
WS01C	4/4/89	C/O	Kel-F #3	K-500 #2	LOX	300	-	-	17,000	124.77	-	-	-	-	Hydrodynamic Load Increased with Time.
WS01D	4/24/89	C/O	Kel-F #3	K-500 #2	LOX	300	-	-	17,000	124.77	-	-	-	-	Established Pumping Forces vs. Rotor Displacement.
WS01E	4/24/89	C/O	Kel-F #3	K-500 #2	LOX	300	-	-	17,000	124.77	-	-	-	-	Established Pumping Forces vs. Rotor Displacement.
WS03C	5/2/89	RF	Kel-F #3	K-500 #2	LOX	300	61	28	17,000	124.77	-	5	8	14149	Test Cut by Incursion Redline. 2 Small Rotor Hot Spots. Seal Stringers.
WS04C	6/23/89	RF	Vespel #4	K-500 #3	LOX	300	61	13	17,000	124.77	-	-	-	20580	Tester Shaft Failed. Rotor Tooth Heat Effected. Seal Worn 0.005".

Speed check out test, a force producing phenomena was measured on the load cell when the shaft was rotating. It was determined that the four bolt heads, which protruded from the flat surface on the back of the test rotor, created a pumping effect. The local low pressure zone on the back surface of the rotor produced a net axial force that prevented the test rotor from contacting the seal specimen. The load, which was proportional to the square of the shaft speed, was measured as high as 175 lbf at 17,000 rpm in test WS30E. To this point in the program only SF tests had been run and the load applied to the shaft by the pneumatic cylinder was always less than the hydrodynamic forces at operating speed. Consequently, only small and non-uniform wear markings were evident on the seal specimens, and these were caused by the initial shaft acceleration when the pumping forces were very small.

For Test WS30F, a RF test, the shaft speed was reduced to 6200 rpm from 17,000 rpm and the pneumatic cylinder applied load was increased to 49 N (220 lbf) to overcome the pumping forces. A Vespel SP211 seal and a Monel K-500 rotor was installed for this test. The test ran the planned duration of 30 seconds, and a maximum temperature of -174°F was measured within the seal at location TC-702 (Figure 26). A drop in temperature can be seen from TC-702, when the other measurements, only 0.047 and 0.094 inch away saw no change. This event could not be adequately explained. The Vespel surface was non-uniformly worn, having only approximately 85% of the surface worn. An average PV of 14,376 psi-ft/sec was measured during this test. The contact pressure was calculated by taking the difference between the measured applied load from the load cell and the pumping force measured during the pre-contact time divided by the rotor contact area.

To overcome the inconsistent wear track problem, originally believed to be caused by hydrostatic forces between the wide rotor tooth and the seal, the Alloy 718 "knife-edged" rotor configuration was employed. The inconsistent wear track was probably caused by seal to rotor misalignment rather than hydrostatic lift. For test WS31, the speed was reset to 17,000 rpm and the applied load was increased linearly throughout the RF test to a maximum value of 611 lbf. At 383 lbf applied axial load, the test was terminated by an incursion limit redline cut. Within the test chamber, the seal had ignited due to excessive frictional heating and as the material burned, the rotor passed though the seal material more readily and triggered the redline cut (Figure 27). Prior to ignition, the seal internal temperatures (Figure 28) rose steadily, until just after the cut off at which time they increased rapidly to over 2000°F.

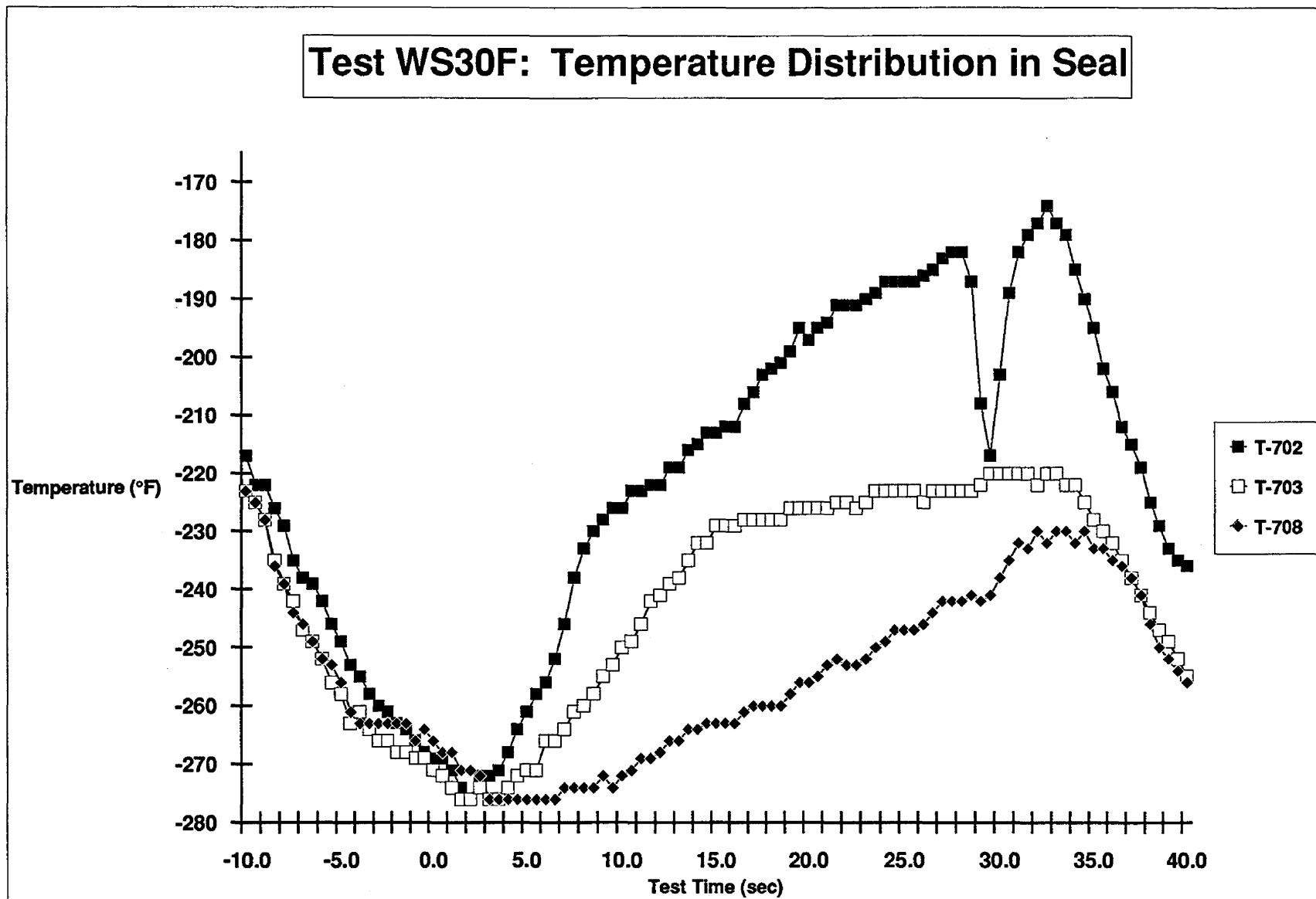


Figure 26

Test WS31 Data

Speed, Torque, Load, & Incursion Profiles

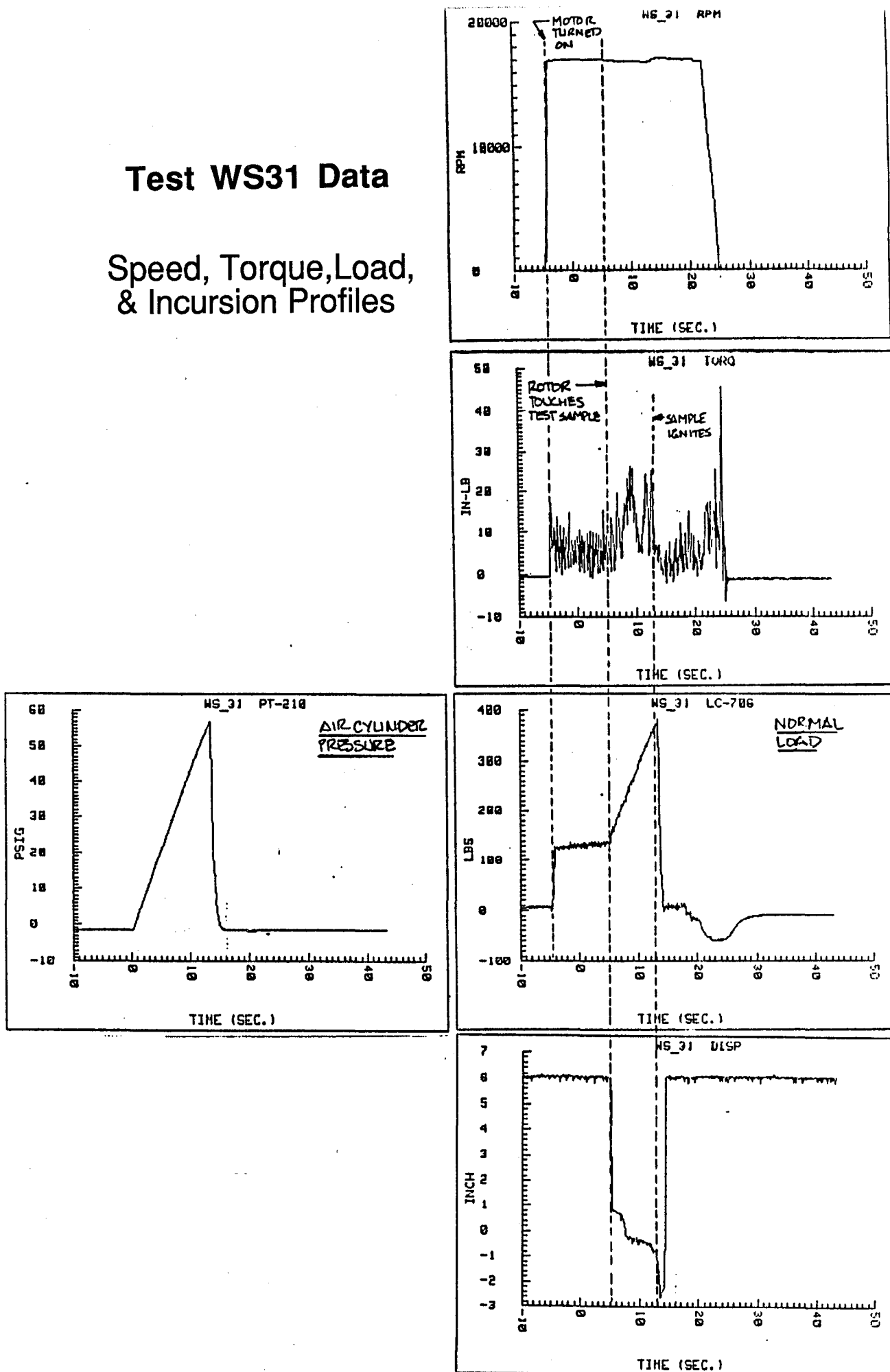


Figure 27

Test WS31: Temperature Distribution

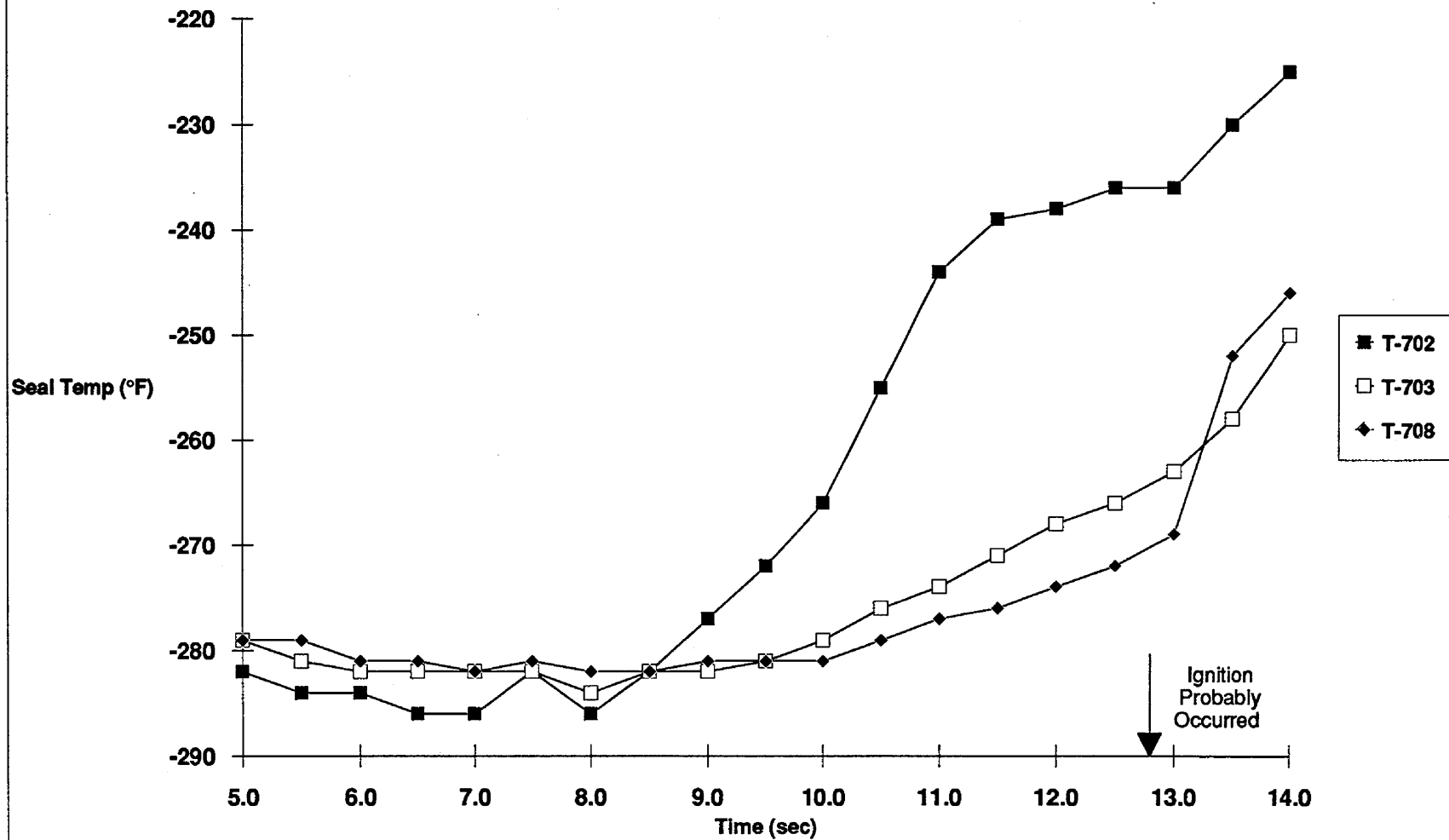


Figure 28

The tester chamber wall burned through at the locations of the chamber vent fittings. The seal specimen was totally consumed, as was most of the seal retainer. The 321 CRES shaft, shown in **Figure 29**, was burned through adjacent to the cavity near the annulus of the seal specimen by the rotor/seal contact. Notice that the INCO 718 test rotor was not destroyed and was only covered with slag from the CRES 321 shaft. A thorough failure investigation was conducted by the WSTF personnel which helped produce these conclusions. The incident report, generated by the WSTF investigation including action items and their dispositions, can be found in **Appendix A**.

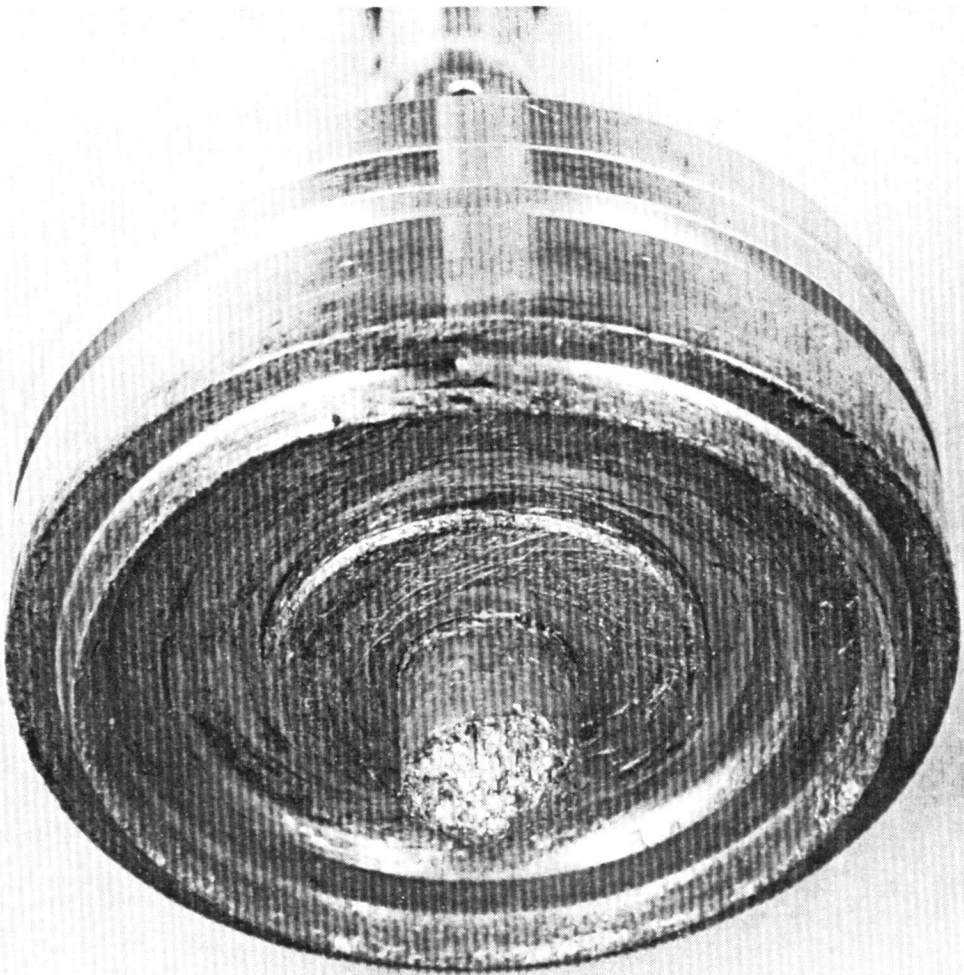
Three significant changes between RF tests WS30F and WS31 were believed to contribute to the failure; the increased speed from 6,200 to 17,000 rpm, the linearly increased applied load to 611 lbf, and reduced contact area (knife-edged) rotor. These changes effectively increased the planned PV product from just over 14,000 psi-ft/sec in Test WS30F to over 1,100,000 psi-ft/sec, to overcome the pumping and hydrostatic forces.

After a complete review of the test incident, the tester shaft was redesigned to eliminate the protruding bolt pattern on the aft end of the test rotor. The high axial loads produced by the initial design created significant pressure fluctuations in the test cavity which complicated the test operations and the repeatability of test conditions. The re-designed test rotor, P/N 7R032078, was machined integrally from raw material bar stock, eliminating all mechanical fasteners and protrusions. The contact tooth for this rotor was also modified to a width of 1.40 mm (0.055 inch) for a contact area of 187.5 mm² (0.291 in²). The same contract area was used for all the shafts fabricated after the incident. The goal of this selection was to obtain the basic wear and heat generation characteristics of the seal materials using a consistent and repeatable heat input. Shafts in this configuration were fabricated from Monel K-500, INCO 718, and A-286, as seen in **Figure 30**.

For structural reasons, the titanium rotor specimen, P/N 7R032079, was configured similar to the previous design. However, in place of the four bolts, a thin nut with threads on the outer diameter was used to secure the titanium sample to a A-286 shaft in the cavity between the rotor and seal contact zone. The 187.5 mm² (0.291 in²) contact area was also selected for this configuration. Two titanium rotor assemblies were procured and balanced.

In addition to the redesigned rotors, the seal specimens were also modified. Another theory that was expressed after WS31 was that the flow of LOX was significantly reduced into the cavity between the rotor and seal specimens when they contacted. Potentially, the reduced LOX flow

Test WS31
INCO 718 Rotor

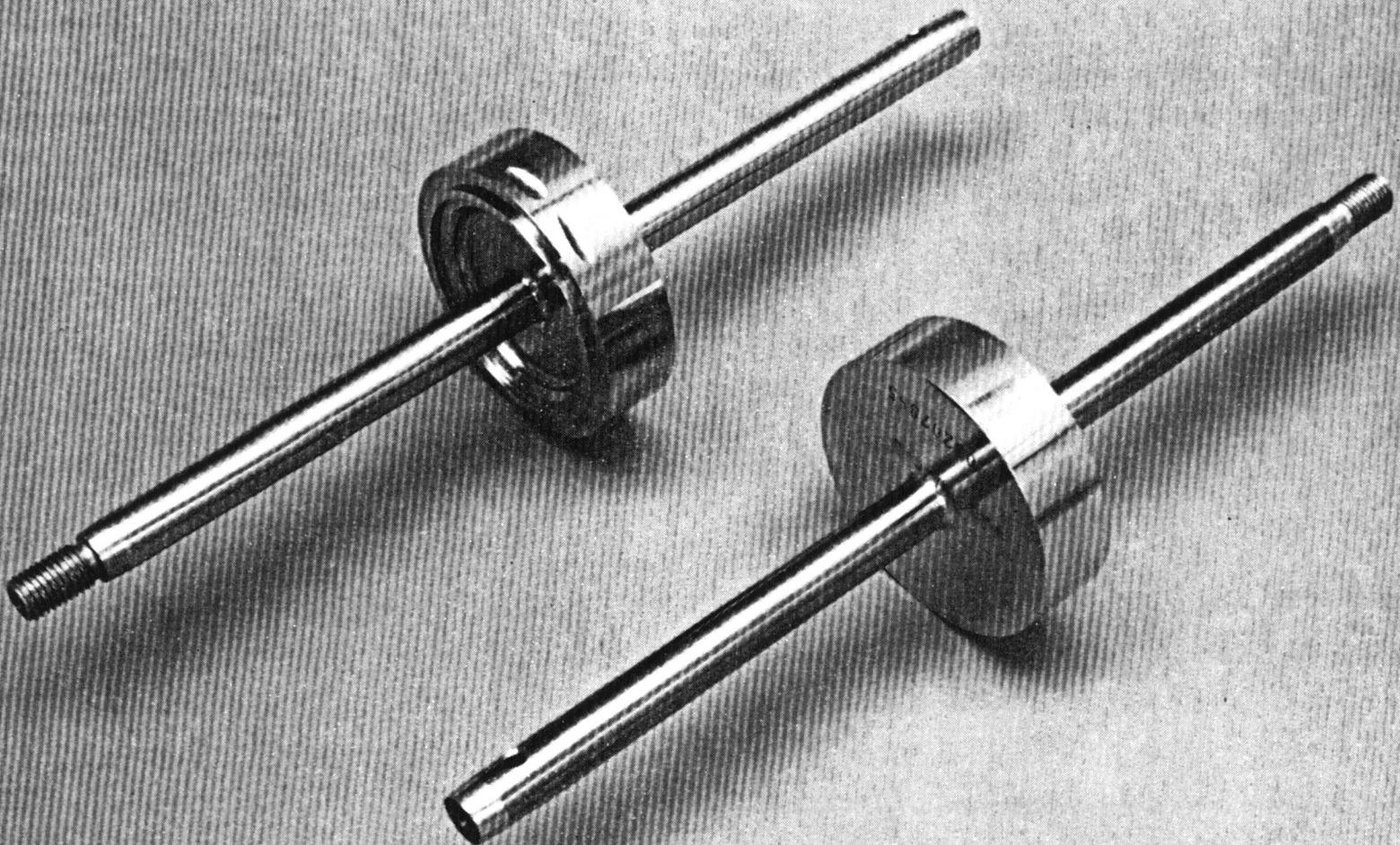


Test Rotor Face
Test Number WS-31
1-31-86

Figure 29

RI/RD90-214

Low Speed Friction and Wear Tester
Re-Designed Rotor Specimens



Rockwell International
Rockwell International

11/11/97/2/03-01

Figure 30

RI/RD90-214

into this area could not sufficiently convect the heat from the contact area, and was converted to gaseous oxygen. Since the heat transfer characteristics of gaseous oxygen are far poorer than LOX, the convective boundary was reduced and more heat was conducted into the seal. To ensure that sufficient coolant passed through this area, slots 0.100 inch wide and 0.100 inch deep were milled into the soft seal specimens creating a new flow path for the test fluid allowing more flow into the cavity between the contact.

During the downtime after test WS31, the positive displacement pump LOX supply system was installed. This modification increased the test durations from one minute to several minutes. In addition, better quality liquid oxygen was delivered to the test chamber. However, the pump produced pulsating pressure and flow which added noise to the tester system measurements.

Test WS01 was run in LN₂ instead of LOX as a check out of the re-designed hardware, however, these changes compromised the operation of the bushing bearing. Intermittent or continuous rubbing contact between the new rotor and bushing caused excessive heating and subsequent shaft seizures. The original configuration utilized a 321 CRES shaft and bronze bushing which worked well. The new design employed a bronze bushing rubbing against, in this case, Monel K-500. Both of these alloys contain percentages of copper by weight. The copper-copper rubbing interface had a high coefficient of friction, and excessive heat was generated. As the interface temperature increased, the operating clearance reduced eventually seizing the shaft in the bushing. The bronze bushing was then replaced with a Vespel SP211 bushing which seemed to have solved the problem when an INCO 718 rotor was used during the check out tests after WS01.

Upon completion of these checkouts, tests WS03A through WS5A were conducted using the redesigned K-Monel rotor and the Kel-F seal specimen. The tests yielded significantly lower pumping forces 25 to 30 lbf compared to 175 lbf, but still resulted in uneven wear. Post test inspections of the sample determined that adhesive build up around the thermocouples caused the seal to be cocked and consequently was not contacted uniformly by the rotor. The tests were repeated as test WS03B, 4B, 5B and WS06, and no test parameters were changed.

The test series from WS03B to WS06 included one 30 second SF test, after which the sample was replaced, followed by three consecutive 20 second RF tests. Light slightly uneven wear tracks were obtained. These samples were reviewed for wear volume loss. A few very small

filamentous wear debris were seen around the wear track. No measureable temperature rise in the Kel-F specimen was seen within the seal in any of the four tests.

Tests WS07 through WS10 were run with a Vespel SP211 sample under similar conditions as WS03B through WS06. Again light evenly distributed wear was seen, and no measureable temperature rise was observed.

Conducted similarly to the previous tests, WS11 through WS14 were run with a Polybon M seal specimen. Light, barely distinguishable wear was observed. It was evident that the applied load in the three previous test series was too low, and was nearly equal to the pumping force.

After these tests, blowdown tests WS01C,D, and E were run to determine if the pumping effect was a function of rotor axial position. In other words, as the rotor moved closer to the seal specimen, did the force holding the rotor away increase? The tests showed that the pumping load was independent of position. However, as seen in **Figure 31**, the axial load increased with time, probably due to the thermal interactions between the bushing bearing, seals, and the test shaft. It was possible that during the previous tests the seal and rotor were in contact for several seconds, but due to this increasing time-dependent force, the rotor was eventually lifted off the seal. In addition, the pulsating test chamber pressure delivered by the positive displacement pump probably contributed to the inconsistent wear.

Test WS03C was run with a new Kel-F specimen against the same Monel K-500 rotor as had been used since WS01, for a planned duration of 30 seconds. The applied axial load for this test was increased to 60 lbf due to the previous results at the lower loads. This test was terminated due to the maximum incursion (0.020 inch) after 5 seconds of contact. Although significant wear was produced, the internal temperature measurements did not increase from the established steady state temperatures. Post test inspections revealed copious quantities of filamentous wear product. The debris was found in the downstream filter, as well as throughout the test chamber (**Figure 32**) and around the shaft (**Figure 33**). This was expected, and was typical of Rocketdyne experience with Kel-F under these conditions. The sample was not available for profilometric measurements, so the incursion data was used in lieu of the detailed measurements. As seen in **Figure 34**, the initial contact of the rotor offset the signal of the displacement transducer by 0.014", and the actual wear due to the input PV was the remainder, 0.008" giving an erroneous cut off. No temperature rise, however, was measured within the seal.

Test WS01C: Axial Load vs Time

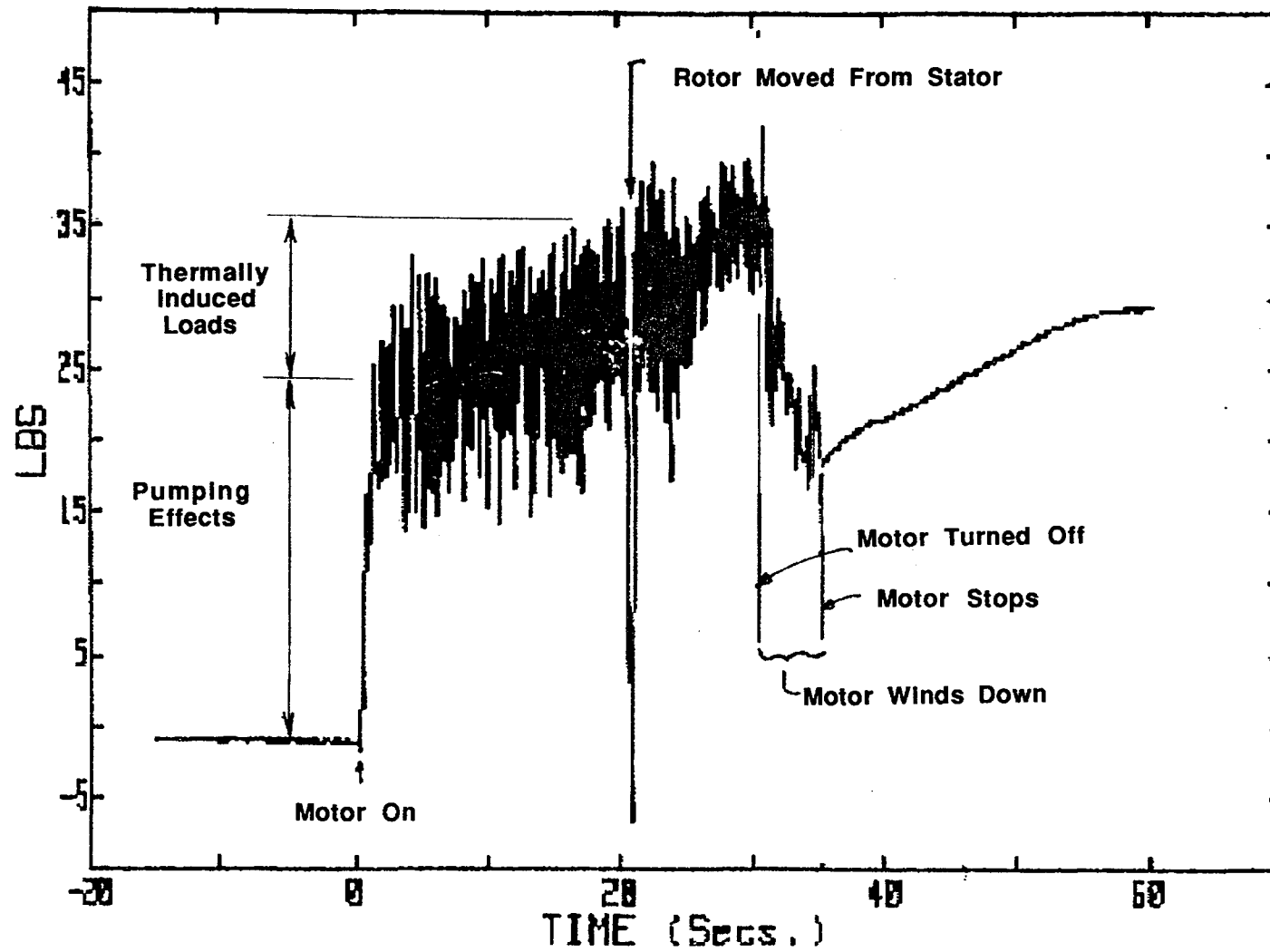


Figure 31

Test WS03C
Kel-F Wear Debris in Test Chamber

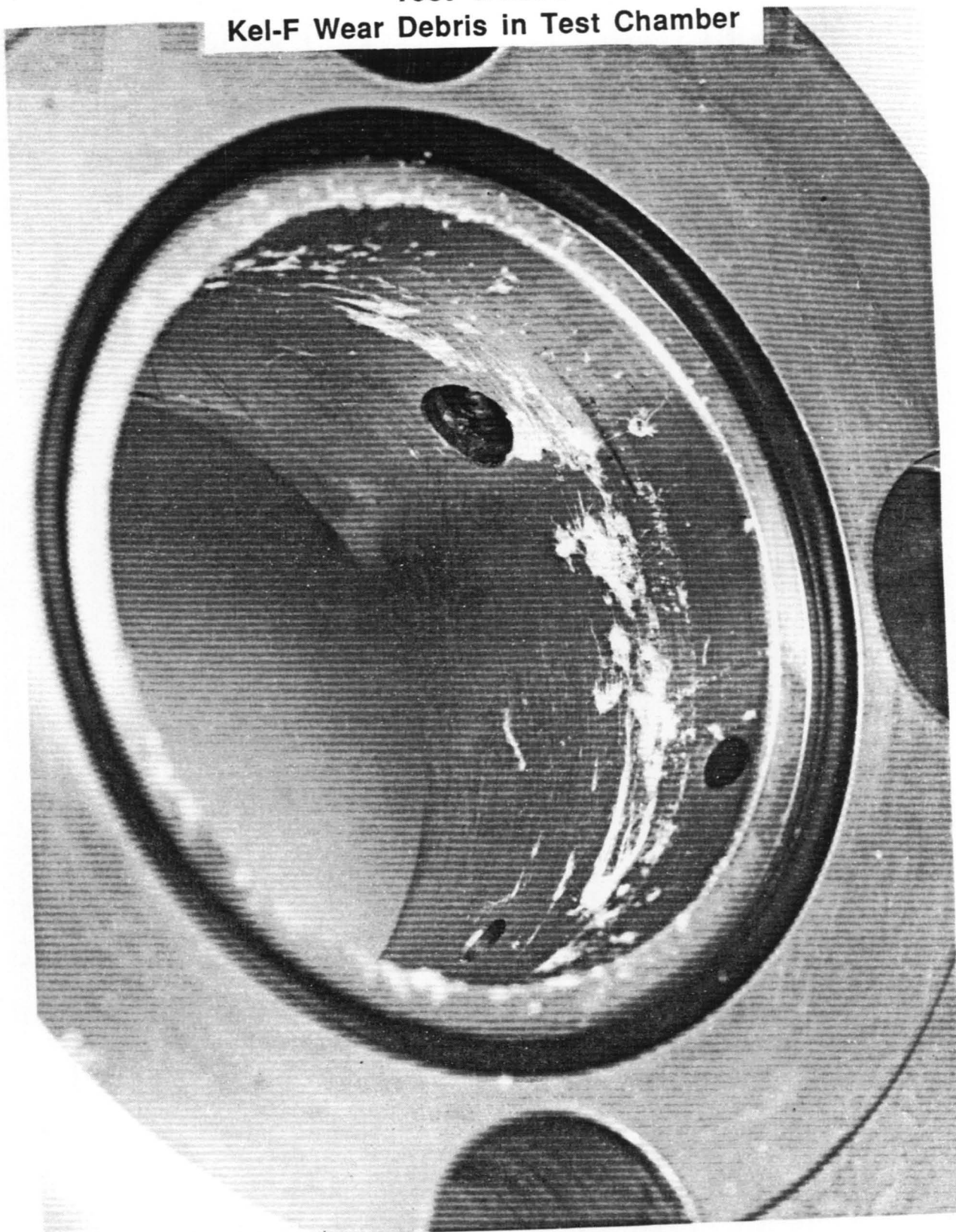


Figure 32

Test WS03C
Kel-F Wear Debris on Monel K-500 Rotor

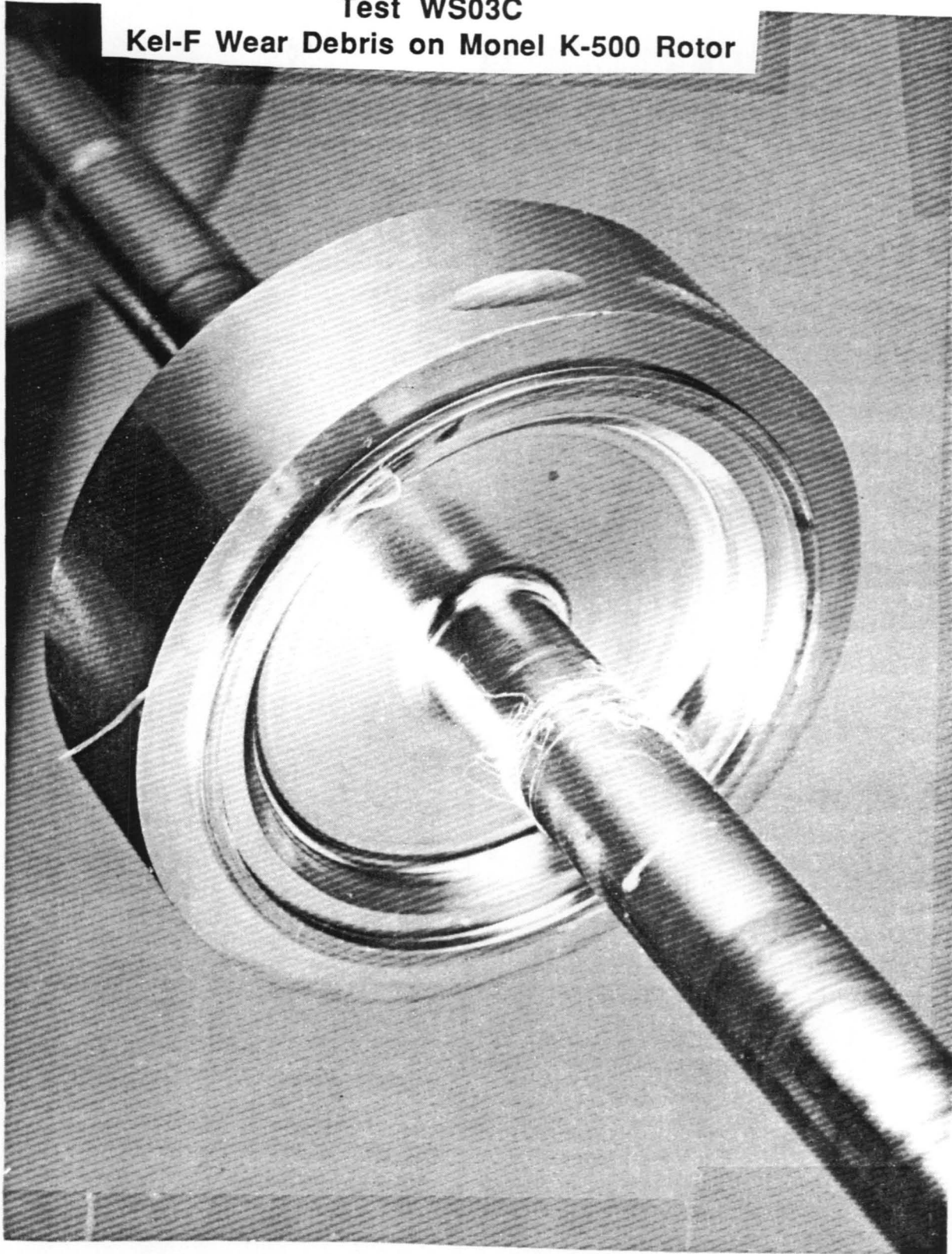


Figure 33

R/RD90-214
65

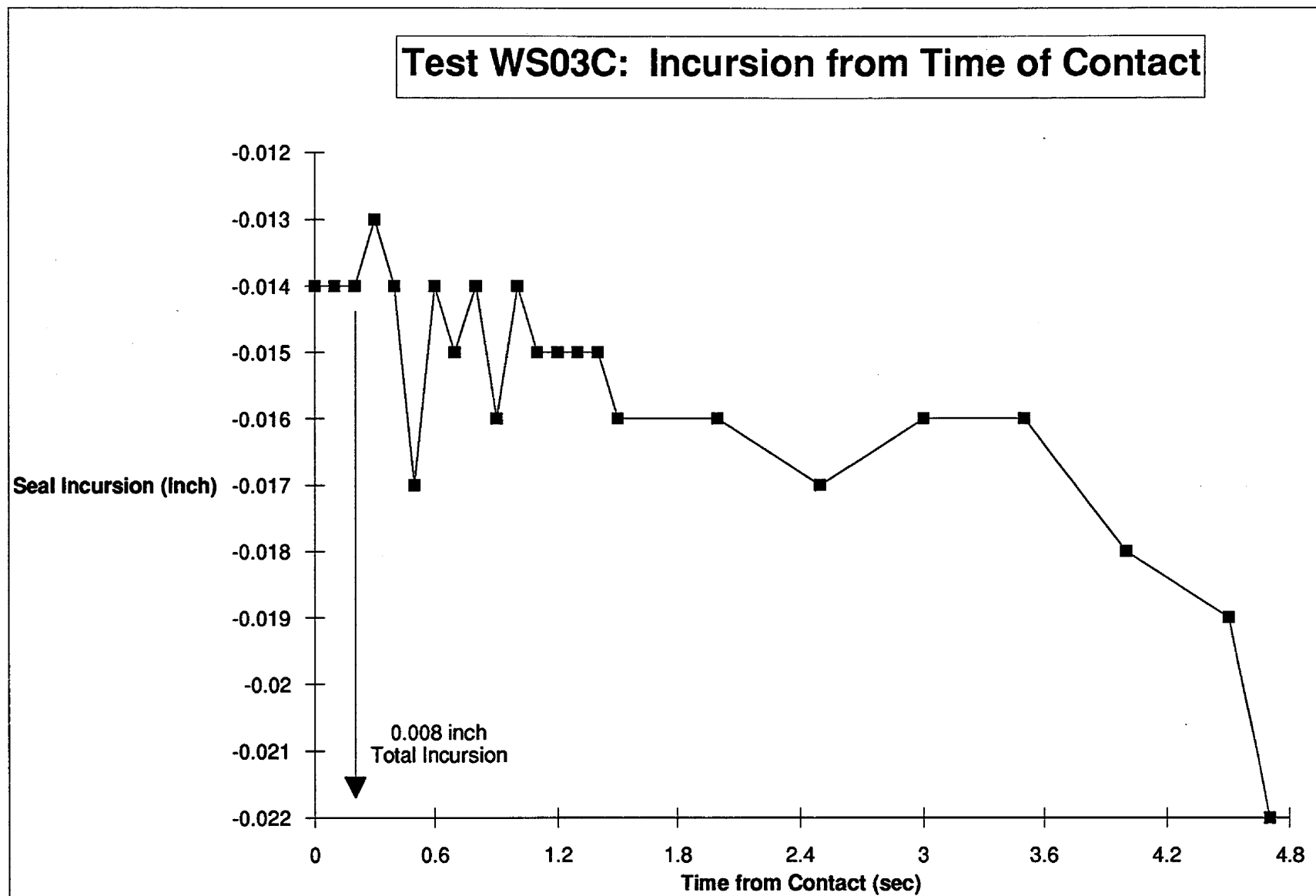


Figure 34

Prior to test WS04C, the purged gas seals were replaced because a low temperature spike was observed in the seal cavities during WS03C signifying a worn or failed part. During the check out test to verify the seal installation, the Monel K-500 shaft sheared into two pieces at the location of the bushing bearing near the pneumatic actuator. Excessive heat affected areas were seen on the bushing and ball bearing. The ball bearing had seized due to thermal-mechanical runaway and created a higher torque through the shaft whose properties were severely degraded by the rubbing induced temperatures. Upon replacement of the shaft seal and bushing and bearing, a check out test was successfully conducted.

Test WS04C was conducted using the same load conditions as WS03C but with the Vespel sample previously used in test WS07. The test ran the planned duration of 30 seconds, however, the tester shaft failed after approximately 22 seconds of rub time on the drive motor side stopping the rotor. The seal wear depth was significantly less than the Kel-F specimen of WS03C, about 0.00325 inch as measured using a profilometer. This is compared to the 0.003" obtained from the incursion data, as seen in **Figure 35**, using the same logic as WS03C. The seal sample indicated 28°C (50°F) temperature rise during the test. However, the temperature measured at TC-702 was not consistent with the other temperatures (**Figure 36**). Post test, heat effected areas were observed on the rotor rubbing face (**Figure 37**) and along the edges of the contact tooth. This test was run at the highest successful PV of 20,923 psi-ft/sec as calculated from the measured axial load shown in **Figure 38**. This seal specimen was reviewed further in the temperature and wear correlations section.

In contrast to the Kel-F specimen, Vespel SP211 and Polybon M generated undetectable wear debris. A 10 micron nominal filter was located downstream of the tester in the test chamber drain line. The filter was inspected after each test series was completed, and no debris was found.

The tester shaft failed, **Figure 39**, in a similar location as the previous failure, only on the opposite side of the test chamber, at the drive motor side bushing bearing. Post test inspections indicated the shaft failed in torsion just as the prior test. As seen in the photograph, the rotor was significantly heated and worn by the bushing bearing causing an eventual torsional overload due to degraded properties. The test program was terminated after this test.

Table 10 summarizes the results of the Running Friction tests that were conducted during this program. The running friction tests provided test data that was more easily reduced and compared to the predictions since the PV values during these tests were relatively constant, and

Test WS04C: Incursion from Time of Contact

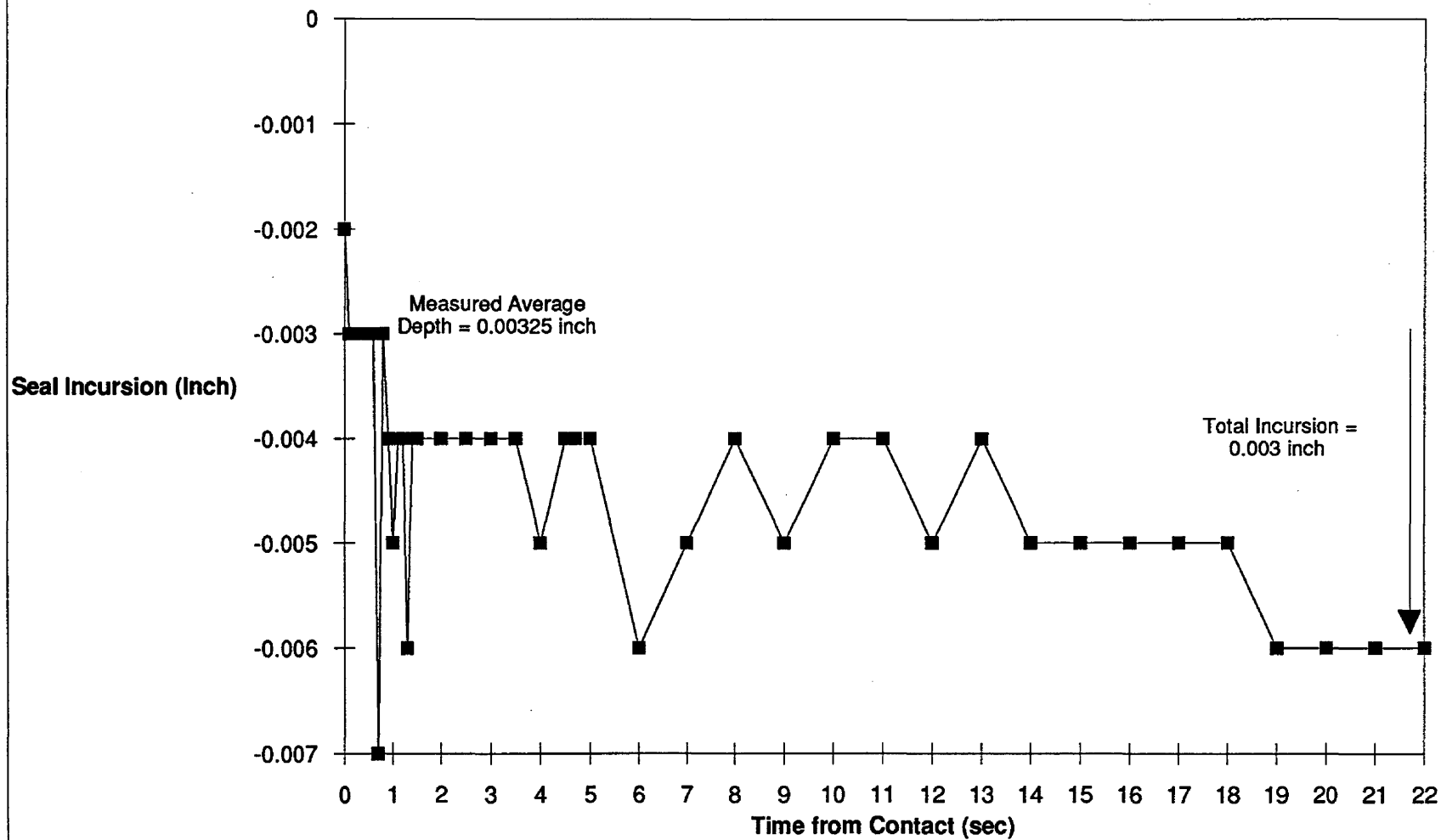


Figure 35

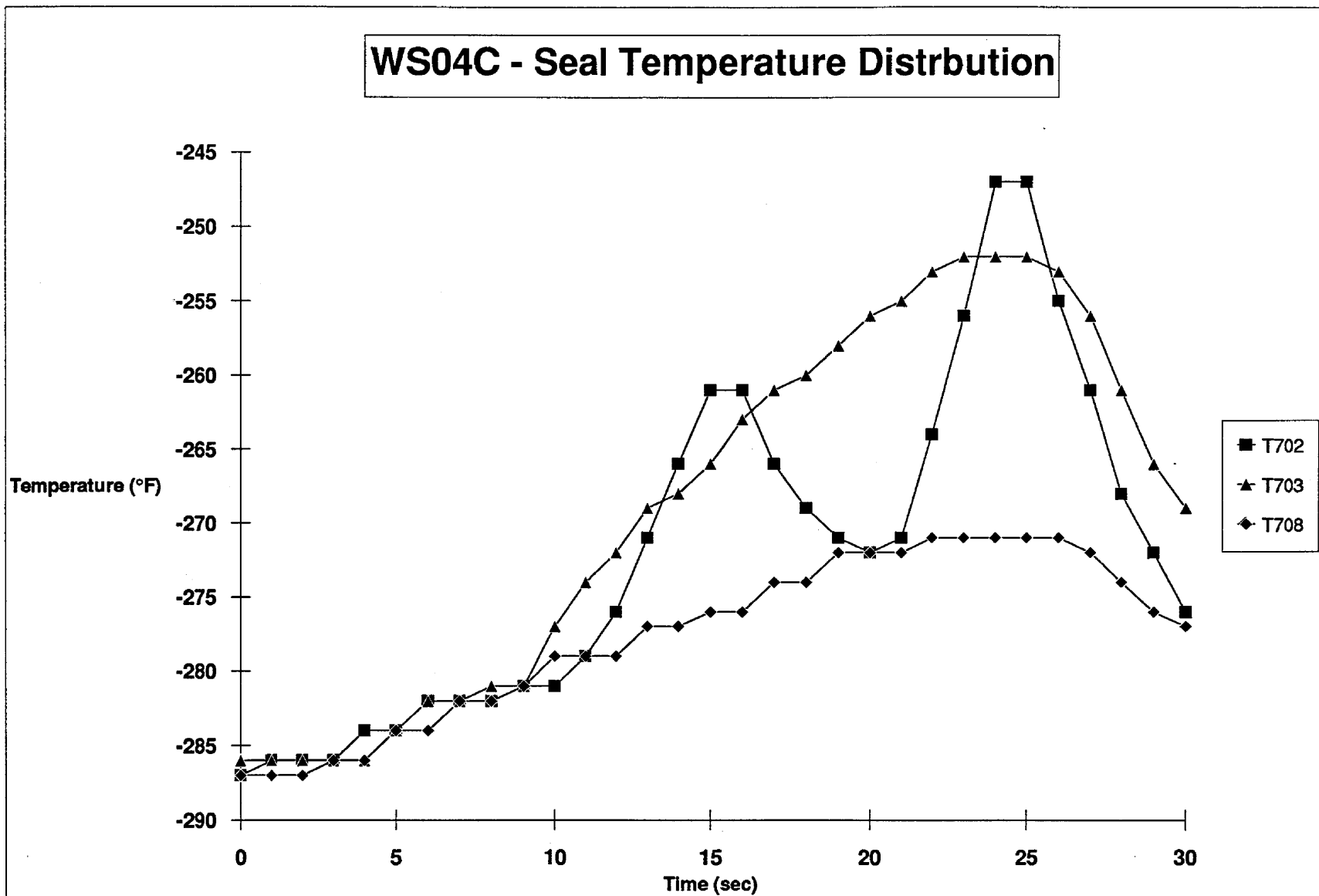
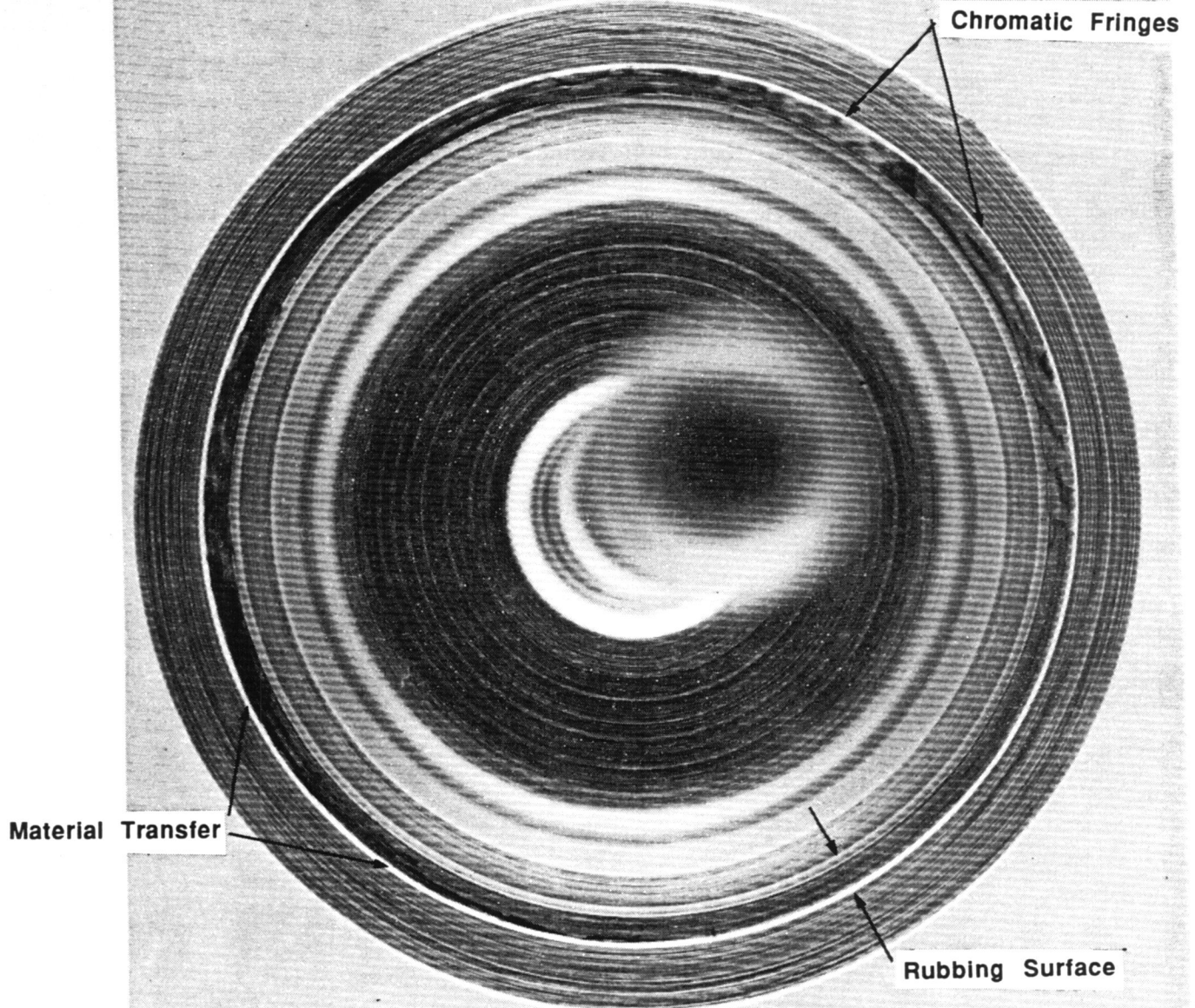


Figure 36

Test WS04C
Heat Effected Monel K-500 Rotor Face



Shaft End View

Figure 37

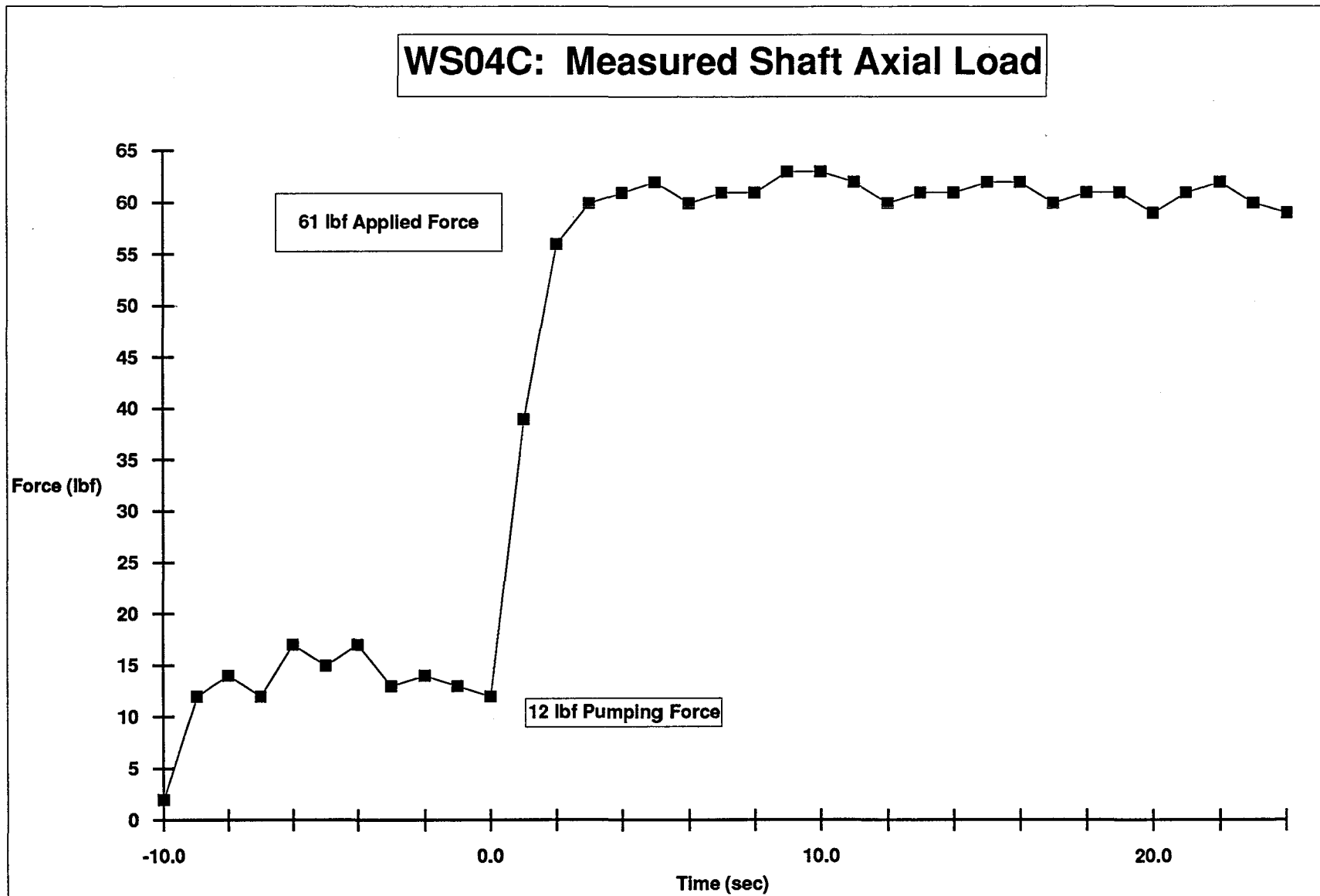


Figure 38

Test WS04C

Post Test - Monel K-500 Rotor and Bushing Bearing

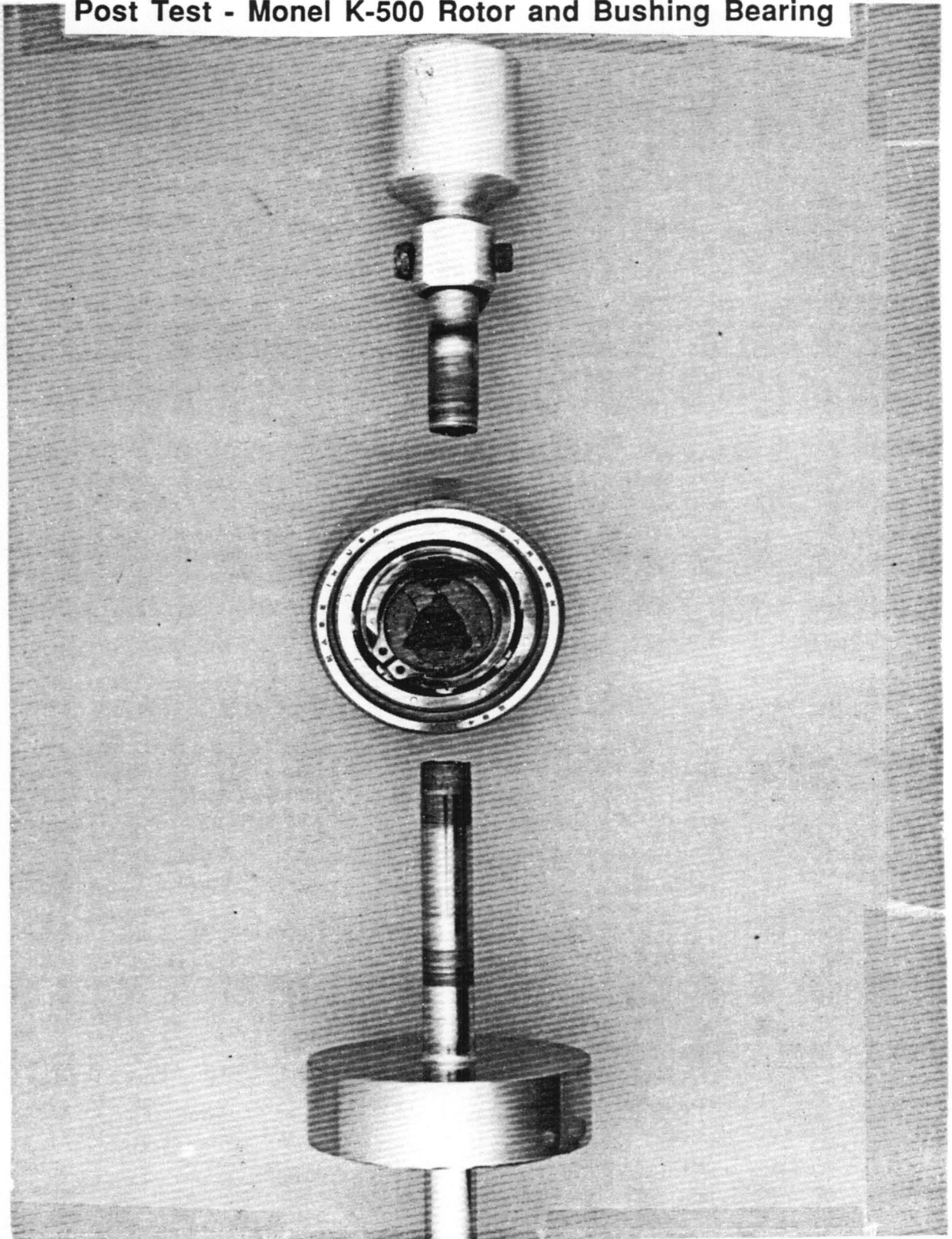


Figure 39

Table 10

Soft Wear Ring Seal Low Speed Test History in LOX

Running Friction Tests

Test Number	Test Date	Test Type	Soft Seal Sample	Test Rotor Sample	Test Duration (sec)	Applied Shaft Load (lbf)	Rotor Pumping Load (lbf)	Avg Shaft Speed (rpm)	Sliding Velocity (ft/sec)	Tare Torque (in-lbf)	Run Torque (in-lbf)	Contact Area (in ²)	Average PV psi-ft/sec	Dyn Coeff Friction μ	Wear Data (inch)	Wear Time (sec)	Wear Measured (inch)	LOX Start Temp (°F)	LOX C/O Temp (°F)
WS30F	1/17/86	RF	VespeI #2	K-500 #1	40.0	216.3	14.8	6,031	48.66	2.2	20.6	0.682	14,376	0.077	0.005	30.6	0.0006	-282	-267
WS31	1/31/86	RF	VespeI #3	Alloy 718#1	20.0	383.0	131.1	16,815	127.08	5.3	25.2	0.054	591,696	0.066	0.025	8.1	-	-282	-236
WS31 *	1/31/86	RF	VespeI #3	Alloy 718#1	20.0	363.0	131.1	16,730	126.43	5.3	25.2	0.054	541,964	0.072	0.018	7.3	-	-282	-282
WS04B	11/18/88	RF	Kel-F #2	K-500 #2	20.0	32.1	14.8	17,032	129.09	5.7	6.6	0.291	7,689	0.043	0.002	22.0		-275	-275
WS05B	11/18/88	RF	Kel-F #2	K-500 #2	20.0	31.8	15.1	17,044	129.18	4.6	5.3	0.291	7,424	0.035	0.000	23.0		-275	-275
WS06	11/18/88	RF	Kel-F #2	K-500 #2	20.0	32.6	15.6	17,050	129.23	5.1	6.0	0.291	7,577	0.044	0.000	22.0	0.0014	-273	-273
WS08	11/28/88	RF	VespeI #5	K-500 #2	20.0	31.5	16.1	17,036	129.12	9.5	6.1	0.291	6,838	-0.184	0.000	22.0		-278	-278
WS09	11/28/88	RF	VespeI #5	K-500 #2	20.0	32.0	23.0	17,054	129.26	6.0	6.0	0.291	4,003	0.000	0.000	20.0		-278	-278
WS10	11/28/88	RF	VespeI #5	K-500 #2	20.0	31.0	22.0	17,085	129.49	6.0	6.0	0.291	4,010	0.000	0.001	21.0	0.0001	-275	-275
WS12	12/9/88	RF	Polybon #2	K-500 #2	20.0	32.3	14.0	17,064	129.33	5.5	6.0	0.291	8,144	0.024	0.003	22.0		-278	-278
WS13	12/9/88	RF	Polybon #2	K-500 #2	20.0	32.3	21.0	17,078	129.44	5.5	5.5	0.291	5,033	0.004	0.000	21.0		-280	-280
WS14	12/9/88	RF	Polybon #2	K-500 #2	20.0	32.8	20.8	17,080	129.45	6.3	4.4	0.291	5,346	-0.132	0.000	21.0	**	-278	-278
WS03C	5/2/89	RF	Kel-F #3	K-500 #2	30.0	61.0	28.3	16,880	127.94	4.8	8.3	0.291	14,396	0.090	0.008	5.0	0.0080	-292	-264
WS04C	6/23/89	RF	VespeI #4	K-500 #3	30.0	61.0	13.0	16,713	126.67	0.0	0.0	0.291	20,923	0.000	0.003	22.0	0.0033	-292	-285

* Slice at 12.6 sec when Ignition Occured

** After WS14 - No Discernable Wear Track

the coefficient of friction could be extracted. Of the RF tests completed, Tests WS03C using Kel-F, and Tests WS30F, WS31, and WS04C using Vespel SP211 produced data that could be adequately investigated and correlated with analytical techniques.

SOFT SEAL DATA CORRELATION

Frictional Heating Theory

As a consequence of reduced seal operating clearances, rotor/seal contact will be an inescapable condition of operation. The seal will be contacted, whether it be instantaneous, intermittent, or continuous, during turbopump start and shut down transients, particularly during transitions through rotor critical speeds. Structurally, the seal materials must be capable of reacting these transient loads and maintaining the interference fits which are necessary to circumferentially and axially locate the seal. Coupled with these loads, extremely high rubbing velocities must be contended, especially in the turbine where tip speeds can be as high as 488 m/sec (1600 ft/sec). The environment within the seal annulus is one of the most severe in the entire turbopump, and seal survivability is key to the performance and reliability of the turbopump.

The rubbing interactions described above can be classified as a frictional heating contact where the kinetic energy of the rotor is transferred to the contact surface. The seal survivability depends on the thermal, mechanical, and chemical mechanisms for dissipating this energy.

Heat Input. The physical interface between the rotor and the seal can be described as a pure rubbing contact. Assuming a semi-infinite solid and a perfect sliding contact, the heat rate generated by friction at the rubbing interface can be described by:

(Eq. 2)

$$Q_f = \mu PVA/J ,$$

where μ is the coefficient of friction, P is the contact pressure, V is the sliding velocity, A is the contact area, and J is the mechanical equivalent of heat. Within the seal itself, the contact load and rubbing speed varies greatly with each seal application. In this analysis, it was assumed that the rotor and seal rubbing contact was continuous, which produced the maximum possible heat generation. At the contact area of the seal and the rotor, the frictional heat rate is transferred to both the rotor and the seal component, as shown:

(Eq.3)

$$Q_f = Q_{\text{seal}} + Q_{\text{rotor}} ,$$

where Q_{seal} is the heat rate into the seal and Q_{rotor} is the heat rate into the rotor. As determined from the transient one-dimensional conduction equation, assuming the contact surface temperature was equal for each component, the ratio of heat rate conducted into each component was defined by:

(Eq. 4)

$$\frac{Q_{\text{Seal}}}{Q_{\text{Rotor}}} = \sqrt{\frac{(k C_p \rho)_{\text{Seal}}}{(k C_p \rho)_{\text{Rotor}}}}$$

The material properties k (thermal conductivity), C_p (specific heat), and ρ (density) of each rubbing material were assumed constant. Therefore, the heat input into the seal can then be defined as:

(Eq. 5)

$$Q_{\text{Seal}} = \frac{Q_{\text{Friction}}}{1. + \frac{1.}{\left(\frac{Q_{\text{Seal}}}{Q_{\text{Rotor}}}\right)}}$$

The heat rate into the metallic rotor component is much greater than that of the polymer seal material due to its significantly higher thermal conductivity and density. For example, the thermal conductivity of Monel K-500 is 10.3 BTU/in-sec-°F, while Vespel SP211 is 0.28 BTU/in-sec-°F. For this material combination at room temperature, the heat load into the rotor is nearly ten times greater than the heat load into the soft seal. Although the heat input to the seal is small compared to the rotor, the low thermal conductivity creates a very steep thermal gradient, and consequently relatively high temperatures at the the rubbing surface.

However, like most metals, the thermal and mechanical properties of polymeric materials vary greatly over a wide temperature range. For Monel K-500 and Alloy 718, rotor materials used in this program, the thermal conductivity as a function of temperature follows the same rate of change, as seen in **Figure 40a**. A normalized ratio of thermal conductivity over the thermal conductivity at room temperature was used to represent the change in properties.

The soft seal materials have not been extensively tested, so many of the material properties were available only at room temperature. The graphite filler used in Vespel SP211 (15% by wt.) and Polybon M (30% by wt.) increases the thermal conductivity of the base polyimide significantly. However, the continuous phase, the polyimide in this case, would dominate the thermal

Thermal Conductivity versus Temperature

Thermal Conductivity of Typical Ni Based Alloys

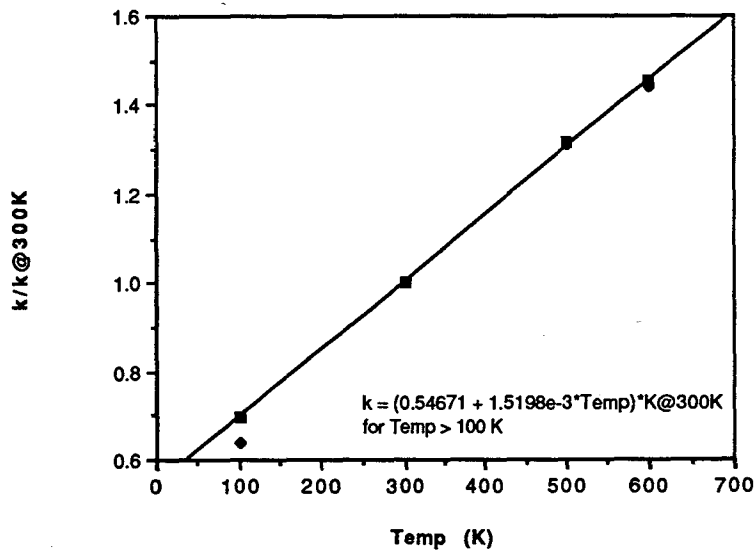


Figure 40a

Alloy and Thermoset Thermal Conductivity

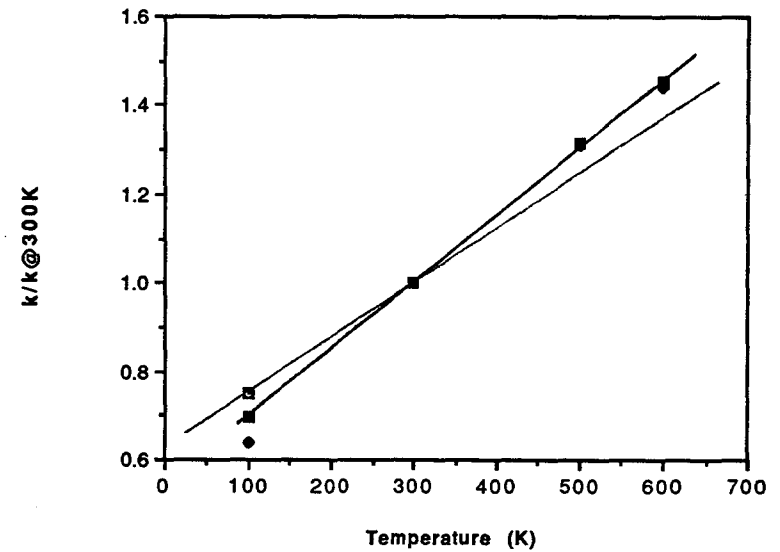


Figure 40b

conductivity as a function of temperature. **Figure 40b** compares the thermal conductivity as a function of temperature for a typical thermoset resin (without fillers), for which data were available and the rotor alloys shown previously. Only the slightly different slopes of the thermoset resin and alloy lines probably indicate a potential change in the heat split from the room temperature calculations. Based on the small difference in slope, the heat split would be relatively small. Heat capacity as a function of temperature was not available so this comparison could not be made.

Heat Dissipation Mechanisms. For polymers the maximum useable temperature is usually lower than for metallic rotor materials. Therefore, the seal must effectively dissipate the heat input so that the bulk temperature of the seal does not exceed the useable limit. By the conservation of energy, the heat rate into the seal must equal the heat dissipated by conductive, convective, radiant, mechanical, and chemical mechanisms as described by:

(Eq. 6)

$$Q_{\text{seal}} = Q_{\text{conduction}} + Q_{\text{convection}} + Q_{\text{radiation}} + Q_{\text{mechanical}} + Q_{\text{chemical}}$$

Conduction. The temperature distribution within the seal can be determined using a two dimensional time dependent conduction equation with constant heat generation as defined by:

(Eq. 7)

$$\frac{\partial^2 T}{\partial x^2} + \frac{1}{r} \left(r \frac{\partial^2 T}{\partial r^2} \right) + \frac{g(x,r)}{k} = \frac{1}{\alpha} \frac{\partial T}{\partial t}$$

Thermal Diffusivity; $\alpha = k/C_p \rho$

where $g(x,r)$ is the seal heat input as a function of x and r . If perfect contact is made by the rotor, the temperature variation in the circumferential direction can be ignored. In reality, contact between the rotor and the seal will never be perfect, and a circumferential load profile will exist due to rotor to stator misalignment. This effect was considered to be a small effect and has therefore been neglected. This equation also assumes a constant thermal conductivity, specific heat, and density, so changes in the thermal properties with temperature were ignored. As seen in the previous figures this was not the case, but due to the limited data available, these characteristics were ignored.

Convection. The boundary conditions around the contact zone can significantly effect the seal temperature distribution within the seal. Convection terms can dominate the heat transfer due to the high velocity fluid swirling through the seal annulus. The Kapinos equation (2) for two

rotating disks, separated by a specific gap, has been used to calculate the heat transfer coefficient on the wear ring seal face.

(Eq. 8)

$$h_c = 0.035 \text{ Re}_{r_o}^{0.7} \text{ Re}_s^{0.1} \left(\frac{r_i}{r_o} \right) \left(\frac{2a}{r_G} \right)^{1.06} \left(\frac{k}{2a} \right)$$

where (Eq. 9)

$$\text{Re}_{r_o} = \frac{\rho \omega r_o^2}{\mu} \text{ and } \text{Re}_s = \frac{\dot{w}}{2\pi(2a)\mu}$$

h_c = heat transfer coefficient

r_i = disc inner radius

r_o = disc outer radius

r_G = average disc radius

$2a$ = gap between discs

ω = disc angular speed

ρ = Fluid density

k = Fluid thermal conductivity

μ = Fluid dynamic viscosity

\dot{w} = Fluid flow rate

The rotational Reynolds number for the equation above is about 3.6×10^6 , using LOX at 300 psi and test WS30F conditions ($N_{\text{shaft}} = 6031 \text{ rpm}$, $V_{\text{tangential}} = 55.6 \text{ ft/sec}$). The average heat transfer coefficient for the seal surface is estimated to be $0.00148 \text{ BTU/in}^2\text{-sec-}^\circ\text{F}$ using the equation above.

The influence of boiling on heat transfer from the seal surface can be made by comparing dimensionless parameters for boiling and forced convection. The two phase Grashof number, defined below, is usually the dimensionless parameter used to evaluate pool (natural convection) boiling.

(Eq. 10)

$$\text{Gr} = \frac{r_o^3 \rho_{\text{vapor}} (\rho_{\text{liquid}} - \rho_{\text{vapor}}) g}{\mu_{\text{vapor}}^2}$$

The ratio of the two phase Grashof number and the square of the rotational forced convection Reynolds number can be used to compare heat transfer effects. When this ratio is less than 0.1, then

boiling can usually be neglected; conversely when this ratio is greater than 10 then forced convection can be considered negligible.

(Eq. 11)

$$\frac{Gr}{Re_{r_0}^2} \left\{ \begin{array}{l} \leq 0.10 \text{ Neglect Boiling} \\ \geq 0.10 \text{ and } \leq 10. \text{ Include Both Effects} \\ \geq 10. \text{ Neglect Forced Convection} \end{array} \right\}$$

The two phase Grashof number using O₂ at 300 psi and saturated conditions, is 6.5×10^{10} ; and the ratio Gr/Re^2 is 0.005. Therefore boiling heat transfer can be considered a negligible effect compared to rotational forced convection.

Radiation. Since the bulk temperature of the seal is not much different than the surrounding housing temperatures, the effect of radiant heat transfer is very small. The large forced convection term in LOX dominates the heat transfer by maintaining bulk temperatures. When testing rubbing metallic cylinders in gaseous oxygen, this term would become more significant since gaseous oxygen is a poor convective heat transfer medium and the metallic sample temperatures are much higher than their surroundings. The forced convection heat transfer coefficient can be compared to an effective radiation heat transfer coefficient that is defined by the following equation.

(Eq. 12)

$$h_{\text{radiation}} = \frac{\sigma(T_1^2 + T_2^2)(T_1 + T_2)}{\frac{1}{\epsilon_1} + \left(\frac{A_1}{A_2}\right)\left(\frac{1}{\epsilon_2} - 1\right)}$$

A conservative estimate of the radiation heat transfer from the seal surface can be made by using this equation with an assumed seal surface temperature of 538°C (1000°F), a chamber wall surface temperature of -176°C (-285°F), and an emissivity of 0.80 for both seal and chamber wall surfaces. The radiation heat transfer coefficient is 7.81×10^{-6} BTU/in²-sec-°F, using these assumed conditions. The rotational forced convection heat transfer coefficient is about 140 times larger than the radiation term, which indicates that radiation heat transfer can be neglected. Typically, heat transfer effects an order of magnitude less than competing effects are considered negligible.

Mechanical. Mechanical processes contribute to the heat dissipation through adhesive wear and mechanical distortion. The simplest loss of heat would be by removal of material from the contact surface through actual machining or by wear. Work terms can be developed for these

processes, however, they were currently not available. In the case of Kel-F, which is relatively soft and the thermal conductivity is low, this term was significant. Extensive thermal and mechanical properties tables as a function of temperature would be required to completely evaluate this mechanism.

Chemical. The final heat dissipation mechanism considered was for chemical changes to the seal created by the rubbing energy input. Heat rate terms for phase change, oxidation, and dissociation were considered but were not developed due to the lack of available information about these materials in these environments. Chemical terms can behave in different ways, for example a phase change is an isothermal process, where oxidation can be an endo- or exothermic reaction. Not enough information exists on the subject to consider these phenomena. This term can become very significant at high PV's as the frictional heating model uncovered from test WS31.

Frictional Heating Model Description

The temperature distribution of soft wear ring seal test specimens has been determined for several key running friction tests. A 2-D axisymmetric thermal model was generated which simulated the test seal specimen and seal retainer, using the ANSYS computer code. A cross-sectional view of the wear ring seal model is shown in Figure 41, which also shows a view of how the wear ring seal was installed in the Low Speed tester. The temperature output of the model was compared with the data from the three thermocouple locations within the soft seal samples.

Frictional heat generation between the seal surface and rotor was calculated from the test data, using the following equation using information from Eqs.(1) & (2):

(Eq. 13)

$$Q_{\text{Friction}} = \frac{\mu F_n V}{778.}$$

Q_{Friction} = Frictional heat load, BTU/sec

F_n = Applied shaft load - Rotor pumping load, lbf

V = Rotor sliding velocity, ft/sec

μ = Coefficient of friction between rubbing surfaces (from Eq. 1)

The heat split between the seal and rotor rubbing surfaces was then determined using Eq (4) & (5). Thermal conductivity, specific heat, and density were obtained for the seal from the Material

Frictional Heating Model Configuration

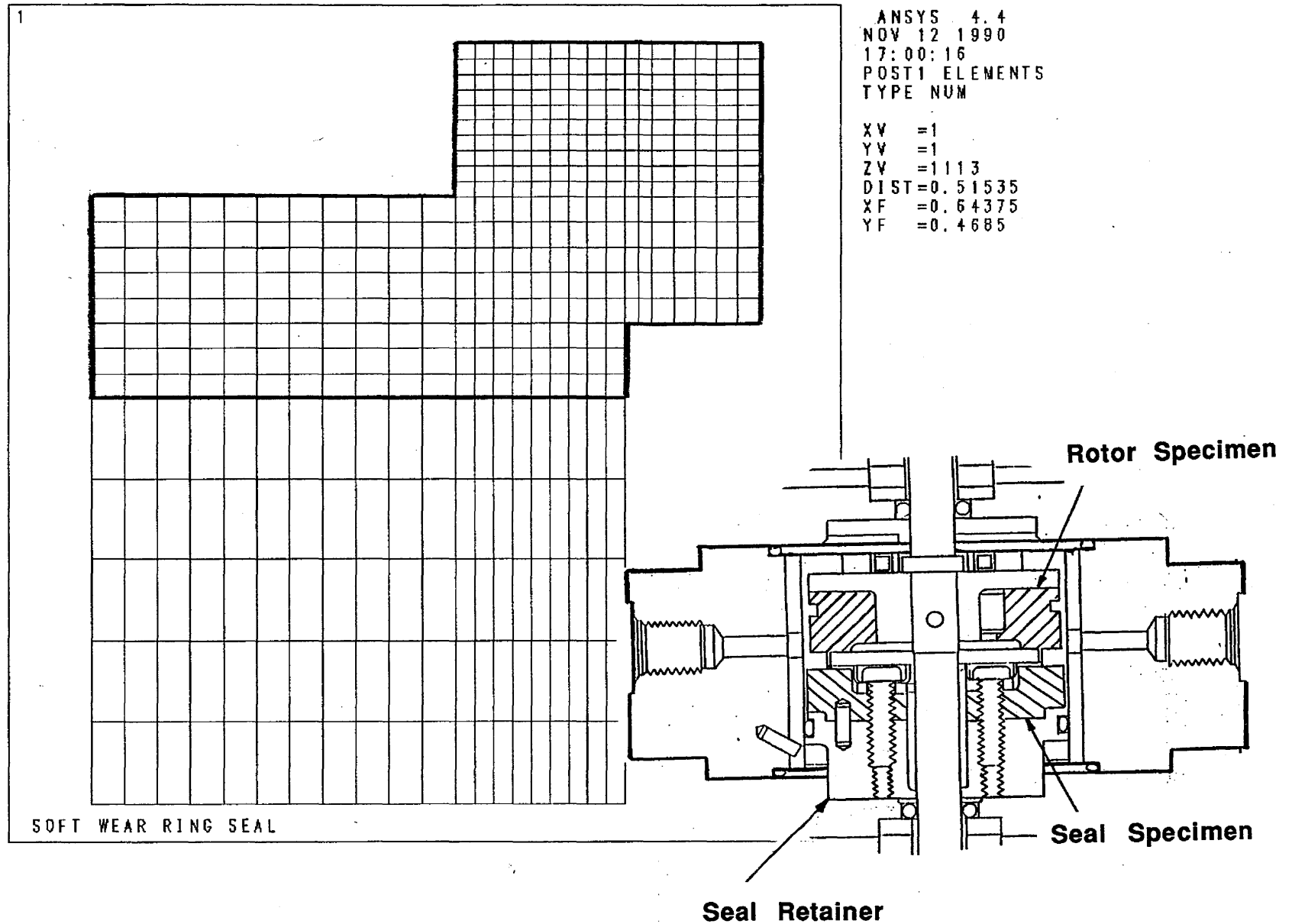


Figure 41

Properties test data (Table 2) and for the rotor from material standards handbooks. The heat load into the wear ring seal was then calculated. The rotor contact surface area was calculated from the rotor outer diameter and the rotor width, w_{Rotor} , and used for the heat input location.

(Eq. 14)

$$A_S = \pi (OD_{\text{Rotor}} - w_{\text{Rotor}})(w_{\text{Rotor}})$$

Liquid oxygen at 300 psi and -285°F (at the start) passed through the tester at a flow rate of 50 lb_m/min. Two primary flow paths, of approximately equal rate, flowed around the circumference of the seal and through the slots in the wear ring seal face (Figure 18). The primary source of convective heat removal from the wear ring seal was from the seal face, near the contact area between the seal and rotor. The LOX flowed through the slots, as well as around the rotor and seal contact area, providing direct cooling to the seal face all around the contact area. LOX also flowed between the seal and the retainer to provide additional coolant. The slots were present in the seal face after the incident of test WS31. The model was created with the slots for simplicity. Therefore the temperature profiles predicted in tests WS30F and WS31 may be slightly less accurate.

The heat transfer coefficient on the seal face, was calculated from Eq. (8) & (9) near the rotor/seal rubbing surface. This term had a strong influence on thermal gradients through the sample seal. Seal temperatures were determined by the thermal model for one Kel-F test, WS03C and three Vespel SP211 tests WS30F, WS31, and WS04C. By adjusting the frictional heat load in the seal thermal model, the temperatures profiles seen in the test data were matched. Frictional heat load into the seal is proportional to load, speed, and the coefficient of friction; and for each test load and speed are measured constants, but the coefficient of friction was calculated from tare torque and operating torque measurements. Due to the inaccuracy of this type of calculation, the heat load was adjusted by varying the coefficient of friction. A constant frictional heat load (except Test WS31 where a linear ramped load was duplicated) and coefficient of friction was applied to the seal thermal model throughout a specific test. The seal model temperature at the thermocouple location closest to the rubbing surface (which is .125 in. from the seal surface) was particularly used to match the test data. Table 11 summarizes the materials, heat split, seal heat load, coefficient of friction and rubbing contact duration for each test.

Frictional Heating Model Results

Kel-F - WS03C. Although, the measured temperatures for test WS03C never exceeded the local propellant temperature, the excessive wear provided by this test was of interest, so a case

was run to estimate the rubbing surface temperature. The duration of the test was only 5 seconds, and the test was terminated due to an incursion limit redline. The coefficient of friction used in the thermal model ($\mu = 0.09$) was the value calculated from the torque data. The maximum surface temperature of the Kel-F was estimated to be 722 °F which far exceeds the melting temperature of this material. This indicates that the seal was operating at or near its melting temperature. Fluoroplastics, like Kel-F, lose their mechanical properties at elevated temperatures. The excessive wear would indicate a local "softening" in the heat affected area and removal due to localized shear failure. This loss of material would relieve the load and allow quenching of the contact area. The model predicted that the heat load over the rub duration was not sufficient to increase the seal temperatures at the thermocouple locations, even though the model did not account for the material loss, as seen in the tabular output from the model in Table 12.

Table 11
Frictional Heat Model Input

Test Number	Seal Material	Rotor Material	$\frac{Q_{Seal}}{Q_{Rotor}}$	Q _{Seal} Seal Heat Load		Coefficient of Friction, μ		Wear Time (sec)
				BTU/sec	Watts	Model	Data	
WS03C	Kel-F	K-Monel	0.067	0.0304	0.534	0.090	0.090	5.0
WS30F	Vespel	K-Monel	0.114	0.0498	0.875	0.039 +	0.078	30.6
WS31	Vespel	Alloy718	0.142	0.338†	5.95	0.066	0.066	8.1
WS04C	Vespel	K-Monel	0.114	0.0656	1.15	0.082	*	22.0

§ Heat Split Calculated from Material Properties at 20°C (70°F).
+ μ used to match test data.
† Does not include Heat of Reaction of Vespel
* No torque data available

Table 12
Frictional Heating Model Results

Temperature vs Time at the Three Thermocouple Locations

Test	Time (sec)	Calculated Surface Temperature		Calculated Location 1 TC-702		Calculated Location 2 TC-703		Calculated Location 3 TC-708	
		°F	°C	°F	°C	°F	°C	°F	°C
WS03C Kel-F & KMonel	0.1	-222.8	-141.5	-285.0	-176.1	-285.0	-176.1	-285.0	-176.1
	2.0	433.8	223.3	-285.0	-176.1	-285.0	-176.1	-285.0	-176.1
	3.0	573.8	301.0	-285.0	-176.1	-285.0	-176.1	-285.0	-176.1
	4.0	662.1	350.1	-285.0	-176.1	-285.0	-176.1	-285.0	-176.1
	5.0	721.8	383.2	-285.0	-176.1	-285.0	-176.1	-285.0	-176.1
WS30F Vespel & KMonel	0.1	-238.8	-150.4	-285.0	-176.1	-285.0	-176.1	-285.0	-176.1
	5.0	204.6	95.9	-276.6	-171.4	-283.2	-175.1	-284.8	-176.0
	10.0	287.7	142.1	-251.0	-157.2	-271.9	-168.8	-281.9	174.4
	15.0	321.5	160.8	-228.9	-144.9	-257.6	-160.9	-275.5	-170.8
	20.0	339.0	170.8	-212.9	-136.0	-245.2	-154.0	-268.2	-166.8
	25.0	349.3	176.3	-201.5	-129.7	-235.5	-148.6	-261.4	-163.0
	30.0	355.8	179.9	-193.4	-125.2	-228.0	-144.4	-255.7	-159.8
WS31 Vespel & Alloy 718	0.1	-83.5	-64.2	-285.0	-176.1	-285.0	-176.1	-285.0	-176.1
	2.0	1000	537.8	-284.3	-175.7	-285.0	-176.1	-285.0	-176.1
	5.0	1000	537.8	-266.9	-166.0	-282.9	-174.9	-284.0	-175.5
	6.0	1000	537.8	-256.9	-160.9	-280.7	-173.7	-282.9	-174.9
	7.0	1000	537.8	-245.9	-154.4	-277.8	-172.1	-281.1	-173.9
	8.0	1000	537.8	-234.9	-148.3	-274.3	-170.2	-278.8	-172.7
	8.1	1000	537.8	-233.8	-147.7	-273.9	-169.9	-278.4	-172.4
WS04C Vespel & KMonel	0.1	-142.6	-97.0	-285.0	-176.1	-285.0	-176.1	-285.0	-176.1
	5.0	500.8	260.5	-277.7	-172.0	-283.3	-175.2	-284.8	-176.0
	10.0	520.8	271.6	-259.8	-162.1	-275.0	-170.5	-282.5	-174.7
	15.0	526.1	274.5	-248.0	-155.5	-266.4	-165.8	-278.3	-172.4
	20.0	528.7	276.0	-240.8	-151.5	-261.3	-162.9	-274.1	-170.0
	22.0	529.3	276.3	-238.7	-150.4	-258.2	-161.2	-272.6	-169.2

VespeI SP211 - WS30F. The maximum seal surface temperature estimated for test WS30F was about 356°F. The actual wear ring seal surface indicated a non-uniform wear pattern, with approximately 85% of the wear ring seal surface in contact with the rotor during the test. For the axisymmetric thermal model, the heat load was distributed uniformly over the contact area, so the thermal model should under predict the actual seal surface maximum temperature. Although the thermocouples were at different circumferential locations around the seal, the points of greatest wear were aligned with these measurements, so the temperature profiles were useful data.

The closest thermocouple to the rubbing surface was still relatively far from the actual contact zone. The steep thermal gradients caused by the low thermal conductivity makes these comparisons less accurate for predicting surface temperatures. For Test WS30F, thermocouple TC-702, located 0.125 inch from the surface, measured a temperature of -125°C (-193.°F) after 30 seconds of rubbing. **Figure 42 through 44** shows a comparison of the measured temperatures and the frictional heating thermal model predictions. **Figure 45** shows a composite comparison of the model predictions against the actual measured thermocouple data. The measured values were slightly higher than the predicted. By slightly increasing the heat load, the temperatures could be matched better. When the coefficient of friction calculated from the test data was used (0.078), the surface temperature predicted was over 538°C (1000 °F) and the temperature profiles within the seal were significantly higher than measured.

The heat transfer coefficient on the seal face, near the rubbing surface, was varied in order to evaluate seal temperature sensitivity to the convective heat transfer assumptions. The estimated heat transfer coefficient on the seal surface was .00148 BTU/sq.in.-sec-°F, and near the rubbing surface (rotor/seal contact) this value increases to .00681 BTU/sq.in.-sec-°F due to the close proximity of the rotor tooth. If a constant heat transfer coefficient of .00148 BTU/sq.in.-sec-°F is used over the entire seal face, then the maximum seal surface temperature increased to 385°F, which is only 30°F higher than the baseline case. Large changes in the heat transfer coefficient (order of magnitude) will produce more substantial changes in rubbing surface temperature.

VespeI SP211 - WS31. In Test WS31 the wear ring seal heat load was so concentrated, due to the knife-edged rotor, that the sample surface temperature rose above 538°C (1000°F) after only a second. The model duplicated the linearly increasing PV profile as was conducted in the test. **Figure 27** shows the load profile from the test data. This high heat flux probably caused the sample to ignite soon after contact. A 1000°F rubbing surface temperature was arbitrarily used in the thermal model simulating a isothermal phase change or decomposition process. The

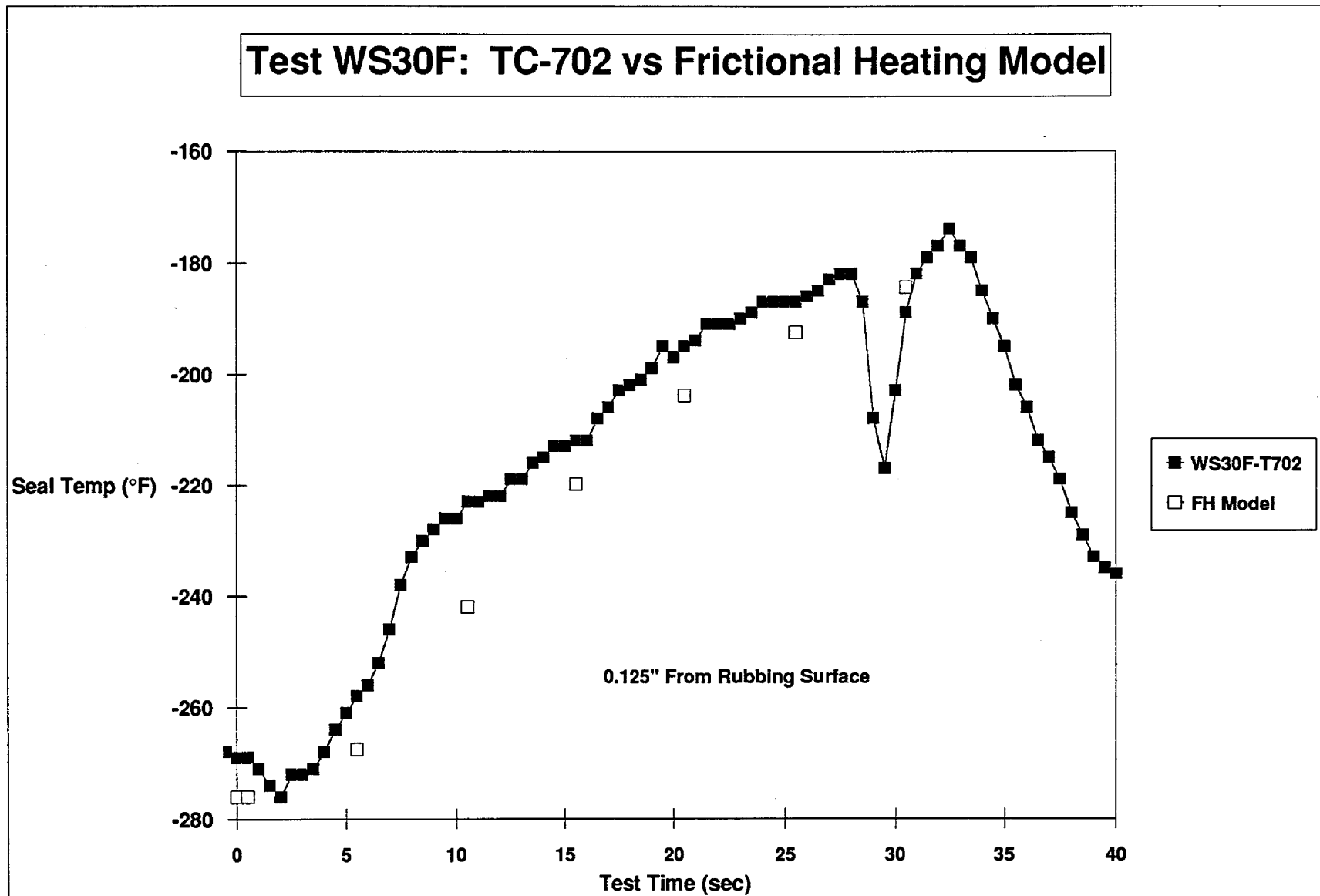


Figure 42

R/RD90-214
86

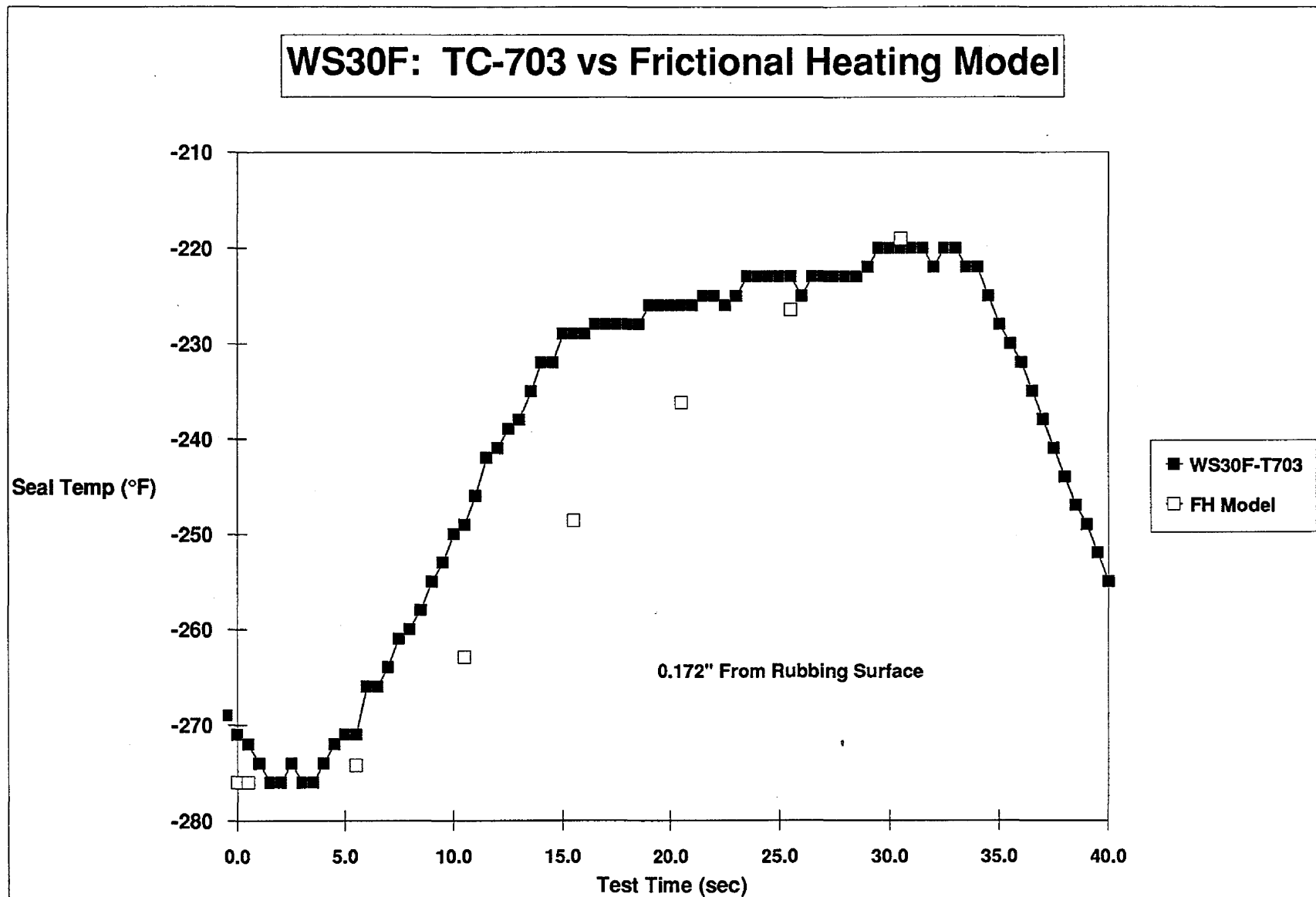


Figure 43

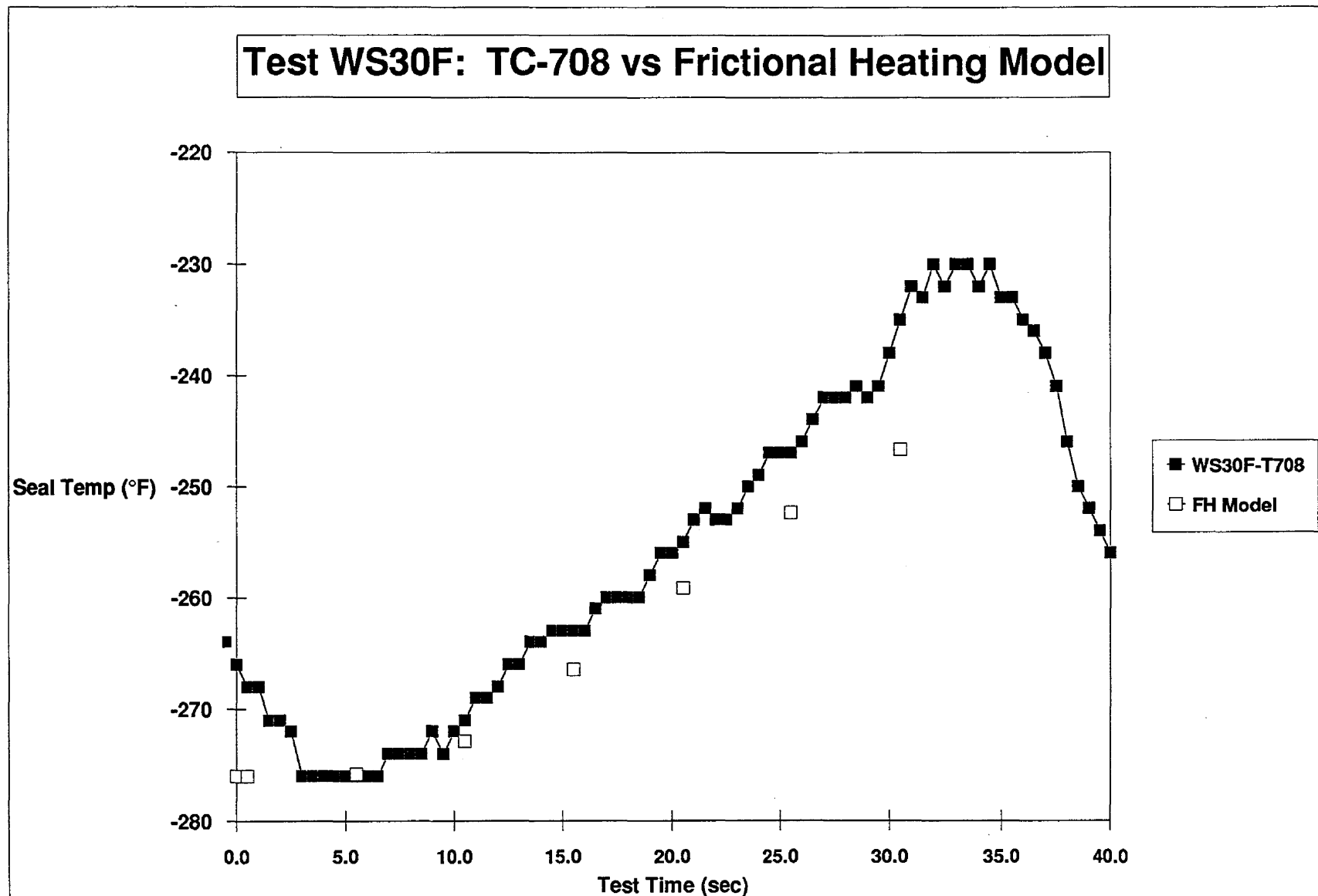


Figure 44

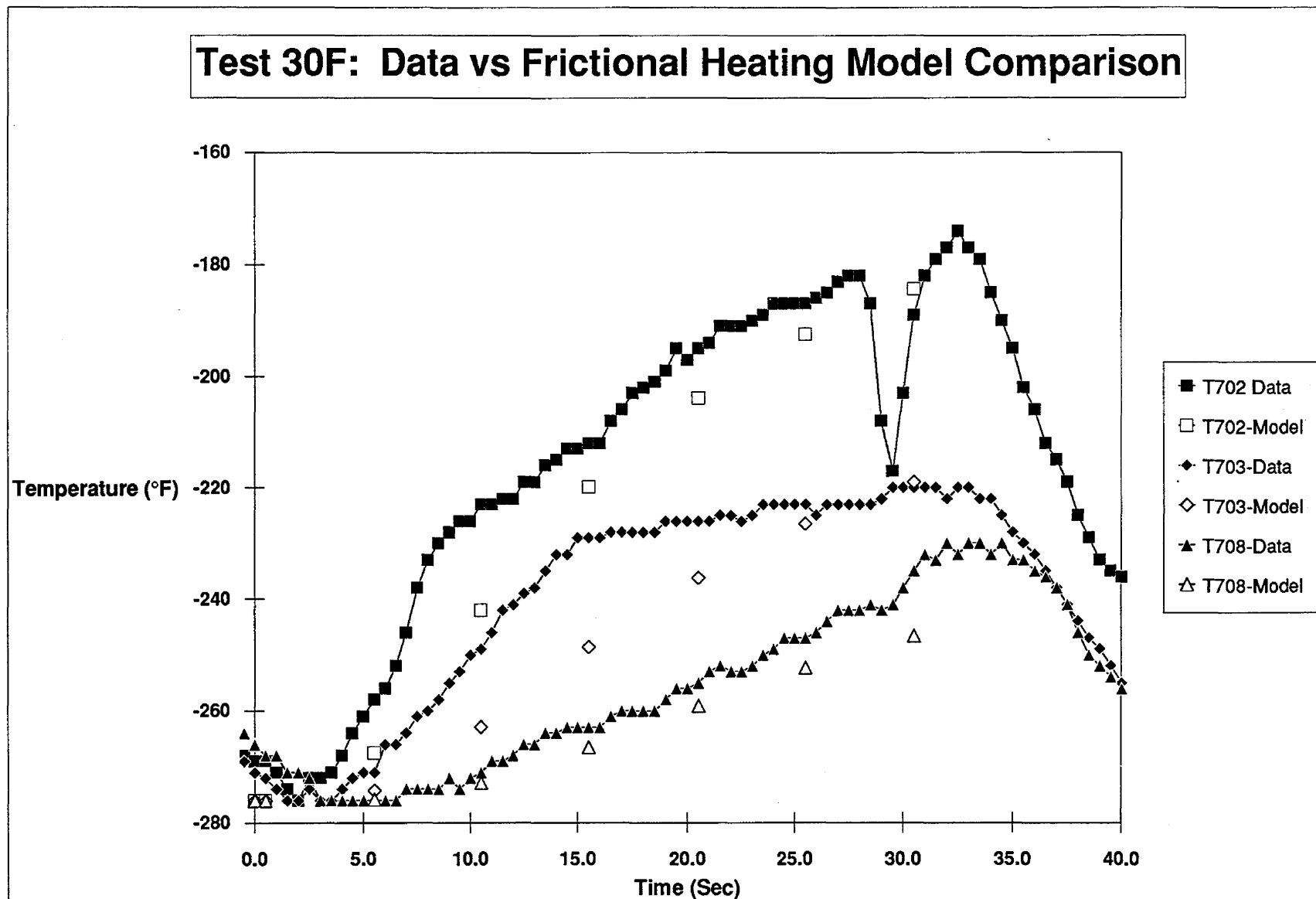


Figure 45

total heat load applied to the rubbing surface of the thermal model required to match the thermocouple data, was about 3.14 BTU/sec. The heat of reaction of the Vespel, as it burned, probably dominated the overall heat transfer into the seal, causing a much higher heat load. Therefore, the chemical heat rate term, instead of dissipating heat, was generating additional heat. Frictional heating from the rotor was only about 0.338 BTU/sec, whereas the estimated heat emersed by the reaction was about 2.80 BTU/sec (more than eight times greater than the frictional heat load). **Figure 46** compares the model predictions against the actual measured thermocouple data prior to the termination of the test. The tapered contact tooth of the test rotor developed a larger contact area as incursion increased, reducing the contact stress. However, the incursion data during this test was difficult to interpret, so a constant contact area was used (rotor tip area). This is not entirely realistic, and imposed a higher heat flux than was actually applied.

Vespel SP211 - WS04C. The thermocouple data from test WS04C appeared to be the most reliable temperature information needed to estimate the rubbing surface temperature and coefficient of friction. However, during this test, as in Test WS30F, the temperature at TC-702 drops after several seconds into the test, while the other thermocouples, which were spaced approximately 0.050 inch further from the surface, continued to increase. This behavior could not be sufficiently explained. The coefficient of friction used by the thermal model was about 0.082, which was close to what was measured during Test WS30F. The maximum surface temperature after the 22 seconds of rubbing contact was about 529°F. **Figure 47** shows a composite comparison of the model and measured temperature profiles.

Temperature contour plots were prepared showing the temperature profile at the end of each test as predicted by the frictional heating model (**Figures 48 to 50**).

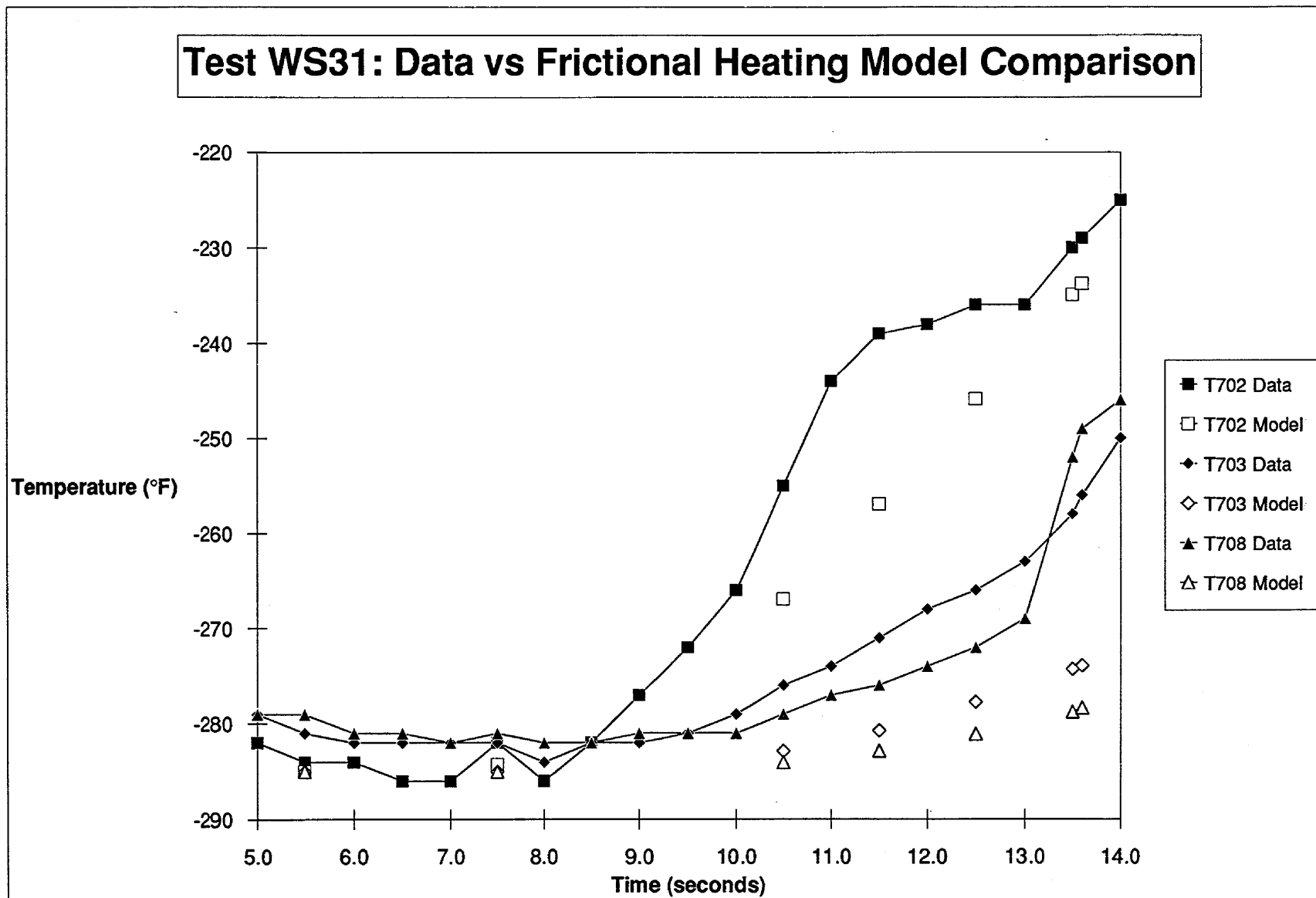


Figure 46

Test WS04C: Data vs Frictional Heating Model Comparison

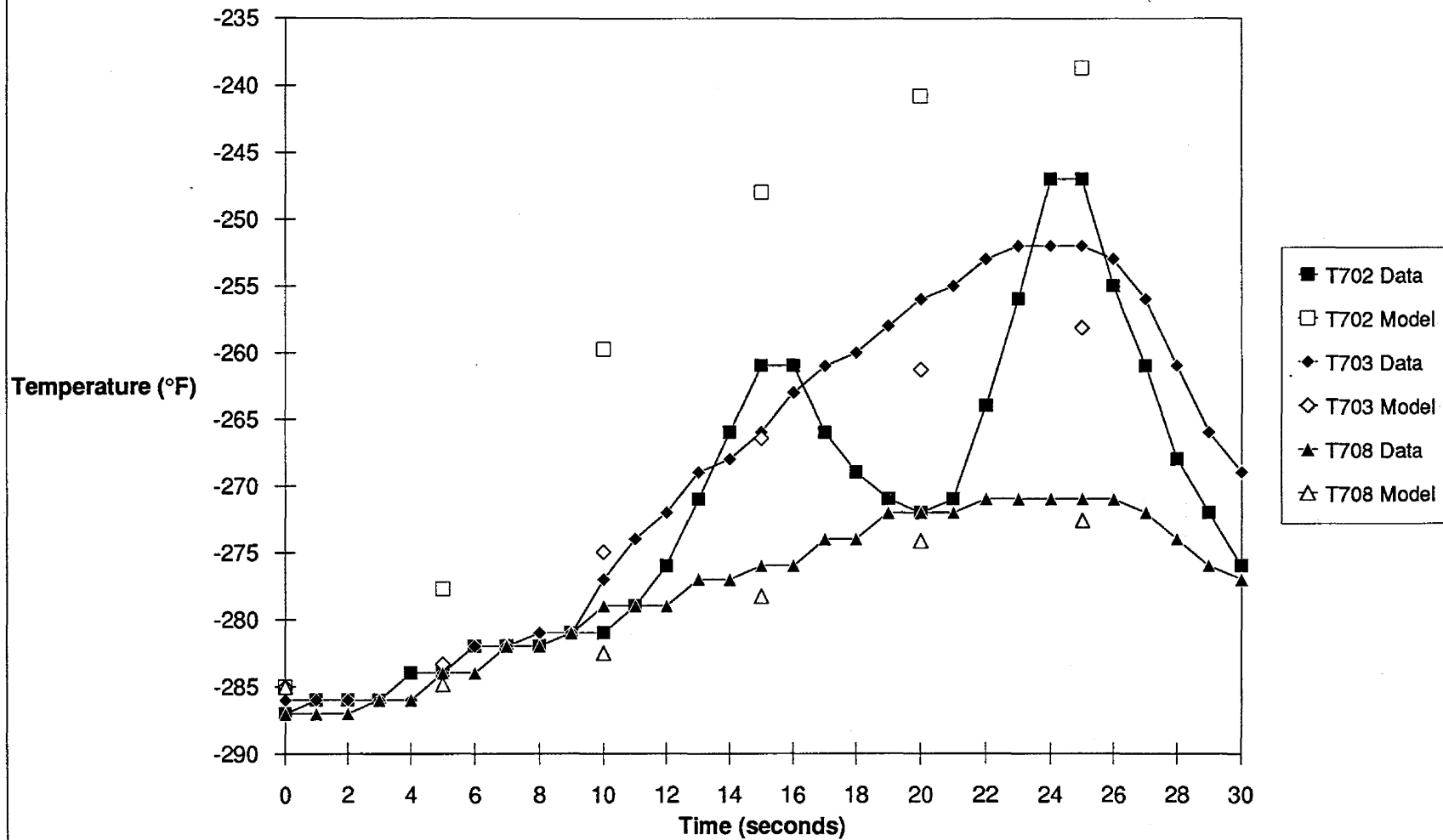


Figure 47

Test WS03C: Kel-F Temperature Contour Plot

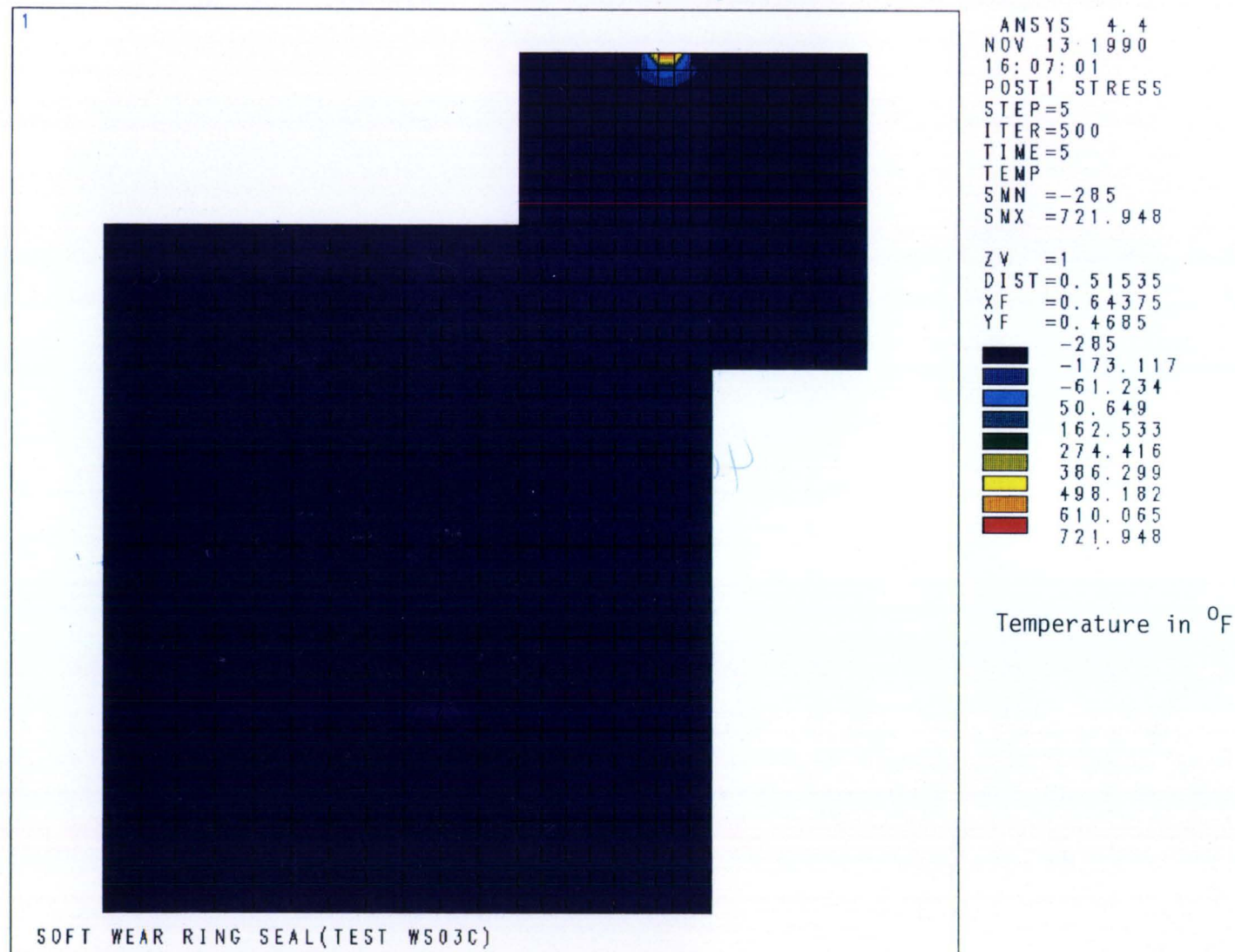


Figure 48

Test WS30F: Vespel SP211 Temperature Contour Plot

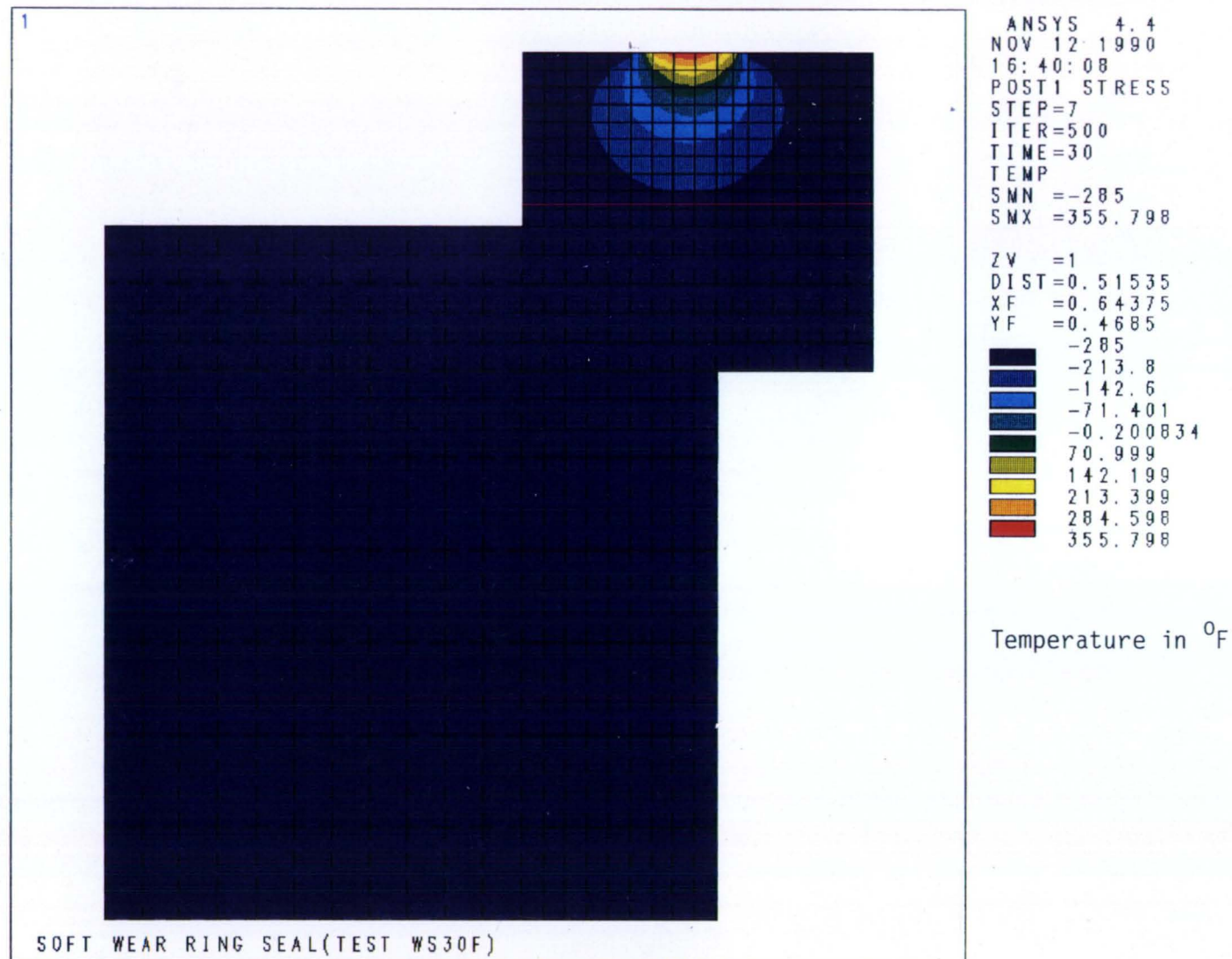
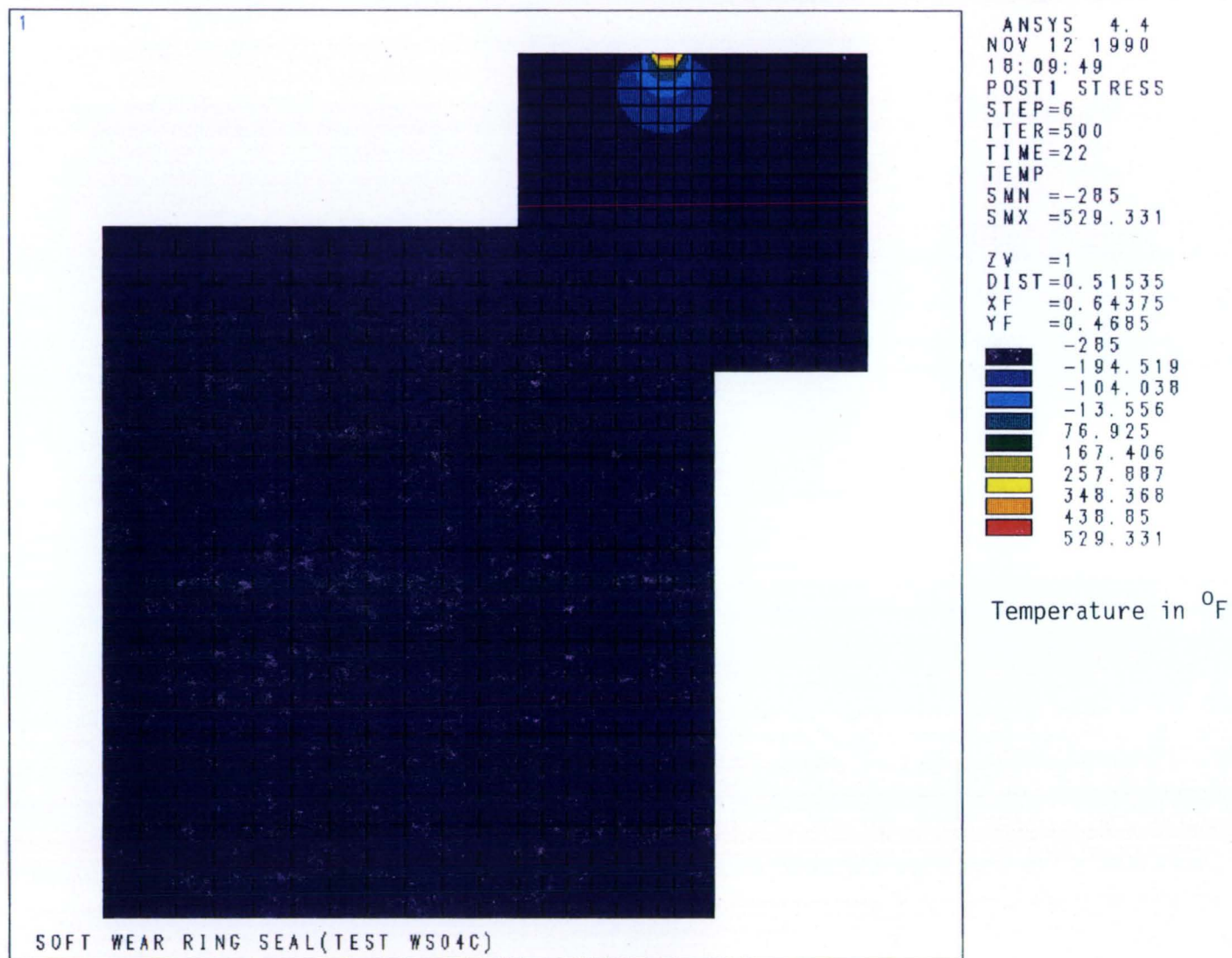


Figure 49

Test WS04C: Vespel SP211 Temperature Contour Plot



R/RD90-214
 94

Figure 50

Seal Specimen Wear Description

Under many conditions of contact the abrasive and adhesive wear of polymeric materials is adequately represented by Archard's Law. This states simply that the volume of material removed, v , is proportional to the contact load, L , and the sliding distance, d , and inversely proportional to the material hardness, H , (3):

(Eq. 15)

$$v = KLd/H$$

The constant of proportionality, K , referred to as the wear coefficient, depends upon the material compatibility and environment and is frequently used to characterize wear regimes.

The practical application of this relationship to the wear of polymers is frequently hindered by the difficulty of defining H . The hardness of many polymeric materials is affected by creep and stress relaxation effects, and these in turn are affected by the sliding speed and surface temperature in the tribological contact (4). To simplify and standardize the reporting of polymer wear, H can be eliminated. The non-dimensional wear coefficient, K , of Archard's equation is then replaced by a specific wear rate:

(Eq. 16)

$$k = v/Ld$$

In studying various polymeric materials it has been noted that conditions exist where the specific wear rate is a constant. The contact conditions are defined by the product of normal stress and sliding velocity (PV), which is directly proportional to the frictional energy dissipated as heat for a constant coefficient of friction (Eq. 2). As discussed, the regime of constant specific wear rate occurs at, or below, a PV product that is low enough for the contact to be considered isothermal, i.e. the frictionally induced temperature rise has an insignificant effect on physical/mechanical properties or surface chemistry. A useful summary of PV independent specific wear rate ($PVISWR$) data is given by Anderson (5) for a range of polymeric materials. Of particular interest are the figures for unfilled thermoplastics, ranging from $10^{-16} \text{ m}^3/\text{Nm}$ for UHMWP to $10^{-13} \text{ m}^3/\text{Nm}$ for PTFE, and the spread for filled polyimide at approximately $10^{-15} \text{ m}^3/\text{Nm}$. These data were obtained at a contact stress of 1 MPa (145 psi) and a sliding speed of 0.03 m/s (0.1 ft/s) against a steel counterface in room temperature air.

Higher PV values result in the development of significant interface temperatures which, in turn, control the friction and wear response of the material. For this to be valid it should be noted that the contact stress generally is limited to approximately one-third of the compressive strength of the polymer. It can be seen that this requirement is met by the tests reported herein, where contact stresses are nominally 0.34 MPa (50 psi). The sliding speeds, however, are approximately 4 orders of magnitude higher than that used to define the PVISWR. Therefore thermal effects are expected to dominate the wear of the polymeric materials in this program. The extent to which the compensating effects of the cryogenic heat sink and aggravating effects of a highly oxidizing environment cannot be determined from this simple analysis.

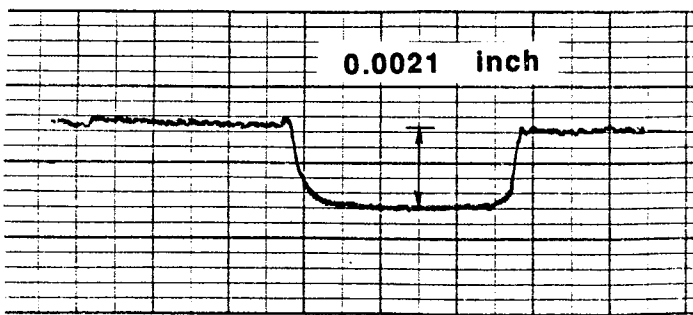
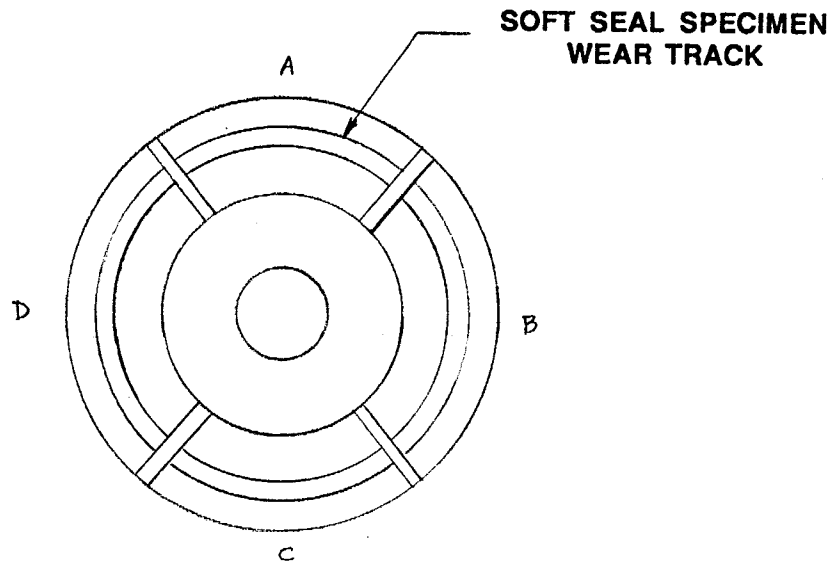
Seal Specimen Wear Results.

The wear volume, v , for a total of six polymeric seal specimens was determined using profilometry. A Rank Taylor Hobson Talyform was used to trace wear track cross-sections in the radial plane. **Figure 51** is typical of the profiles obtained. Four traces, one per sector, were measured. Mean wear track widths and depths were calculated and the wear volume was then determined from the product of the mean wear track cross-sectional area and the wear track circumference. A summary of the wear track dimensions and calculated specific wear rates is presented in **Table 13**.

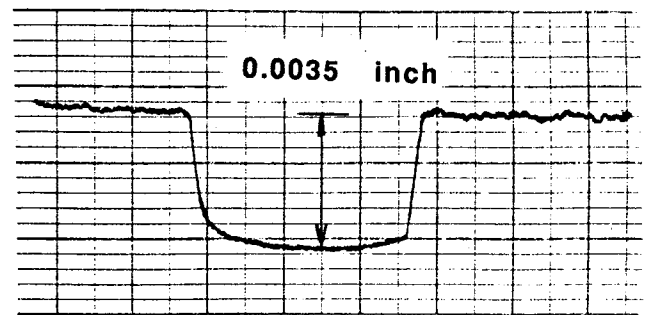
Kel-F Wear Analysis. **Table 14** presents a post-test summary for four Kel-F tests. WS03C was run at approximately double the PV of the the other three tests. The measured incursion rate was high and the test was terminated after 5 seconds when a redline triggered the cut off. The resulting wear is shown in **Figure 52**. A large quantity of filamentous debris was generated and material extrusion was clearly seen at the trailing edge of each of the four coolant channels which interrupt the contact area. This wear mode was consistent with the predicted interface temperature of 722 °F predicted by the frictional heating model, exceeding the material's melting range (350 - 425 °F) by a wide margin. The surface probably was not at the melting temperature, because Kel-F's mechanical properties degrade severely above ambient temperature. The seal operated above ambient temperature in the contact area which allowed the rotor to easily remove the softened material. It is clear that the seal was well established in the "softening-wear" regime and that the contact PV exceeded the acceptable operational value for this material in this environment. The specific wear rate for this test, estimated using incursion data at $k = 1.3 \times 10^{-12} \text{ m}^3/\text{Nm}$, was the highest value obtained in the program.

PROFILOMETRIC ANALYSIS OF VESPELL SP211 SAMPLE TEST WSO4C

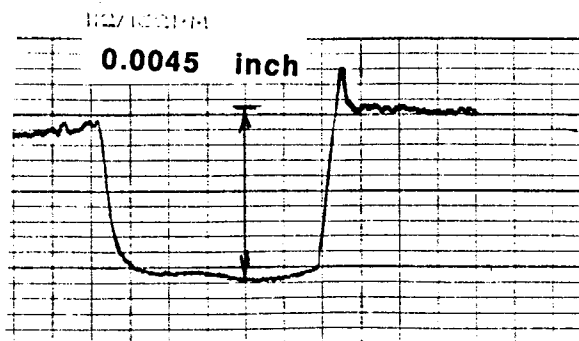
NOTE: Wear track was measured radially from the inside to the outer edge of the wear track



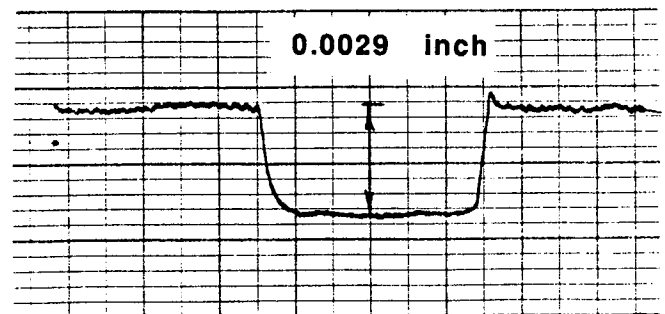
SECTOR A



SECTOR B



SECTOR C



SECTOR D

Figure 51

Table 13
Summary of Seal Sample Wear Track Profilometry

Test No.	Seal Material	Mean Wear Depth	Mean Track Width	Wear Volume v		Specific Wear Rate k	
		inch	inch	inch ³	meter ³	in ³ -min/ ft-lbf-hr	m ³ /N-m
WS03C	Kel-F	0.00800	0.055	2.114x10 ⁻³	3.465x10 ⁻⁸	6.3x10 ⁻⁶	1.3x10 ⁻¹²
WS04B	Kel-F	0.001428	0.0554	4.165x10 ⁻⁴	6.826x10 ⁻⁹	1.8x10 ⁻⁷	3.5x10 ⁻¹⁴
WS05B							
WS06							
WS08	Vespel	0.000121	0.0608	1.925x10 ⁻⁵	3.156x10 ⁻¹⁰	1.3x10 ⁻⁸	2.7x10 ⁻¹⁵
WS09							
WS10							
WS30F	Vespel	0.000562	0.1093	3.565x10 ⁻⁴	5.843x10 ⁻⁹	7.7x10 ⁻⁸	1.5x10 ⁻¹⁴
WS04C	Vespel	0.00325	0.055	9.417x10 ⁻⁴	1.543x10 ⁻⁸	4.4x10 ⁻⁷	8.8x10 ⁻¹⁴
WS11	Polybon	0.000390	0.0526	1.082x10 ⁻⁴	1.772x10 ⁻⁹	7.8x10 ⁻⁸	1.6x10 ⁻¹⁴

Table 14
KEL-F Wear Summary

Test	Mean PV		Specific Wear Rate k		Interface Temp		Wear Product Observations
Number	psi-ft/ sec	N-m/ sec	in ³ -min/ ft-lbf-hr	m ³ / N-m	°F	°C	
WS03C	14,396	30.26	6.3x10 ⁻⁶	1.3x10 ⁻¹²	722	383	Significant Filamentous Debris (see Figs. 32, 33, 52)
WS04B WS05B WS06	7,561	15.89	1.8x10 ⁻⁷	3.5x10 ⁻¹⁴	N/A	N/A	Smooth Wear Track. No Extruded Wear Product.

Test WS03C
Worn Kel-F Seal Specimen

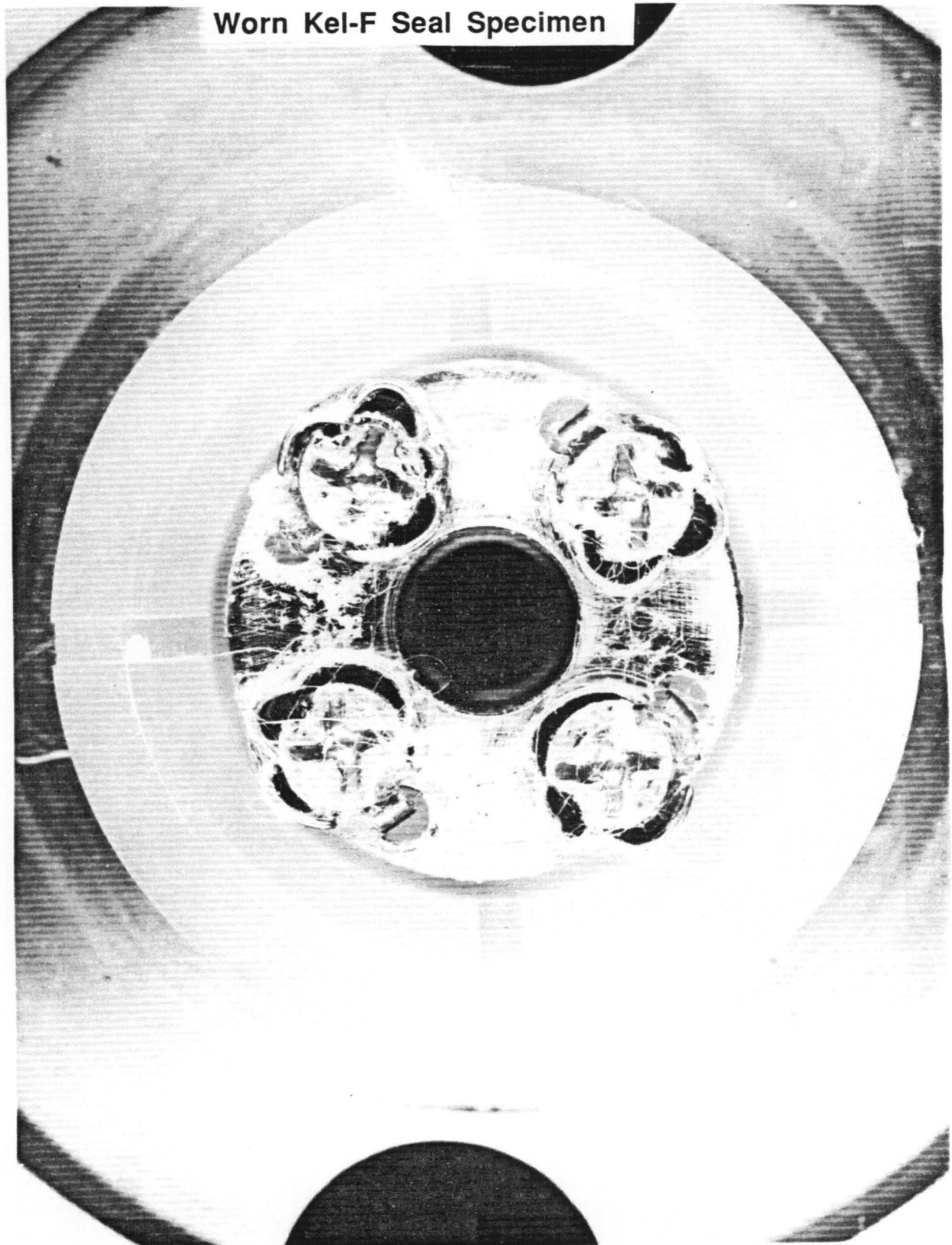


Figure 52

A cumulative specific wear rate for the tests WS04B through WS06, which were run consecutively, was determined using profilometric measurements. In contrast to test WS03C, the wear for these tests was milder. The value of $3.5 \times 10^{-14} \text{ m}^3/\text{Nm}$ lies within the acceptable range of PVISWR for many unfilled thermoplastics (5). While no interface temperature estimate was made, it is clear from the lack of filamentous debris that the surface temperature was below the threshold of the "softening wear" regime during these tests, and that the contact PV of approximately 7000 psi.ft/s lies within the limit for the test environment used.

VespeI SP211 Wear Analysis. A more comprehensive evaluation of material performance was possible with VespeI SP211 due to the greater amount of data obtained. Three specific wear rate values were calculated from a total of 5 tests. These are summarized in **Table 13** and plotted against contact PV in **Figure 53**. The figure clearly shows rapidly accelerating specific wear rate in response to increasing contact PV. At the low end, the results approach the published data for VespeI SP211 in air. For example, Friedrich (6) showed that k is independent of pressure and sliding speed at PV values less than 5 MPa-m/s (2380 psi-ft/s). The PVISWR given for the SP211 material in his study is $4.3 \times 10^{-16} \text{ m}^3/\text{Nm}$. This is included in **Figure 53** for reference purposes.

At the higher PV values, increasing interface temperatures accompany the rapidly escalating specific wear rates. The heat transfer analysis predicts surface temperatures of 355 °F (179 °C) and 529 °F (276 °C) for tests WS30F and WS04C respectively. This general trend in temperature dependent wear is well documented. For example, Tanaka has shown a rapid increase in specific wear rate, leading to a speed dependent maximum, for an unfilled polyimide (7). For a filled polyimide, containing 15 wt% graphite and 10 wt% PTFE (similar in composition to SP211), Anderson (5) has shown an increase in PVISWR of an order of magnitude over the temperature range from 50 °C to 250 °C. In both cases the initial increase is primarily due to temperature dependent loss in mechanical properties. At higher temperatures, the onset of thermal degradation ("charring") at isolated hot-spots is expected to have a major impact on the wear rate. Indications of surface oxidation on the rotor, **Figure 54**, corroborates the interface temperature estimate for test WS04C, and visual evidence of substantial material transfer, **Figure 55**, for this test suggests failure of the lubricating fillers that would normally provide a barrier against adhesion of the matrix material to the rotor counterface. A close-up photograph of the seal wear track from this test (**Figure 56**) displays surface irregularities consistent with the transferred material on the rotor. The seal surface wear track was smooth and uniform as shown in **Figure 57**. Since post-test evaluation of surface chemistry was not conducted, it was not

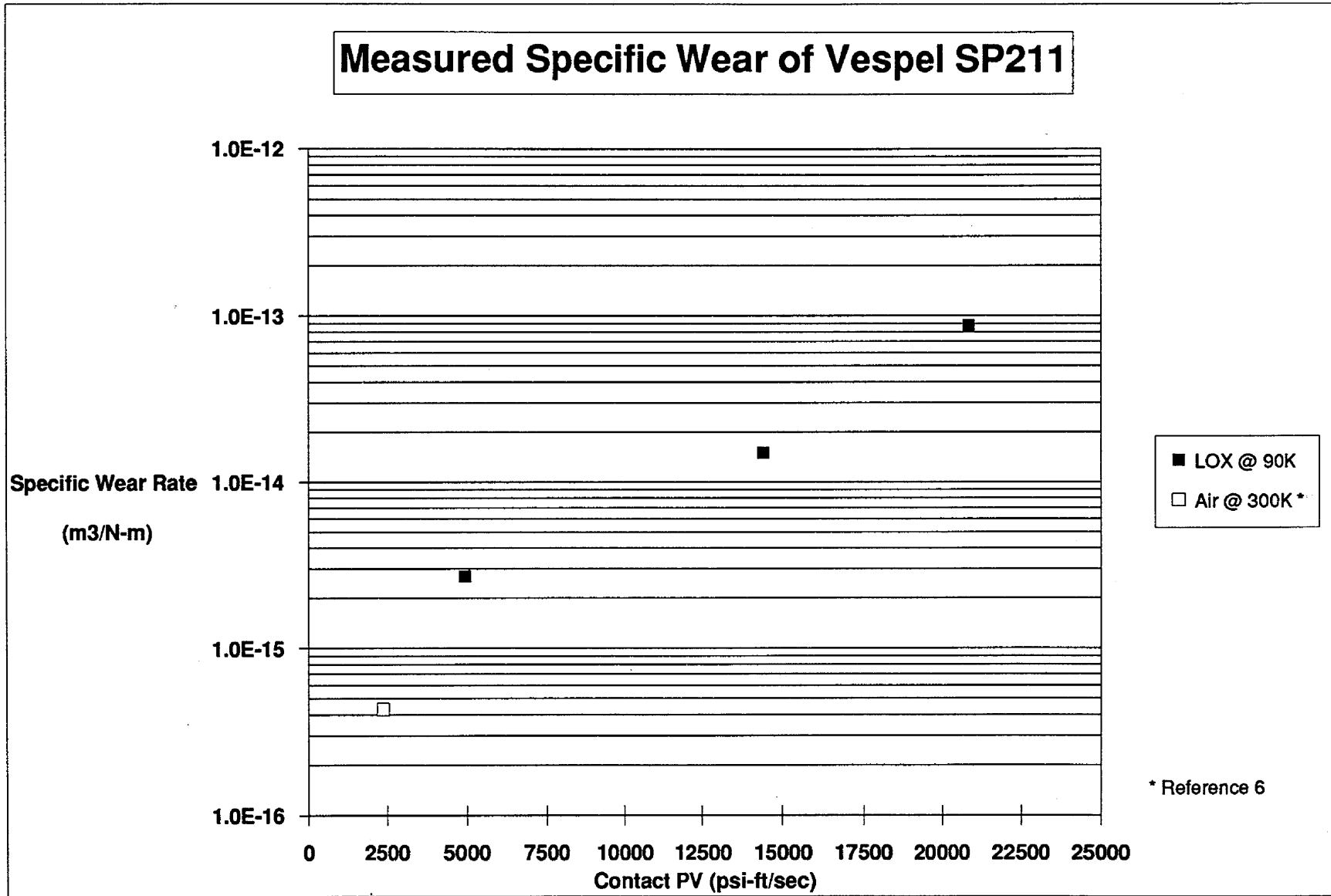


Figure 53

Test WS04C
Monel K-500 Rotor Showing Surface Oxidation

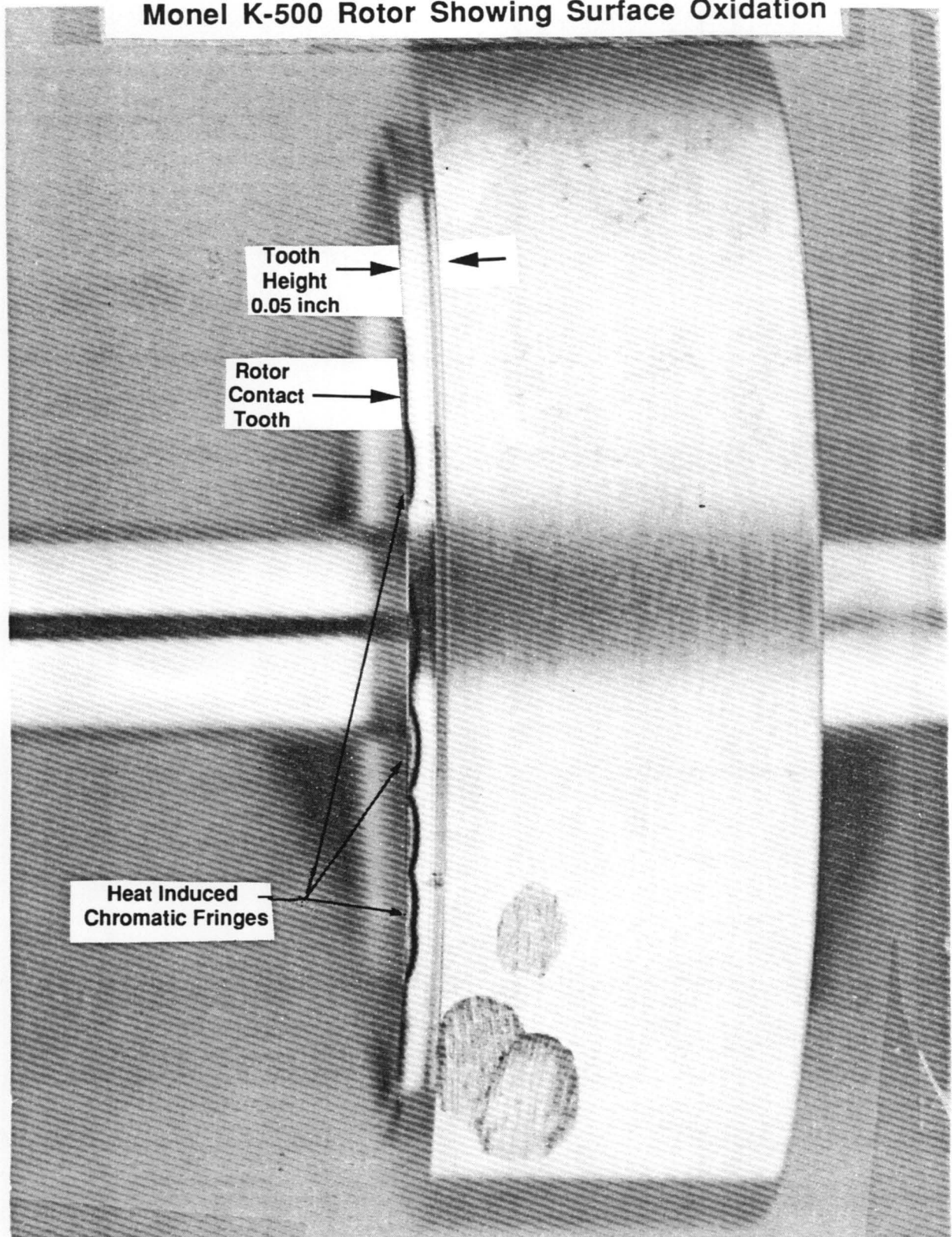


Figure 54

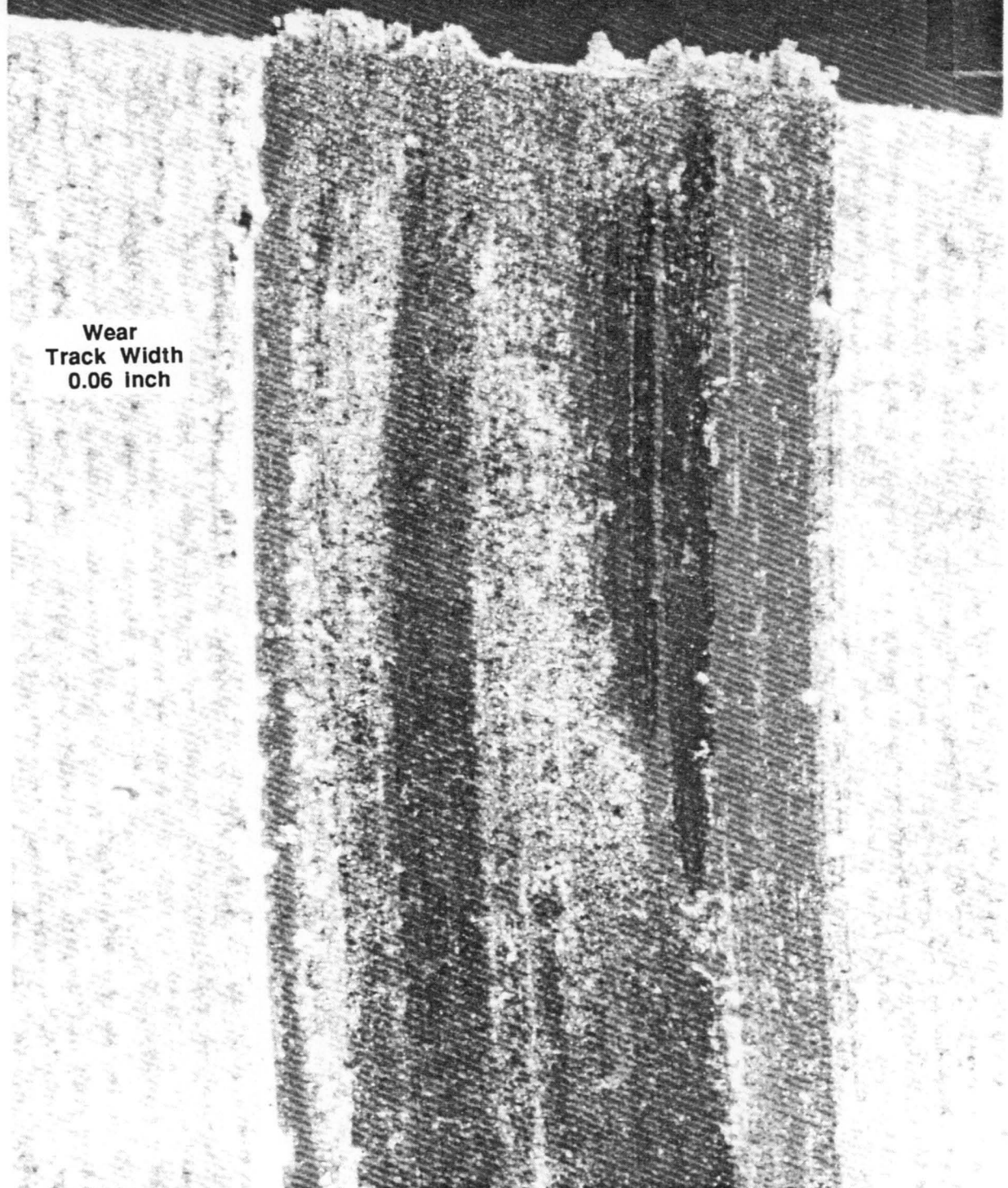
Test WS04C
Monel K-500 Rotor Showing Material Transfer

Rotor Contact
Tooth Width
0.055 Inch

Transferred
Vespel SP211
On Monel K500

Figure 55

Test WS04C
Vespel SP211 Seal Specimen Wear Track



Wear
Track Width
0.06 Inch

Figure 56

Test WS04C
Worn Vespel SP211 Seal Specimen

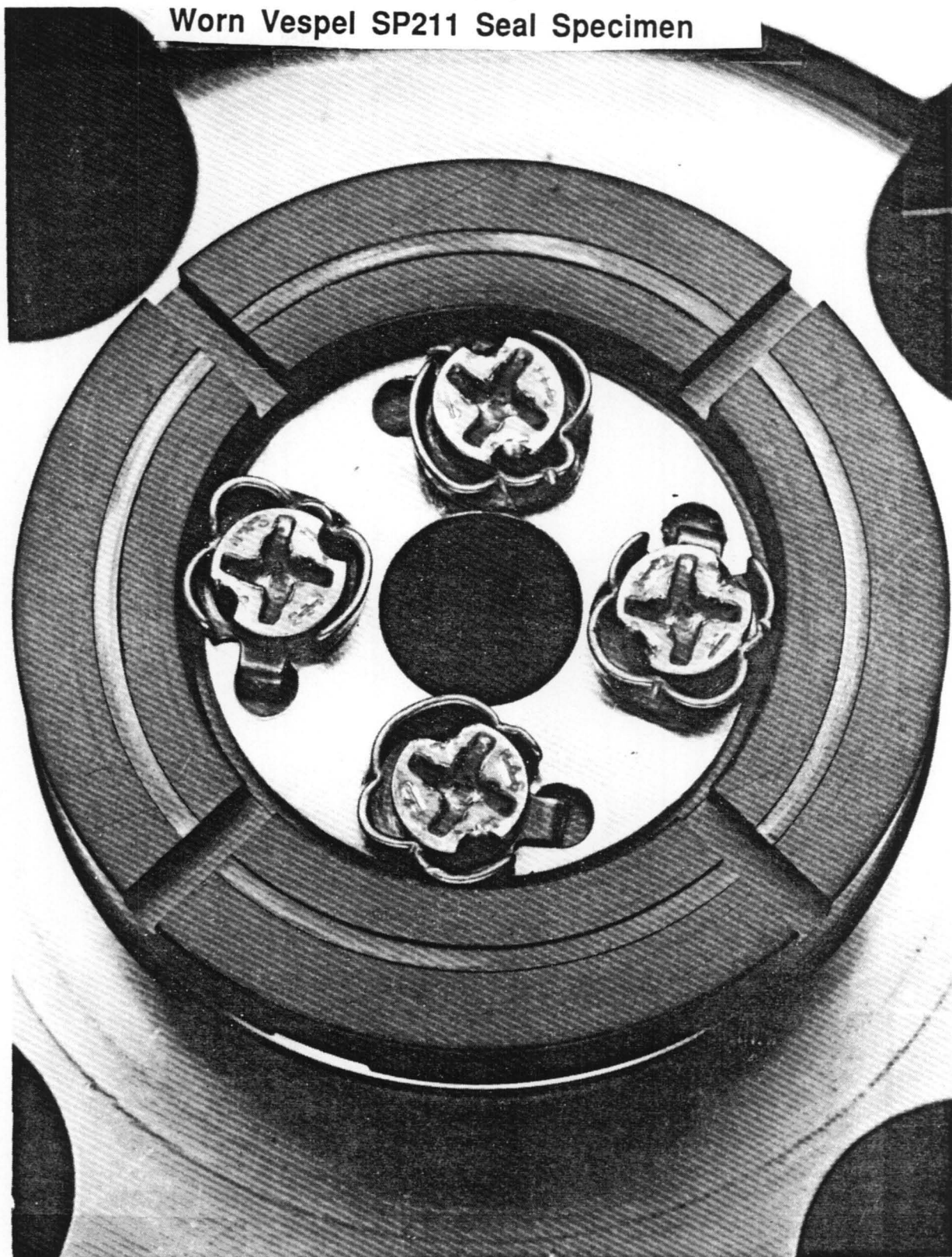


Figure 57

possible to relate PV and k with predominant wear rate mechanisms. Therefore, a positive correlation of charring with specific test conditions could not be made without further work in this area.

The chromatic interference fringe pattern seen on the rotor in **Figure 54** corresponds to the variation in thickness of the surface oxide film. Its variability, seen also on the rotor face in **Figure 37** follows the distribution of temperature at the interface. This occurs because heat generation is proportional to local contact stress (Eq. 2), which in turn produces localized thermal growth. Thus small deviations from perfect surface conformity produce an unstable situation leading to the development of "hot-spots". This process is referred to as "thermoelastic instability" and is reviewed in detail by Johnson (8). Three hot spots can be seen in **Figure 37**, at approximately the 12, 3, and 5 o'clock positions.

Polybon M Wear Analysis. While profilometric data was obtained for a total of four tests, the wear track could not be identified for the series WS12, WS13 and WS14 and therefore no data was recorded for these tests in **Table 13**. Wear track dimensions were obtained for WS11, however, and a specific wear rate of $1.6 \times 10^{-14} \text{ m}^3/\text{Nm}$ was calculated. Since this was a static friction (SF) test, accurate PV data were not available and so a comparison with the other polyimide based material (VespeI) could not be made. Published PVISWR's for filled polyimides are approximately one order of magnitude or more lower than this value (5).

CONCLUSIONS

The combined efforts of Tasks B.3 and B.5 have culminated in an evaluation of potential soft seal materials for applications in liquid oxygen turbopumps where reduced operating clearances improve performance and reliability at the expense of frictional rubbing contact with the rotor. Potential soft seal materials were tested, including Vespel SP211, Polybon M, and Torlon 4301 to establish their capabilities in future turbopump designs. Along with these new seal materials, Kel-F, which has been used extensively in both liquid oxygen and liquid hydrogen turbopumps, was similarly tested as a basis for comparison.

These materials were subjected to various LOX compatibility tests, including autogenous ignition, promoted ignition, and LOX impact tests. Vespel SP211 displayed the most benign oxygen environment sensitivity. Vespel showed no visible reactions or dissociation when heated to 427°C (800°F) in the autogenous ignition tests. The other three materials showed various signs of distortion, swelling, dissociation (residue in sample holder), and in the case of Kel-F, melting. Vespel, although having the third slowest burn rate at 0.113 inch/sec in the promoted ignition tests, burned evenly and completely. The Polybon (0.078 in/sec) and Torlon 4301 (.102 in/sec) sparked and sputtered while combusting. Kel-F was consumed very rapidly (0.290 in/sec) and dripping was also witnessed. Finally during the LOX impact testing, Vespel passed the testing at the NASA HDBK 8060.1 requirement of 10 kg-m. Torlon 4301 was the worst at 4 kg-m and because of this was eliminated from the LOX low speed friction and wear test plan. Kel-F and Polybon MT-747 passed the 8 kg-m level and were included in the LOX low speed friction and wear tests.

Low speed friction and wear tests provided insight into the several heat dissipation mechanisms which constitute the frictional heating environment of the various soft seal applications. Although the test program was not entirely successful in demonstrating the operating limits of these materials, the test data, together with an analytic model did demonstrate the differences in seal materials selected for LOX application.

A frictional heating model was constructed to better understand the low speed friction and wear test data. By adjusting the model frictional heat input, the temperature profiles were matched to test data. The differences between the analytical heat input and the measured heat input was used to determine what other heat transfer mechanisms were significant. The model utilized conduction and convection mechanisms exclusively to predict the temperature distributions in

the seal samples. Although this was probably an adequate assumption for Vespel SP211, this was not so for Kel-F which included the wear process as a prominent heat transfer mechanism.

Specific wear rates were determined for six soft seal low speed friction and wear test specimens and compared to published data as a function of both nominal contact PV and predicted interface temperature. The measured specific wear rates were, in general, an order of magnitude or greater than published values. This discrepancy was due to a combination of factors, including significantly higher sliding speeds (up to 4 orders of magnitude), cryogenic temperatures, and the highly oxidizing environment. It might be expected that the higher sliding velocities and LOX environment would increase these wear rates, while the effect of cryogenic temperatures on the material hardness would act to depress them. This study, however, did not include sufficient data for determining the relative effects of these factors against the literature. Specific wear rates were found to increase with applied PV and interface temperature. This agrees qualitatively with other published data for polymeric materials and with the current state of understanding of the wear mechanisms occurring with these materials.

It was determined that interface "softening" or mechanical properties degradation was the limiting damage mechanism for the fluoroplastic material (Kel-F). While sufficient data was not obtained to completely characterize this transition in wear mode, it can be stated that the "PV limit" for this material in the reported test configuration and environment lies between 7000 and 14000 psi-ft/sec.

No PV limit was identified for the polyimide based materials. While thermal degradation might be expected to mark their limits of performance, unequivocal evidence relating this mechanism to particular specific wear rate, interface temperature or PV values was not obtained.

Several seal locations, including impeller labyrinths, inducer tip, pump interstage, turbine tip, and turbine interstage seals have been identified for potential soft seal applications based on their turbopump performance and reliability benefits. These different seal applications, however, require different seal material characteristics due to differences in sealing requirements, operational rubbing speeds, rotor geometry, rotor contact loads, and surrounding fluid conditions. The seals' objective, however, really should dictate the type of seal material that would fit the application. For example, an impeller labyrinth or turbine tip seal, which is used to minimize leakage only, should utilize a "softer" soft seal material because the rotor could more easily wear into the seal to define its optimum clearance without resistance. The rotor geometry for these types of seal tend to be sharp toothed configurations which produces a high contact

stress, and consequently, a high PV. Plastics similar to Kel-F would be considered the best for this application, because of their low thermal conductivity which localizes the heat and promotes a material softening wear which probably dominates the heat dissipation mechanisms. However, the Kel-F wear debris generated at the PV level of about 14,000 psi-ft/sec was large and copious. At the lower PV level (approximately 7000 psi-ft/sec) no debris was observed. Similar thermal, mechanical, and chemical properties with less debris would be the desired material replacement for Kel-F in future turbopumps.

For seal applications which provide leakage control and provide rotor load carrying capability, such as pump and turbine interstage seals, a harder "soft" seal would be more beneficial. In these applications, the rotor and seal geometry tends to be a long cylindrical shape where a circumferential clearance is necessary. Due to the conforming geometries of the seal and rotor, the normal contact pressure is reduced. In these applications, minimizing wear is the primary concern. In the case of a hydrostatic bearing or a load sharing seal, the clearance and annulus pressure provide the load carrying capability, and seal wear reduces these capabilities. Contrary to Kel-F, the "harder" materials, such as the filled polyimides Vespel SP211 and Polybon MT-747, maintain their mechanical strength over a wider temperature range, so these materials, under similar frictional heating conditions, tend to dissipate heat via conduction rather than through material removal. The higher thermal conductivity of these materials, provided by the graphite fillers, coupled with the mechanical strength at the elevated temperatures, aided in this type of heat dissipation. The filler in the Vespel SP211 also provided additional lubrication at the lower PV products tested (6000 psi-ft/sec), but at the higher PV products (>20000 psi-ft/sec) the teflon transfer film seemed to breakdown. Based on the demonstrated oxygen compatibility and wear resistance, Vespel SP211 would be the best selection for this type of application.

The successful design and integration of soft seals into future turbopumps really depends on the ability to initially determine the purpose of the seal and the rubbing contact (PV) environment for which it must survive.

REFERENCES

1. RI/RD85-201, Orbit Transfer Rocket Engine Technology, Soft Wear Ring Seals, Task Order B.3 Final Report. Prepared by T. Irvin, Rockwell International, Rocketdyne Division.
2. Kapinos, V. M., "Convection Heat Transfer in Rotating Systems", Advances in Heat Transfer, Vol 5, Pg. 192, Academic Press, 1968.
3. Archard, J.F., "Wear Theory and Mechanisms", in Wear Control Handbook, Peterson, M.B., and Winer, W.O., (eds), ASME, 1980, pp. 35-80.
4. Lee, L-H., "Fracture Energetics and Surface Energetics of Polymer Wear", in Polymer Wear and its Control, Lee, L-H., (ed), ACS, 1985, pp. 27-38.
5. Anderson, J.C., "The Wear and Friction of Commercial Polymers and Composites", in Friction and Wear of Polymer Composites, Friedrich, K. (ed), Elsevier, 1986, pp. 329-362.
6. Friedrich, K., "Sliding Wear Performance of Different Polyimide Formulations", Tribology Int., 1989, Vol. 22, No. 1, pp. 25-31.
7. Tanaka, K., and Yamada, Y., "Effect of Temperature on the Friction and Wear of Some Heat-Resistant Polymers", in Polymer Wear and its Control, Lee, L-H., (ed), ACS, 1985, pp. 103-128.
8. Johnson, K. L., "Contact Mechanics", 1985, Cambridge University Press.

APPENDIX A

TEST WS31 FAILURE INVESTIGATION REPORT BY WSTF

EVENT REPORT
AND FAILURE ANALYSIS REPORT
FOR THE
JANUARY 31, 1986
FIRE IN THE LOX FRICTIONAL HEATING TEST SYSTEM
IN THE 800 AREA TEST CELL 111

Issued By
National Aeronautics and Space Administration
Johnson Space Center
White Sands Test Facility
Laboratories Test Office

Prepared By:

Joel Stoltzfus
J. Stoltzfus, Lockheed-EMSCO

John Homa
J. Homa, Lockheed-EMSCO

EVENT REPORT

REPORT NO. ER86-002

DATE ISSUED 9/5/86

TO: Distribution

FROM: Stoltzfus/Homa

SUBJECT: Failure Analysis - LOX FHT

DATE OF EVENT 1/31/86 TIME OF EVENT _____

LOCATION OF EVENT 800 Area, Test Cell 111

TYPE OF EVENT Fire in the LOX Frictional Heating Tester

PERSONNEL INVOLVED John Homa-TC, Leo Hall, Bruce Havenor-Technicians

TPS OR DR NO. USED TO DOCUMENT AND CORRECT TPS 8-HPF-4507 E1

WAS LOST/DESTRUCT REPORT INITIATED? NO X YES _____ REPORT NO. _____

DETAILS (WHO? WHAT? WHEN? WHERE? HOW? WHY?) ATTACH STATEMENT OF
PERSONNEL INVOLVED. USE CONTINUATION SHEETS AS REQUIRED. _____
See attached report.

DISPOSITION. USE CONTINUATION SHEETS AS REQUIRED. _____
See attached report.

John Stoltzfus / John Homa
SIGNATURE

DISTRIBUTION:

NASA
LTO CHIEF 3 COPIES
SAFETY 1 COPY

LOCKHEED
LTO MANAGER 3 COPIES
SAFETY 1 COPY
PROPERTY 1 COPY
(IF LOST/DESTRUCT REPORT INITIATED)

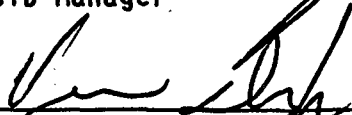
RECORD OF CONCURRENCE OF FAILURE ANALYSIS COMMITTEE



Frank Benz, NASA
Laboratories Test Office



Craig Bishop, Lockheed-EMSCO
MCTD Manager



Vernon Diaz, Lockheed-EMSCO
MTF Supervisor




Mike Pedley, Lockheed-EMSCO
LPS Supervisor



Bob Johnson, Lockheed-EMSCO
LSS Supervisor



John Homa, Lockheed-EMSCO
Engineer



Joel Stoltzfus, Lockheed-EMSCO
Engineer

TABLE OF CONTENTS

	<u>Page</u>
EVENT REPORT FORM	i
RECORD OF CONCURRENCE BY FAILURE ANALYSIS COMMITTEE	11
LIST OF FIGURES	1v
1.0 INTRODUCTION	1
2.0 TEST SETUP	1
2.1 TEST SYSTEM	1
2.2 TEST MATERIALS AND CONFIGURATION	6
2.3 TEST CONDITIONS	8
3.0 DETAILS OF TEST WS-31	9
4.0 FAILURE ANALYSIS	10
4.1 COMMITTEE MEETING OF 02/03/86	10
4.2 COMMITTEE MEETING OF 02/05/86	28
4.3 DISCUSSION OF POSSIBLE FAILURE MECHANISMS	46
5.0 CONCLUSIONS	56
APPENDIX - TPS 8-HPF-4507 E1	A-1

LIST OF FIGURES

<u>Figure</u>		<u>Page</u>
1	LOX Frictional Heating Test Chamber	2
2	LOX Frictional Heating Test System Schematic	3
3	Photograph of WSTF LOX Frictional Heating Test System	4
4	Vespel SP-211 Test Sample Mounted in Frictional Heating Tester	7
5	Location of Mechanical Stops After Test WS-31 Fire	12
6	View of Frictional Heating Tester after WS-31	14
7	Cell 111 After Test WS-31	15
8	View of Tester from the Air Cylinder End	16
9	Damage to Video Equipment Cables	17
10	View of Equipment Behind Tester	18
11	Close-up View of Test Chamber	19
12	Top View of Test Chamber	20
13	Torque Transducer and Test Chamber	21
14	Front View of Test Chamber	22
15	Test Chamber Outlet Ports and Vent Lines	23
16	Close-up View of Test Chamber Outlet Ports	24
17	Schematic of Test Chamber Outlet Lines	25
18	Correlation of Events Observed on the Video Recording with Those Ascertained from the Digital Data	29
19	Test Chamber Outlet Filter Before Disassembly	31
20	View of the Inside of the Test Chamber Outlet Filter Fittings	32
21	Filter Element and Chamber Housing	33
22	Bottom View of the Test Chamber and Its Associated Vent Lines and Fittings After Being Removed from the Test System	35
23	Test Chamber Outlet Ports	36
24	Inside of Test Chamber as Seen from the Drive Motor End	37
25	Test Chamber End-Section with Sample Holder and Test Chamber Mid-Section	38

LIST OF FIGURES - (Continued)

<u>Figure</u>		<u>Page</u>
26	Test Rotor and Test Chamber End-Section	39
27	End-Section Located on Drive Motor Side of Test Chamber	40
28	Test Setup Used to Determine the Deformation of the Test Sample Material Due to Load Applied to Sample Prior to WS-31	43
29	Deformation of Sample Material at Ambient Temperature	44
30	Deformation of Sample Material at Cryogenic Temperature	45
31	RPM, Torque, Normal Load, Air Cylinder Pressure, and Displacement Data from Test WS-31	53
32	Pressure Data from Test WS-31	54
33	Temperature Data from Test WS-31	55

1.0 INTRODUCTION

On January 31, 1986, a fire occurred in the Liquid Oxygen (LOX) Frictional Heating Test System in Test Cell 111 in the 800 Area. The test was being conducted for the NASA Lewis Research Center, using an Inconel 718 rotor, which was being rubbed against a Vespel SP-211 test sample. This report describes the test setup, details of Test WS-31, actions taken by the failure analysis committee, and the committee's conclusions regarding the cause of the fire.

2.0 TEST SETUP

2.1 Test System

The test system used was the White Sands Test Facility (WSTF) Frictional Heating Test System (Figure 1). In this system, a rotating test sample or test rotor is attached to the chamber shaft, which can be rotated at 17,000 rpm. The test rotor is loaded against the stationary test sample using a pneumatic cylinder actuator. The cylinder pressure is controlled in order to establish the desired load profile on the test sample.

Plumbing modifications were made to the test system in order to provide a continuous flow of LOX through the test chamber during the performance of a test (Figures 2 and 3). Prior to a test, LOX was fed into the system from a 150-gallon-capacity (568 l) dewar to chill the system to cryogenic temperature. A gaseous nitrogen (GN_2) purge system was used to prevent excessive chilling of the chamber shaft seals (Figure 1), and was later used to inert the system at the conclusion of a test. When the

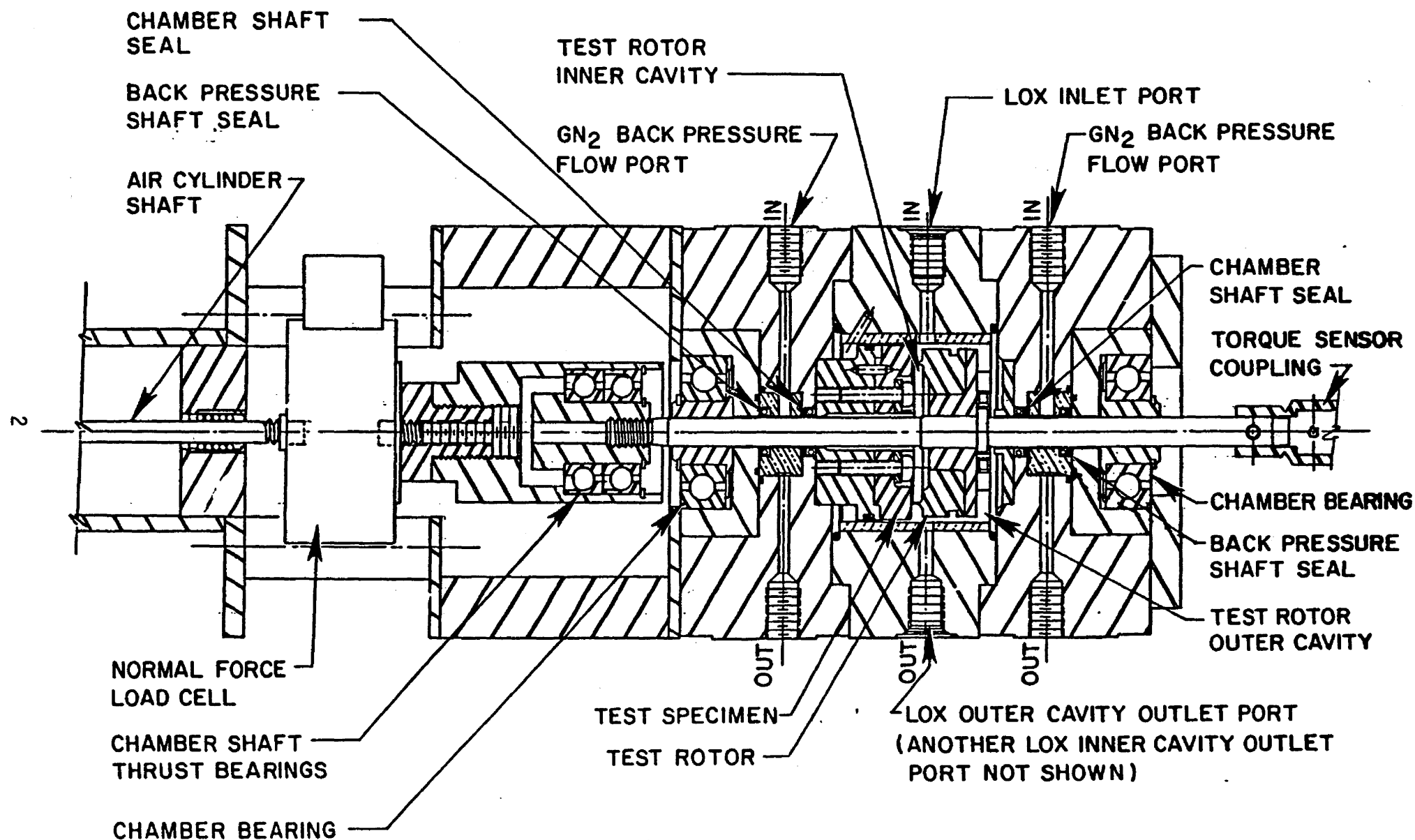
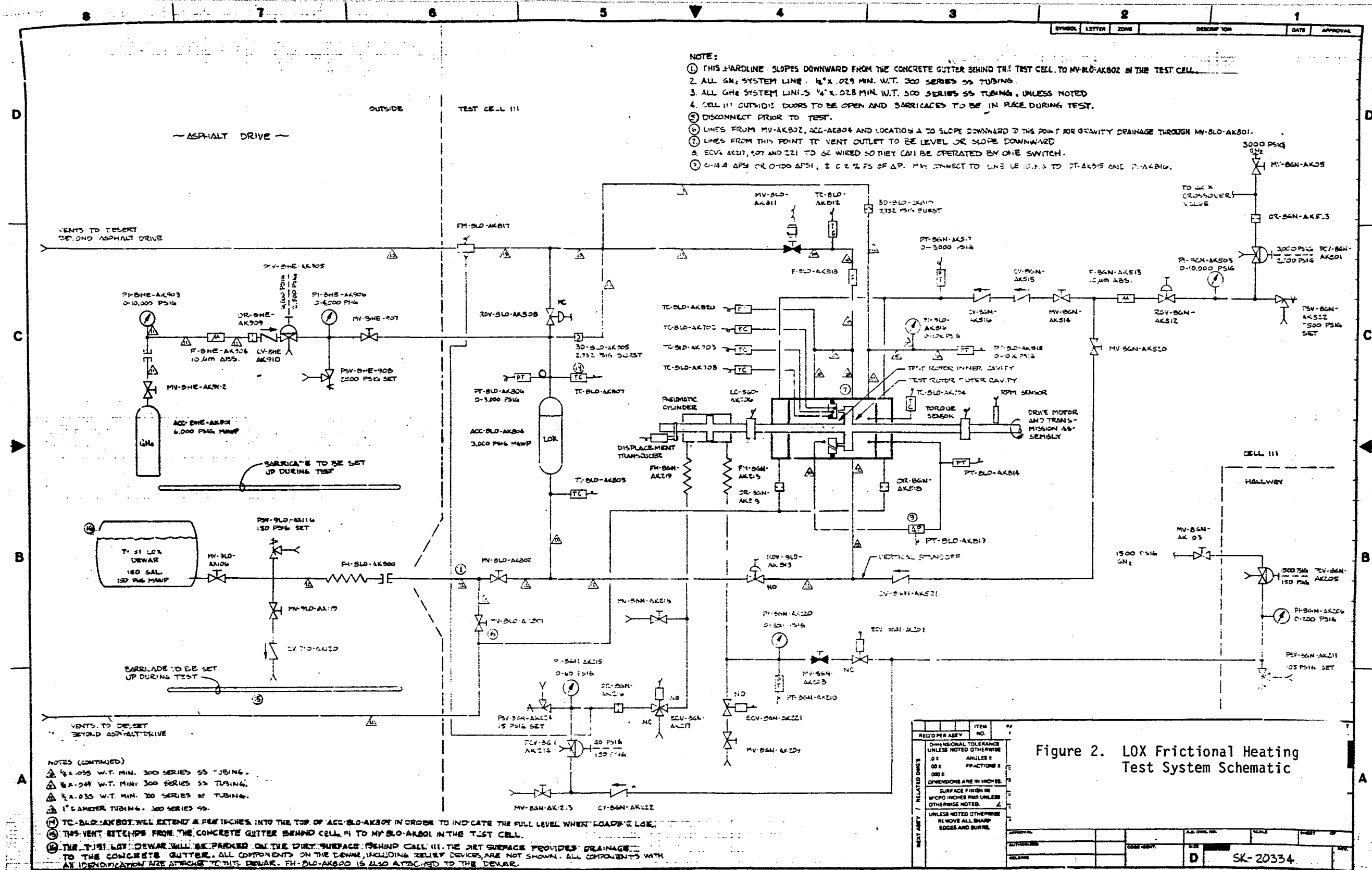


Figure 1. LOX Frictional Heating Test Chamber



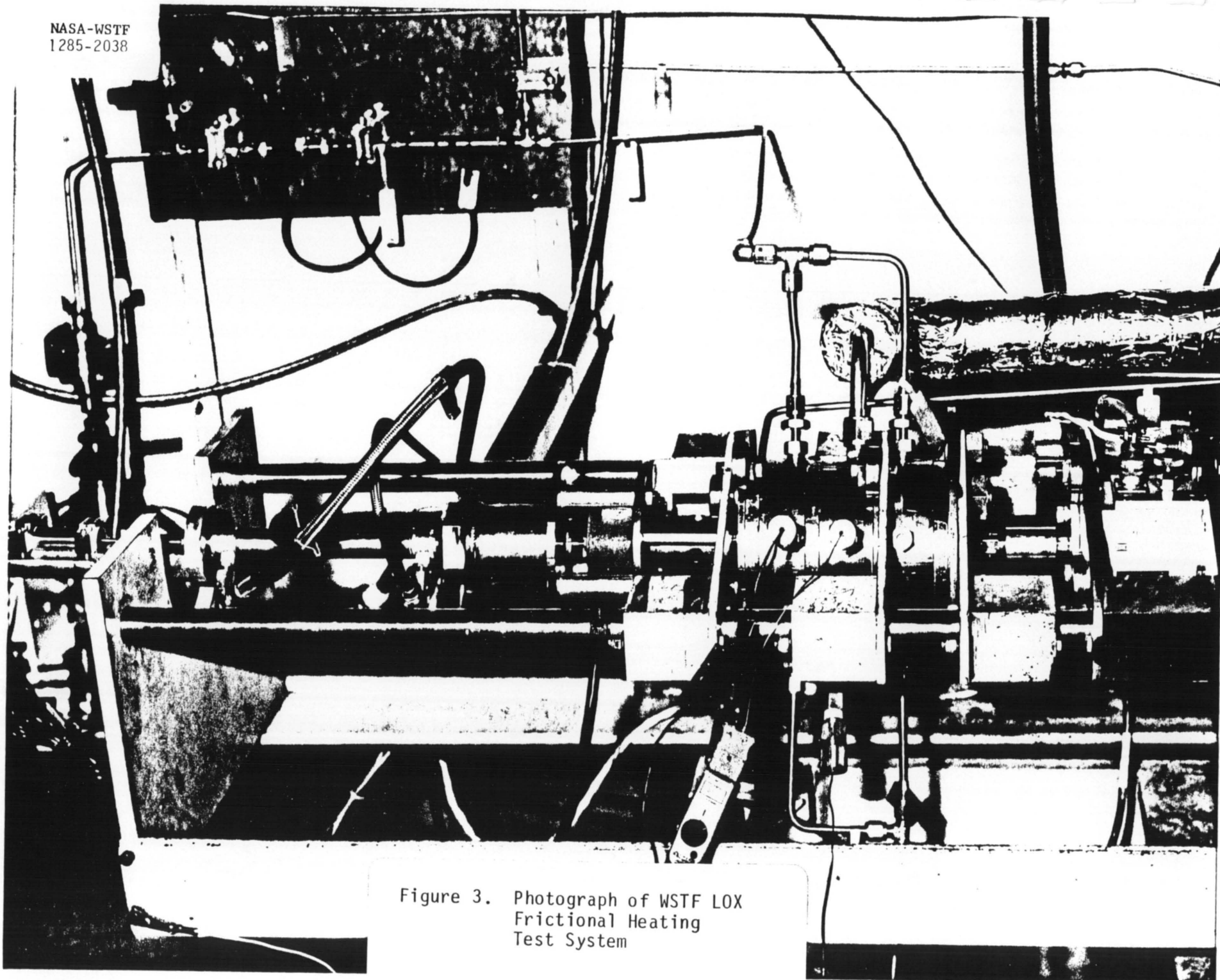


Figure 3. Photograph of WSTF LOX
Frictional Heating
Test System

system was fully chilled, a LOX accumulator with an approximately 3-gallon capacity (11.4 l) was filled and the test system was isolated from the LOX dewar.

A gaseous helium (GHe) system provided ullage pressure to the LOX accumulator, which allowed LOX to flow through the test chamber with chamber pressures up to 1800 psig (12.5 MPa). A metering valve downstream of the test chamber was adjusted to provide approximately one minute of LOX flow before the accumulator was drained.

Test system data was recorded at 100-millisecond intervals throughout a test. The following data were collected:

	<u>Designation</u>
LOX Accumulator Pressure	PT-AK806
Test Chamber Pressure at Outer Diameter	PT-AK815
Test Chamber Pressure at 1/2 the Radius	PT-AK814
Test Chamber Differential Pressure (Inner/Outer Cavities)	PT-AK819
GN ₂ Purge Pressure	PT-AK517
Pneumatic Cylinder Pressure	PT-AK210
Sample Temperature (3 Locations)	TC-AK702, 703, 708
Test Chamber Temperature	TC-AK704
Temperature at Vent Port of Inner Cavity	TC-AK820
Test System Main Vent Line Temperature	TC-AK812

LOX Accumulator Outlet Temperature	TC-AK803
LOX Accumulator Overflow Temperature	TC-AK807
Chamber Shaft Speed	RPM
Chamber Shaft Torque	TORQ
Chamber Shaft Displacement	DISP
Chamber Shaft Tension Load	LC-AK706

In addition, the test system was monitored using standard (30 frames/second) video recording equipment.

2.2 Test Materials and Configuration

The test sample material used in Test WS-31 was Vespel SP-211. The test sample was attached to the sample retainer with four bolts and a retaining pin (Figure 4). The test sample was held stationary throughout the test by the sample retainer. An O-ring in the sample retainer separated the LOX inner cavity from the LOX outer cavity. Four channels machined into the test sample allowed LOX to flow from the outer cavity, through the test sample, into the inner cavity, after the test rotor contacted the test sample. This configuration provided a continuous flow of LOX to the inner portion of the test sample once the test rotor formed a seal by contacting the test sample. The test rotor material used for this test was Inconel 718. The test rotor surface was tapered down to a 0.010-inch-thick rubbing surface to contact the test sample, as shown in Figure 28.

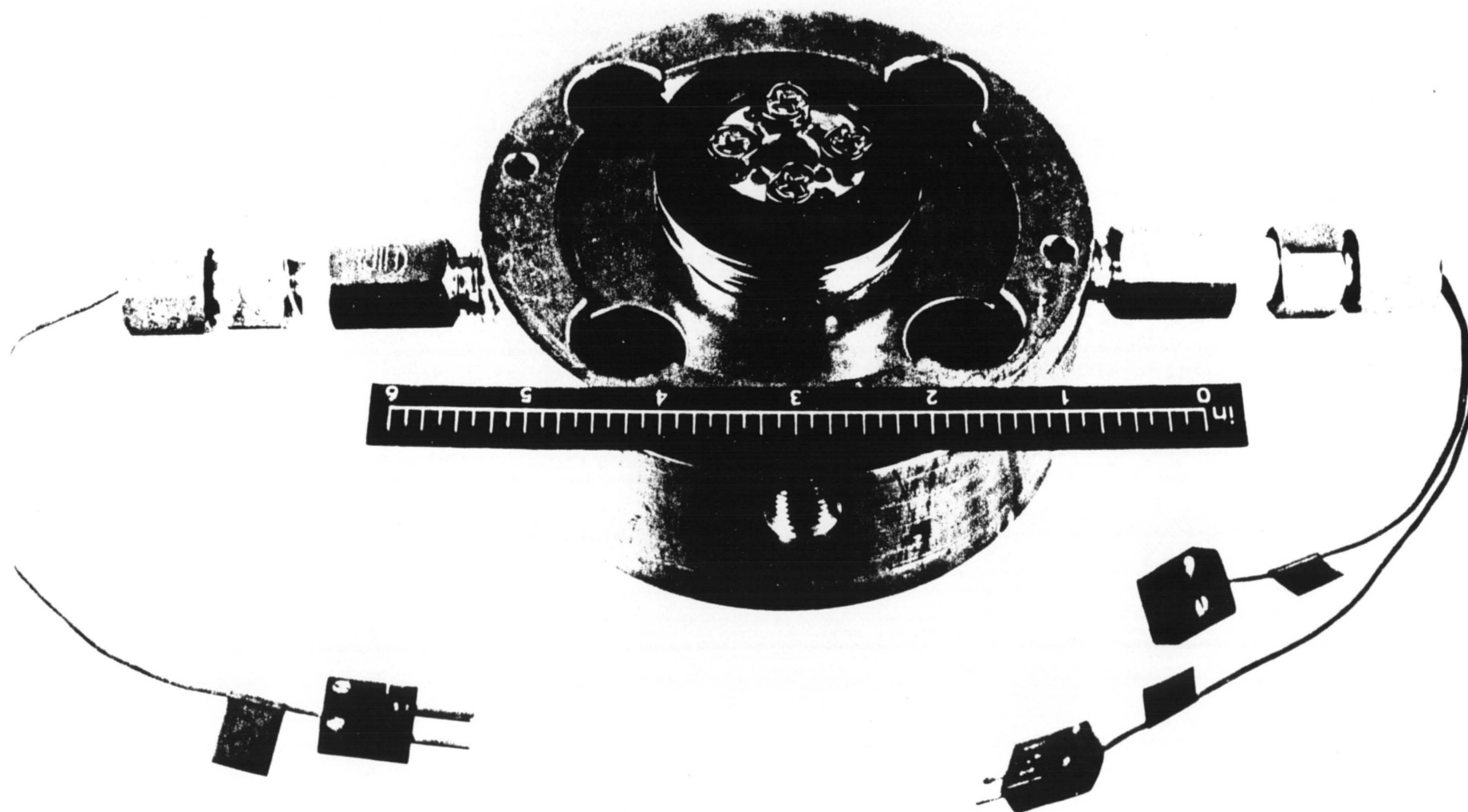


Figure 4. Vespel SP-211 Test Sample
Mounted in Frictional
Heating Tester

Additional materials in the test chamber environment were a Monel 400 test chamber with copper liner, 300 series stainless steel sample retainer and chamber shaft, stainless steel hardware, Teflon chamber shaft seals, and Viton chamber O-ring seals.

2.3 Test Conditions

The test conditions for Test WS-31 were as follows:

Chamber Shaft Speed	17,000 rpm
Chamber Pressure	300 psig
Seal Purge Pressure	150 psig
Maximum Normal Load (Pretest)	611 lbf
Load Ramp	27 lbf/second
Test Shutdown Temperature Limit	100 °F
Test Shutdown Incursion Limit	0.020 inch
Maximum Test Duration	30 seconds
Test Rotor - Inconel 718	S/N 7R030268-5
Test Sample - Vespel SP-211 (Mat'l A)	S/N 7R030265-9
Test Type: RF (Running Friction) - Test rotor increased to desired velocity prior to contacting sample	
Total LOX in System	Approx. 3 1/2 gallons

3.0 DETAILS OF TEST WS-31

LOX frictional heating Test WS-31 was conducted on January 31, 1986, using TPS-8-HPT-1627R, Mod. 1. The test sample and test rotor were installed in the chamber. The test chamber was installed in the test system and proper assembly was verified. The pneumatic cylinder maximum load was set to 611 lbf. The load ramp was adjusted to increase from 0 to 540 lbf in 20 seconds. The displacement transducer was reset to indicate "zero" when the samples were loaded to 611 lbf. A mechanical incursion limit stop was set to allow a maximum test rotor incursion of 0.030 inch. An additional mechanical stop was set to prevent the test rotor from contacting the back of the test chamber when the test rotor was positioned away from the test sample.

The system was chilled to LOX temperature and the LOX accumulator was filled. When all thermocouples indicated stable temperatures of approximately -300 °F, the LOX dewar was disconnected from the system. The displacement "zero" reading was checked and indicated no change from the pre-chilled reading. The accumulator ullage pressure was set to 400 psig, which resulted in approximately 300 psig chamber pressure under flow conditions. The LOX metering valve was preset to two turns open, as determined by previous testing. Instrumentation readouts were checked for proper readings prior to initiating the test sequence. The chamber isolation valve was opened to allow LOX to pre-flow through the system and establish steady-state conditions in the test chamber. Microprocessor control was initiated with a 10-second countdown. At T=-5 seconds, the

drive motor was turned on and verified at 17,000 rpm. An approximately 120-lbf load was observed on the chamber shaft load cell, due to the pumping action of the test rotor. At T=0 second, the pneumatic cylinder was actuated automatically and the load ramp began. At T=5 seconds, the pneumatic cylinder load surpassed the opposing test rotor pumping force. The test rotor subsequently displaced towards the test sample. At T=13 seconds, the test sequence was automatically terminated due to the test rotor incursion reaching the incursion limit of 0.020 inch. This caused the pneumatic cylinder to cycle and displace the test rotor away from the sample. Approximately 5 seconds later, a test technician monitoring Test Cell 111 indicated that a fire had commenced. The emergency shutdown procedure was initiated,, which included turning off the drive motor, venting the LOX accumulator ullage pressure, closing facility GOX and compressed air supplies, and shutting down power to Test Cell 111. Dense smoke was observed in the test cell. The smoke was cleared by the ventilation system after approximately 30 seconds, with no further evidence of fire in the test chamber. An incident investigation, TPS-8-HPF-4507 E1, was initiated to complete the test system shutdown. The test system was left undisturbed and Test Cell 111 was maintained "OFF LIMITS" until the first failure analysis committee meeting on February 3, 1986.

4.0 FAILURE ANALYSIS

4.1 Committee Meeting of 02/03/86

On February 3, 1986, the first failure analysis committee meeting was convened. The attendees were:

Frank Benz	NASA	Committee Member
David Dixon	NASA	
David Baker	LEMSCO	
M. D. Pedley	LEMSCO	Committee Member
C. V. Bishop	LEMSCO	Committee Member
Vernon Diaz	LEMSCO	Committee Member
Ralph Williams	LEMSCO	
Jim Dugan	LEMSCO	
G. L. Squyres	LEMSCO	
John Schneider	LEMSCO	
Bruce Havenor	LEMSCO	
Leo Hall	LEMSCO	
John Homa	LEMSCO	Committee Member
Ken McCardle	LEMSCO	
Bob Johnson	LEMSCO	Committee Member
Joel Stoltzfus	LEMSCO	Committee Member

The video tape of the fire was viewed, a description of the test was presented, and members were assigned to the committee, as noted above. Eight action items were assigned by the committee. Listed below are the items and their dispositions.

1. Verify the safety of turning on the facility power, so that the other test cells can be powered up.

DISPOSITION: The test cell was checked out to ensure that all damaged electrical equipment and wiring was disconnected from the power source, and the power was turned on.

2. Check the location and tightness of the mechanical stops on the air cylinder shaft. These stops limited the incursion of the rotor into the test sample and kept the rotor from rubbing against the drive-motor end of the chamber.

DISPOSITION: Both collars were tightly fixed to the air cylinder shaft. The shaft was fully displaced in the drive-motor direction and the mechanical stop (Collar A in Figure 5), which was designed to stop the rotor from rubbing on the drive-motor end of the chamber was pressed against the end of the air cylinder. The gap between the incursion limiting mechanical stop (Collar B in Figure 5) and its stop measured 0.091 inch.

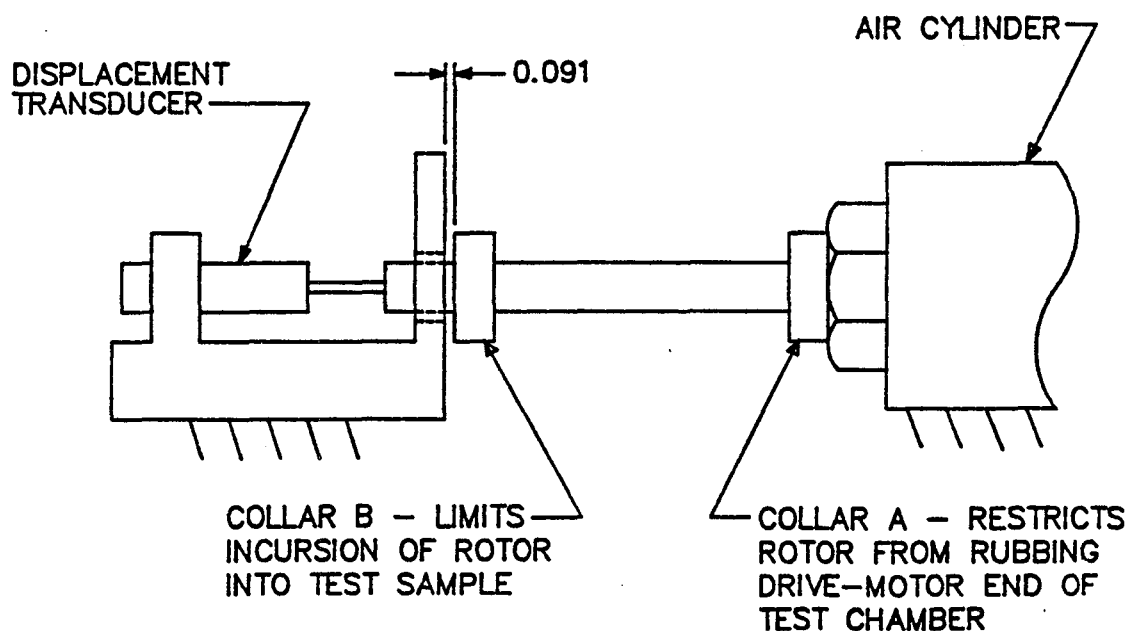


Figure 5. Location of Mechanical Stops After Test WS-31 Fire

3.0 Obtain photographs of test cell and test apparatus.

DISPOSITION: Eleven photographs were taken, and are included as Figures 6 through 16.

4.0 Verify the channel identification of all thermocouples to ensure that they are configured according to the DAS

schematic. Label the connector halves prior to separating them.

DISPOSITION: All thermocouples were connected as indicated on the system schematics. The connectors were labeled and separated.

5.0 Locate and tag ejected pieces.

DISPOSITION: The outlet fittings from the inner cavity and the outer cavity of the test chamber were the only pieces that were ejected from the test chamber. The outer cavity outlet fitting was found lying on the floor 18 inches inside the doorway leading to the High Pressure Test Area (HPTA) hallway. The piece is shown in Figure 7. The inner cavity fittings, which included thermocouple TC-AK820, were found lying on the FRT base plate, underneath the test chamber. The backup nut from the thermocouple fitting is shown in the lower right-hand corner of Figure 11, and the thermocouple and its fittings can be seen in Figure 12, which is an overhead view of the test chamber.

6.0 Carefully inspect the system for additional data.

DISPOSITION: The following observations were noted during this inspection:

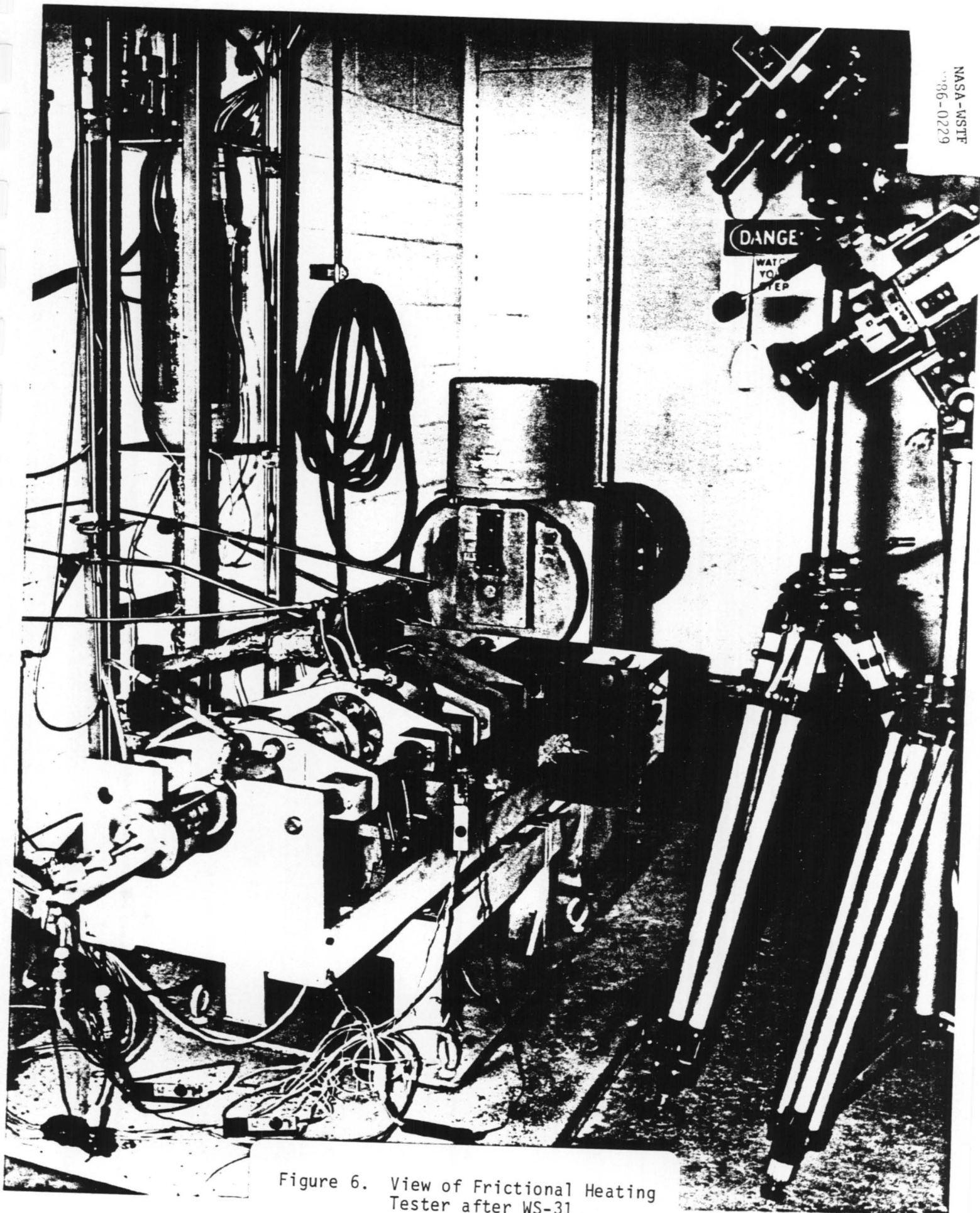


Figure 6. View of Frictional Heating Tester after WS-31

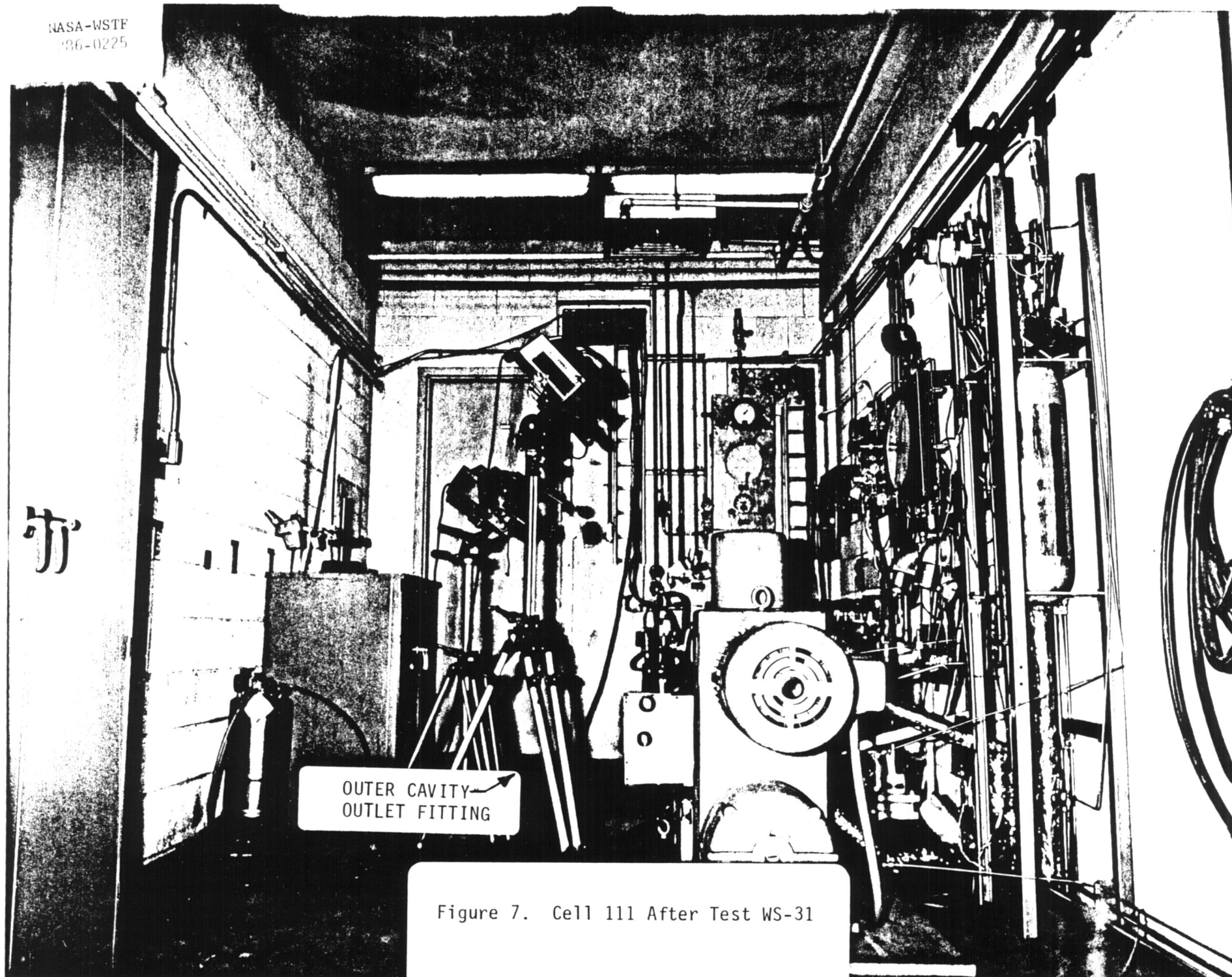


Figure 7. Cell 111 After Test WS-31

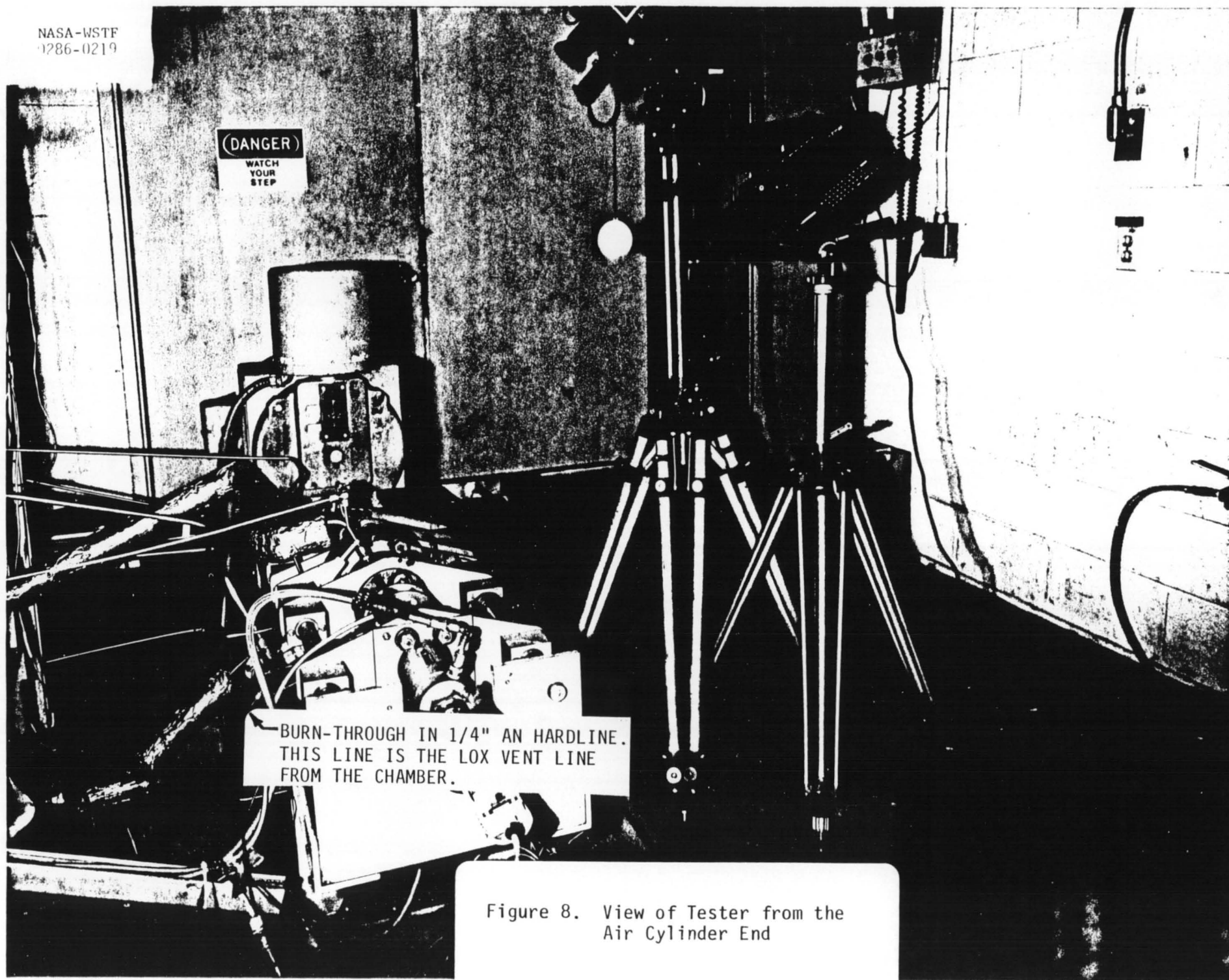


Figure 8. View of Tester from the Air Cylinder End

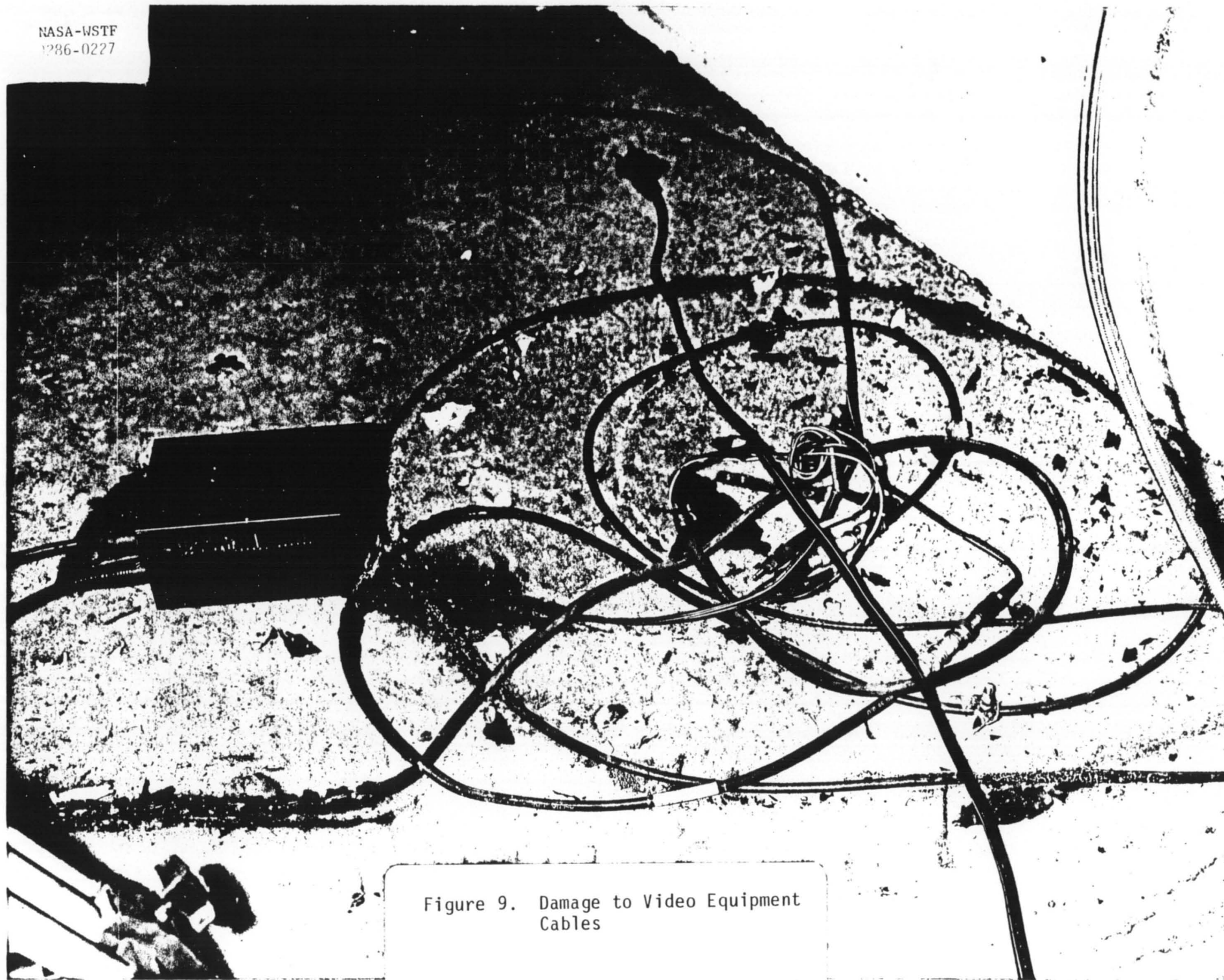


Figure 9. Damage to Video Equipment
Cables

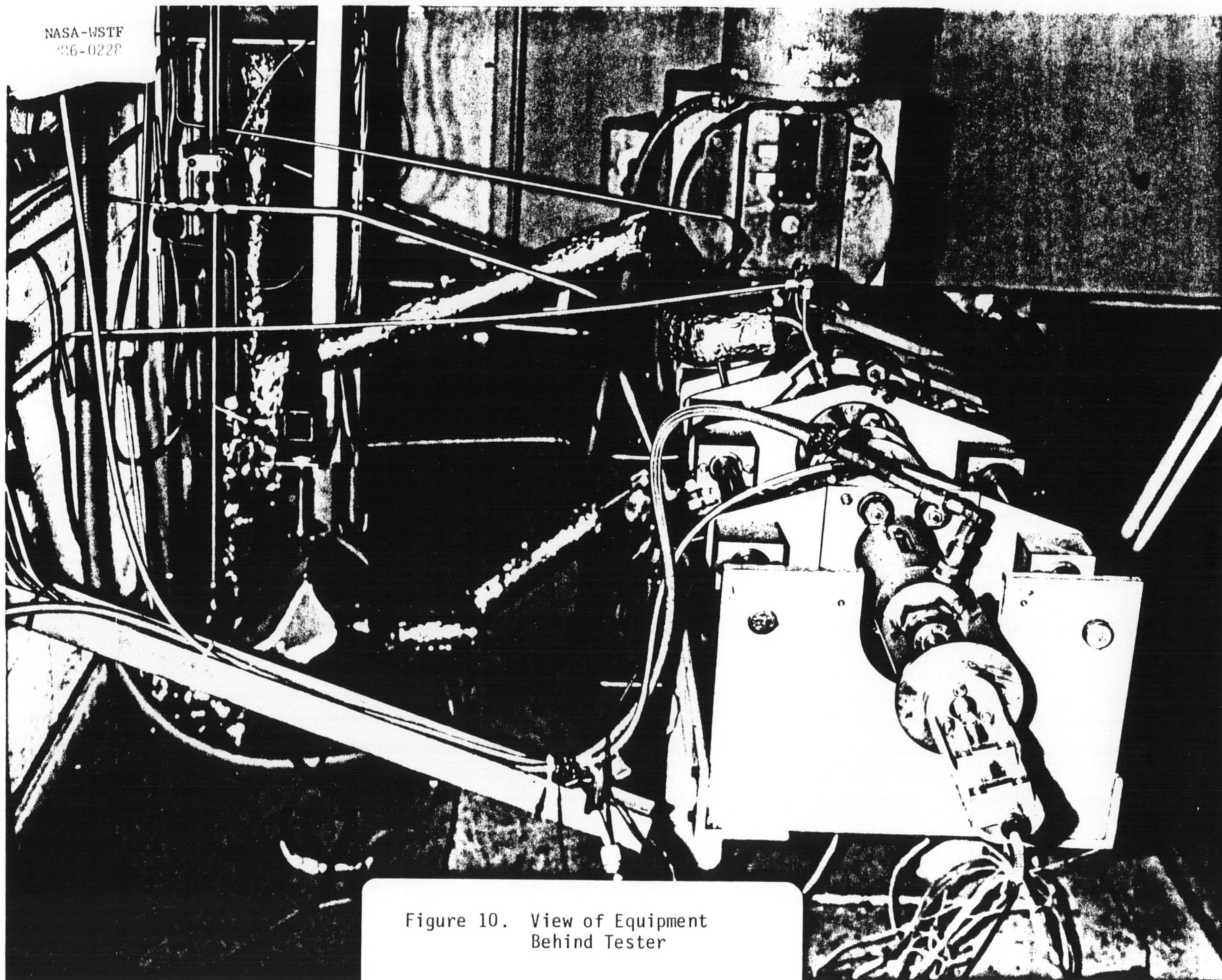


Figure 10. View of Equipment
Behind Tester

NASA-WSTF
1286-0226

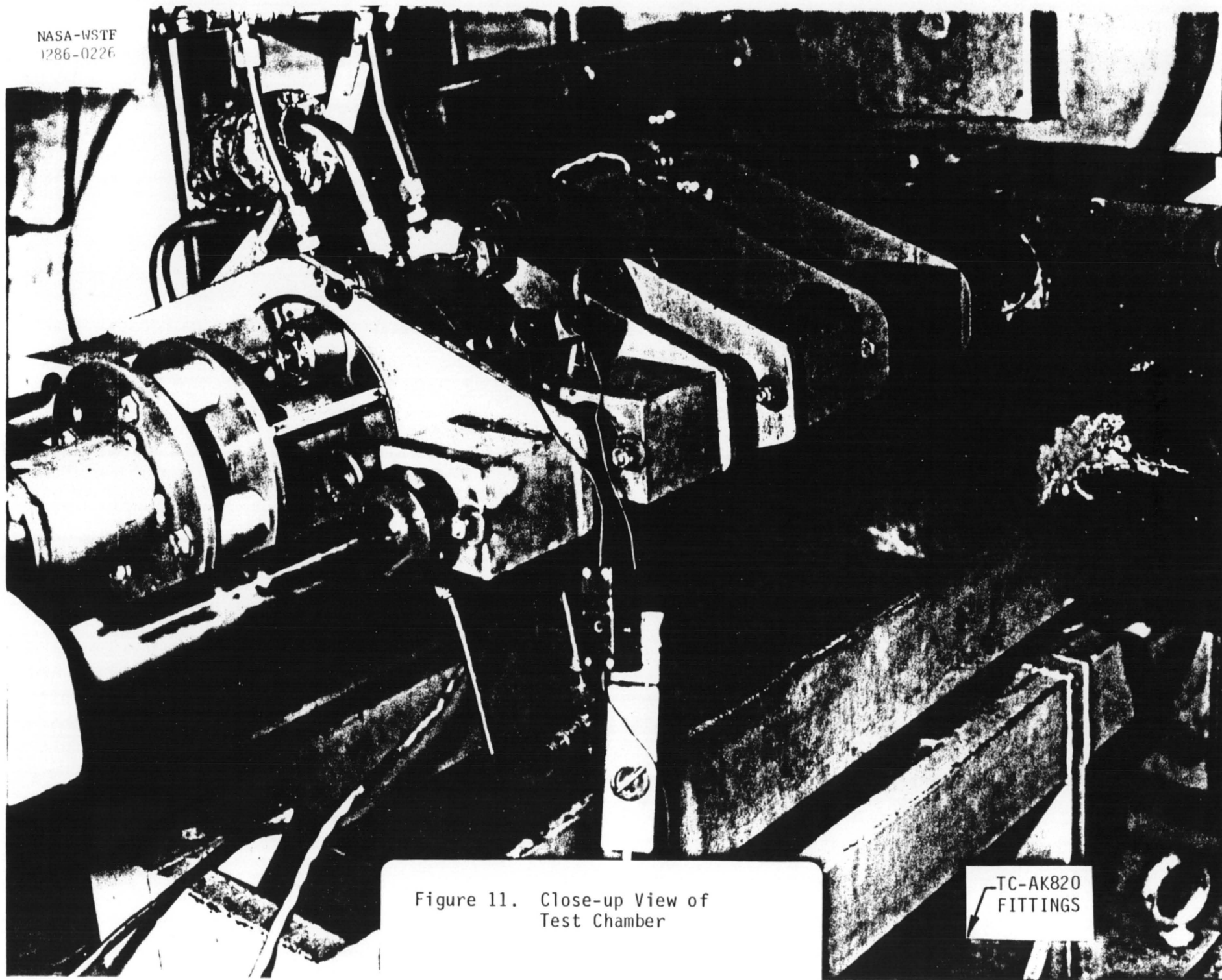


Figure 11. Close-up View of
Test Chamber

TC-AK820
FITTINGS

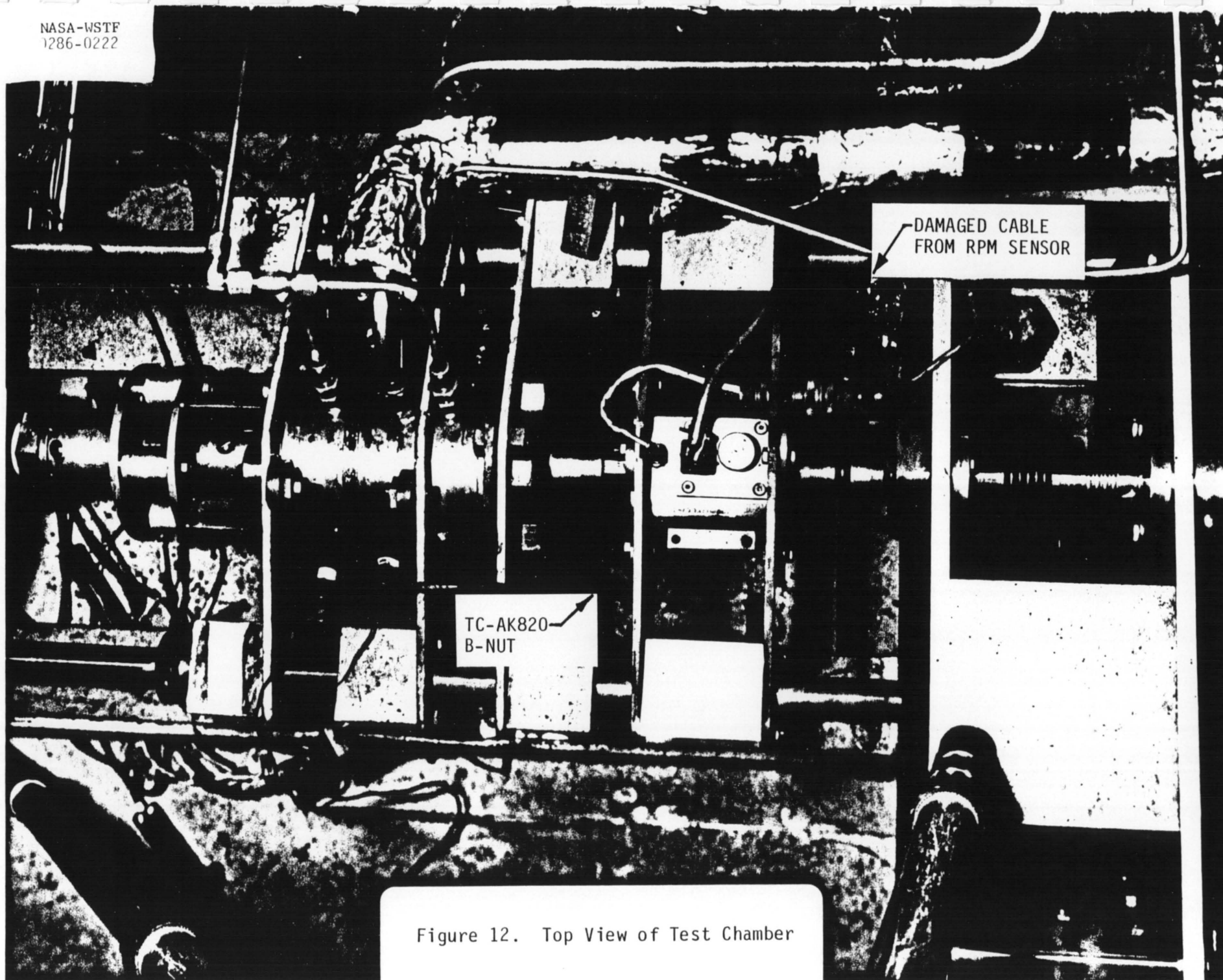


Figure 12. Top View of Test Chamber

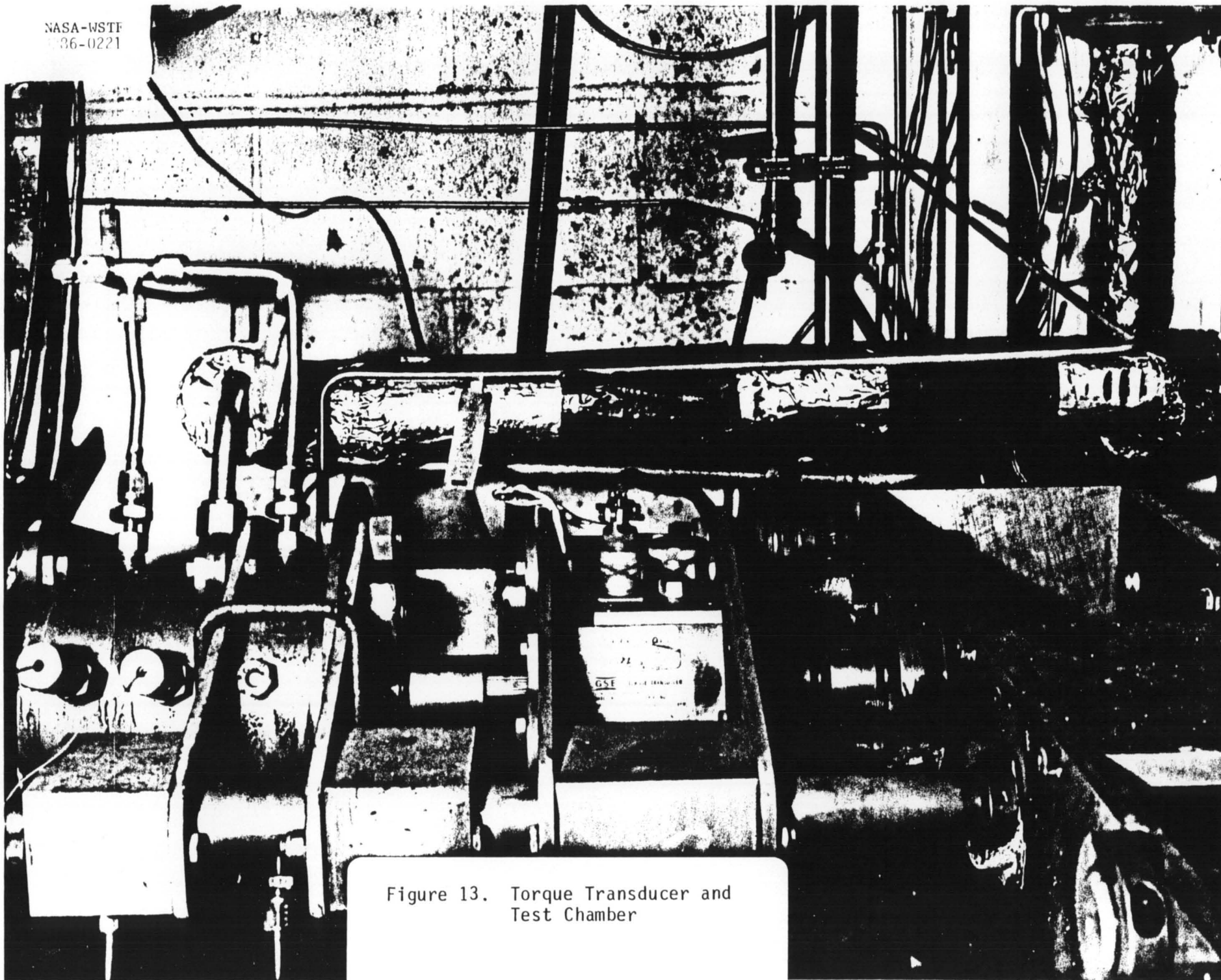


Figure 13. Torque Transducer and
Test Chamber

NASA-WSTF
86-0220

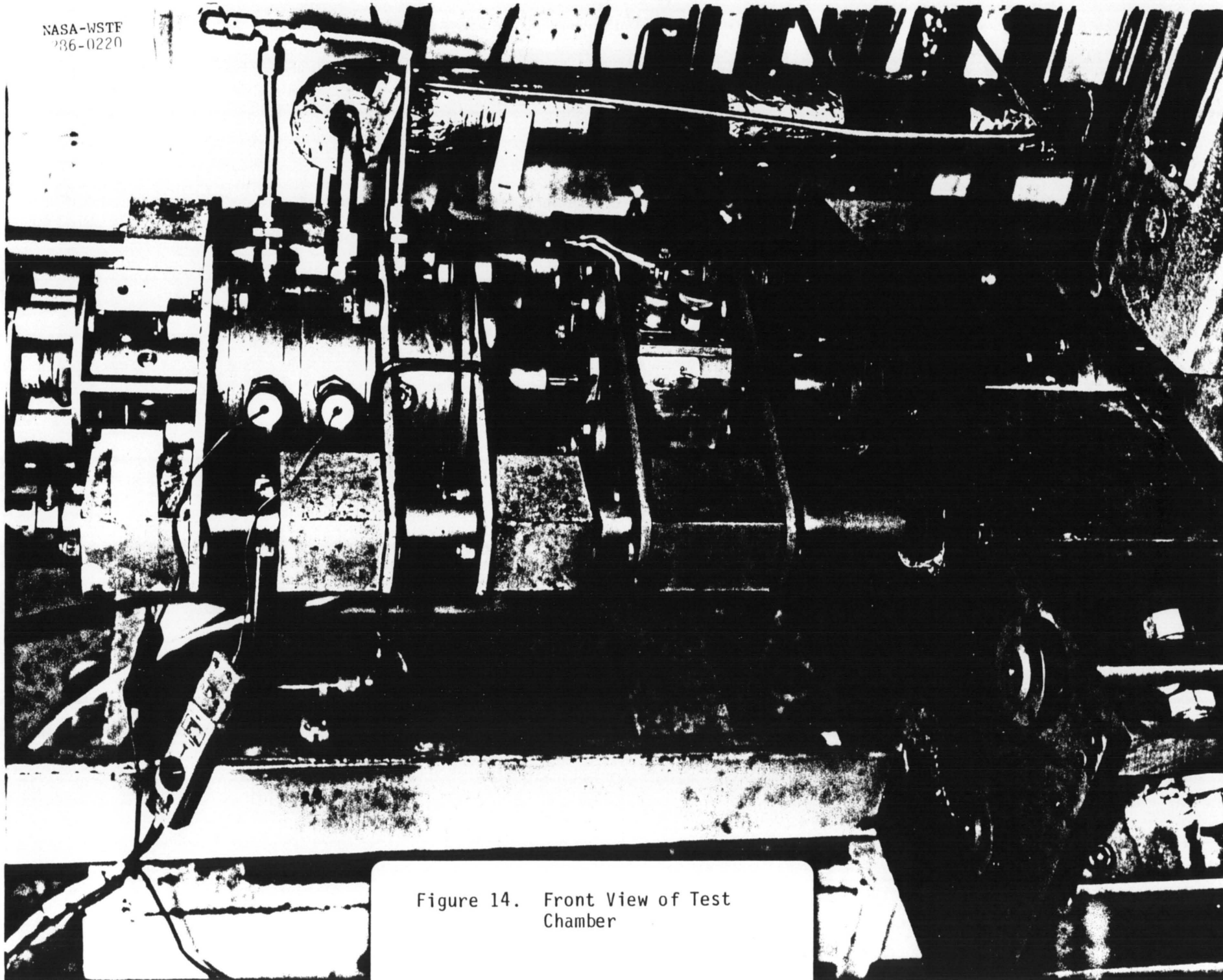


Figure 14. Front View of Test Chamber

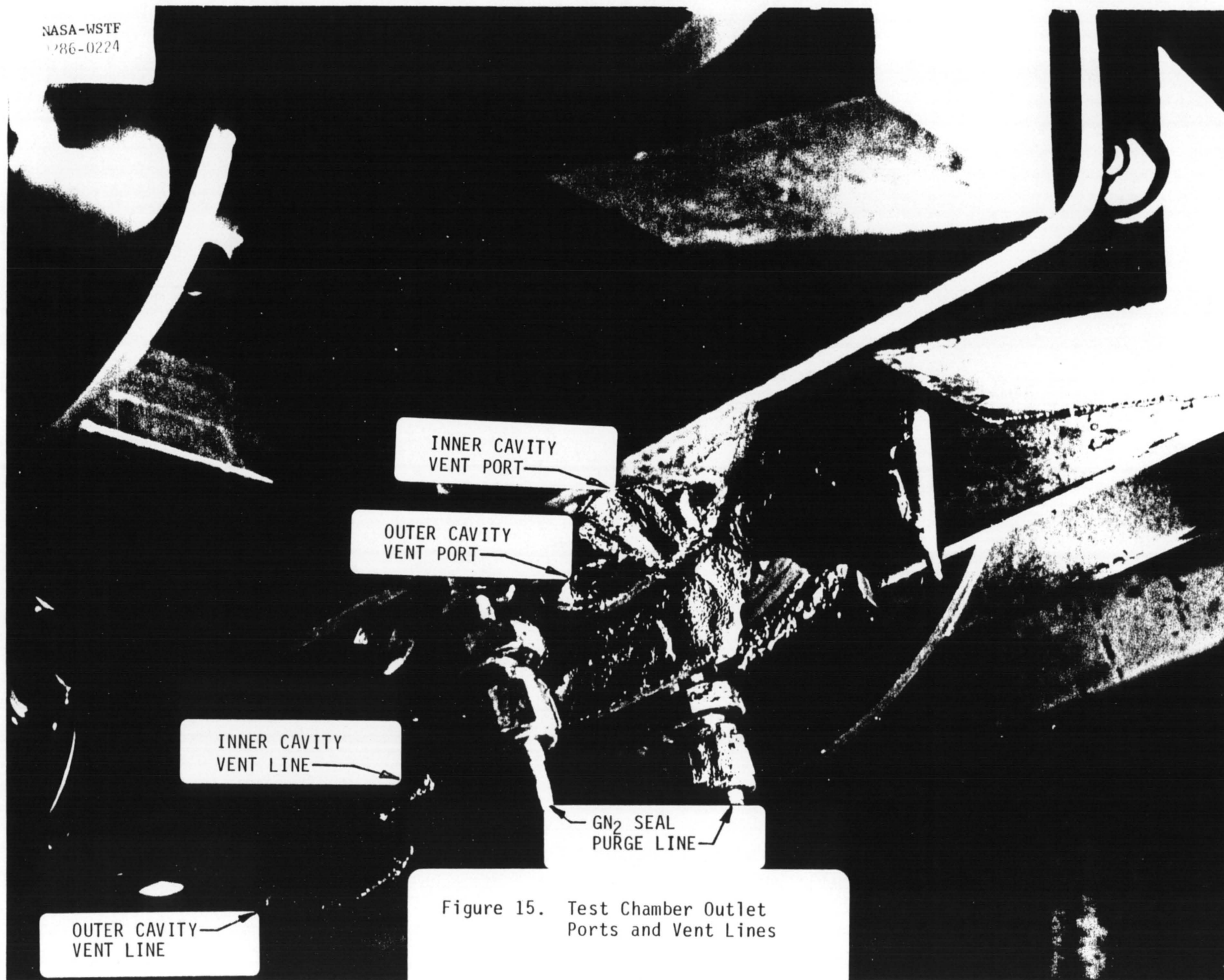


Figure 15. Test Chamber Outlet Ports and Vent Lines

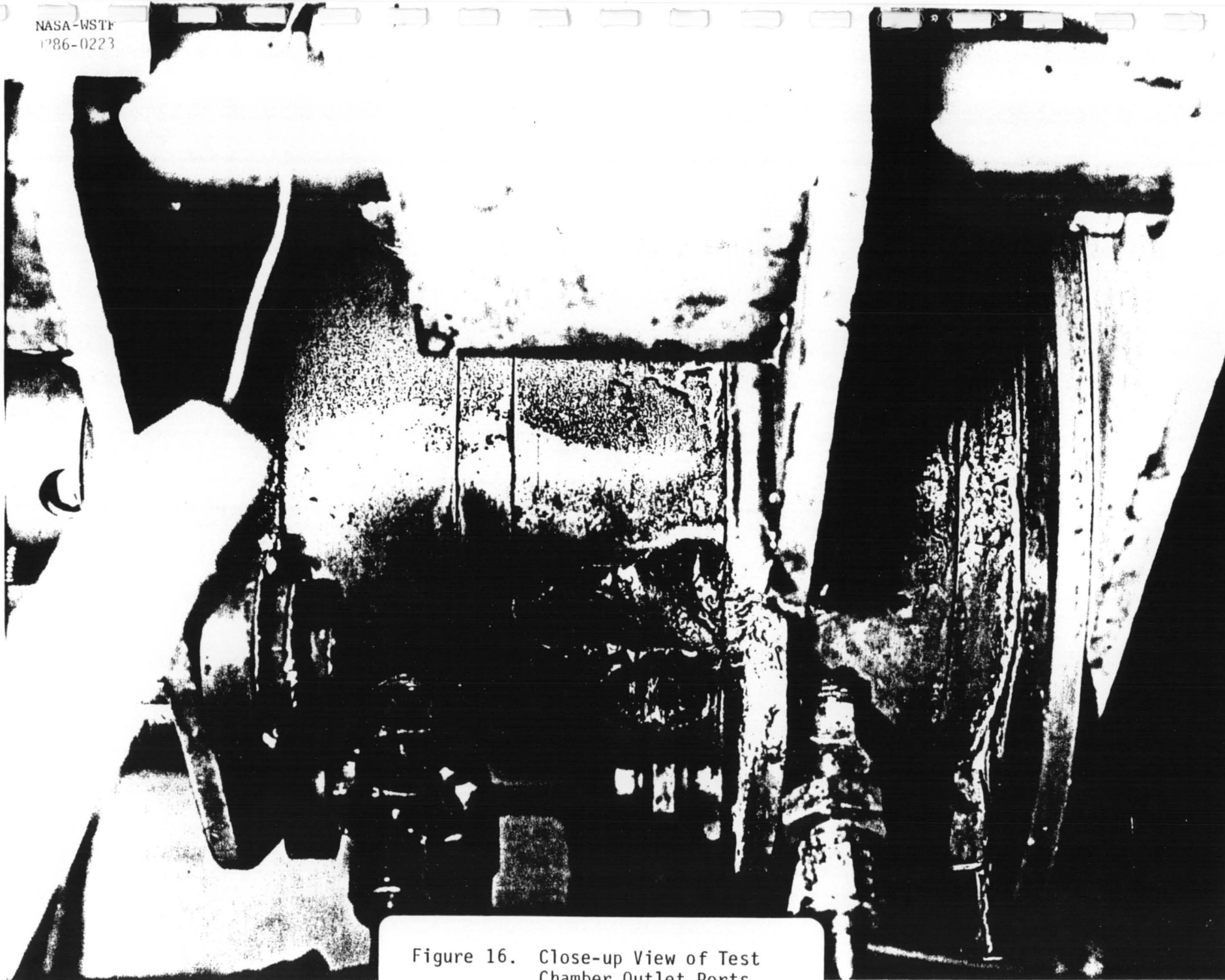


Figure 16. Close-up View of Test Chamber Outlet Ports

1. The LOX outlet fittings from the test chamber inner and outer cavities were burned and had been ejected from the chamber. The two 1/4-inch AN hardlines connected to the outlet fittings were burned several inches back, as shown in Figure 15. A schematic of the outlet lines is shown in Figure 17.

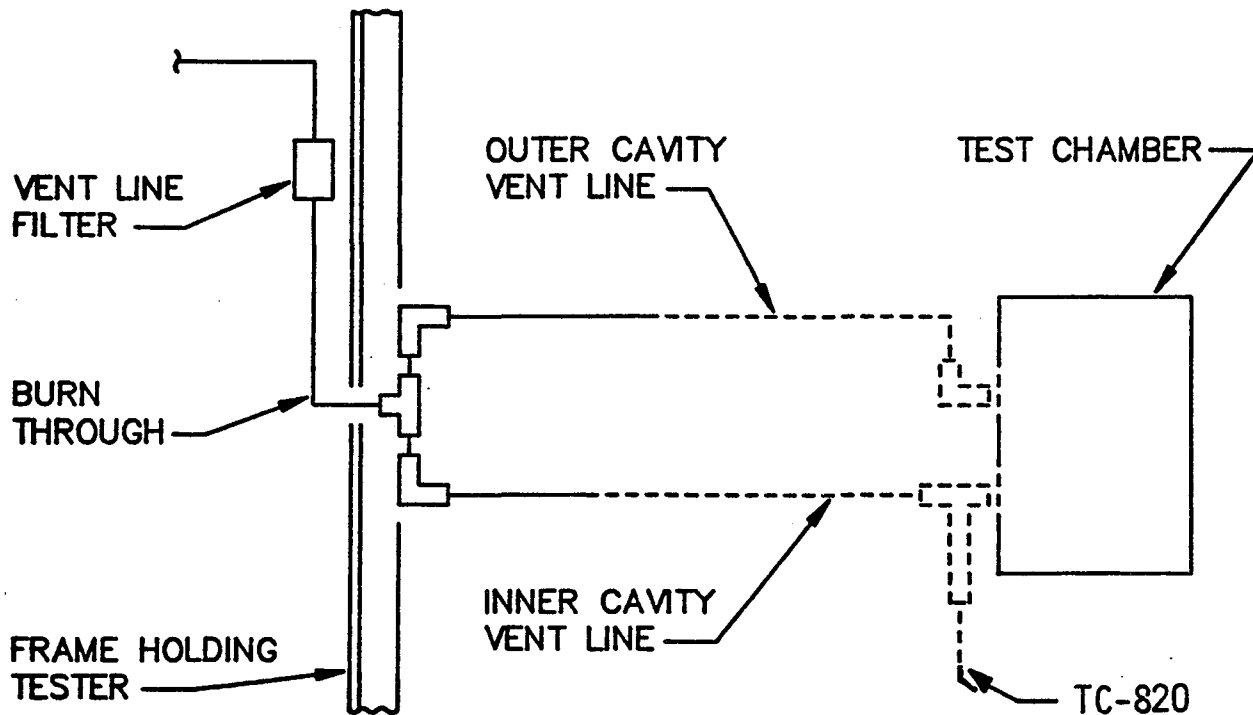


Figure 17. Schematic of Test Chamber Outlet Lines

It was noted that there was a burn-through in the wall of the AN tubing at the 90° bend downstream of the connection of the two outlet lines, as shown in Figure 17. The burn-through is also shown in Figure 8. From this photograph it should be noted that the location of the burn-through is behind the frame of the tester, when viewed from the video camera.

2. All the electrical cables that were damaged, other than very minor damage, were in the immediate vicinity of the test chamber, or were lying on the floor. The cables for thermocouples TC-AK707, TC-AK703, TC-AK704, TC-AK708, TC-AK820, and TC-AK812 were damaged. The reference junctions for TC-AK704 and TC-AK702 were burned and melted. The cable for the rpm sensor was badly damaged (see Figure 12) and the plastic casing of the 480V power cord to the drive motor was slightly damaged. The power cables for the video cameras were badly damaged, as shown in Figures 8 and 9.

7.0 Using a borescope, inspect the inside of the test chamber.

DISPOSITION: The fire burned through the test chamber at the inner and outer cavity vent ports (Figures 15, 16). The most damaged portion of the chamber was the portion that was seen through the inner cavity vent port. Looking through this port, the following was observed:

- A. The flange portion of the air-cylinder-end fluorogold seal. The cup portion and the spring were missing.
- B. The burned end of the shaft on the rotor side was seen. The shaft on the air cylinder end was burned back to the fluorogold seal.
- C. The sample material was completely consumed and the sample holder was partially consumed. The face of the rotor could be seen..
- D. The face of the rotor was intact. The knife-edge was covered, in places, with slag.
- E. The air-cylinder-end of the protective copper sleeve was burned/melted away, especially on the side of the chamber nearest the inner cavity vent port.
- F. Two of the socket-head screws that held the sample holder to the test chamber and section were still intact.

Looking through the outer cavity vent port, it was noted that there appeared to be little or no damage to the drive motor end of the test rotor, shaft, and fluorogold seal.

- 8. Check the damage done to the electrical cables and make recommendations to ensure that they are better protected in the event of another fire.

DISPOSITION: The damage to the electrical cables was noted in paragraph 2 of the the disposition for Action Item 6. It was recommended that the cables be rerouted so that they would be out of the direct line of fire of any fire that may occur in the test chamber. The reference junctions for the thermocouples should be moved from near the test chamber to a

more remote, protected location. Instrumentation and electrical chambers should not be located near the ends of the chamber, where the shaft penetrates the chamber. A protective shield should be placed between the test chamber and the video cameras.

In addition to the eight actions listed on the previous pages, the video tape of the test chamber was reviewed and an attempt was made to correlate the events recorded on the tape with the events noted from the digital data. The framing rate of the video camera was 30 frames per second. A diagram depicting the results of this correlation is shown in Figure 18.

4.2 Committee Meeting of 02/05/86

On February 5, 1986, the second meeting of the failure analysis committee was held. The attendees were:

Frank Benz	NASA
C. V. Bishop	LEMSCO
M. D. Pedley	LEMSCO
Bob Johnson	LEMSCO
Ralph Williams	LEMSCO
John Homa	LEMSCO
Tim Irvin	ROCKETDYNE (818) 710-3605

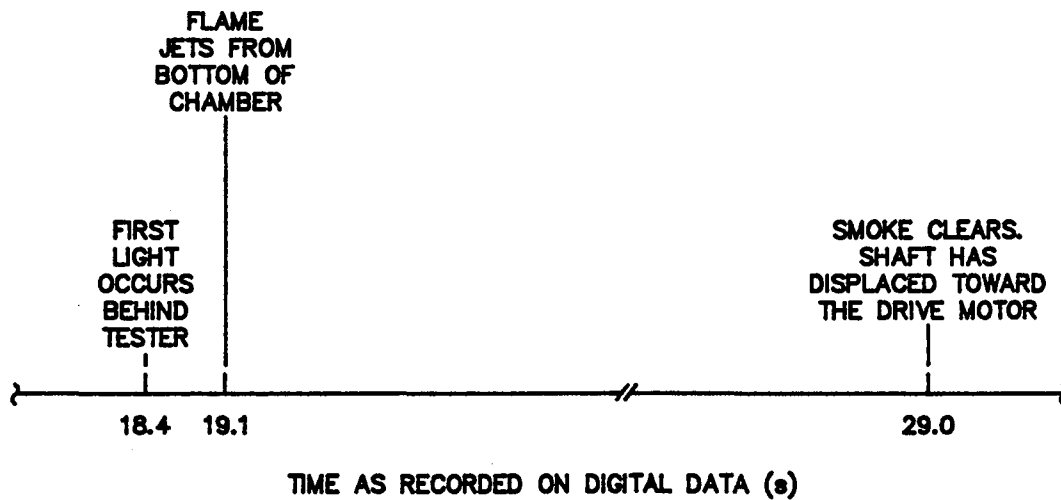
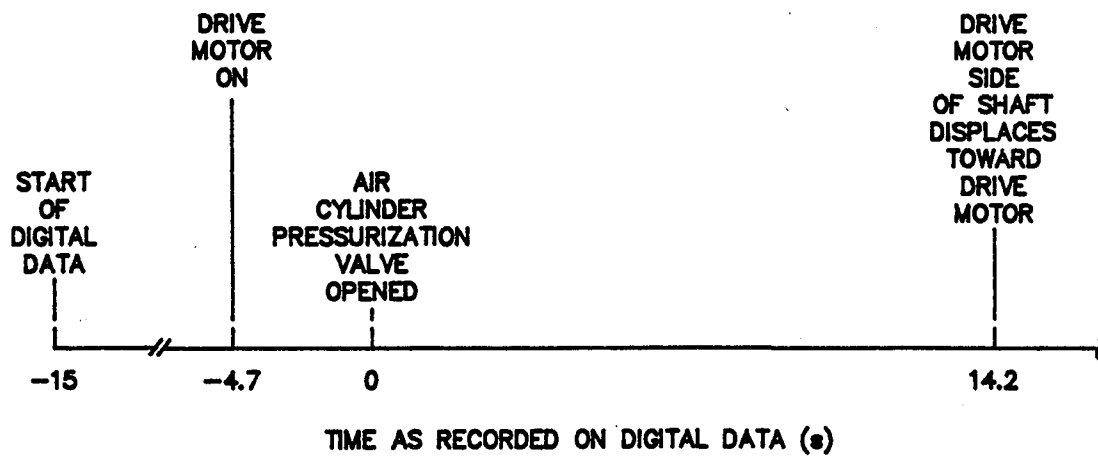


Figure 18. Correlation of Events Observed on the Video Recording with Those Ascertained from the Digital Data

The results of the action items from the February 3rd meeting were discussed and the test data were reviewed. In light of the results of those action items, postulated failure mechanisms were discussed. Six action items were assigned by the committee. Listed below are the items and their respective dispositions:

1. Disassemble the lines downstream of the test chamber and inspect the filter carefully for burned and unburned test sample material.

DISPOSITION: The lines and the filter were carefully removed and the filter was carried and opened in a manner that did not disturb its contents. The removed filter is shown in Figure 19. Slag from the fire can be seen on the inlet fitting. In Figure 20, it can be seen that slag and other debris were located in the inlet fitting and on the upstream side of the filter element. Although the downstream side, or outlet fitting, was discolored, it did not contain any slag or other debris. The filter element was still intact, as shown in Figure 21.

2. Review the method of setting and checking the normal load and rotor displacement prior to the next test. Consider the possibility of ramping the normal load to the desired level and holding it constant.

DISPOSITION: Several discussions with the customer were held and plans to accomplish these items were made.

Test Chamber outlet filter
Test number WS-31
1-31-86

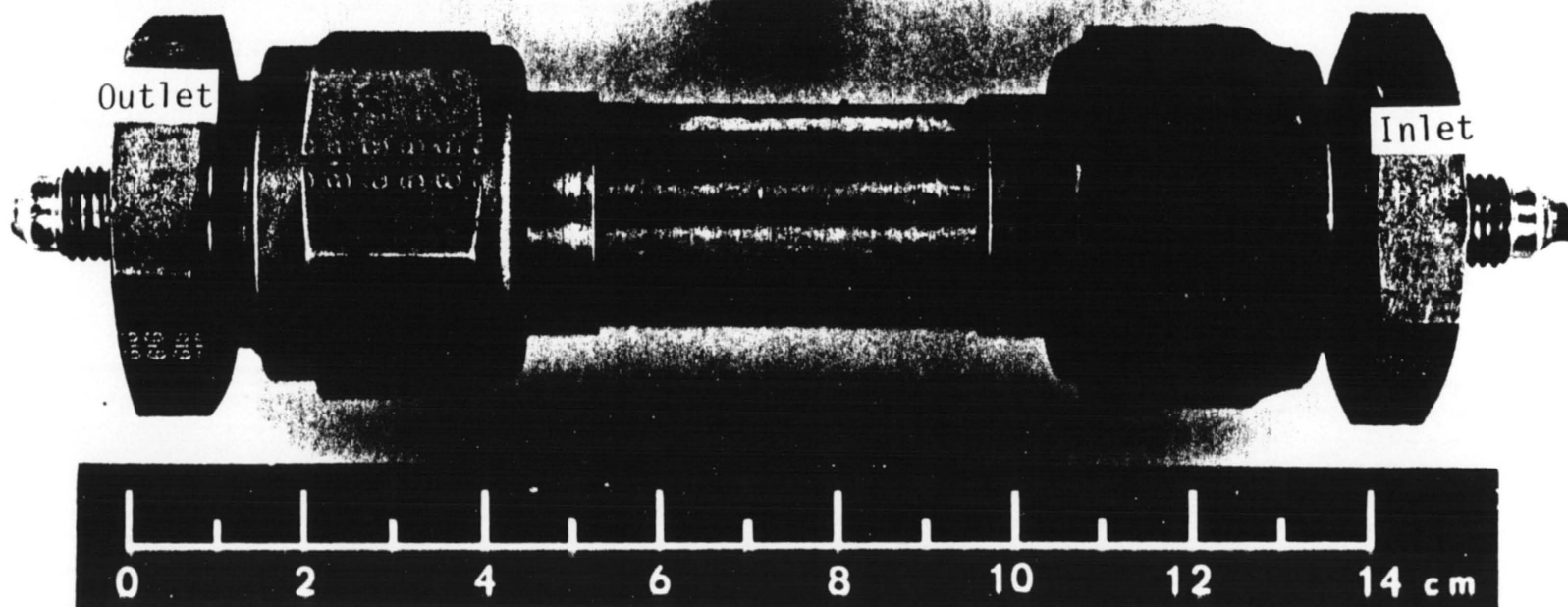


Figure 19. Test Chamber Outlet
Filter Before Disassembly

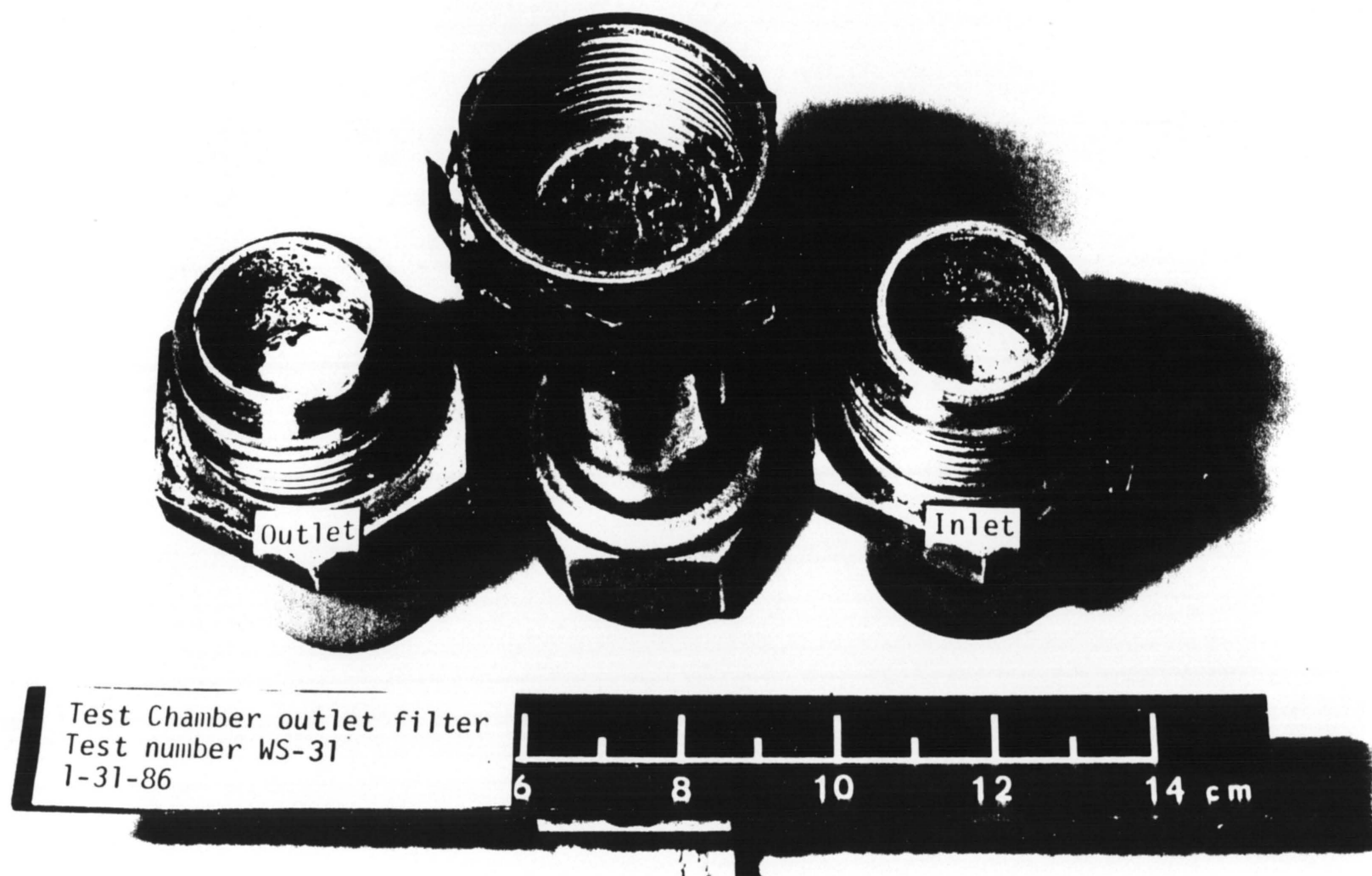


Figure 20. View of the Inside of the
Test Chamber Outlet

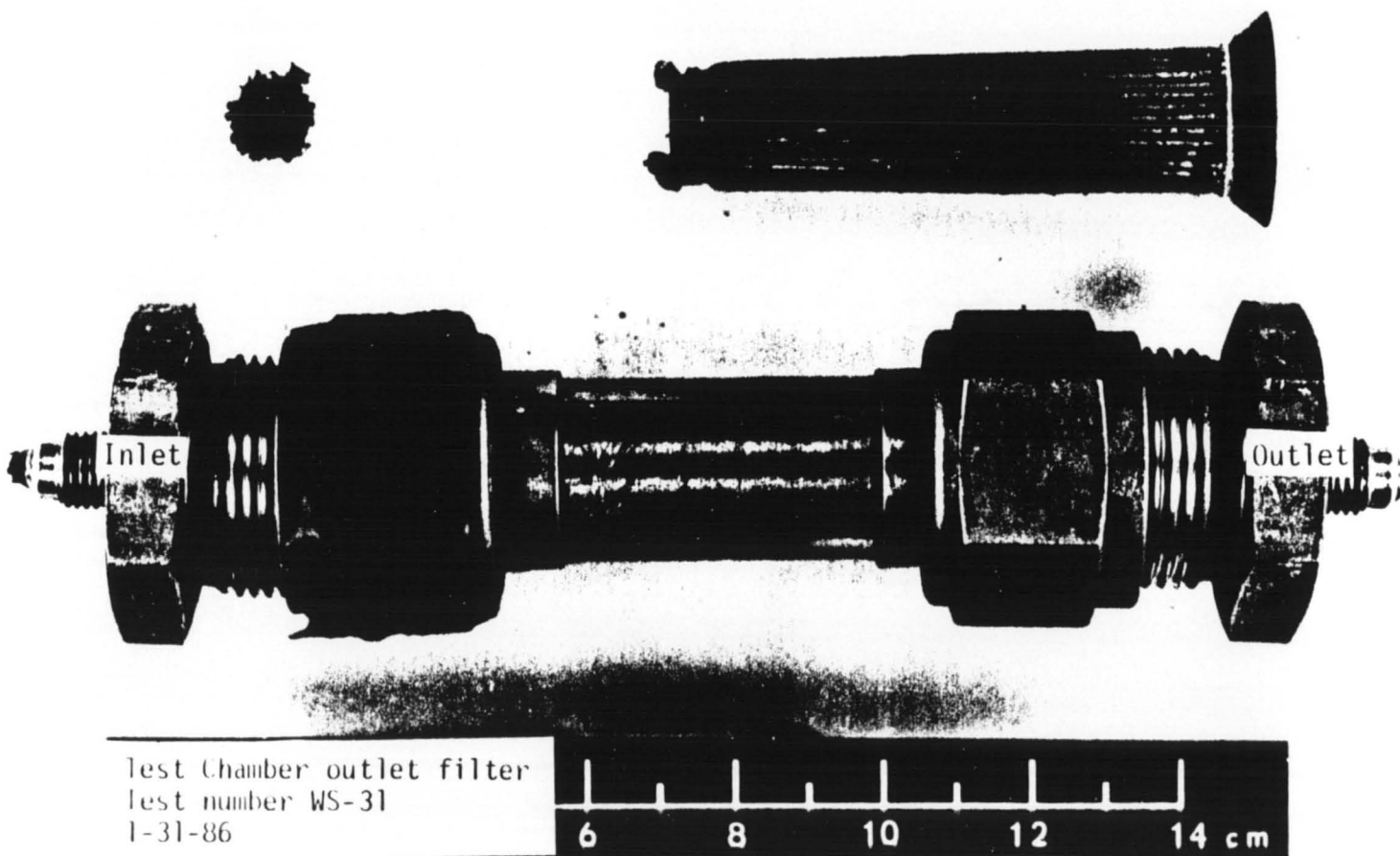


Figure 21. Filter Element and
Chamber Housing

3. Disassemble and photograph the test apparatus.

DISPOSITION: The test apparatus was disassembled and the test chamber was removed to the Low Pressure Laboratory for disassembly. Two photographs of the test chamber, taken prior to disassembly, are shown in Figures 22 and 23. In Figure 22, the bottom of the chamber and the associated fittings and lines are shown. The location in the 1/4-inch hardline where the first fire burned through can be seen at the far left.

To the right of the site of the first burn-through, the tee joining the inner cavity vent line (top) and the outer cavity vent line (bottom) can be seen. The inner and outer cavity vent line fittings are shown in the locations that they were in before the test. TC-820, the inner cavity vent thermocouple, is shown installed in the inner cavity vent line fittings. Figure 23 depicts another bottom view of the test chamber, in which the damage to the inner and outer cavity vent ports can be seen. Most of the damage occurred at the inner cavity vent port.

Four photographs of the disassembled test chamber are shown in Figures 24 through 27. A view of the test chamber from the drive motor end is shown in Figure 24. It can be seen that the test sample was totally consumed, and that the rotor blade had rubbed into the sample holder. The top and bottom of the test chamber, as it was oriented in the test apparatus, is indicated. The bottom of the test sample holder was totally consumed, while the top was left partially intact. This indicates that the test sample melted and dripped or fell to the bottom of the chamber as it

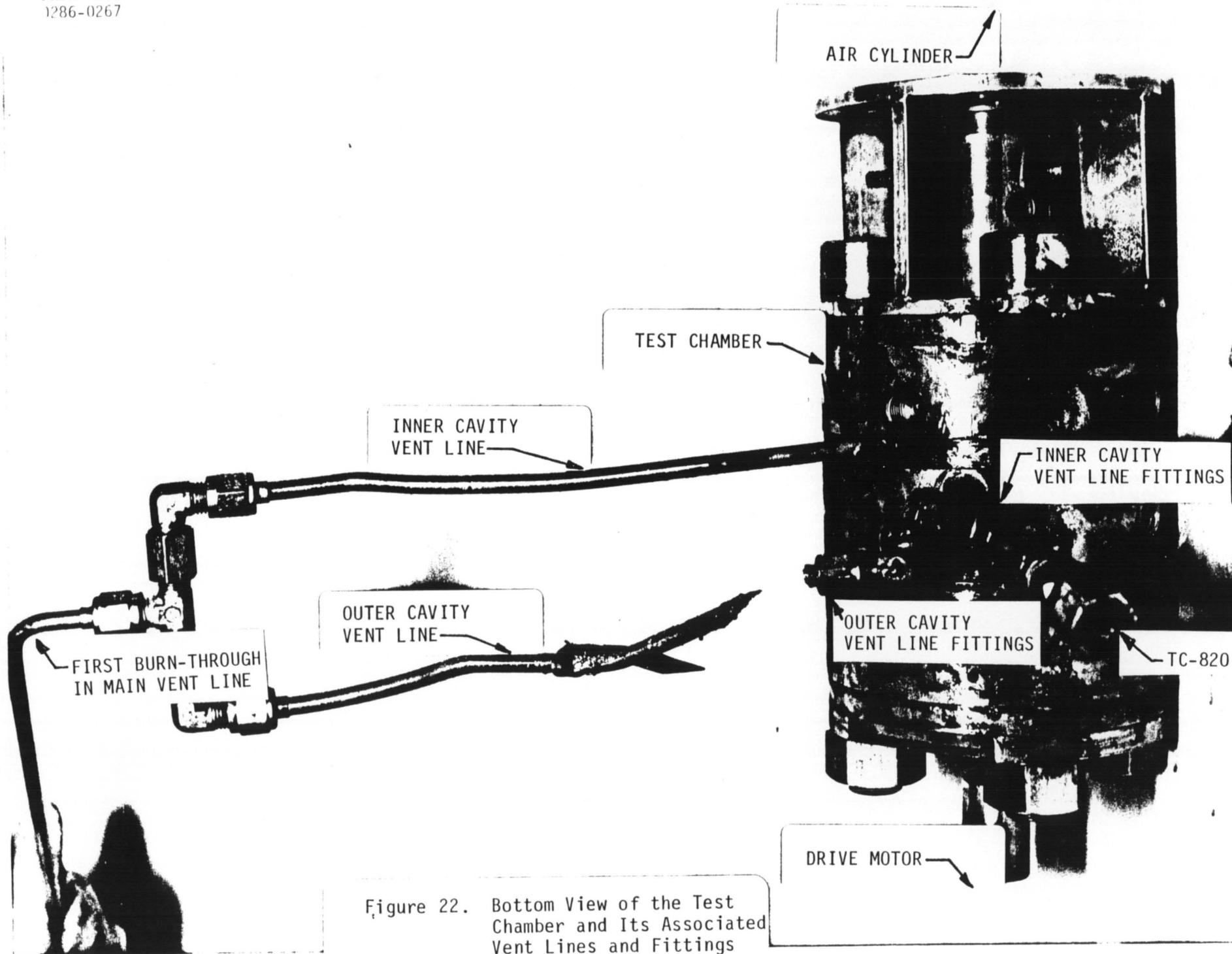


Figure 22. Bottom View of the Test Chamber and Its Associated Vent Lines and Fittings After Being Removed from the Test System

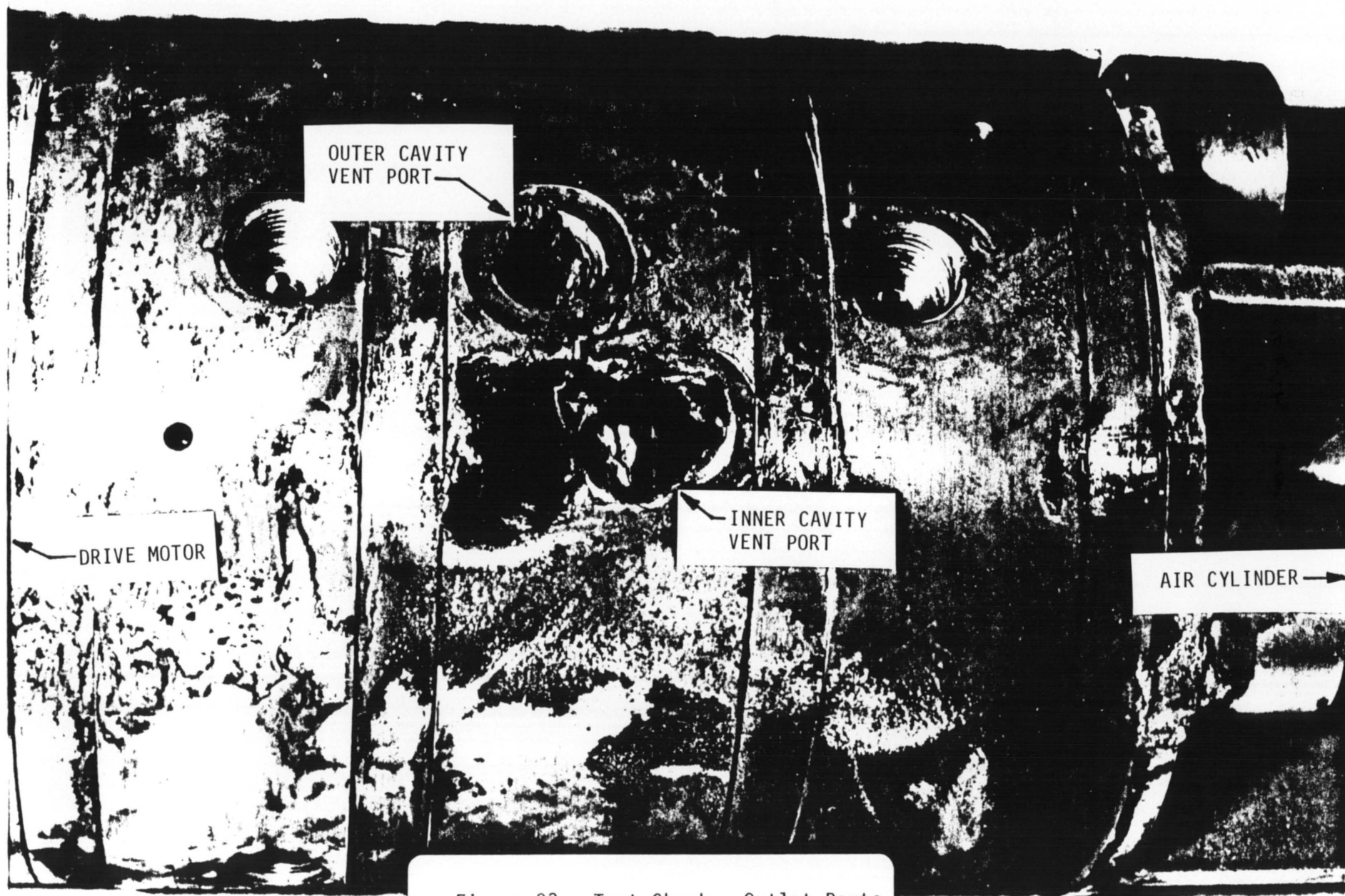


Figure 23. Test Chamber Outlet Ports

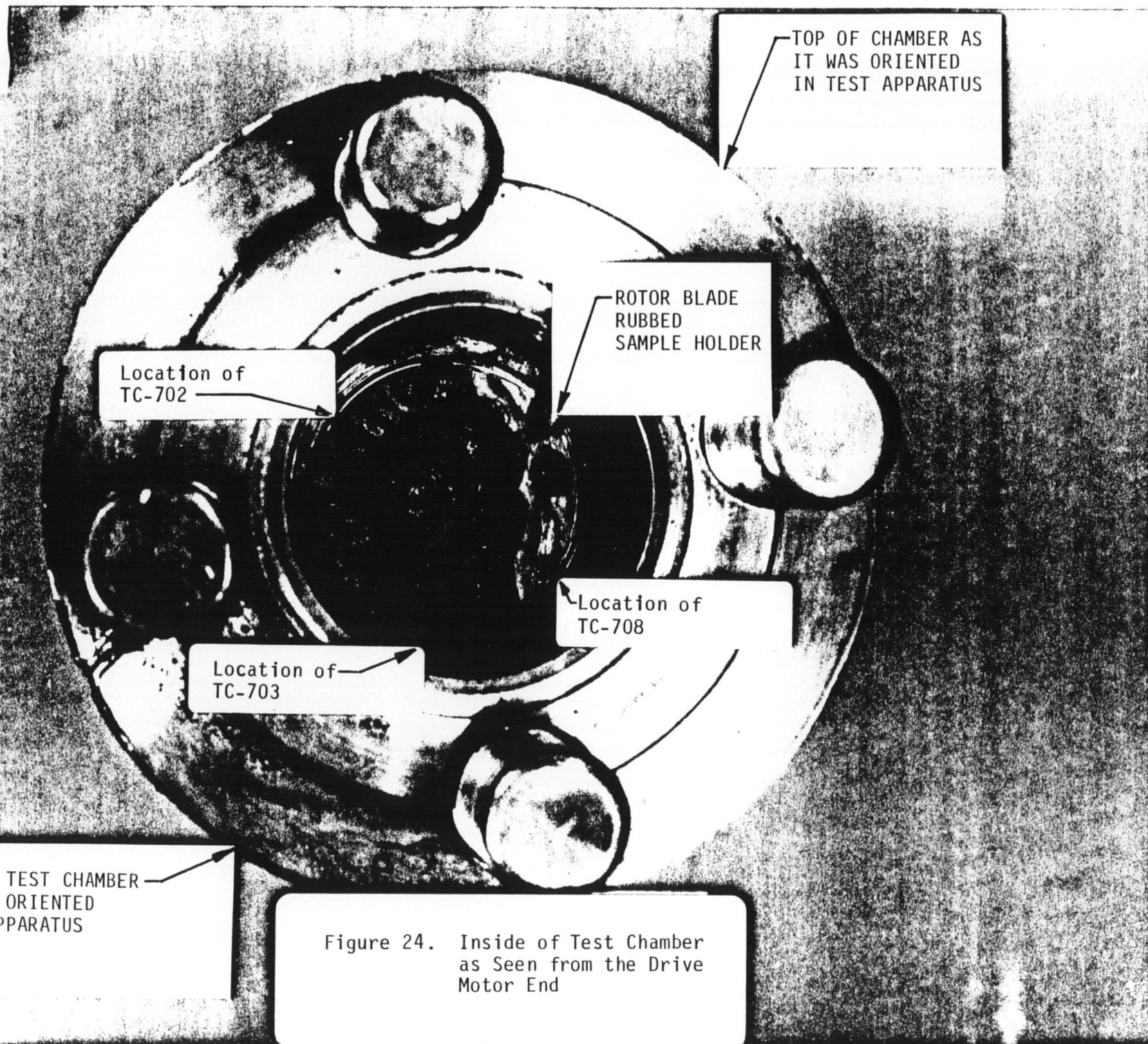


Figure 24. Inside of Test Chamber
as Seen from the Drive
Motor End

BOTTOM OF TEST CHAMBER
AS ORIENTED IN TEST
APPARATUS

38

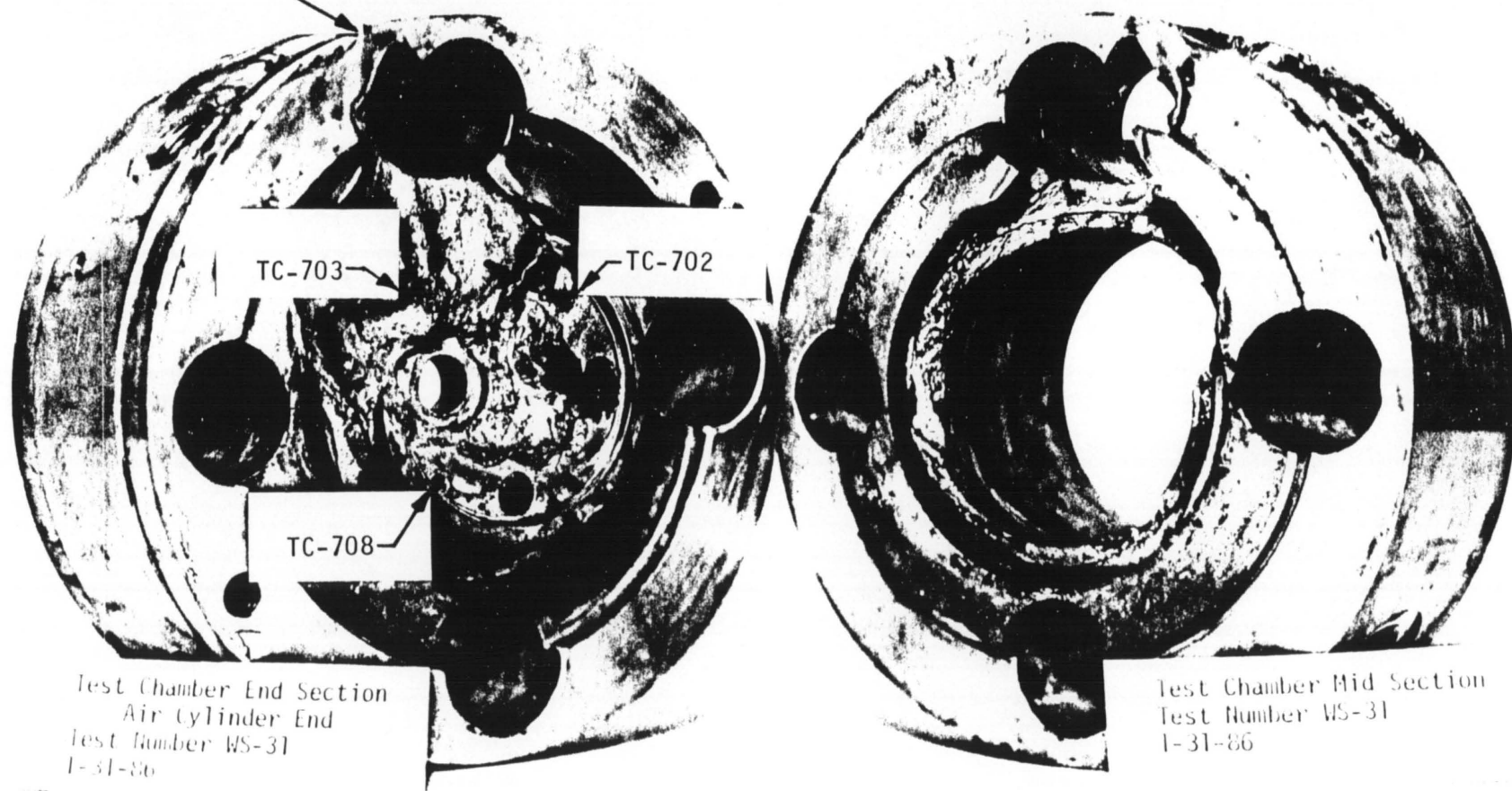


Figure 25. Test Chamber End-Section
with Sample Holder and
Test Chamber Mid-Section

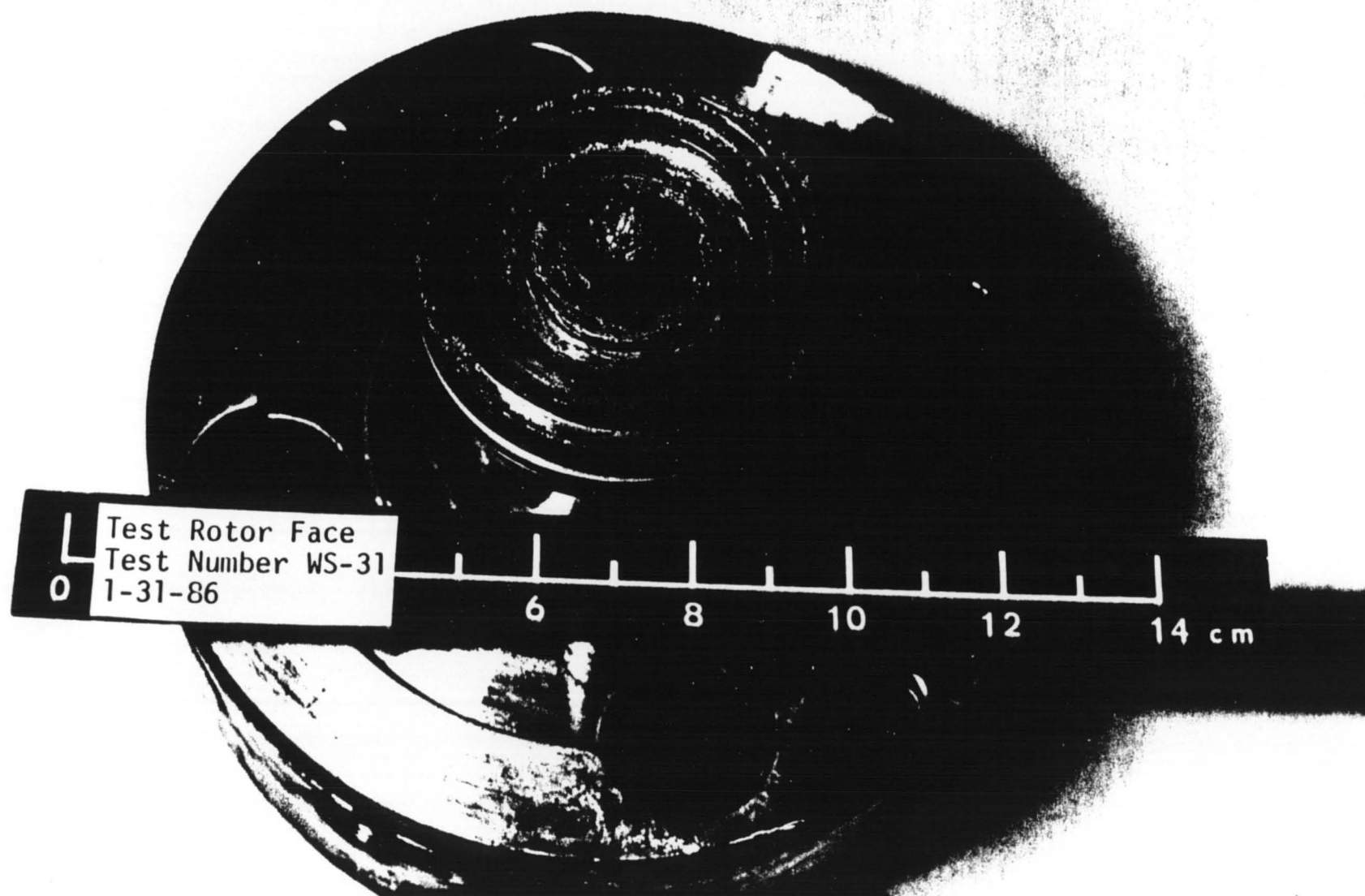


Figure 26. Test Rotor and Test Chamber End-Section



Test Chamber End Section
Drive Motor Side
Test Number WS-31
1-31-86

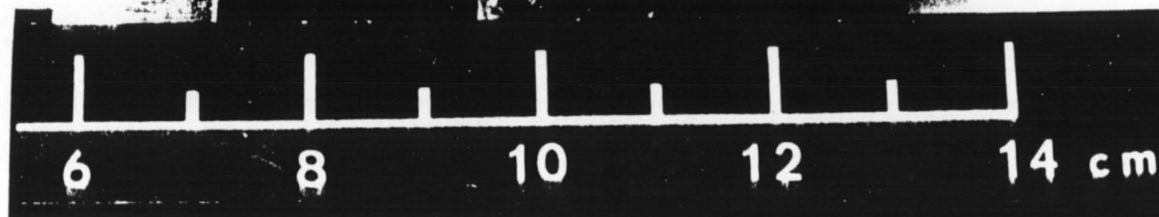


Figure 27. End-Section Located on
Drive Motor Side of
Test Chamber

burned. The locations of the three thermocouples that were imbedded in the test sample are also shown in this figure. The yellow chamber shaft seal and the burned end of the shaft can be seen at the center of the chamber.

The damage done to the portion of the test chamber which contained the test sample can be more clearly seen in Figure 25. This photograph shows the test chamber mid-section and the test chamber end section that was located on the air-cylinder-end of the chamber. The bottom and top of the chamber, as it was positioned in the test apparatus, and the location of the test sample thermocouples, are indicated. Nearly all of the damage sustained by the test chamber occurred in this area, indicating that this was the most probable location of the cause of the fire.

The rotor face, shown in Figure 26, was relatively undamaged, compared to the test sample. The other end of the burned portion of the shaft is shown in this photograph. It should be noted that the portion of the rotor and test chamber located behind the rotor face are undamaged. This indicates clearly that the fire originated in the section of the test chamber containing the test sample. The undamaged test chamber end section that was located on the drive motor end of the chamber is shown in Figure 27.

4. Determine if the temperature spike indicated by TC-704 at 12.3 seconds is real, or if it was caused by electrical noise.

DISPOSITION: This spike was caused by a single data point in the digital data that was being taken at a rate of 10 points per second, and it had a magnitude of approximately 70 F. It is possible that the thermocouple could have responded that quickly if the driving function was sufficiently large. The only thing that could have caused a temperature gradient large enough to cause this spike would be a bubble of hot GOX that passed quickly by the end of the thermocouple. Whether or not a bubble such as this existed in the test chamber at that time in the test is unknown.

5. What is the strength of the 17-4 PH shaft at the test temperature?

DISPOSITION: While investigating this action item, it was determined that the shaft material was 304 SS, rather than 17-4 PH, as it was supposed to be. The strength of 304 SS at the test conditions is greater than at ambient temperature.

6. Determine the possible deformation of the test sample material under a normal load that was as large as the one used in the pretest setup that was done prior to Test WS-31.

DISPOSITION: It was determined that the VespeI SP-211 sample material had been subjected to an 11,300-lb/sq in load during the pretest setup procedure. A test setup was made using 3/4-inch-diameter discs made from VespeI SP-211 and a rotor, as shown in Figure 28. Four 0.060-inch-thick

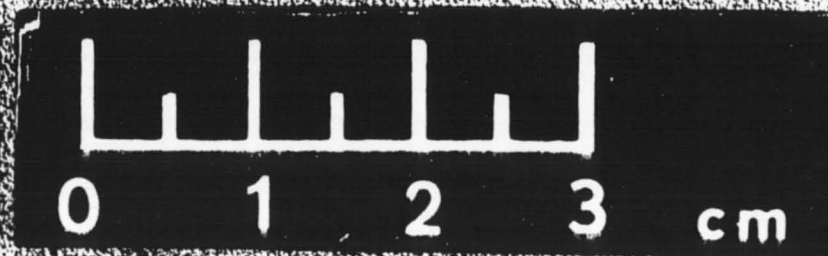
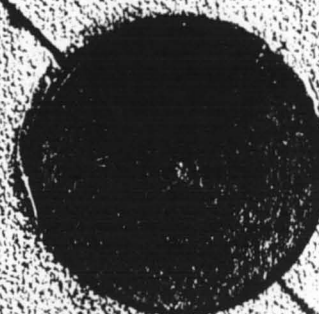
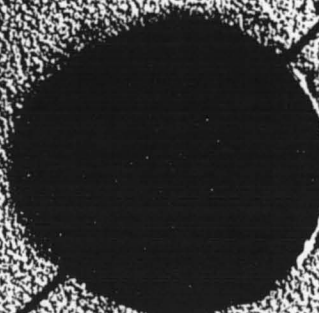
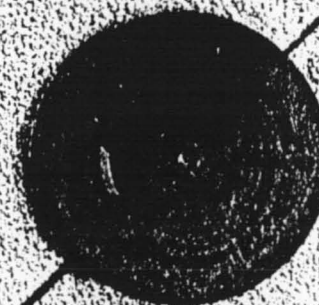
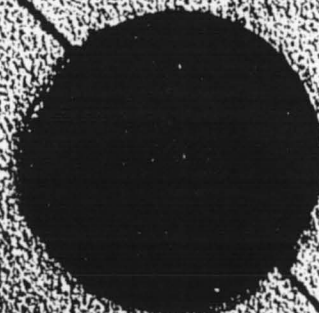
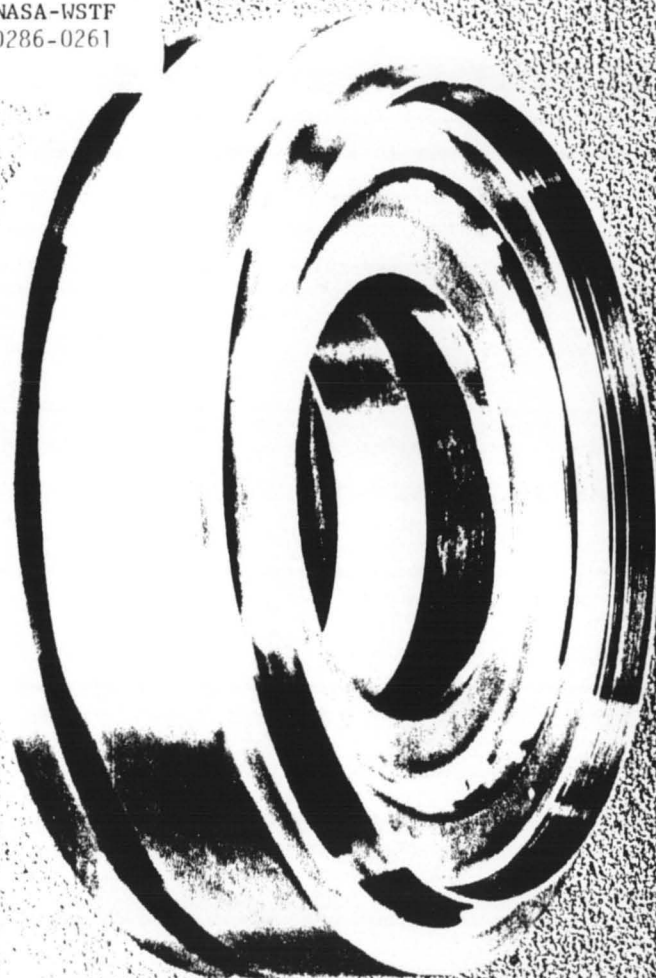


Figure 28. Test Setup Used to Determine the Deformation of the Test Sample Material Due to Load Applied to Sample Prior to WS-31

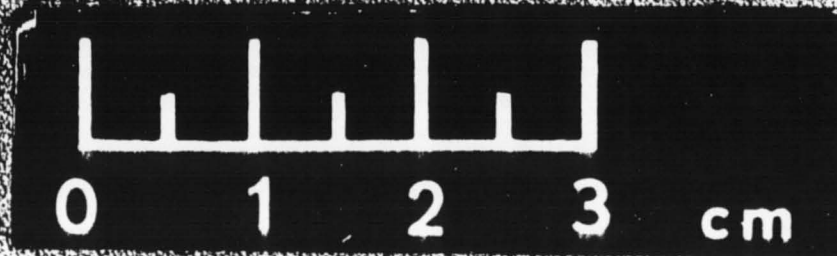
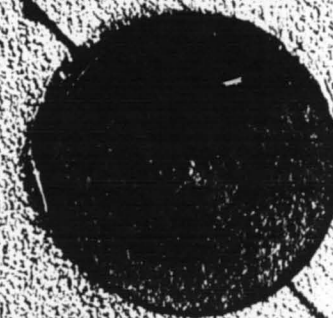
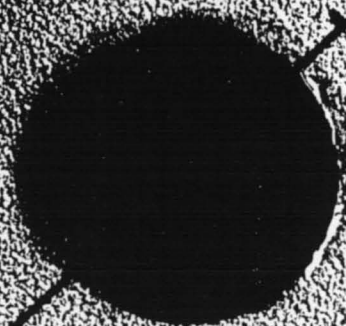
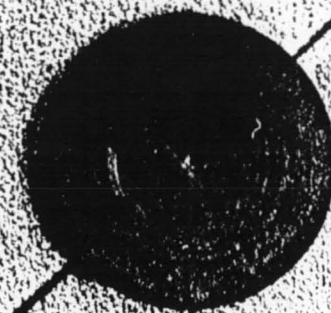
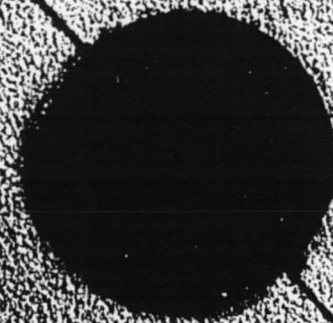
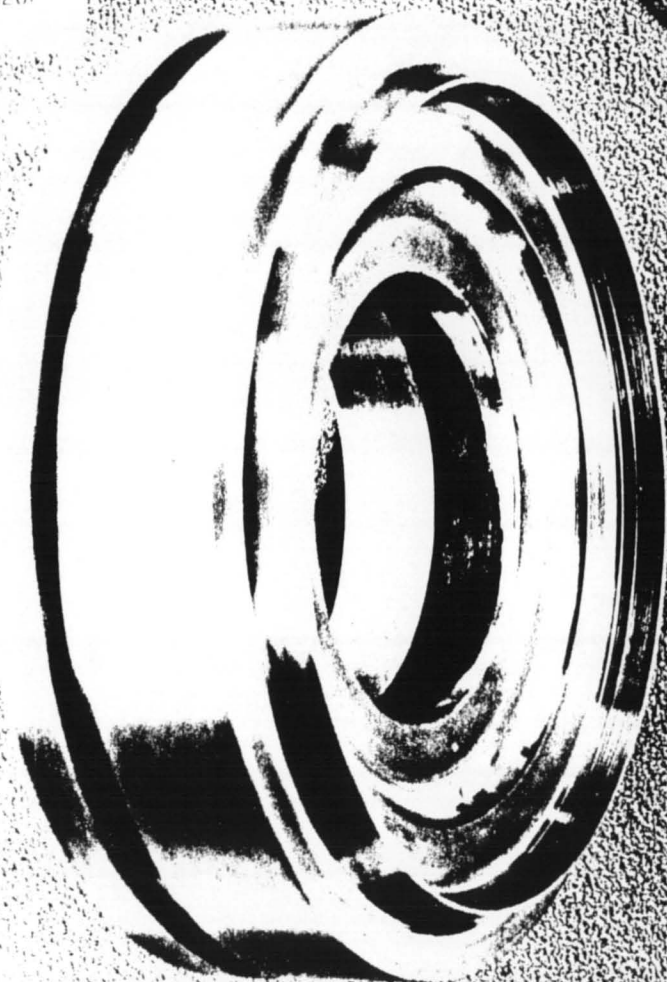


Figure 29. Deformation of Sample
Material at Ambient
Temperature

NASA-WSTF
0286-G262

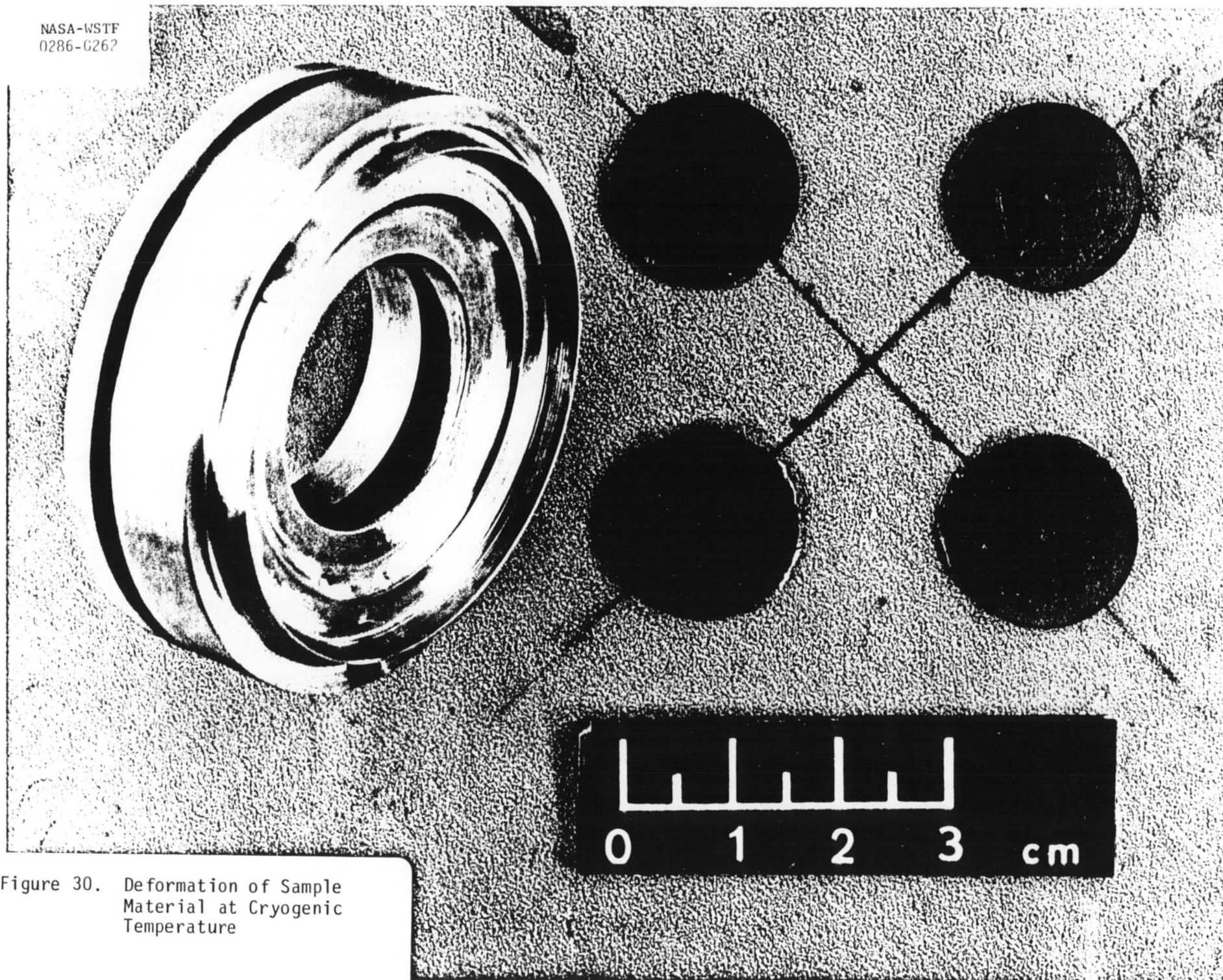


Figure 30. Deformation of Sample Material at Cryogenic Temperature

discs were attached to a 1/4-inch-thick, stainless steel plate using epoxy. The rotor was placed on top of the discs and an 11,300 lb/sq in load was applied and held for several seconds. The results of the experiment are shown in Figure 29. The rotor made a slight, nearly imperceptible mark in the surfaces of the discs. The experiment was then repeated after the rotor and the discs were cooled in liquid nitrogen, and the results are shown in Figure 30. Again, it was found that only a very slight impression had been made in the test sample material. As a result of this experiment, it was determined that the load applied to the samples in the pretest setup did not damage the test sample surface.

4.3 Discussion of Possible Failure Mechanisms

Several failure mechanisms were considered as possible causes of the fire in the LOX Frictional Heating Tester. They were (a) rubbing of the rotor bolts on the drive motor end of the test chamber, (b) the shaft broke, (c) the test was performed with GOX instead of LOX, (d) the sample was damaged due to the load applied during the pretest setup, (e) a shaft seal burned, and (f) the test sample ignited. Each of these possible causes of the fire are discussed below.

(a) Rubbing of the Rotor Bolts on the Test Chamber. If this had occurred, then there would be signs of rubbing on the rotor bolts and the test chamber end section nearest the drive motor, and these parts of the test apparatus would be burned. In fact, as can be seen in Figures 26 and 27, there was no damage to this portion of the apparatus.

- (b) The shaft broke. For the shaft to have broken, a large force would have been required or the shaft material would have had to have decreased strength at the test conditions. None of the data indicate that a large force was exerted on the shaft, e.g., the rpm, normal load, torque load, and the displacement. The shaft material, 304 SS, has a higher strength at cryogenic temperatures than at ambient temperature.
- (c) The test was performed with GOX rather than LOX. All the thermocouples, from the LOX accumulator to the main vent line, indicated lower than -270 °F, and the pressure was greater than 240 psia until just a few seconds prior to the first fire burning through the test system. During the fire, the supply accumulator temperature was below -300 °F, and its pressure was greater than 350 psig. At these pressures and temperatures the oxygen is a saturation mixture of vapor and liquid.
- (d) The sample was damaged due to the normal load that was applied in the pretest setup. The experiment performed in response to Action Item 6 from the February 5th committee meeting (see Section 4.2) indicated that the application of this load did not seriously damage the sample (see Figures 28, 29, and 30).
- (e) A shaft seal burned. In 1982, a seal in the WSTF Frictional Heating Tester did fail and cause a fire (Event Report ER82-001, R. Shaw). In that case, the oxygen from the test chamber was vented to the seal area and the seals, the chamber shaft bearing, and the portion of the shaft from the seal outward were destroyed. The fire burned

from the seal outward, the direction that the oxygen was being vented. In the case of Test WS-31, the major portion of the damage to the test apparatus occurred in the area of the test sample. Only a small portion of the chamber seal was destroyed. The burning of the seal appeared to be as a result of the fire, rather than the cause of it. If the fire had started in the seal, then the oxygen would have been vented through the seal, and the fire would have burned from the seal outward, as it did in the seal fire of 1982. This would have caused a loss of chamber pressure. In this case, the burning occurred within the test chamber and the chamber pressure was maintained until the fire burned through the vent line downstream of the test chamber. These things indicate that the fire did not start at the shaft seal.

(f) The test sample burned. The most likely of all the possible failure mechanisms discussed was that the test sample burned. A description of the scenario is given below. Refer to Figures 31 through 33.

<u>Time (s)</u>	<u>Event</u>	<u>Consequence/Discussion</u>
-4.7	Drive motor turned on.	RPM increases from 0 to 17,000 in 1 second. Torque increases from 0 to 11 in-lbs, the break-out torque, and then decreases to approximately 5 in-lbs, the tare torque, and remains constant. The pressure at 1/2 radius of test chamber (PT-814) decreases from 330 psia to 250 psia and then begins a slight decrease to 230 psia in approximately 10 seconds. The differential pressure between PT-814 and the inner cavity changes from 0 to -70 psid (a negative psid indicates that the inner cavity pressure is greater than the outer cavity pressure). One second later the chamber pressure decreases from approximately 325 to 315 psig. The

<u>Time (s)</u>	<u>Event</u>	<u>Consequence/Discussion</u>
		normal load (LC-706) increases from 0 to approximately 125 lbf, and then begins a gradual increase to approximately 135 lbf in 10 seconds.
0.0	Command given by micro-processor to increase air cylinder pressure.	After a delay of 0.2-0.3 second, the air cylinder begins to increase from 0 to 59 psig at a rate of 4.5 psi/s.
5.2-5.3	The normal load caused by the air cylinder surpasses that caused by the pumping of the rotor.	The rotor is abruptly displaced toward the test sample (DISP). The normal load (LC-706) indicates an increase from approximately 135 lb to 390 lb at a rate of 29.6 lb/s. The pressure at 1/2 the radius and at the circumference of the test chamber both indicate a slight increase. This is most likely due to changes in the hydrodynamic forces caused when the rotor touches the test sample. The torque load begins to increase.
5.3	The rotor wears into the test sample.	The displacement indicates a gradual change from 0.0085 to 0.0055 at a rate of 0.008 in/s.
7.0		The displacement indicates an abrupt incursion of the rotor into the test sample from 0.0055 to -0.002 at a rate of 0.0083 in/s. This may be due to melting of the sample surface. A slight increase in TC-702 is noted at approximately 8 seconds. Due to an expected time delay in the response of the thermocouple, this temperature rise is associated with this incursion.
7.9	The rotor wears into the test sample.	The displacement indicates a gradual change from -0.002 to -0.0075 at a rate of 0.0011 in/s. The rate of this incursion indicates that the rotor is wearing into the test sample in the same fashion as it did at 5.3 seconds.
9.3		An unexplained cycle occurs in the torque load measurement in which it goes from 20 to 7 to 20 in-lbs in a time of nearly 3 seconds.

<u>Time (s)</u>	<u>Event</u>	<u>Consequence/Discussion</u>
12.3		The temperature in the outer cavity of the chamber (TC-704) indicates a 75 °F spike of approximately 0.2 second duration.
12.8- 12.9	Test sample ignites.	An abrupt incursion of the rotor into the test sample from -0.0075 to -0.0265 at a rate of 0.05 in/s occurs. This type of incursion is similar to that noted during ignition in other frictional heating tests conducted previously. The temperatures in the test chamber outer cavity, in the inner cavity vent line, and in the main vent line, indicate a temperature rise of approximately 75 °F in 1 second. These rises in temperature are probably due to the vaporization and heating of the LOX in the chamber, which arises from the combustion at the surface of the test sample. The torque load drops from 50 to 5 in-lbs (the tare torque load). The pressure at 1/2 the radius in the outer chamber cavity increases abruptly from 238 to 270 psia, and there is a corresponding decrease in the differential pressure measurement. This increase is due to the changes in the pumping action of the rotor, because it is now pumping a gas (at least partially) instead of a liquid. An abrupt increase in the delta P occurs at 13.2 seconds.
13.2	Microprocessor gives command to separate the rotor from the test sample.	The rotor continues to move toward the test sample. The air cylinder valve is actuated.
13.4	Air cylinder pressure begins to decrease.	The air cylinder pressure and the normal load decrease to pretest conditions and the displacement indicates that the rotor begins to move away from the test sample. The torque load decreases from 5 to 2 in-lb. The differential pressure decreases abruptly from -85 to 0 psid

<u>Time (s)</u>	<u>Event</u>	<u>Consequence/Discussion</u>
		<p>because the rotor has moved away from the sample and the inner and outer cavity pressures now equalize. The pressure at 1/2 the radius of the outer chamber cavity increases from 270 to 393 psia in 0.5 second, and the pressure at the chamber circumference increases from 315 to 330 psig in 0.3 second. These pressure increases occur due to the rapid vaporization of LOX as a result of the burning test sample. (It should also be noted that the normal load has decreased to 0, in spite of the fact that the rotor is still spinning at 17,000 rpm. This gives a further indication that the LOX in the area surrounding the rotor has been vaporized. If it hadn't, then the pumping action would have caused a normal load. The pressure increase in the test chamber causes a reduction of flow from the LOX supply accumulator and the supply pressure increases from 360 to 370 psig. The rpm increases from slightly less than 17,000 to 17,000 rpm in 1 second.</p>
14.2	Rotor is fully displaced away from test sample and test sample continues to burn.	<p>Displacement indicates 0.060, the pretest position. Torque is at a reading slightly lower than it was prior to the start of rubbing. The lower torque value is due to the fact that the test chamber is now filled with warm GOX, rather than LOX, as it was prior to rubbing. The temperatures in the outer cavity of the test chamber, the vent line from the inner cavity, and the main vent line increase abruptly by 100 to 1200 °F. The chamber pressures and the supply accumulator pressure increase approximately 0.30 psi in a period of 5 seconds. The test sample burns at a rather slow rate and in an uneven fashion, as indicated by the thermocouples imbedded in it. At T=15.8, the fire reaches the location of</p>

<u>Time (s)</u>	<u>Event</u>	<u>Consequence/Discussion</u>
		TC-703 (the thermocouple located in the middle position) and burns it. At T-16.8, the fire reaches the location of TC-708 (the thermocouple located in the position farthest away from the rubbing surface) and burns it. And at T-18.0, the fire reaches the location of TC-702 (the thermocouple nearest the rubbing surface) and burns it.
18.0	The shaft is burned.	The normal load indicates a negative value.
18.1		The thermocouple in the inner cavity vent line (T C-820) is burned.
18.4	The fire burns through the system plumbing at the elbow in the 1/4" AN hardline in back of the tester.	The first light is observed coming from behind the tester. The pressure on the supply accumulator begins to drop.
19.0	The fire burns through the bottom of the test chamber where the vent lines connect to the chamber.	The flame is observed coming from the bottom of the test chamber. The test chamber pressures drop from approximately 380 to 30 psi in just under 2 seconds, and then drop to ambient within 7 seconds after that.
22.3	The drive motor is turned off.	The rpm decreases to 0. The torque load increases as the motor slows down.
24.7	The drive motor stops.	The torque load goes to 0.

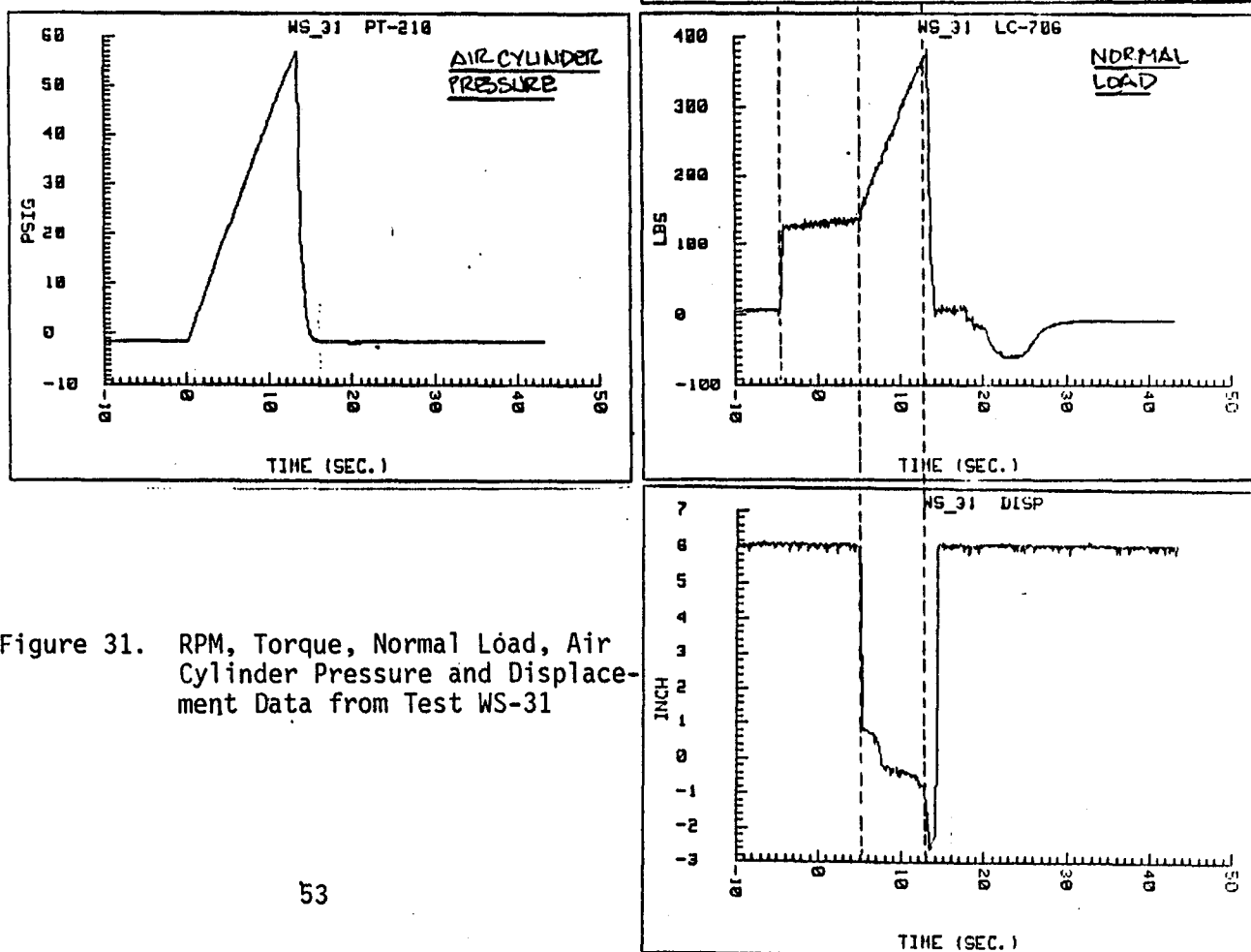


Figure 31. RPM, Torque, Normal Load, Air Cylinder Pressure and Displacement Data from Test WS-31

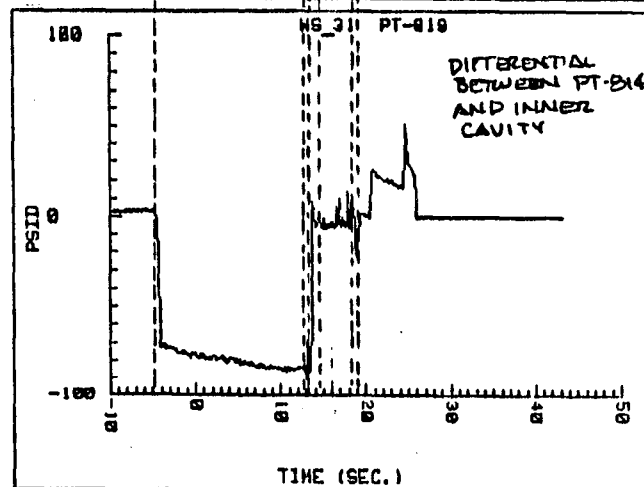
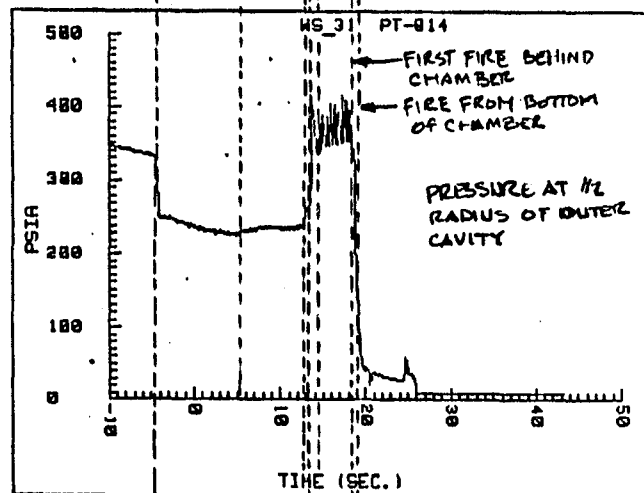
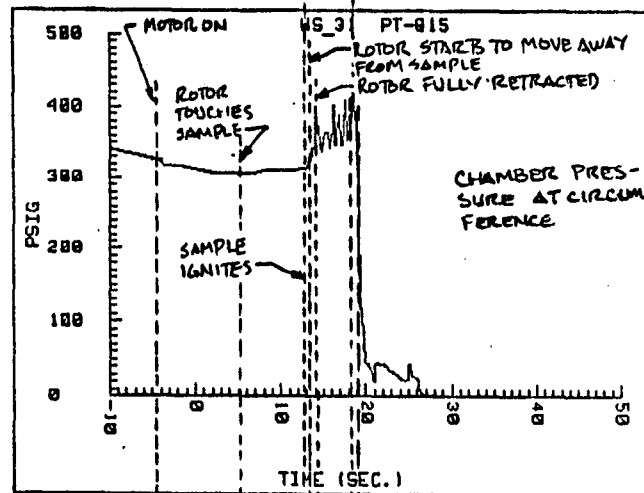
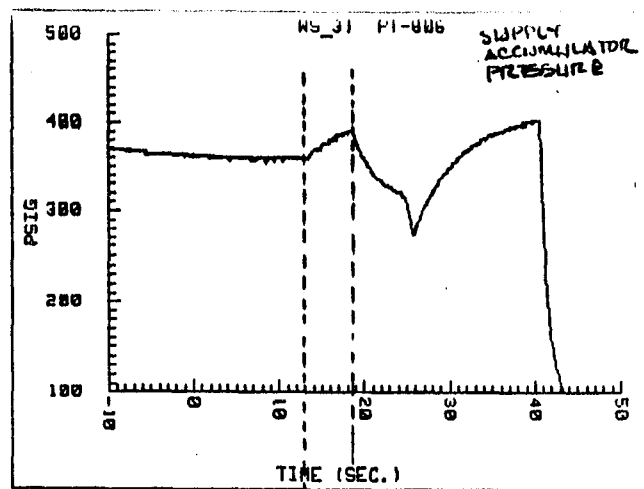


Figure 32. Pressure Data from Test WS-31

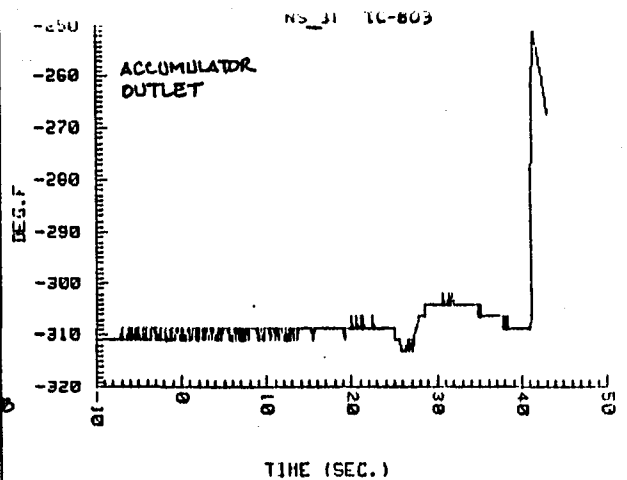
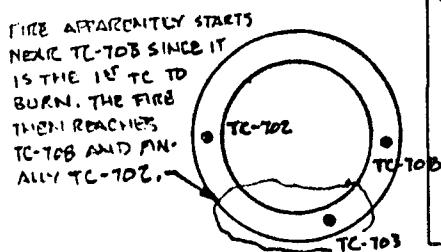
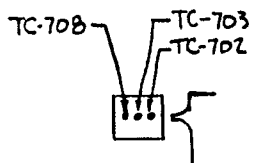
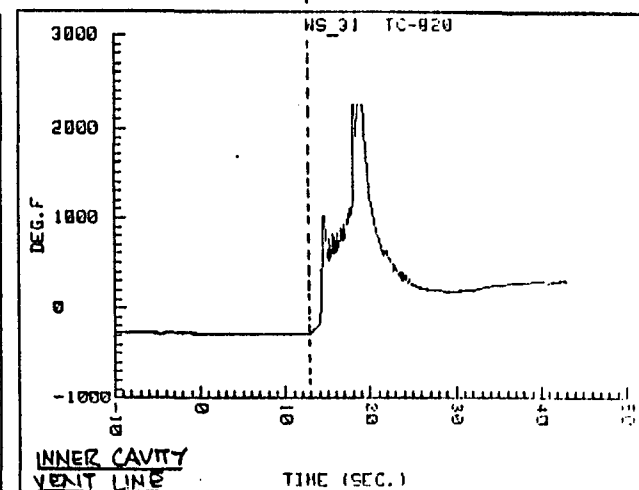
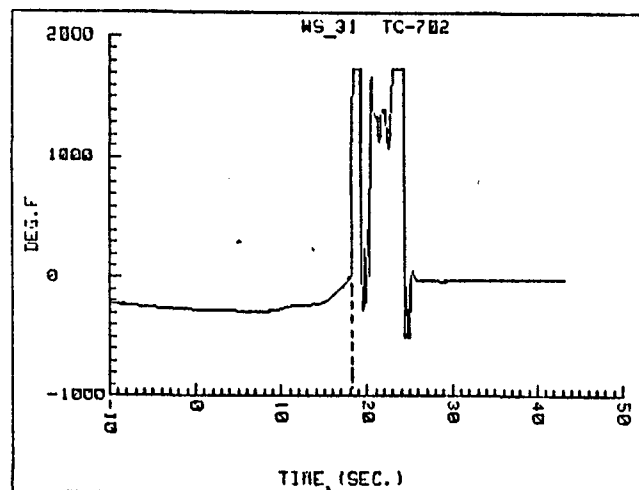
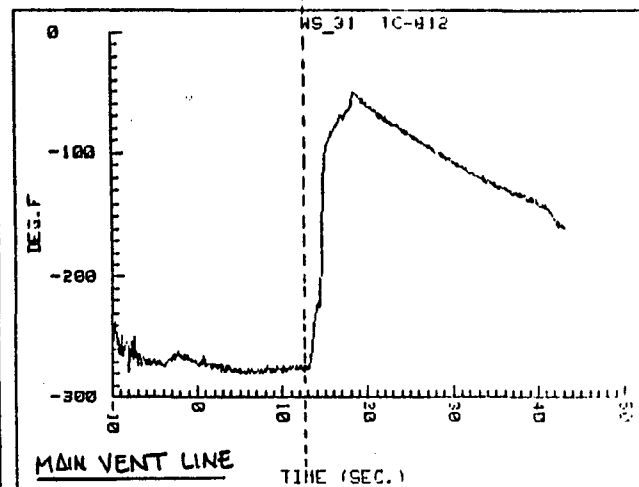
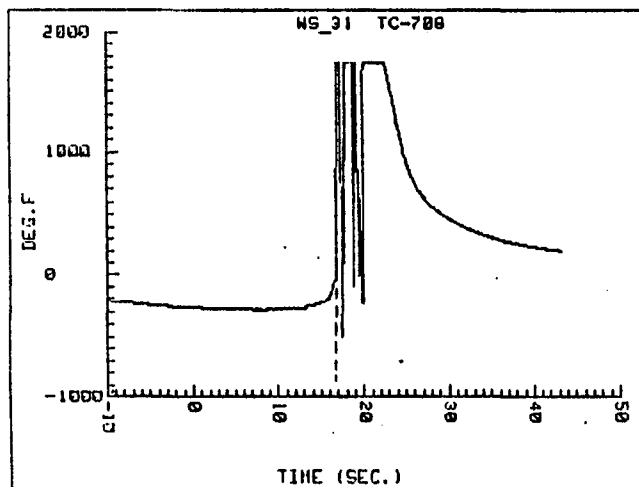
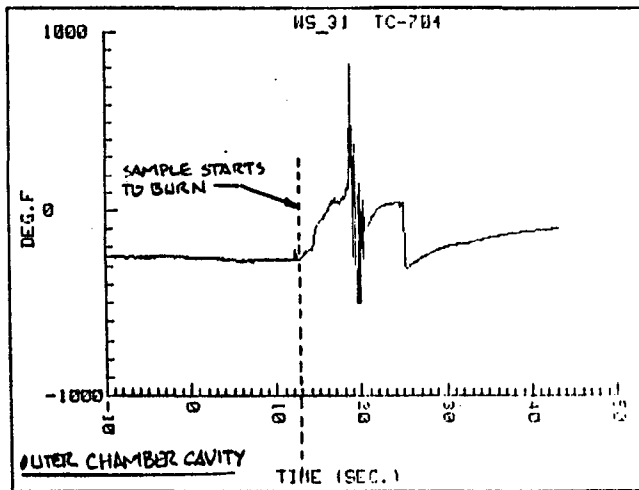
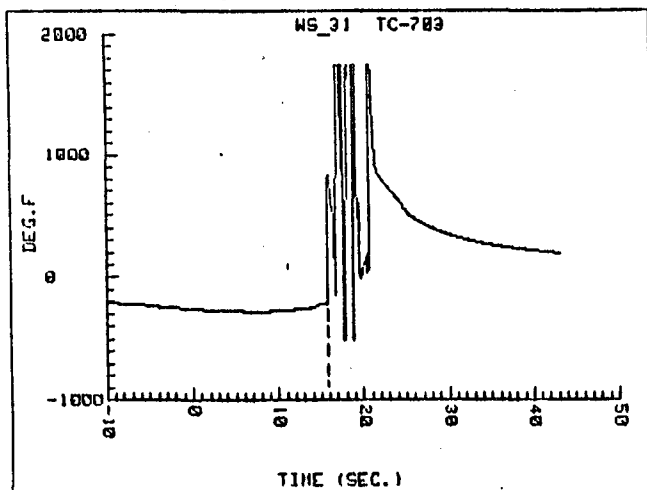


Figure 33. Temperature Data from Test WS-31



5.0 CONCLUSION

The fire in the LOX Frictional Heating Test System occurred as a result of the Inconel 718 rotor rubbing against the Vespel SP-211 test sample. It was surmised that the rubbing of the rotor on the sample caused local heating of the sample, which in turn heated the oxygen near the rubbing area. A bubble of gaseous oxygen formed which reduced the heat transfer away from the test sample. The temperature of the sample was increased to its ignition temperature, and the sample ignited, causing the fire.



NASA JSC WSTF
TEST PREPARATION SHEET



1/31/86

TPS NO. 8 HPF = 4507E1
TYPE: A - Configuration Change
B - No Configuration Change ☒

SYSTEM

LOX FRICTION RUBBING TEST - CELL III

MOD SHEET NO.

DRAWING(S), DOCUMENTS, OCP(S), PART NO(S) & DCN(S)
SK-20334

PAGE 1 of 7

PREPARATION DATE
1/31/86

TPS SHORT TITLE

INCIDENT INVESTIGATION

REASON FOR WORK

FIRE IN FRICTIONAL HEATING TEST SYSTEM

TASK ORDER NO.

F38

NEED DATE

CONSTRAINTS

SPECIAL SAFETY
REQUIREMENTS

☐ YES
☒ NO

MATERIALS
REQUIRED

☐ YES
☒ NO

ITEM
NO.

DESCRIPTION (TYPE OR PRINT)

WORKED

SHOP

INSPECTED

NASA

THIS IS AN INVESTIGATIVE TPS TO AUTHORIZE
THE INVESTIGATION OF THE FIRE THAT
OCCURED IN TEST CELL III ON 1/31/86.

1. PLACE "DO NOT OPERATE" TAGS ON THE FOLLOWING
CIRCUIT BREAKERS TO ENSURE THAT DRIVE MOTOR,
WALL OUTLETS, ARE NOT POWERED ON:

JMS
1/31/86

PANEL PA CB-3

PANEL LC CB-5, CB-9, CB-10,
CB-23, AND CB26

2. DUMP DATA STORED DURING TEST.

JMS
1/31/86

3. ENSURE THAT ALL LOX HAS BEEN VENTED

JMS
1/31/86

PREPARED BY:

J. STOLTZTUS

ORGANIZATION:

LCMSO

COMPLETION DATE:

9-5-86

SHOP

J.H.

NASA

CONTRACTOR AUTHORIZED SIGNATURES

NASA AUTHORIZED SIGNATURES

[Signature]

[Signature]


TEST PREPARATION SHEET CONTINUATION SHEET

PAGE 2 OF 1

TPS NO.

3-HPF-4507 E1

MOD. NO.

ITEM NO.	DESCRIPTION CONTINUED	WORKED	INSPECTED
		SHOP	NASA
	FROM ACC-3LO-AK804 AS INDICATED BY		
	TC-7T807 AND TC-803 READING ABOVE		
	-100 °F.		
4.	PLACE CELL IN AMBER STATUS.. ENTER		
	CELL AND REMOVE ANY SMOLDERING		
	DEBRI FROM THE CELL ^{SHUT OFF MASTER (LOAD) POWER SWITCHES} PLACE CELL IN		
	RED STATUS. ^{UNPLUG ALL 110 AC POWER CORDS}		
	<i>J. Stoltz</i>  1/31/86		
5.	ENSURE SYSTEM IS SHUT DOWN		
	A. PLACE CELL IN AMBER		
	B. CLOSE MV-AK05		
	C. CLOSE MV-AK03		
	D. CLOSE MV-AK02		
	E. CLOSE MV-AK902		
	F. FULLY REDUCE PCV-AK501		
	11 PCV-AK205		
	11 PCV-AK905		
	11 PCV-AK214		
	11 PCV-AK202		
	G. DISCONNECT FILL & DRAIN LINES.		
	H. SHUT DOWN CONTROL CONSOLE 111.		
CONTRACTOR AUTHORIZED SIGNATURES		NASA AUTHORIZED SIGNATURES	
<i>J. Stoltz</i>		<i>[Signature]</i>	

TEST PREPARATION SHEET CONTINUATION SHEET

PAGE 2 OF 4

TPS NO. 8-HPF-4507E
MOD. NO.

ITEM NO.	DESCRIPTION CONTINUED	WORKED	INSPECTED
		SHOP	NASA
I	PLACE CELL IN RED		
J	PLACE "DO NOT OPERATE" TAGS ON CELL DOORS AND CONTROL CONSOLE.		
K	PLACE CELL IN AMBER		
6	VERIFY SAFETY OF BRINGING UP FACILITY POWER, SO THAT OTHER CELLS CAN BE POWERED UP.	JH 2-3-86	
7	CHECK LOCATION AND TIGHTNESS OF MECHANICAL STOPS ON AIR CYLINDER SHAFT. BOTH COLLARS TIGHT. GREEN COLLAR AGAINST AIR CYL. BODY. .041" GAP BEHIND INCUSION LIMIT COLLAR.	JMS 2/3/86	
8	PHOTOGRAPH TEST CELL AND TEST APPARATUS	JH 2-4-86	
9	VERIFY THERMOCOUPLE CONNECTORS AND TAG PRIOR TO SEPARATING CONNECTORS	JMS 2/4/86	
10	LOCATE, TAG, AND MAKE NOTE OF ELECTRODES	JMS	
11	CHECK FACILITY CABLE DAMAGE. MAKE RECOMMEND- ATIONS REGARDING PROTECTING CABLES		
12	PERFORM BORESCOPE INSPECTION OF TEST CHAMBER	JMS 2/4/86	
CONTRACTOR AUTHORIZED SIGNATURES		NASA AUTHORIZED SIGNATURES	
J. Stultz		F. Berry	

MOD. NO.

PAGE 7 OF 7

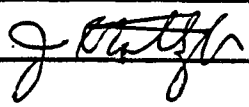
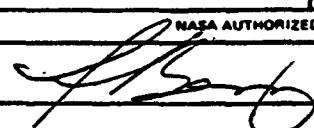
A-4

TEST PREPARATION SHEET CONTINUATION SHEET

PAGE 2 OF 1

TPS NO. 8 - HPF - 4507 E1



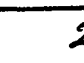
MOD. NO.

ITEM NO.	DESCRIPTION CONTINUED	WORKED	INSPECTED
		SHOP	NASA
18.	INVESTIGATE THE EXTENT OF TEST ROTOR INCURSION INTO VESPEL SP21 MATERIAL UNDER THE STATIC LOADING CONDITIONS USED IN THE PRE-TEST ADJUSTMENTS FOR TEST WS-31, 11,300 psi sample LOADING, AMBIENT & CRYOGENIC TEMPERATURES.	JH 2-7-86	
19.	SUBMIT THE FOLLOWING COMPONENTS FOR CALIBRATION AND CLEANING. NOTE ANY SIGNIFICANT DIFFERENCE BETWEEN NEW CALIBRATION DATA AND PREVIOUS DATA.	Bb 2/10/86	
	PT - AK 815 8848		
	PT - AK 819 3117		
	PSV - AK 211 092277-10		
	PT - AK 816 68819		
	PI - AK 903 2959		
	PT - AK 806 3118		
	VPT - AK 517 3119		
	PT - AK 210 2104		
	LC - AK 706 92191		
	DISP 36420		
	VPT - AK 814 2519		
CONTRACTOR AUTHORIZED SIGNATURES		NASA AUTHORIZED SIGNATURES	
			

TEST PREPARATION SHEET CONTINUATION SHEET

PAGE 1 OF 1

TPS NO. 8-HPF-4507 E1
MOD. NO.

ITEM NO.	DESCRIPTION CONTINUED	WORKED	INSPECTED
		SHOP	NASA
19	CON'T'D		
	A. ENSURE SYSTEM IS PROPERLY VENTED		
	B. REMOVE COMPONENTS LISTED ABOVE.		
	C. CAP OPEN LINES ON SYSTEM.		
	D. SUBMIT COMPONENTS FOR CALIBRATION AND CLEANING.		
	<i>John Ham</i> 2-7-86 <i>Berry</i> 2/7/86 		
20	A. LOAD TEST ROTOR & VESPEL SP211 MATERIAL WITH LOAD DETERMINED IN STEP 18, USING MET-LAB COMPRESSION TESTER, AT AMBIENT TEMPERATURE.	<i>B 16</i> 2/7/86	
	B. REPEAT AT LN ₂ TEMPERATURE.		
	1) FILL LN ₂ DEWAR PER LJI-32034024 FROM TANK T-130.		
	2) TRANSPORT LN ₂ DEWAR TO MET-LAB		
	3) PROPER PROTECTIVE GEAR MUST BE WORN WHILE TRANSPORTING CRYOGENIC LIQUIDS.		
	4) DIP TEST ROTOR AND VESPEL SP211 MATERIAL INTO LN ₂ BATH UNTIL BOILING CEASES.		
	5) LOAD MATERIAL IN COMPRESSION TESTER & TEST WITH PRESCRIBED LOAD.		
CONTRACTOR AUTHORIZED SIGNATURES		NASA AUTHORIZED SIGNATURES	
<i>John Ham</i> 2-7-86 <i>Berry</i> 2/7/86 		<i>John Ham</i> 2-7-86 <i>Berry</i> 2/7/86 	


TEST PREPARATION SHEET CONTINUATION SHEET

PAGE 1 OF 1

TPS NO.

8-HPF-4507E1

MOD. NO.

ITEM NO.	DESCRIPTION CONTINUED	WORKED	INSPECTED
		SHOP	NASA
21	REMOVE "ALL "DO NOT ENTER" AND "DO NOT OPERATE" TAGS PLACED ON CELL IN DOORS AND CELL IN CONTROL PANEL IN STEPS 1 & 5 OF THIS TPS.	JH 2-7-86	
22	PERFORM FUNCTIONAL CHECKOUT OF CELL IN CONTROL CONSOLE ELECTRONICS.	JH 2-7-86	
	John Hone 2-14-86  2/14/86 F. Boring 2/14/86		
	The failure analysis was completed as described in the steps above. Event report number ERB6-002 was generated. This report is stored in the Materials and Component Test Department Office in the 200 Area. The conclusion drawn was that the test sample material burned after being rubbed by the test rotor as.	J. Stoltzfus 2/5/86 F. Boring	
CONTRACTOR AUTHORIZED SIGNATURES		NASA AUTHORIZED SIGNATURES	
J. Stoltzfus		F. Boring	

1. Report No. NASA CR189055		2. Government Accession No.		3. Recipient's Catalog No.	
4. Title and Subtitle Orbit Transfer Rocket Engine Technology Soft Wear Ring Seals Technology - Task Order B.5				5. Report Date 14 February 1992	
				6. Performing Organization Code	
7. Author(s) B. W. Lariviere				8. Performing Organization Report No. RI/RD90-214	
				10. Work Unit No.	
9. Performing Organization Name and Address ROCKWELL INTERNATIONAL Rocketdyne Division 6633 Canoga Avenue Canoga Park, California 91304				11. Contract or Grant No. NAS 3-23773	
				13. Type of Report and Period Covered Final Technical Report 1985 to 1990	
12. Sponsoring Agency Name and Address National Aeronautic Space Administration - Lewis Research Center Research and Technology Branch 21000 Brookpark Road Cleveland, Ohio 44135				14. Sponsoring Agency Code	
15. Supplementary Notes Task Manager, Joseph Hemminger, NASA Lewis Research Center, Cleveland, Ohio					
16. Abstract LOX Compatibility Tests, including Autogenous Ignition, Promoted Ignition, and LOX Impact Tests, and Friction and Wear tests at different PV products were conducted for several polymer materials as a verification of implementing soft wear ring seals in advanced rocket engine turbopumps. Thermoplastics, polyimide based materials, and polyamide-imide base materials were compared for oxygen compatibility, specific wear coefficient, wear debris production, and heat dissipation mechanisms. A thermal model was generated that simulated the frictional heating input and calculated the surface temperature and temperature distribution within the seal. The predictions were compared against measured values. Heat loads in the model were varied to better match the test data and determine the difference between the measured and the calculated coefficients of friction.					
17. Key Words (Suggested by Author(s)) Oxygen Turbopumps, Polymer Wear, Frictional Heating, Lox Impact, Promoted Ignition, Autogenous Ignition, PV Product				18. Distribution Statement Unclassified - Unlimited	
19. Security Classif. (of this report) Unclassified	20. Security Classif. (of this page) Unclassified	21. No. of Pages 190	22. Price		

